



HAL
open science

The role of the low-energy electrons in the process of radiosensitization

Barbora Sedmidubská

► **To cite this version:**

Barbora Sedmidubská. The role of the low-energy electrons in the process of radiosensitization. Radiochemistry. Université Paris-Saclay; České vysoké učení technické (Prague), 2024. English. NNT : 2024UPASF069 . tel-04905867

HAL Id: tel-04905867

<https://theses.hal.science/tel-04905867v1>

Submitted on 22 Jan 2025

HAL is a multi-disciplinary open access archive for the deposit and dissemination of scientific research documents, whether they are published or not. The documents may come from teaching and research institutions in France or abroad, or from public or private research centers.

L'archive ouverte pluridisciplinaire **HAL**, est destinée au dépôt et à la diffusion de documents scientifiques de niveau recherche, publiés ou non, émanant des établissements d'enseignement et de recherche français ou étrangers, des laboratoires publics ou privés.

The role of the low-energy electrons in the process of radiosensitization

*Le rôle des électrons de basse énergie dans le processus de
radiosensibilisation*

**Thèse de doctorat de l'université Paris-Saclay et de Czech Technical
University in Prague**

École doctorale n° 571, Sciences chimiques : molécules, matériaux,
instrumentation et biosystèmes (2MIB)
Spécialité de doctorat : Chimie
Graduate School : Chimie. Référent : Faculté des sciences d'Orsay

Thèse préparée dans les unités de recherche **Institut de Chimie Physique (Université
Paris-Saclay, CNRS)** et **J. Heyrovský Institute of Physical Chemistry of the CAS**,
sous la direction de **Mehran MOSTAFAVI**, Professeur,
la co-direction de **Marie DAVÍDKOVÁ**, Chargée de recherche,
le co-encadrement de **Sergey DENISOV**, Chargé de recherche,
le co-encadrement de **Jaroslav KOČIŠEK**, Chargé de recherche.

Thèse soutenue à Prague, le 22 novembre 2024, par

Barbora SEDMIDUBSKÁ

Composition du Jury

Membres du jury avec voix délibérative

Václav ČUBA

Maître de conférences, Doyen d'université
Czech Technical University in Prague

Président

Hassan ABDOUL-CARIME

Maître de conférences, HDR, Claude Bernard University Lyon 1
(IP2I, UMR 5822)

Rapporteur & Examineur

Štefan MATEJČÍK

Professeur, Comenius University in Bratislava

Rapporteur & Examineur

Viliam MÚČKA

Professeur, Czech Technical University in Prague

Examineur

Mojmír NĚMEC

Maître de conférences, Chef de département
Czech Technical University in Prague

Examineur

Gérard BALDACCHINO

Chargé de recherche, HDR, Institut Rayonnement-Matière de Saclay
(LIDYL, EMR9000)

Examineur

Czech Technical University in Prague
Faculty of Nuclear Sciences and Physical Engineering
Department of Nuclear Chemistry



DISSERTATION

The role of the low-energy electrons in the process of
radiosensitization

Role nízkenergetických elektronů v procesu radiosensitizace

Le rôle des électrons de basse énergie dans le processus de
radiosensibilisation

Prague 2024

Ing. Barbora Sedmidubská


Bibliographic Entry

<i>Author</i>	Ing. Barbora Sedmidubská Czech Technical University in Prague, Faculty of Nuclear Sciences and Physical Engineering, Department of Nuclear Chemistry J. Heyrovský Institute of Physical Chemistry of the Czech Academy of Sciences, v.v.i., Department of Dynamics of Molecules and Clusters Université Paris-Saclay, Faculté des Sciences d'Orsay Institut de Chimie Physique, UMR 8000, CNRS, Département Chimie
<i>Title of Dissertation</i>	The role of the low-energy electrons in the process of radiosensitization
<i>Degree Programme</i>	Applied Natural Sciences —
<i>Field of Study</i>	Nuclear Chemistry Sciences Chimiques : Molécules, Matériaux, Instrumentation et Biosystèmes (2MIB); Chimie Physique, BioPhysique et Analytique (CPBA)
<i>Supervisors</i>	Marie Davídková, Ing. CSc. Nuclear Physics Institute of the Czech Academy of Sciences, v.v.i., Department of Radiation Dosimetry
<i>Supervisor specialists</i>	Prof. Mehran Mostafavi Institut de Chimie Physique, UMR 8000, CNRS Université Paris-Saclay, Faculté des Sciences d'Orsay Mgr. Jaroslav Kočíšek, Ph.D. J. Heyrovský Institute of Physical Chemistry of the Czech Academy of Sciences, v.v.i., Department of Dynamics of Molecules and Clusters
<i>Academic Year</i>	Dr. Sergey Denisov Institut de Chimie Physique, UMR 8000, CNRS Université Paris-Saclay, Faculté des Sciences d'Orsay 2023-2024
<i>Number of Pages</i>	168
<i>Keywords</i>	Electron attachment spectroscopy, pulse radiolysis, secondary low-energy electrons, favipiravir, RRx-001, fullerenols

Declaration

I hereby declare that except where specific reference is made to the work of others, the content of this dissertation is original. I carried out this work independently and only with the cited sources, literature and other professional sources.

In Prague 6.9.2024


.....
Ing. Barбора Sedmidubská

Acknowledgment

I would like to take this opportunity to express my gratitude to everyone with whom I had the honour of working and without whom this complex work would not have been possible. My most enormous thanks belong to my supervisors.

I would like to thank my supervisor, Marie Davídková, Ing., CSc., from the Nuclear Physics Institute of the CAS, for her valuable advice, experiences, consultations, and great willingness and support throughout my studies. I would like to express my gratitude to my supervisor specialist, Mgr. Jaroslav Kočíšek, PhD, from the JH Institute of Physical Chemistry of the CAS, especially for his valuable advice and consultations, for his support and patience, and for providing me with many opportunities to develop my skills and broaden my knowledge. Finally, I would like to thank him for guiding my work for most of my studies. I would like to thank both of them for allowing me to build my dissertation framework on my previous works and develop the topic more deeply regarding the real impact. From the Institut de Chimie Physique and Université Paris-Saclay in Orsay, I am very grateful to my supervisor, Prof. Mehran Mostafavi, for the opportunity to conduct my research in his research group and use the experimental platform ELYSE. I also wish to thank him, especially for his precious discussions about pulse radiolysis experiments and his guidance during my stay in Orsay. My thanks belong to my supervisor specialist, Dr. Sergey A. Denisov, for his valuable comments, advice, discussions, and guidance during measurements on the ELYSE platform.

I would like to thank my colleagues from the Department of Dynamics of Molecules and Clusters at the JH Institute of Physical Chemistry in Prague for the friendly atmosphere, enriching discussions, valuable advice and support in gaining my practical and theoretical knowledge. I thank my colleagues at the Institut de Chimie Physique in Orsay, especially J.P. Larbre, for his patience and extraordinary commitment in the case of the platform ELYSE, without which I could not perform the experiments there. Many thanks to Denis Dobrovolskii and Dr. Zhiwen Jiang for their willingness to introduce me to some measurement procedures.

I would like to thank my colleagues with whom I worked on the publications for their valuable interdisciplinary insights into the complex tasks solved; special thanks to Prof. Milan Ončák for his *ab initio* calculations, illuminating some parts of our experimental work. I am grateful to Ing. David Chvátíl and his scientific team at the microtron for the opportunity to irradiate our solutions there and for their willingness and total commitment during the experiments. I would like to thank Mgr. Jiří Pinkas, Phd. for his great willingness and commitment to analysing irradiated samples on the microtron using NMR spectroscopy.

I must thank the institutions that allowed me to conduct research at the ICP, Orsay. My one-year stay there was financially supported by the European Cooperation in Science and Technology via short-term scientific missions (STSMs) and the French Ministry of Foreign Affairs via the France Excellence Eiffel Scholarship Program.

Finally, I thank my family for their unwavering support.

Ing. Barbora Sedmidubská

Title : The role of the low-energy electrons in the process of radiosensitization

Keywords : Electron attachment spectroscopy, pulse radiolysis, secondary low-energy electrons, favipiravir, RRx-001, fullerenols

Abstract : Concomitant chemoradiotherapy is one of the crucial methods of cancer treatment. Still, there is an effort to increase its effectiveness and keep the toxicity for healthy cells as low as possible. Its most significant advantage is the synergistic effect resulting from many complex interactions between both treatment modalities (i.e. chemotherapy and radiotherapy). It was shown that one of its causes could be the interaction of the chemical component (so-called radiosensitizer) with secondary low-energy electrons produced in large numbers during radiolysis in the irradiated tissue. In this work, I focus on the radiosensitization process to investigate the radiosensitizing potential of molecules and reveal their mechanisms of radiosensitization based on interaction with low-energy electrons. The motivation was to obtain new information to design novel, more effective radiosensitizers with lower toxicity.

The work consists of a theoretical part and an experimental part. The theoretical part is based on the research of existing radiosensitizers and their model compounds from the point of view of interaction with low-energy electrons.

The experimental part combines electron attachment experiments in the gas phase on two experimental systems and ab initio calculations of the electron affinities of the studied molecules and their fragments. Pulse radiolysis experiments in solution and microtron irradiation with NMR spectroscopic evaluation.

In this work, the antiviral agent favipiravir was studied, for which we confirmed its radiosensitizing potential based on interaction with low-energy electrons. Next, the radiosensitizing mechanism of the RRx-001 molecule, a confirmed radiosensitizer and chemotherapeutic, was investigated in relation to its interaction with secondary low-energy electrons as a possible source of synergism in chemoradiotherapy. The significance of such an interaction in the case of the RRx-001 molecule was revealed in this work. Finally, a strong interaction of solvated electrons with fullerenols was revealed. Fullerenols were studied for use within a platform that would demonstrate sensitivity to low-energy electrons and simultaneously be used for drug delivery in concomitant chemoradiation therapy.

Titre : Le rôle des électrons de basse énergie dans le processus de radiosensibilisation

Mots clés : Spectroscopie d'attachement d'électrons, radiolyse pulsée, électrons secondaires de basse énergie, favipiravir, RRx-001, fullerénols

Résumé : La chimioradiothérapie concomitante est l'une des méthodes importantes de traitement du cancer. Il existe des efforts pour augmenter son efficacité tout en maintenant la toxicité pour les cellules saines à un niveau supportable. Son plus grand avantage réside dans l'effet synergique découlant de nombreuses interactions complexes entre les deux modalités de traitement (la chimiothérapie et la radiothérapie). L'une des causes pourrait être l'interaction de la composante chimique (le radiosensibilisateur) avec les électrons secondaires de basse énergie produits en grand nombre lors de la radiolyse de l'eau dans le tissu irradié. Ce travail se concentre sur le processus de radiosensibilisation afin d'examiner le potentiel radiosensibilisateur des molécules et les mécanismes de radiosensibilisation. La motivation était d'obtenir de nouvelles informations pour la conception de nouvelles radiosensibilisateurs plus efficaces et moins toxiques.

La thèse se compose de parties théorique et expérimentale. La partie théorique présente les connaissances sur les radiosensibilisateurs existants et de leurs composés modèles du point de vue de

leur interaction avec les électrons de basse énergie. La partie expérimentale combine des expériences de capture d'électrons en phase gazeuse, des expériences de radiolyse pulsée en solution, ainsi que des irradiations sur microtron avec évaluation par spectroscopie RMN et des calculs ab-initio des affinités électroniques des molécules étudiées et de leurs fragments.

Dans ce travail, l'antiviral favipiravir a été étudié, pour lequel j'ai confirmé son potentiel radiosensibilisant. Ensuite, le mécanisme de radiosensibilisation de la molécule RRx-001, un radiosensibilisateur et agent chimiothérapeutique confirmé, a été étudié en relation avec son interaction avec des électrons secondaires de basse énergie. Cette interaction, qui pourrait être l'une des sources possibles de synergisme en chimioradiothérapie, a été révélée pour la molécule RRx-001 dans ce travail. Enfin, une forte interaction des électrons solvatés a été révélée avec les fullerénols étudiés pour une utilisation comme plateforme sensible aux électrons de basse énergie pour la délivrance de médicaments dans le cadre de la thérapie chimioradiative concomitante.

Název : Role nízkoenergetických elektronů v procesu radiosensitizace

Klíčová slova : Elektronová záchytová spektroskopie, pulsní radiolýza, sekundární nízkoenergetické elektrony, favipiravir, RRx-001, fullerenoly

Abstrakt : Konkomitantní chemoradioterapie je jedna z důležitých metod léčby rakoviny. Stále existuje snaha zvýšit její účinnost a udržet toxicitu pro zdravé buňky na snesitelné úrovni. Její největší výhodou je synergický efekt plynoucí z mnoha komplexních interakcí mezi oběma léčebnými přístupy (tzn. chemoterapie a radioterapie). Bylo ukázáno, že jednou z příčin synergismu může být interakce chemosložky (tzv. radiosensitizeru) se sekundárními nízkoenergetickými elektrony vznikajícími v hojném počtu během radiolýzy v ozářené tkáni. V této práci se zaměřuji na proces radiosensitizace s cílem prozkoumat radiosensitizační potenciál molekul a odhalit radiosensitizační mechanismy na bázi jejich interakce s nízkoenergetickými elektrony. Motivací této práce bylo získat nové informace pro návrh nových a více účinných radiosensitizerů s menší toxicitou.

Práce sestává z teoretické a experimentální části. Teoretická část je postavena na rešerši již existujících radiosensitizerů a jejich modelových sloučenin z pohledu interakce s nízkoenergetickými elektrony.

Experimentální část kombinuje experiment elektronového záchytu v plynné fázi na dvou experimentálních zařízeních, experiment pulsní radiolýzy v roztoku, dále ozařování na mikrotronu s NMR spektroskopickým vyhodnocením a ab-initio výpočty elektronových afinit studovaných molekul a jejich fragmentů.

V této práci bylo studováno antivirotikum favipiravir, pro který jsme na základě interakce s nízkoenergetickými elektrony potvrdili jeho radiosensitizační potenciál. Také byl zkoumán mechanismus radiosensitizace již potvrzeného radiosensitizeru a zároveň chemoterapeutika RRx-001 z pohledu jeho možné interakce se sekundárními nízkoenergetickými elektrony, která byla v této práci potvrzena. Nakonec byla odhalena silná interakce solvatovaných elektronů s fullerenoly studovanými pro použití v rámci platformy, která by prokazovala citlivost na nízkoenergetické elektrony a užívala by se pro dodávání léků v rámci konkomitantní chemoradiační terapie.

Contents

List of Abbreviations	19
Introduction	21
1 State-of-the-art in chemoradiotherapy	23
1.1 A concomitant chemoradiotherapy	23
1.1.1 Synergism	25
1.1.2 Side effects	26
1.2 Cytostatics and radiosensitizers	27
1.2.1 Chemotherapeutic drugs: Alkylating agents	28
1.2.2 Chemotherapeutic drugs: Antimetabolites	30
1.2.3 Cytostatic agents with radiosensitizing potential	31
1.3 Secondary LEEs in chemoradiotherapeutic synergism	34
1.3.1 Formation and properties of secondary LEEs	34
1.3.2 Reactions of LEE-attachment	37
1.4 Motivation for a design of novel radiosensitizers and goals of the work	37
1.5 Molecules investigated in the present work	40
1.5.1 Antiviral: Favipiravir	40
1.5.2 Chemotherapeutic: RRx-001	41
1.5.3 Fullerenes as a part of a π - π complex	42
2 Experimental & theoretical approaches	46
2.1 CLUster Beam apparatus	47
2.1.1 Experimental device	47
2.1.2 Calibration of energy scale using CO ₂	51
2.2 Electron attachment spectrometer	53
2.2.1 Experimental device	53
2.2.2 Calibration of electron-energy scale using SF ₆	55
2.3 Mass resolution of mass spectrometers	56

2.4	Experimental ELYSE platform	57
2.4.1	Experimental device	57
2.4.2	Sample preparation and sample inlet	60
2.5	Microtron MT25	63
2.6	<i>Ab initio</i> calculations using Gaussian software	64
3	Overview of results & discussion	66
3.1	Studies on the molecule of favipiravir	67
3.2	Studies on the molecule of RRx-001	68
3.2.1	Studies on the molecule of RRx-001 in cooperation with University of Innsbruck	68
3.2.2	SHORT TIME-SCALE: Intermediates	69
3.2.2.1	Electron attachment to RRx-001 in gas phase (CLUB)	69
3.2.2.2	Picosecond pulse radiolysis of RRx-001 in ethanol . .	75
3.2.3	LONG TIME-SCALE: Products of radiolysis	84
3.2.3.1	Radiolysis of RRx-001 in ethanol solution on microtron	84
3.2.4	Final discussion and conclusion of the experiments with RRx-001	90
3.3	Studies on fullerenes considering π - π complex	93
3.3.1	Pulse radiolysis experiments on fullerenes	95
3.3.2	Picosecond pulse radiolysis experiments on fullerenols	96
3.3.3	Fluorescence spectroscopy for 2-aminopurine in water	100
3.3.4	Final discussion and conclusion of fullerenes study	102
	Conclusion	103
	Bibliography	105
	Author's publications	117

List of Abbreviations

AEA: associative electron attachment
C₆₀: buckminsterfullerene
C₆₀-PTA: C₆₀ pyrrolidine tris-acid
CCD: charge-coupled device
CL: cross-links
CLUB: cluster beam apparatus
DSB: double-strand break
DEA: dissociative electron attachment
DFT: density functional methods
DMSO: dimethyl sulfoxide
DNA: deoxyribonucleic acid
EA: electron attachment
EAS: electron attachment spectroscopy
ELYSE: a platform for lysis of sample by electrons
EPR effect: extended permeability and retention effect
ESI: electrospray ionisation
FWHM: full width at half maximum
HF: Hartree-Fock methods
HOMO: highest occupied molecular orbital
IR: ionizing radiation
JH IPC: J. Heyrovský Institute of Physical Chemistry of the CAS
LEEs: low-energy electrons
LET: linear energy transfer
LUMO: lowest unoccupied molecular orbitals
NMR: nuclear magnetic resonance
pH: potential of hydrogen
PR: pulse radiolysis
QMS: quadrupole mass spectrometer
R: mass resolution
RNA: ribonucleic acid
rTOF: reflectron time-of-flight spectrometer
SSB: single-strand break
TEM: trochoidal electron monochromator
tRNA: transfer ribonucleic acid
UPS: Université Paris-Saclay
VD: direct line
VMI: velocity map imaging

Introduction

Concomitant chemo-radiation therapy is one of the crucial strategies for anticancer treatment. Its best advantage is a synergistic effect caused by many complex interactions between both treatment modalities (ionizing radiation and cytostatics). [1] Simultaneously, it strives to improve efficiency and maintain toxicity to healthy tissue at an endurable level. A natural effort to alleviate side effects either builds on adjustment of the parameters of well-established treatment or involves developing entirely new treatments together with newly designed drugs. These can significantly increase the irradiation effect in cooperation with ionizing radiation and thus cause a maximal effect in chemoradiotherapy - the synergistic effect. [2, 3] Hence, the proposal of novel drugs emphasizes on radiosensitizing properties, toxicity, and the size of drugs that affect targeted drug delivery properties [4]. Also, it requires a more profound knowledge of the mechanisms of their action as a possible source of the synergistic effect. One of these mechanisms causing the synergism was shown in pioneering work by Leon Sanche's research group [5, 6]. This mechanism lies in the interaction of administered drugs with secondary low-energy electrons (LEEs) produced as the most abundant secondary species after the passage of high-energy radiation through the tissue [7]. The above-mentioned key themes and their interrelationships relevant to the present work are elaborated in more detail in Chapter 1: State-of-the-art in chemoradiotherapy.

The work was generally motivated by the rational design of novel radiosensitizing agents with low side effects for chemoradiotherapy. Specifically, the work was driven by an effort to understand better synergism-causing mechanisms based on interactions of the secondary LEEs with radiosensitizers in cancer chemoradiotherapy. The motivation is described in more detail in Chapter 1.4, as well as the goals of the work. The aim was to reveal new information for the rational design of novel therapeutic agents with radiosensitizing properties. The work focuses on studying the radiosensitizing potential of selected compounds in connection with targeted drug delivery from the point of view of LEE-induced chemistry.

For this purpose, the work was split into two primary directions: literature research and experimental research. The research direction was focused on the current state-of-the-art in the field, which will help us focus future investigations in a better direction and provide a real-time impact on rational drug development. To do so, I prepared a detailed review of all the works studying the attachment of LEEs to radiosensitizers that was used as a base for our perspective publication in journal *Phys. Chem. Chem. Phys.* [8]. The main goal of the work was to conduct experimental research on interactions between secondary LEEs and selected molecules.

It is a highly complicated task since electrons in the biological environment are only intermediate species with an extremely short lifetime. Hence, there are two complementary approaches for studying their reactions: a) electron attachment spectroscopy carried out at the J. Heyrovský Institute of Physical Chemistry of the CAS (JH IPC) in Prague and b) ultrafast spectroscopy being performed at Institut de Chimie Physique (ICP), UMR8000 in Orsay. While the first technique allows us to characterize the entrance channels for LEEs in detail, the second experimental technique can identify the reaction channels in a natural biological environment. Combining these complementary techniques was one of the primary goals of the present doctoral thesis. Experimental and theoretical approaches applied in this work are subjects of Chapter 2: Experimental & theoretical approaches.

The foremost part of the experimental research combines theoretical and experimental research to study the reductive properties of selected compounds. The studied molecules were selected as promising candidates for a radiosensitizing agent (favipiravir) and already confirmed for the chemotherapeutic and radiosensitizing effect (RRx-001). These molecules are presented in Chapters 1.5.1, resp. 1.5.2. In the first case, the crucial aim was to reveal radiosensitizing potential based on the reductive properties of the molecule. In the second case, there was an essential effort to uncover the part of the radiosensitizing mechanism of the molecule coming from its interaction with secondary low-energy electrons. These studies build on the electron attachment spectroscopy method (Chapters 2.1, 2.2) for studying electron attachment reactions to selected molecules. The further experimental approach is a pulse radiolysis technique (Chapter 2.4) applied to study behaviour of LEE in the form of quasi-free and solvated electrons in solution and their scavenging by the studied molecule. From the theoretical perspective, Gaussian software was also used to compute electron affinities (Chapter 2.6). Electron attachment spectroscopy and *ab initio* calculations were carried out at the JH IPC in Prague. Pulse radiolysis experiments were performed at the ICP, UMR8000 in Orsay. The study of antiviral favipiravir is summarized in the Chapter 3.1 and the attached article. Chapter 3.2 deals with the results of the investigation of the RRx-001 molecule and is extended by the article in the attachment.

The minor part of the work focuses on fullerenes, introduced in Chapter 1.5.3, to examine their potential to be used as a LEEs-sensitive platform for drug delivery in concomitant chemo-radiation therapy. The bi-molecular complex could work as a radiosensitizer while benefiting from the best properties of both molecules, e.g., the good targeted drug delivery properties of fullerene and the high radiosensitizing potential of the second molecule. The π - π complex should consist of water-soluble fullerene and molecules with high electron affinity. This investigation requires the application of a method of pulse radiolysis (Chapter 2.4) to study the scavenging of secondary low-energy electrons in a solution by fullerene. These experiments were performed at the ICP, UMR8000 in Orsay and are presented in Chapter 3.3.

The gained theoretical and experimental information is essential for revealing fundamental mechanisms driving synergy in concomitant chemo-radiation therapy. The outcomes of this complex study are summarized in the Conclusion chapter.

State-of-the-art in chemoradiotherapy

In the first instance, the theoretical part of this work briefly summarizes in the Chapter 1.1 a field of concomitant chemoradiotherapy and its main advantages and disadvantages in cancer treatment. In the following Chapter 1.2, a great emphasis is placed on cytostatics and radiosensitizers. In the case of cytostatic agents, the work presents chemotherapeutics from groups of alkylating agents and antimetabolites. Subsequently, the chapter discusses in more detail only selected molecules with already clinically proven radiosensitizing properties, for which these molecules have been studied from the perspective of interaction with LEEs as one of the possible sources of synergism. This chapter is freely extended by an already published article (attached in the appendix [8]) dealing with essential molecules from the series of modified DNA components, nitroimidazoles, and organometallics, which were studied for their interaction with low-energy electrons considering their (potential) use in chemoradiotherapy as radiosensitizers. The next Chapter 1.3, deals with the radiosensitizing effect, formation and properties of secondary electrons and mainly secondary low-energy electrons, and their crucial role in chemotherapeutic synergism and thus in this work. This introduction outlines the current progress in developing agents to make a concomitant chemoradiotherapy treatment more effective and less toxic to healthy tissue.

In Chapter 1.4, based on the previous chapters, I put forward my motivation and goals of the present work, which study LEEs interactions with selected molecules to facilitate the rational design of novel therapeutic agents with radiosensitizing properties. On this account, the last Chapter 1.5 aims to introduce the molecules investigated in this work with applied strategies such as drug repurposing and targeted drug delivery. The first presented molecule is an antiviral drug - favipiravir, which was studied to examine its radiosensitizing potential. Next, the molecule RRx-001 is introduced as a proven chemotherapeutic radiosensitizer, successfully passing clinical tests. To the third, I present a buckminsterfullerene C_{60} and its two water-soluble derivatives, fullerenols and C_{60} -pyrrolidine tris acid, which are attractive to explore for targeted drug delivery.

1.1 A concomitant chemoradiotherapy

Since the beginning of human existence, humankind has struggled with various diseases, some of which have gradually evolved into diseases of affluence. One of them is a cancer. The history of cancer goes back to ancient Egypt. Still, in response to new knowledge and tools for diagnostics and treatment, medical theoretical approaches and cancer treatment have developed progressively since then. Still, new therapeutic attitudes and options are being sought. [9]

Nowadays, cancer treatment can be divided into curative and palliative treatment, which primarily mitigates the symptoms. If the goal is to cure cancer, modern medicine offers five primary forms of treatment: classic surgery, radiotherapy, chemotherapy, an increasingly used hormonal therapy, and biological treatment.

However, many studies show the crucial importance of combination therapy for cancer treatment, where the effects of the individual modalities affect each other positively or negatively [10]. The opportunity to combine treatment approaches is also one of the options for responding more efficiently to the individuality of cancer cases. Specifically, it is possible to combine individual drugs [11, 12] in a case of chemotherapy and individual treatment approaches such as chemotherapy and radiotherapy into chemoradiotherapy [13] and others.

The chemoradiotherapy itself is used as a treatment strategy, especially for the treatment of solid tumours in advanced stages of cancer. It is generally assumed that this combined therapy can increase the lethal effect on tumour cells and keep the remaining side effects on healthy tissues tolerable. Chemotherapeutic cytotoxic drugs called cytostatics in tumour cells can reinforce the efficiency of ionizing radiation. In particular, these are appropriate for cytostatic and timing combining chemotherapeutic and irradiation parts, which can also significantly increase the potential overall therapeutic effect. Chemoradiotherapy provides several types of treatment according to the timing of the combination.

This work is motivated by the rational design of novel drugs for concomitant chemoradiotherapy. It thus touches on topics like combining the most promising novel approaches of rational drug design, drug repurposing, targeted therapy, and secondary low-energy electrons-induced synergism. Therefore, the whole chapter is devoted to concomitant chemoradiotherapy, its principles, utilization, and advantages and disadvantages.

A concomitant chemoradiotherapy and its utilization

This type of combination therapy became a widely used approach for the treatment of diverse localizations of cancer [14]. And even if I talk about chemoradiotherapy, the primary modality remains radiotherapy [10]. The breadth of the utilization of this specific treatment increases with the number of performed clinical trials for various cancers. However, it is necessary to consider that in addition to the synergistic effect, there is a multiplication of side effects arising from both types of treatments, which require additional care to reduce them. For this reason, such treatment is very complicated, and the scope of its primary use remains relatively narrow. Even so, from the point of view of local control of tumour and treatment response, the appropriately indicated application of concomitant chemoradiotherapy belongs among one of the most effective treatments. Thanks to the strong occurring synergistic effect and the shorter time-duration of treatment, it suppresses neo-adjuvant and adjuvant chemo-radiotherapeutic approaches. [10] The most significant curative effects have been shown, especially in the case of locally advanced solid tumours of the head and neck, where this combined treatment became the first method of choice because of its efficiency [15, 16]. It is also very often used for the treatment of lung cancer and tumours in the pelvic area (rectum, anus, vulva, cervix). However, it can also be used in the case of the treatment of bladder and anal cell carcinoma. In addition,

mutilating surgery is not often necessary after such combined treatment [2]. Also, it has been proven an improved survival for pancreatic, small-cell lung, head and neck, colorectal and cervical cancer [17].

Effects of a concomitant chemoradiotherapy

Combining chemotherapy with radiotherapy can lead to three conceivable final effects, which reflect the ratio of positive and side effects: subadditive, additive, or supra-additive (also called synergistic). The subadditive effect is when a low dose of cytostatics can increase the total effect of radiotherapy. However, the overall effect of combination therapy does not reach the sum of effects from both individual treatments. An additive effect equals the sum of individual effects from chemotherapy and radiotherapy. A synergistic effect means that the overall effect originating from combining both treatment modalities surpasses the sum of both individual effects. The effect can also be theoretically antagonistic when the combination of both approaches causes the effect to be lower than that of one of the used therapies alone. [2, 18] Naturally, concomitant chemoradiotherapy aims to reach the additive effect at least but the synergistic effect at the best case. Although the aim is clear, it, unfortunately, turns out that conditions in the laboratory and experiments in vitro differ from conditions in vivo clinical practice. Synergistic effects can still be reached more easily in vitro experiments than in clinical practice, where often only additive or subadditive effects are observed, and the main advantage arises from the fewer side effects. [14] Both synergistic and side effects will be depicted in the next subchapters 1.1.1, resp. 1.1.2.

1.1.1 Synergism

Synergistic effect benefits from the chemoradiotherapeutic combination applied more or less concurrently to the tumour area. The basis of synergism is manifold and diverse interactions between both treatment modalities, which are difficult to describe in their complexity and interconnectedness [14]. Specific interactions on cellular and vascular levels, which are behind the synergistic effect, are mentioned in Chapter 1.2.3. However, the positive consequences of these interactions are narrated here.

It is known that concomitant chemoradiotherapy can lead to the combined mechanism of efficiencies as spatial cooperation [19], independent cell killing, debulking, enhanced tumour control and response, recruitment, redistribution and total semi-synchronization of tumour cell lines, activations or deactivations of enzyme properties with impact on pharmacokinetic, metabolic pathways of a drug, inhibition of DNA repair processes, lethal and sublethal damages of DNA, increasing of apoptosis index, prohibition of formation of tumour cell clones resistant to individual types of treatment, and others [2, 18]. These findings have been summarized in Steel's model [20], which proposes five mechanisms that describe interactions of chemotherapy and radiotherapy and thus manage together a synergistic effect. These are: i) spacial cooperation, ii) cytotoxic enhancement, iii) temporary modulation and iv) normal tissue protection, and v) biological cooperation [20].

On these lines, the listed sources of synergism on a biological level will be described in more detail. **Spatial cooperation** represents a situation when radiotherapy acts locoregionally, while chemotherapy fights against micrometastases, but individual treatments do not influence each other, only cooperate [19]. The effect of **independent cell killing** is based on the assumption that chemotherapy and radiotherapy dispose of certain anticancer activities that add up due to combination but without interaction. **Debulking** is an decrease of tumour size. It may be caused by adjuvant or neo-adjuvant chemotherapy that follows up with concomitant chemoradiotherapy to influence potential micrometastases in the surrounding area positively. It allows for the better insertion of cytostatics into tumour tissue, higher oxygenation of tumour cells, and decreased radiotherapy toxicity because of a smaller target volume. A typical interaction between chemotherapeutic and radiotherapeutic approaches achieves **enhanced tumour control and response**. **Recruitment** involves the transition of cells from the G0 phase to a repopulation cell cycle; **redistribution** means that individual cells are shifted to a cell cycle phase where they can be more sensitive to radiation (it is known that cells are most sensitive during a transition between cycle phases G2 and M). **Semi-synchronization of tumour cells** is a shift of a part of tumour cells to more radiosensitive phases in a cell cycle (G0 and G1 phases are practically radio-resistant). This shift is caused by irradiation or cytostatics alone, like, e.g., 5-fluorouracil, cisplatin, and taxanes. Suitable synchronization of cells can lead to higher cell deaths after irradiation. The overall effect of concomitant chemoradiotherapy is also influenced (positively or negatively) by **activations or deactivations of enzyme properties and the following impact on the pharmacokinetic metabolism of a drug**. **Inhibition of DNA repair processes** is another way to increase chemoradiotherapy efficiency. It can be achieved with cytostatics such as cisplatin, bleomycin, hydroxyurea, and anthracyclines. DNA sensitization for damages (e.g. caused by high-reactive radicals forming after irradiation) leading to a **lethal or sublethal effect in a cell** can be reached by incorporating cytostatics into the DNA strands. A combination of chemotherapy and radiotherapy can induce **apoptosis** in the cell. This combination is also a guarantee for **prohibiting the formation of tumour cell clones**, which could be resistant to individual types of treatment. [10, 2, 18]

Another advantage of the concomitant treatment is that when chemotherapy is used, the total irradiation dose can be decreased (10-25%), reducing the probability of acute and chronic damage to healthy tissues. [2, 3]

1.1.2 Side effects

Both components of combination therapy are unfortunately known for their toxic effects on healthy tissue, and the side effects can be further enhanced during the combined treatment. Hence, it is important to consider the indication of chemoradiotherapy very carefully in addition to the overall medical state of a patient. [2, 3]

According to the toxicity response, one can recognize early reactive tissue (a response on toxicity appears during irradiation) and lately reactive tissue. Chemotherapy is mainly responsible for toxicity in early reactive tissue like intestines and bone marrow. However, it also causes late toxic effects after treatment in tissues such as the

heart and nervous system. Radiotherapy is a source of acute toxic effects but can also lead to chronic irreparable changes in tissues. Thus, toxicity can be divided into acute toxicity (local - e.g. radiation dermatitis, mucositis, or systemic - e.g. leukopenia, postirradiation syndrome) and chronic toxicity (as organ damage, carcinogenesis and immunosuppression) according to the period when side effects appear. Acute toxicity shows up to 3 months after therapy; by contrast, the chronic effect appears from 3 to 18 months in case of late effect or later than several years after treatment in case of a very late effect. The safety of concomitant chemoradiotherapy is reflected in the damage rate of vital organs (heart, lungs, liver, kidneys, intestines, central nervous system, bone marrow). [2]

Treatment by concomitant chemoradiotherapy can be cancelled when sensitive structures (in case of solid tumours of the head and neck, lung cancer and tumours in the pelvic area (rectum, anus, vulva, cervix)) are undergoing significant side effects. Irradiation can lead to infectious complications during the healing of the affected area. Hematologic toxicity increases when using a combined therapy. Also, toxicity in the intestines is higher, but the right timing of chemotherapy can mitigate it. Mucositis as an acute toxicity is an inflammation of the oral cavity, oesophagus and pharynx that occurs in the case of head and neck tumours, oesophagus and lungs; it is usually treated by application of growth factors. Another substantial problem is xerostomia, which requires treatment with pilocarpine to stimulate the salivary glands. Mucositis and xerostomia can be positively influenced by treatment with amifostine. Skin reactions are the next important side effect that occurs with the frequency and severity of dermatitis after external irradiation (especially for rectal and anus cancer). It is treated with boric acid or antibiotics. The final consequences of cancer and its treatment with combined therapy can be somatic and genetic damage and also secondary tumours, which can appear as a very late effect after treatment. The effort is to prevent the side effects as best as possible. It can be achieved with accurate irradiation planning (using 3D planning and conform radiotherapy), then a special source of irradiation (Leksell gamma knife, proton beams, pencil beams, emerging flash radiotherapy) but also radioprotective substances such as amifostine or others which allow increasing a dose delivered to the volume for irradiation without increasing of risk of damages in healthy tissue in the surrounding. [3]

1.2 Cytostatics and radiosensitizers

Chemical agents used in chemoradiotherapy are usually cytostatic and radiosensitizing agents, and this chapter is dedicated to them. According to the definition, "The cytostatic is a substance that slows or stops the growth of cells, including cancer cells, without killing them. These agents may cause tumours to stop growing and spreading without causing them to shrink in size" [21]. In contrast, "radiosensitizing agent is any substance that makes tumour cells easier to kill with radiation therapy. Some radiosensitizing agents are being studied in the treatment of cancer" [22].

It should be emphasized that not every cytostatic disposes of radiosensitizing properties, and simultaneously, not every radiosensitizer may have properties of the proper cytostatic drug and be used for pure chemotherapeutic purposes. [9] The most interesting are the compounds combining cytostatic and radiosensitizing properties since they can exhibit so-called synergistic effects when combined. These compounds and the nature of the synergism are of primary interest in the present work.

From a historical point of view, cytostatics are the cornerstone of the chemotherapeutic attitude to cancer treatment. Cytostatics have been used in pure chemotherapy as drugs that can damage tumour cells to stop their growth, division and reproduction. Even though the designation of chemotherapy may intimate the synthetic origin of cytostatics, this is not the case. A significant amount of cytostatic origin is natural, and its utilization can be found not only in oncology. [23] Chemotherapy in oncology is characterized by the administration of drugs that have a cytotoxic and cytostatic effect and thus have the potential to kill tumour cells. Nevertheless, cytostatics' effects are not specific to tumour cells; unfortunately, they also damage healthy cells, which is one of the reasons the chemotherapeutic effects go hand in hand with side effects. It must be noted that various cytostatics produce diverse side effects with different intensities. Chemotherapy allows the administration of cytostatic drugs alone or combined with more drugs (combination chemotherapy) and is often divided into cycles with various schedules. Drug administration may be orally (liquid, tablets, or capsule forms), locally cutaneously (liquid, ointment forms), intramuscularly, subcutaneously, intralesionally (= directly into the tumour), intraarterially, or intravenously. [24] Chemotherapeutic agents can be divided into several main groups according to their mechanism of action: Antimetabolites, Alkylating agents, topoisomerase inhibitors, mitotic inhibitors, antibiotics, protein kinase inhibitors and others. All representatives are bound to at least one phase of the cell cycle in which they are toxic to the cell.

A combination of chemotherapy and radiotherapy permitted the application of a lower amount of chemo-drug and a dose of irradiation. It multiplied the maximal achievable effect called synergism, which results from combining both treatment modalities and exceeds the sum of their individual effects. Behind this phenomenon were hitherto unknown, complex interactions between chemo-part and ionizing radiation.

The concomitant chemo-radiation therapy mainly operates with cytostatics from two groups: alkylating agents (Fig. 1.1) and antimetabolites (Fig.1.2) present below.

1.2.1 Chemotherapeutic drugs: Alkylating agents

In the case of anticancer actions, these chemotherapeutic agents inhibit DNA within the transcription of DNA, which leads to the inhibition of whole protein synthesis. The basis of this mechanism lies in the substitution of hydrogen atoms by alkyl groups on the DNA molecule. Thus, cross-links are formed within the DNA chain, which results in cytotoxic, carcinogenic, and mutagenic effects. It is not specific to tumour cells, but due to the rapidly dividing division cells in tumour tissue, the effect of these agents on tumour cells is higher than on healthy tissue. The explanation is that faster proliferating tumour cells do not have time for reparation mechanisms.

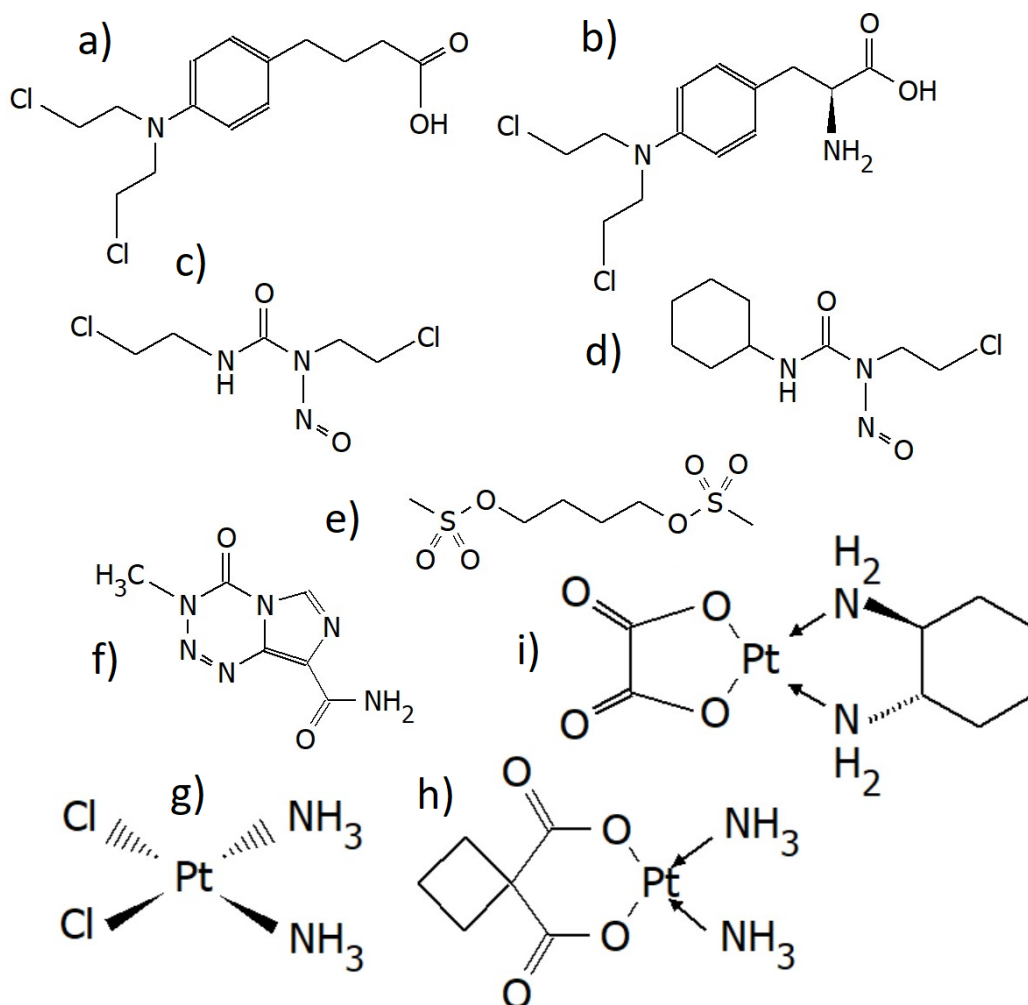


Figure 1.1: The structural patterns of selected alkylating agents: nitrogen mustards; a) chlorambucil; b) melphalan, nitrosoureas; c) carmustine; d) lomustine, alkyl sulfonate; e) busulfan, triazenes; f) temozolomide and antineoplastic agents containing platinum; g) cisplatin; h) carboplatin and i) oxaliplatin.

For the same reason, naturally, faster-dividing cells as hematopoietic, reproductive, and endothelial cells are also primarily damaged. It is a source of side effects of the alkylating agents such as amenorrhea, impaired spermatogenesis, anaemia, pancytopenia, intestinal mucosal damage, increased risk of malignancy, and alopecia. The end of the alkylation process leads to the misreading of the DNA code, inhibition of DNA and RNA, and inhibition of a protein synthesis that supports cell death (apoptosis) in tumour cells. The alkylating agents are generally separated into six classes which are with their representants listed below: The nitrogen mustards (mechlorethamine, melphalan, chlorambucil cyclophosphamide, ifosfamide), methylenamine and ethylenamine derivatives (altretamine, thiotepa), nitrosoureas (carmustine, lomustine), alkyl sulfonates (busulfan), triazenes (dacarbazine, temozolomide, procarbazine), antineoplastic agents containing platinum (cisplatin, carboplatin, oxaliplatin) also called platinum coordination complexes. These last-mentioned causes covalent DNA adduct by no alkylation but different other pathways. [25]

Alkylating agents are generally high-toxic but predominantly are toxic for the gastrointestinal tract and the bone marrow. Several alkylating agents (temozolomide, cyclophosphamide, and chlorambucil) cause a clinically apparent acute liver injury; others can also cause veno-occlusive disease (by high doses) and nodular regenerative hyperplasia (by prolonged periods). [26]

1.2.2 Chemotherapeutic drugs: Antimetabolites

Antimetabolites are one of the oldest and most used chemo-drugs; their utilization for leukaemia treatment goes back to the 1940s. The mechanism of action of these molecules is based on mimicking molecules essential for cell growth. Cells use antimetabolites instead of the appropriate molecule. Then, antimetabolites are incorporated into the DNA as building blocks, which turn off DNA replication and whole-cell proliferation. Such a mechanism goes primarily against cells with higher proliferation, which tumour cells have.

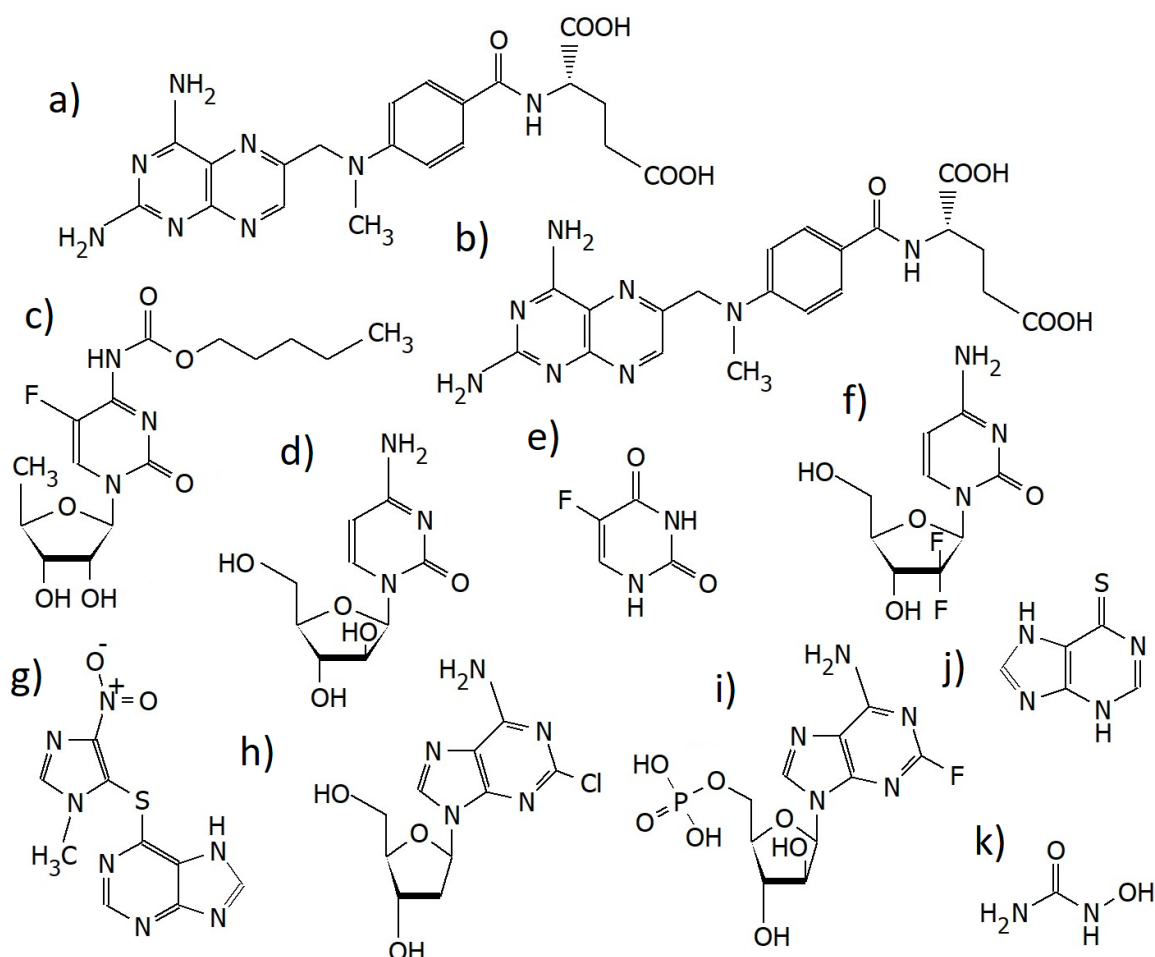


Figure 1.2: The structural patterns of selected antimetabolites: antifolates; a) methotrexate; b) pemetrexed, pyrimidine analogues; c) capecitabine; d) cytarabine; e) 5-fluorouracil; f) gemcitabine, purine analogues; g) azathioprine; h) cladribine; i) fludarabine; j) mercaptopurine and ribonucleotide reductase inhibitors and k) hydroxyurea.

Antimetabolites can be divided into four groups according to the type of structure, basis, and mechanism of action. Groups and their representant chemotherapeutics are antifolates (methotrexate, pemetrexed, pralatrexate, trimetrexate), pyrimidine analogues (azacitidine, capecitabine, cytarabine, decitabine, floxuridine, fluorouracil, gemcitabine, trifluridine/tripracil), purine analogues (azathioprine, cladribine, clofarabine, fludarabine, mercaptopurine, nelarabine) and ribonucleotide reductase inhibitors (hydroxyurea). Figure 1.2 shows the structural patterns of selected antimetabolites. Utilization of antimetabolites can be found in the treatment of cancer of the breast, intestinal tract and ovary. Their mean of administration differs; it depends only on certain antimetabolites. As side effects, antimetabolites cause nausea, diarrhoea, light sensitivity, lower concentration of white blood cells, hair loss, and increased concentration of liver enzymes. [27]

1.2.3 Cytostatic agents with radiosensitizing potential

Radiosensitizers are used to increase concomitant chemoradiotherapy efficiency [28]. They can interact with ionizing radiation in various ways, and many of these ways are still unknown. Several cytostatics have been proven to have radiosensitive potential; the most famous are cisplatin, 5-fluorouracil, hydroxyurea, gemcitabine, and doxorubicin with their structural patterns shown in the figure 1.3 [29, 2]. Several specific examples of interactions between ionizing radiation and radiosensitizers are mentioned here.

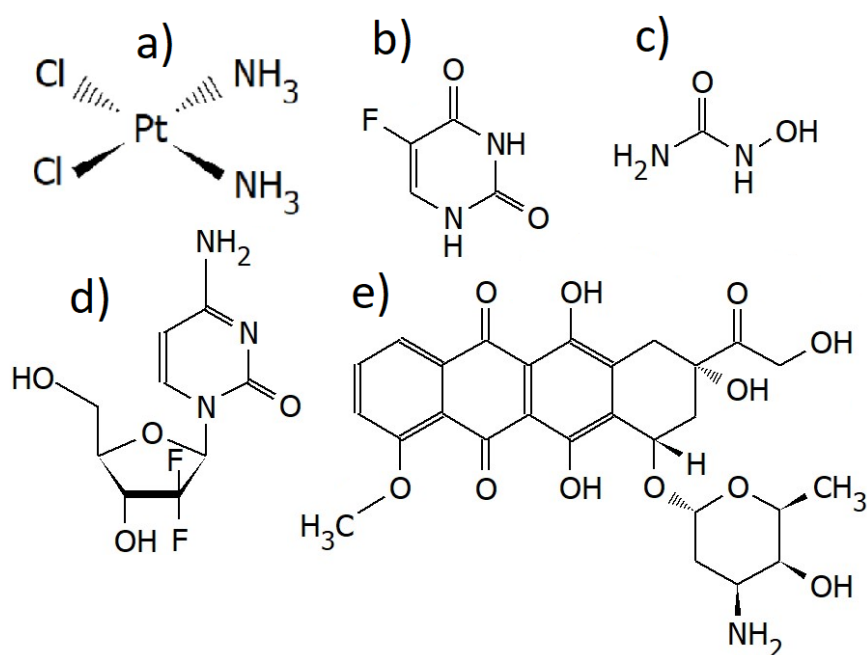


Figure 1.3: The structural patterns of the most famous radiosensitizing chemotherapeutic molecules of a) cisplatin, b) 5-fluorouracil, c) hydroxyurea, d) gemcitabine and e) doxorubicin.

Cisplatin

Radiosensitizing properties of cisplatin (cDDP) (figure 1.3a) were revealed in 1974. Cisplatin acts mainly in phase G1 (it is instead a radio-resistant phase) and S-G1 phases of the cell cycle. The mechanism of cisplatin is based on its ability to crosslink purine bases on DNA, which can disable the DNA repair mechanism in cancer cells [2]. Cisplatin can be bound via Pt to two nucleobases at the same or both DNA fibres. These crosslinks change the structure of DNA, which thus becomes more susceptible to radiation damage [30, 5].

In recent works of Sanche [7, 31, 32, 30, 5], an alternative mechanism was proposed as a source of synergism. The mechanism is based on DNA damages caused by low-energy electrons, which form as secondary species after irradiation. Such damages are enhanced by cDDP presence. Damages of DNA modified with cisplatin by electrons are characterized by three typical electron energy resonances: around 5 and 10 eV (energy of transient molecular anions), then around 14 and 18 eV (for SSB), and from 1.6 to 3.6 eV (bonding of cisplatin induces DSB which is finished by electrons with these energies) [31] [5]. Then, it was found that two electron-transfer mechanisms exist when transient anions are formed simultaneously in the DNA-cisplatin complex [30]. The presence of cisplatin increases the reaction rate of reaction between the oligonucleotide and solvated electrons, and the reaction rate is controlled by diffusion [32].

Such a mechanism does not prevent healthy tissue damage [33]. However, it can enhance DNA damage in tumour cells loaded by cDDP [5]. The efficiency of cisplatin targeting differs according to the organ. The majority of pure cisplatin complex settles in the liver (22.65%), then in the lungs (8.72%), spleen (9.72%), kidneys (10.57%) [34]. For this reason, a patient undergoing chemotherapeutic/chemoradiotherapeutic treatment can be exposed to nephrotoxic, hematotoxic, cardiotoxic, and other effects [33, 35]. An intensity of side effects can be alleviated by using analgesics [35] or by application of combination treatment (cisplatin with other drugs [36, 37] or cisplatin with radiotherapy [38, 39]). Hypoxia or higher fractionation of drug administration can lead to an increase in the radiosensitizing effect of cisplatin. Another analogue of cisplatin is carboplatin, which acts similarly. Cisplatin is useful in colorectal cancer, lung cancer, and oesophageal cancer. [2, 3]

5-Fluorouracil

5-fluorouracil in the figure 1.3b is a chemo-drug belonging to the pyrimidine analogues group. Its action lies in a cell synchronization in the S phase of the cell cycle, then inhibition of reparations after irradiation and activates apoptosis of the cell [40]. In the case of 5-fluorouracil, timing is a crucial parameter that can influence its radiosensitizing efficiency, and the best results are when 5-fluorouracil is administered 5 minutes to 8 hours after irradiation. Also, its toxicity seems to remain the same for both hypoxic and anoxic cells; for this reason, it could be used to treat hypoxic tumour cells. It is worth mentioning because it is known that hypoxic tissue generally contains less oxygen, which leads to higher resistance to ionizing radiation. The utilization of 5-fluorouracil can be found in colorectal cancer, stomach cancer, pancreatic cancer, cervical tumours, head and neck tumours and oesophageal cancer. [2, 41, 42]

Hydroxyurea

Hydroxyurea (figure 1.3c), as a ribonucleotide reductase inhibitor, belongs to antimetabolites cytostatic and affects a cell cycle in its S phase, which is relatively resistant to ionizing radiation and thus causes an only additive effect in combination with irradiation. It is used for the treatment of chronic myeloid leukaemia. The radiosensitizing properties of this molecule proved to be useful for the treatment of cervical tumours. However, its use is gradually declining. [2, 43]

Gemcitabine

The molecule of gemcitabine shown in the Figure 1.3d belongs in antimetabolites cytostatic and specifically in pyrimidine antagonists. It can block DNA synthesis and support apoptosis. Concomitant chemoradiotherapy using this cytostatic is followed by many side effects resulting from gemcitabine's high toxicity. Despite this, gemcitabine was utilized to treat head, neck, pancreatic, lung, and thyroid tumours. [2, 44]

Doxorubicin

Doxorubicin (figure 1.3e) is an anthracycline antibiotic used as a cytostatic. It has strong intercalating properties and is becoming popular in targeted drug delivery [45, 46, 47]. It is assumed that the mechanism of the radiosensitizing action of doxorubicin is based on increasing oxygen concentration in hypoxic tumour cells (also in the case of cisplatin and 5-fluorouracil). Doxorubicin administration leads to the formation of oxygen radicals and higher sensitivity to ionizing radiation. This molecule could inhibit the enzyme repair mechanism, which would occur in case of single-strand breaks or double-strand breaks due to DNA damage by irradiation. Doxorubicin can be bound to DNA or tRNA, but the structure changes after binding only in the case of DNA, and this intercalation causes the anti-tumour activity of doxorubicin. Doxorubicin binds to DNA via intercalation with surrounding nucleobases; however, binding to the tRNA occurs via groove binding when the drug is located in the vicinity [48]. However, doxorubicin binding on RNA is less investigated than binding on DNA [49]. The maximal efficiency of doxorubicin is gained when it is administrated after irradiation. Unfortunately, it shows cardiotoxic effects. It is used, e.g., in the case of breast tumours and urogenital tumours. [2]

The previous chapters have been devoted to chemoradiotherapy and its advantages (synergism) and side effects. The present chapter dealt with the chemotherapeutic components and those cytostatics with a radiosensitizing proven effect. The radiosensitizing effect and secondary low-energy electrons will be the subject of the next chapter, as will their role in synergism.

1.3 Secondary LEEs in chemoradiotherapeutic synergism

As mentioned, the present work is motivated by the rational design of novel radiosensitizing agents with low side effects. Chemoradiotherapy side effects can be suppressed by synergism, allowing for lower doses of chemotherapy and radiotherapy, or by better drug targeting in the organism, resulting in lower cytotoxicity for healthy tissue. In the pioneering works of Sanche [7, 5], it has been proposed that the synergism may be caused by the interaction of administered drugs with LEEs as a secondary species arising after the passage of high energy radiation through the tissue. Together with the following other studies [50, 51, 52, 53], it has been shown that synergism can be caused by the interaction of secondary low-energy electrons with a radiosensitizing molecule. This feature can be practically indicated by measuring the cross-section for such a reaction. However, electron affinity is the most crucial characteristic describing molecules' willingness to interact with electrons. High electron affinity is a prerequisite for radiosensitization via mechanisms based on the reactions of low-energy electrons [7, 5], but may play a role also in other biochemical processes, particularly the drug transfers through cellular membranes. If the theories above are true, then molecules with high electron affinities can be envisaged as promising candidates for radiosensitizers. [7, 5] Despite that the current knowledge of the undergoing processes does not enable the rational design of novel drugs for concomitant chemoradiotherapy based on the action of the low-energy electron, they allow for estimation of synergistic potential (section 1.3.2), which can be used in rational drug design or their repurposing [52, 50, 51, 54].

1.3.1 Formation and properties of secondary LEEs

Secondary electrons are all electrons arising via ionisation as a result of interactions occurring between all types of primary ionising radiation with different energies and irradiated matter. In the case of ionizing radiation, these are specifically α -radiation, β -radiation, X-rays, and γ -rays. However, fission fragments or accelerated heavy ions that pass the matter with energies sufficient to overcome the ionisation potential can also be mentioned. [55]

Electrons with sufficiently high energies can escape a significant distance from the place of primary ionisations and initiate further ionisations. These electrons are named delta electrons by J. J. Thomson [56]. Delta rays are electrons ejected from orbitals by fast-moving, heavy-charged particles (e.g., α -particles). Delta electron can be observed in the Wilson cloud chamber at the beginning of the track of a heavy-charged particle. [55]

However, not all secondary electrons reach high energies. The formation of secondary electrons with their energy distribution was investigated in liquid water by S. M. Pimblott with J. A. LaVerne [57] and in liquid and amorphous solid water by M. Dingfelder [58]. [55]

Chemoradiotherapy leads to irradiation of the cells composed naturally of 75-80% water. Therefore, during the irradiation, the radiolysis of water necessarily occurs, and the water becomes a key environment where the synergistic effect, e.g., between the secondary ionising radiation (LEEs) and the radiosensitiser may happen. For this reason, the present paragraph aims to describe the formation of LEE in the context of water radiolysis, which occurs after the irradiation of water with ionising radiation. After irradiation of water volume, it can be expected that during a physical stage in time to 10^{-16} s, electrons as a secondary species are released from the electron shell via ionisation processes. Free secondary electrons gradually lose their energy; when their energy is less than 7.4 eV, they become subexcitation electrons. The thermalisation process of subexcitation electrons characterises a physico-chemical stage at 10^{-13} s. The causes of electron energy loss are dipole relaxation and the excitation of vibrational energy levels in surrounding water molecules. Thermalised electrons undergo solvation processes and become solvated electrons [59]. This time stage is a source of electron attachment processes, also discussed in this subchapter.

The formation and following reactions of secondary electrons in water were also studied by E. Alizadeh and L. Sanche [60]. Figure 1.4 shows the cross-sections' dependencies on the secondary electron's energy for individual possible events. A graph in the Figure 1.5 presents the convolution of these cross-sections with the energy distribution function of secondary electrons and thus testify to the relative importance of these processes in radiation chemistry. [55]

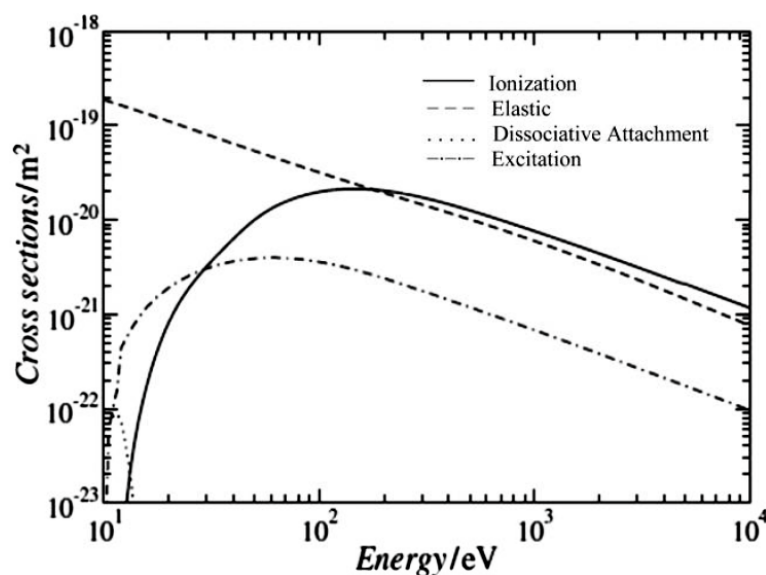


Figure 1.4: Dependence of cross-sections for DEA (dissociative electron attachment), excitation, elastic scattering and ionisation on electron energy in liquid water [60].

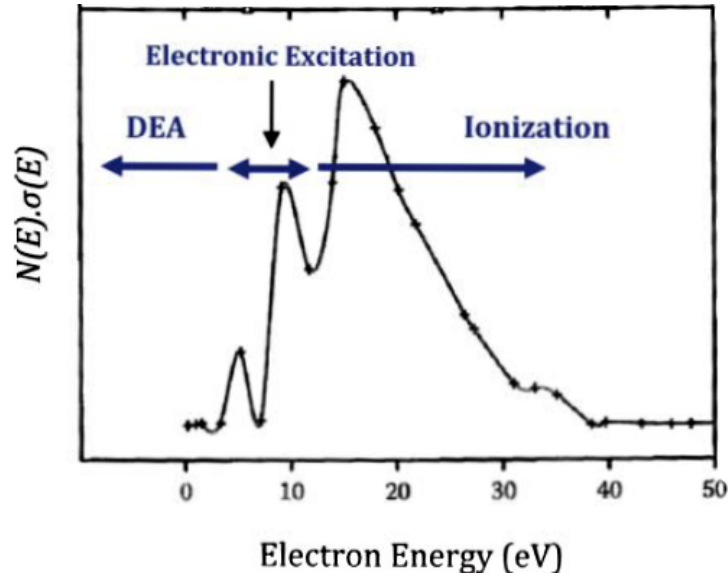


Figure 1.5: Dependence of a product of cross sections (dissociative electron attachment, excitation, and ionisation) and electron-energy distribution on the energy of electrons [60].

The graph in the Figure 1.5 shows four possible ways of interacting low-energy electrons with matter. At the lowest electron energies, elastic scattering can occur while the potential energy of the molecule does not change [55]:



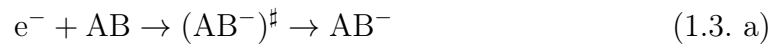
The inelastic scattering can take place when vibrational, rotational, or electronic excitation of a molecule occurs:



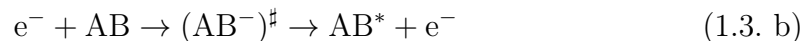
Also, an electron can be captured, and the transient negative ion can form:



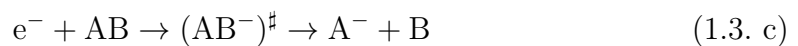
The transient negative ion can then stabilize to form a stable anion (associative attachment):



Alternatively, it can decay with releasing of an electron (autodetachment):



In the last case, the transient negative ion can disintegrate into fragments (dissociative electron attachment).

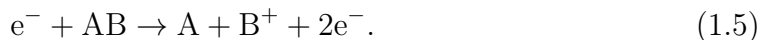


With higher energies of the electron, an electron ionisation occurs:

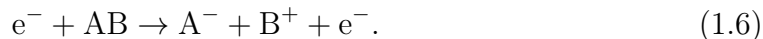
1. Molecular:



2. Dissociative:



3. Ion-pair formation:



1.3.2 Reactions of LEE-attachment

Besides the general fact that low-energy electrons can play an important role in a synergistic effect considering the radiosensitizing potential of chemical agents (Chapter 1.1.1) [7], it has also been shown that secondary electrons with low energies can efficiently cause complex molecular damage in irradiated volume tissue, which can result in considerable cellular toxicities [61]. From the point of view of real chemical reactions that LEEs undergo and thus fulfil their role in a synergistic effect, it is important to highlight a reaction of the electron attachment (EA). That reaction on radiosensitizers can be objectively experimentally examined, and based on the result, the radiosensitizing potential of the studied radiosensitizer can be determined. For this reason, a reaction of EA becomes essential for this research work. The electron attachment is characterized by the formation of a transient, unstable anion that can stabilize in associative electron attachment (AEA) (equation 1.3. a) or can decay into fragments in the case of dissociative electron attachment (DEA) (equation 1.3. c). Both reactions are crucial in terms of the hypothetical mechanism of action of secondary low-energy electrons on the molecule of a radiosensitizer. The products released as a result of both reactions can be heat or highly reactive fragments. These products may break chemical bonds or generally deform the biostructures of a cell's surroundings, which can lead to cell death. [55]

1.4 Motivation for a design of novel radiosensitizers and goals of the work

Whereas the previous chapters dealt with the basics of concomitant chemoradiotherapy for cancer treatment, with a focus on the synergism, cytostatics/radiosensitizers, and secondary low-energy electrons, driven by the idea of higher therapeutic and lower side effects, the present chapter aims to examine and highlight work motivation in more depth and the resulting scientific goals for this work.

The general motivation for this work is built on the importance of secondary LEEs and their reaction of electron attachment EA in many biological processes. This reaction was investigated by the Pshenichnyuk and Modelli groups for various biological processes [19]. The electron reduction properties can affect the drug transport through biological membranes as well as their target binding properties [53, 62]. Nevertheless, when diving deeper into this problem, a key fact for this work is that

low-energy electrons and the reaction of EA directly touch the synergism which was observed in the concomitant chemoradiotherapy of cancer [5, 63]. That relation between LEEs and synergistic action of radiation with a range of radiosensitizing chemotherapeutics [64] was examined for two facts. First, the irradiated tissue gives rise to many secondary low-energy electrons [60, 65]. Secondly, irrespective of the possible modes of action, most known small radiosensitizing molecules contain essential functional groups with high electron affinities [66]. As possible sources of synergism observed in concomitant chemo-radiation therapy, several processes have been proposed such as the formation of reactive anions and radicals via dissociative electron attachment [67, 68] leading to enhanced linear energy transfer [69]; improved transport properties due to associative electron attachment [53]; or DNA sensitization [70, 71]. Various processes have been used to suggest novel radiosensitizers [51, 67]. However, in numerous cases, the suggested molecules with these "ideal" electron-attachment properties failed to exhibit the synergism [72] or were biologically incompatible [52]. These issues may be solved by drug repurposing [73] as aimed in the present project. [62]

The ultimate goal of the present project is to provide new fundamental information for the rational design of novel therapeutic agents with radiosensitizing properties.

The research part of the work can be divided into two sections. The first major section will focus on theoretical and experimental research on the reductive properties of two selected compounds as hopeful candidates for a radiosensitizing agent. The studied compounds will be chosen from drugs already used as chemotherapeutics or antiviral agents. The first molecule is an antiviral agent - a molecule of favipiravir. The molecule will be experimentally studied using electron attachment spectroscopy, and two experimental devices will be used to study the electron attachment reaction to the molecule. The experimental study will be combined with *ab initio* calculations dealing with, among other things, electron affinities using Gaussian software for computation. In the case of favipiravir, the aim is to examine its radiosensitizing potential on the level of electron attachment reaction in the gas phase. The second molecule, RRx-001, is a drug successfully passing through the last phases of clinical studies as a stand-alone chemotherapeutic and a radiosensitizing agent. Its high electron-affine bromo and nitro groups invite to explore the interaction of LEEs with this molecule as a possible source of the already confirmed radiosensitizing effect, which could subsequently be a source of possible synergism. Therefore, this molecule will be examined using electron attachment spectroscopy in the gas phase and pulse radiolysis in the solution on platform ELYSE. The aim will be to reveal the postirradiation mechanism after electron attachment/capturing to/by RRx-001. Also, the irradiation in the solution on the microtron will be carried out to study the final radiolysis products.

The second and minor research section of the work deals with the fullerenes and the examination of their potential for their implementation in bi-molecular π - π complex, allowing better targeting in the body. The choice of this group of spherical nano-molecules lies in their size and geometry; they can be used as carriers of other molecules for better-targeted drug delivery in the organism, thanks to the EPR effect. A molecule can become a carrier after derivation when the transmitted particle is inside the structure or attached to its surface. The central molecule chosen for

the research is the Buckminster fullerene C_{60} molecule. This molecule and its two water-soluble derivatives were investigated using pulse radiolysis in suitable solutions. Experiments in the gas phase are out of the question, as the temperature stability of the derivative leads to their disintegration before reaching the sublimation temperature (around 500°C). This part of the work was driven by future vision, where it would be possible to create a π - π complex of two molecules, shown in the Figure 1.6, which as a whole could function as a radiosensitizer while benefiting from the best properties of both molecules and as well-targeted drug delivery properties. On the following lines, the concept of the π - π complex with its mechanism will be briefly outlined. The potential π - π complex should consist of a water-soluble derivative of C_{60} and a molecule with high electron affinity. C_{60} is suitable for good targeting properties because of its nano-size, and it is also highly reactive with low-energy electrons. The idea of the discussed complex is that the water-soluble derivative of C_{60} as a good electron scavenger will be bound with some appropriate electron-affine molecule via the π - π complex.

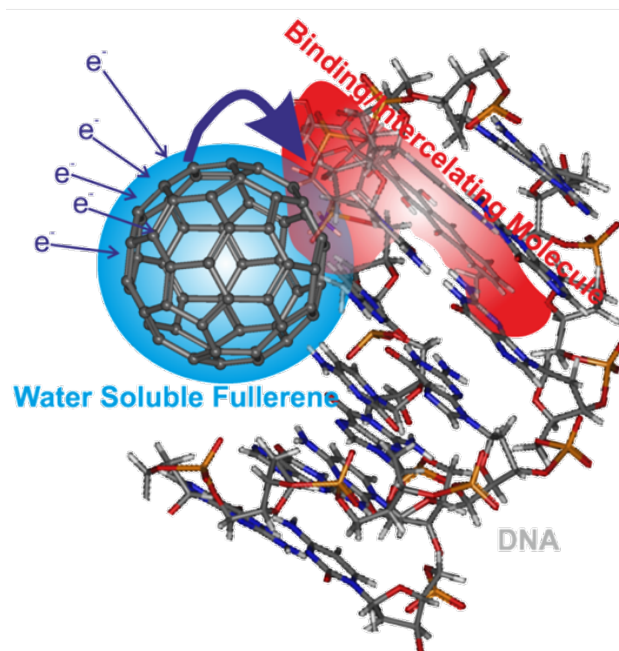


Figure 1.6: The π - π complex of fullerene and electron affine molecule bound to DNA. (by J. Kočíšek, modified)

The aim is to examine the ability of C_{60} water-soluble derivatives to absorb LEEs after irradiation. Realization of the following potential steps cannot be considered for the time-limited frame of the present work. However, it would require observing that the electron can be transferred to the electron affine molecule in a complex, and then if the electron affine molecule can be released from the complex or if the energy or highly reactive fragment can be released into the surrounding and there cause damages. For this purpose, it would require combining experimental techniques such as electron attachment spectroscopy using electrospray (because of chemical decomposition), which is not available in the JH IPC, and ultrafast spectroscopy performed in the ICP UMR8000 to study both parts of the complex separately and

finally in the form of the complex as a whole. The complex interaction process of LEEs with a complex may be modelled theoretically using MBN studio to enrich or support the experimental part.

The information gained through this complex interdisciplinary work can help better understand LEE's mechanism of action and provide information for the rational design of novel radiosensitizers.

1.5 Molecules investigated in the present work

This chapter presents selected perspective molecules studied in the present work that could be or are already being studied for repurposing as radiosensitizing agents. Most proposed molecules have already been used in clinical treatment, and their biocompatibility has been verified. Also, their pharmacokinetics is described. That, in the case of positive results, ultimately speeds up the process of drug implementation into clinical practice. Another criterion for selecting drugs was their simple structure, allowing the analysis of theoretical and experimental studies to be as straightforward as possible.

1.5.1 Antiviral: Favipiravir

The favipiravir molecule was studied as an exciting molecule for drug repurposing.

Drug repurposing (also called "drug repositioning" or "drug reprofiling") is generally a process of revealing the new medical potential of already being used compound (investigational, approved, using, discontinued, and shelved therapeutics) for its utilization in a case of different disease [74, 75]. Such an approach is advantageous because these drugs are described in many studies, and information about their safety, pharmacokinetic, and manufacturing processes is provided. These studies can be used next for further research on other exploitations in the interest of drug repurposing. At the same time, the biocompatibility of the drug is ensured, and the pre-clinical testing process can thus be speeded up just as it requires reduced costs. It is estimated that about one-third of all recent novel drugs were approved based on a drug repurposing process. Because this approach has several advantages, it is an increasingly applied process. [75] This strategy is widely used in developing novel radiosensitizing chemotherapeutics for chemoradiotherapy and, generally, for cancer treatments. With increasing knowledge of the hallmarks of cancer and with an understanding of the development of data-driven approaches, it is possible to target search of radiosensitizers among representatives of chemotherapeutic drugs or non-oncologic drugs associated with the multitargeted strategy, which can bring benefits [76].

Molecules with radiosensitizing properties are searched among the representatives of classical chemotherapeutics and antiviral in the first place [73] because they are already a guarantee of biocompatibility as one of the essential properties. Radiosensitizers newly designed from chemo-radiotherapeutics are, for example, already mentioned cisplatin, 5-fluorouracil, gemcitabine, and other drugs listed in Chapter 1.2.3.

Because these drugs are chemotherapeutics and radiosensitizers, they allow a synergistic effect when used in chemoradiotherapy. Another important group of drugs are antiviral agents, where a mechanism of antiviral effect is utilized. It is known that antiviral agents can bind to DNA or RNA and can lead to the inhibition of DNA or RNA synthesis in case of a virus [77, 78, 73]. It is already well known that some viruses (human papillomavirus, hepatitis C virus) can cause cancer; thus, antiviral agents can be a part of treatment and also as a prevention for several types of cancer due to the probability of tumour recurrence or risk of another cancer appearing after undergoing cancer therapy. [79].

Favipiravir ($C_5H_4FN_3O_2$), with structural pattern in the figure 1.7, is an antiviral and also a modified pyrazine analog. This molecule has already been considered as a broad-range antiviral. Its biocompatibility is excellent, and its pharmacokinetics are very well described, which would facilitate the process of drug repurposing if it were found to have other properties that predetermine its further use. Molecules of favipiravir are utilized for therapeutic use in resistant influenza cases, Ebola virus, COVID-19 and Lassa virus. Its mechanism of antiviral action is based on targeting RNA-dependent RNA polymerase (RdRp) enzymes, which are essential for the transcription and replication parts of viral genomes. Recently, it was shown that the RNA inhibitor efficiency of favipiravir tautomers is related to the energy difference between its highest occupied (HOMO) and low-lying unoccupied (LUMO) molecular orbitals. Unoccupied orbitals can become singly occupied upon electron attachment and appear as shape resonances in the electron scattering spectrum. A present study of the electron attachment to favipiravir may provide an important key to better understanding its activity. [62]

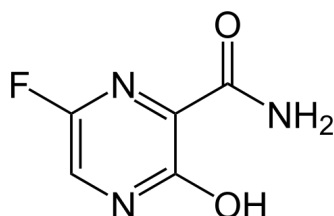


Figure 1.7: The structural pattern of favipiravir.

1.5.2 Chemotherapeutic: RRx-001

2-Bromo-1-(3,3-dinitroazetidin-1-yl)ethan-1-one ($C_5H_6BrN_3O_5$), also referred to as RRx-001 with its structural pattern shown in the figure 1.8, is a hypoxic cell chemotherapeutic with already demonstrated radiosensitization in chemo-radiation therapy and minimal toxicity. [80] Currently, this compound is being studied in phase 2 and 3 clinical trials for treating multiple solid tumour malignancies and as a supportive care drug [81]. Apart from its ability to release free radicals in tumours and thus increase the tumour blood flow [82], the molecule contains three electron affine groups: two NO_2 groups and one Br group, that appear to be chemically interesting when competing for incoming LEEs [80]. This possible sensitivity for LEEs seems promising for proven radiosensitization and a potential synergistic effect. Consid-

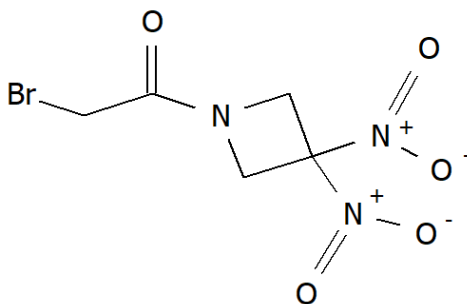


Figure 1.8: Structural pattern of molecule RRx-001.

ering these facts and since this molecule is biocompatible, it appears an exciting candidate for studying its already proven radiosensitization from the point of view of interaction with LEEs to examine its radiosensitizing mechanism and revealing mechanism action that may contribute to synergism. These findings would be valuable for understanding the synergistic effect followed by the rational design of novel radiosensitizers. RRx-001 is well-soluble in ethanol and DMSO.

1.5.3 Fullerenes as a part of a π - π complex

We decided to study water-soluble derivatives of fullerenes as an exciting system for targeted drug delivery. **Targeted drug delivery** is a method of drug delivery to a patient so that the concentration of the drug increases in some parts of the body relative to others. This method aims to deliver a specific drug directly to the targeted area in the body, thus overcoming non-specific toxic side effects from conventional drug delivery. Due to the targeting delivery of a drug, the required amount of drug can be reduced [4]. The most common targeting approach is based on the extended permeability and retention effect (EPR effect) - a controversial phenomenon showing that macro or nano-size molecules are better stored in tumours than in healthy tissue. The principle can be seen in the figure 1.9. Tumour growth stimulates the formation of new blood vessels to supply nutrients and oxygen. However, these are larger, poorly aligned by defective cells, have different architectures, and lack lymphatic drainage compared to healthy tissue. These modifications result in abnormal fluid and molecular transport dynamics for macromolecular and nano-sized drugs. They are extravasated in solid tumour tissues, to which many pathophysiological factors (e.g. nitric oxide) contribute. One of the reasons for increased retention is missing lymphatics in tumours, commonly filtering pathophysiological particles. Knowing of this principle is thus the driving force for the design of new radiosensitizing molecules of nano-sizes [83, 84]. Other approaches are based on the targeted release of the drug triggered by an external impulse. It may be a change in the pH (tumour vs healthy tissue), light impulse in the photodynamic therapy, and ionizing radiation, which is most interesting for the use in combined chemoradiotherapy [85, 86].

Considering targeted drug delivery via the EPR effect, the fullerene molecule should be in a bimolecular complex with a drug delivery platform. In the present work, fullerenes were selected for their unique properties. Fullerenes are one group of extraordinary carbon molecules named after the renowned American architect, inven-

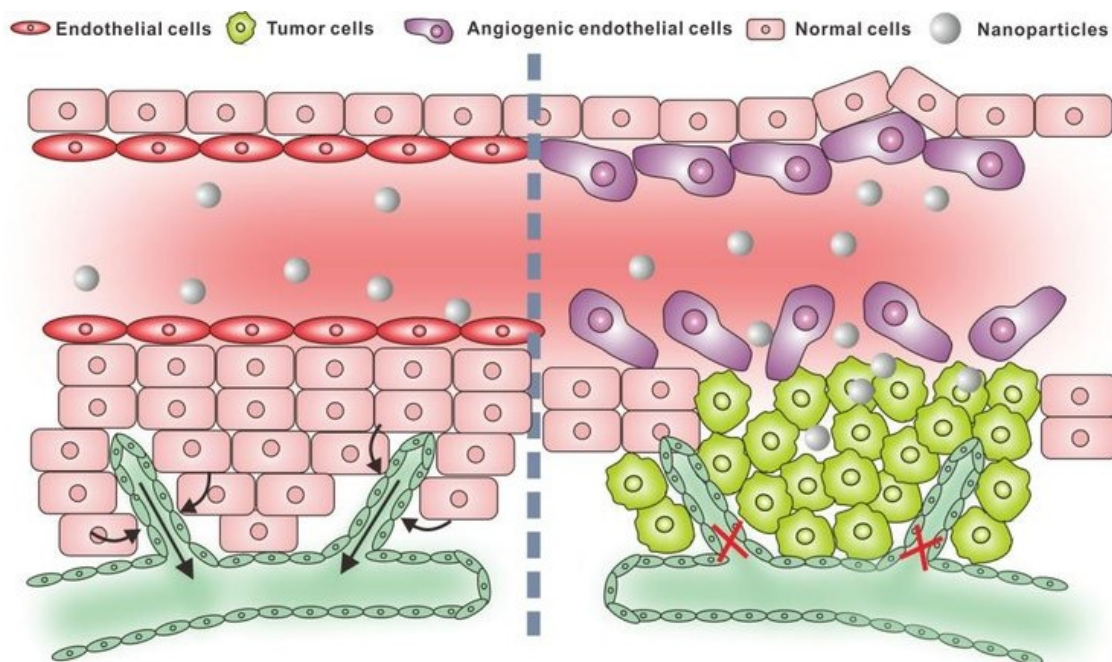


Figure 1.9: Schematic drawing of the EPR effect [87].

tor, visionary and artist - Richard Buckminster Fuller (1895-1983), who became famous in architecture, in addition to other achievements, for numerous designs of geodesic domes of immense dimensions.

C_{60} and its water derivatives C_{60} pyrrolidine tris-acid and fulleranol

Among buckyball clusters, the smallest fullerene molecule can be considered buckminsterfullerene. Buckminsterfullerene (C_{60}) with the structural pattern seen in the Figure 1.11a) is the molecule consisting of 20 hexagonal and 12 pentagonal rings under the condition that the edge is not shared by two pentagons (and precisely this geometric requirement is in contrast with other buckyballs fullerenes). This compound can often be found in soot. It is also the smallest fullerene molecule with hexagonal and pentagonal geometric shapes.

Fullerene C_{60} is a strong acceptor of low-energy electrons, so an electron attachment reaction to this molecule seems very promising. Generally, C_{60} is a good candidate for targeted drug delivery and a radiosensitizer purpose. For targeted drug delivery, a diameter around 0.7 nm could be ideal for both retention effect and transfer through the cell membranes. It can cause better targeting and better C_{60} deposition in living target tissues (lower loss in kidneys and higher uptake by tumours via EPR). Also, the size of C_{60} predetermines this molecule for inserting different molecules inside C_{60} and double-drug targeting. Such C_{60} with a molecule inside is called endofullerene. Fullerenes have been used in the past as diagnostics agents. Even though fullerenes are commonly believed to have antioxidant effects, and the toxicity of their combined treatment should be low, their ability to efficiently penetrate cellular membranes makes this topic quite controversial.

For a radiosensitizer function, it is known that C_{60} is extremely interesting for LEEs.

It has a very broad electron-attachment spectrum [88] seen in the Figure 1.10 and can scavenge secondary electrons in a wide range of energies.

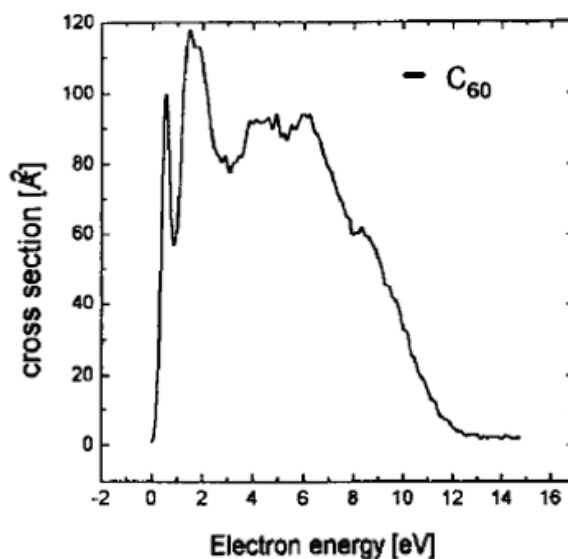


Figure 1.10: A broad electron-attachment spectrum of C_{60} [88].

For radiosensitization purposes, fullerene molecules must be transferred into cells in living tumour tissue, which brings requirements on their solubility in an aqueous medium. However, C_{60} is not soluble in water or any biological medium. Therefore, for these purposes, it is necessary to consider a water-soluble derivative of C_{60} . There are two water-soluble derivatives: C_{60} pyrrolidine tris-acid and fullerenols, with their structural pattern seen in the figure 1.11b), resp. 1.11c), has a declared mass concentration in water about 0.5 mg/ml [89], resp. 50 mg/ml [90]. A handful of fullerene complexes was explored concerning radiosensitization [91, 92]. Similarly unclear is their radioprotective/radiosensitization effect that strongly depends on their functionalization [93]. Endofullerenes with incorporated metal atoms are particularly interesting and they are commonly used as contrast agents in magnetic resonance imaging. Their functionalization may result in novel theranostic approaches.

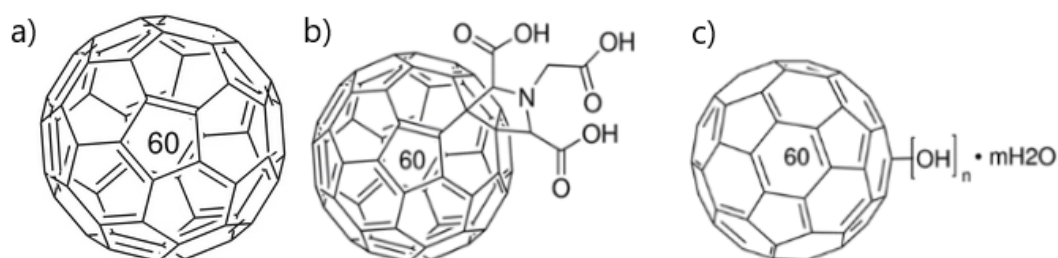


Figure 1.11: The structural patterns of a) C_{60} [94], b) C_{60} pyrrolidine tris-acid [89], and c) fullerenols molecules [90].

Fullerenes and their water-soluble form -fullerenols have been explored for years as possible carriers of drugs due to the ease of their modifications [95, 96, 97, 98, 99]. It resulted in many targeted therapy models and complexes for photodynamic therapy [100]. Particularly interesting properties were observed for cisplatin [101], doxorubicin complexes [102], [103], oxazole complexes [104], and malonic acid complexes. Fullerenes can form stable π - π complexes. The energy of these π - π complexes is often calculated and experimentally determined for estimation of the stability of these complexes, which needs to be known to discuss their potential for different types of utilization. Stability of π - π complexes was calculated by using the quantum-mechanic methods (Gaussian software [104]) and was studied experimentally by fluorescence quenching of this chrome (reference dye) [104].

Experimental & theoretical approaches

The present work combines minor theoretical *ab initio* calculations and experimental approaches using three experimental techniques and four experimental devices to uncover processes occurring after the interaction of LEEs with selected molecules. This chapter will be devoted to describing these applied theoretical and experimental approaches and experimental devices.

A vast majority of this study is experimental. Firstly, it aims to combine two experimental state-of-the-art techniques for studying short time-scale processes under the formation of transient negative ions. The first experimental method is electron attachment spectroscopy (EAS), applied in the Department of Dynamics of Molecules and Clusters in the JH IPC (Prague, Czech Republic). The method of EAS uses two measuring devices: the Cluster Beam apparatus (CLUB) and the Electron attachment spectrometer. The second experimental method is ultrafast spectroscopy in a solution at the ICP, UMR8000 (Orsay, France). The method of ultrafast pulse spectroscopy uses the ELYSE electron pulse radiolysis platform.

While the EAS technique allows for the detailed characterization of the entrance channels for LEEs processes, ultrafast spectroscopy allows for identifying essential channels in the natural biological environment. Unique information obtained by combining these two techniques can help better understand the mechanism of action of the LEEs and provide information for the rational design of novel therapeutic and theranostic agents.

Cluster Beam Apparatus allows electron attachment to molecules in their isolated or cluster forms in the gas phase to be studied. The significant advantage is that the micro-solvated molecules can be studied and, thus, the effect of the environment on the electron attachment reaction. The reflectron spectrometer in the CLUB provides a high-mass resolution R equal to 1489, and whole mass spectra are gained from one measurement. However, the energetic resolution is low (FWHM \approx 700 meV) because of the missing electron monochromator.

An electron attachment spectrometer enables measuring electron attachment to the isolated molecule in the gas phase only. Quadrupole mass spectrometer allows gaining electron energetic dependence for each select mass per one measurement. However, this experimental device offers a higher energetic resolution FWHM equals 172 meV, but a lower mass resolution ($R \approx$ 100).

The ELYSE platform allows us to directly measure the production of short-lived transient species forming in the solution of the sample after its irradiation with electrons. The sample is required as a liquid, but a solid sample can be dissolved in a solvent. The main requirement applied to a solvent is its low reactivity with electrons; therefore, aromatic compounds are inappropriate solvents.

Long time-scale processes- specifically the formation of reaction products- were also examined. For this purpose, irradiation of samples in their solutions on microtron with highly accelerated electrons was done, and the solutions were further studied with NMR spectroscopy (in cooperation with Mgr. Jiří Pinkas, PhD.; JH IPC, Prague, Czech Republic)

A minor part of this work is dedicated to the *ab initio* calculations of electron affinities based on the quantum computational chemistry methods using the Gaussian software.

2.1 CLUster Beam apparatus

2.1.1 Experimental device

The CLUster Beam apparatus (CLUB) is the universal experimental equipment used for various experiments with clusters. Working with clusters makes it possible to study the development of the properties of individual molecules upon solvation. Thanks to the micro-solvation technique, the effect of the water environment on the reaction can be studied. This option gives the unique opportunity to approach a real bio-environment in living tissues, whose interaction with secondary electrons after irradiation motivates our work. The main techniques used to probe the reactivity of molecules and clusters in the beam include velocity map imaging (VMI) to study photodissociation and a reflectron time-of-flight mass spectrometer (rTOF) used in this study, and a quadrupole mass spectrometer utilized for measurements of the speed of neutral clusters in molecular beam (for example for estimation of molecular pickup cross-sections together with pickup cell in the Sel chamber). The elementary diagram of this experimental device is shown in the figure 2.1. A graphical representation of the part of the experiment used in the present study can be seen in the Figure 2.2.

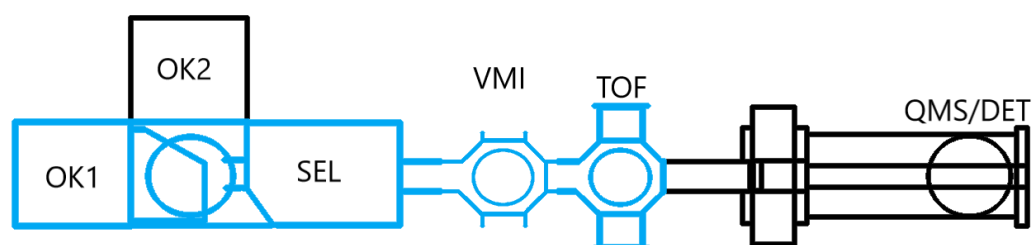


Figure 2.1: Schematic drawing of the experimental device CLUB. The parts of the CLUB apparatus actively used in this work are marked in blue.

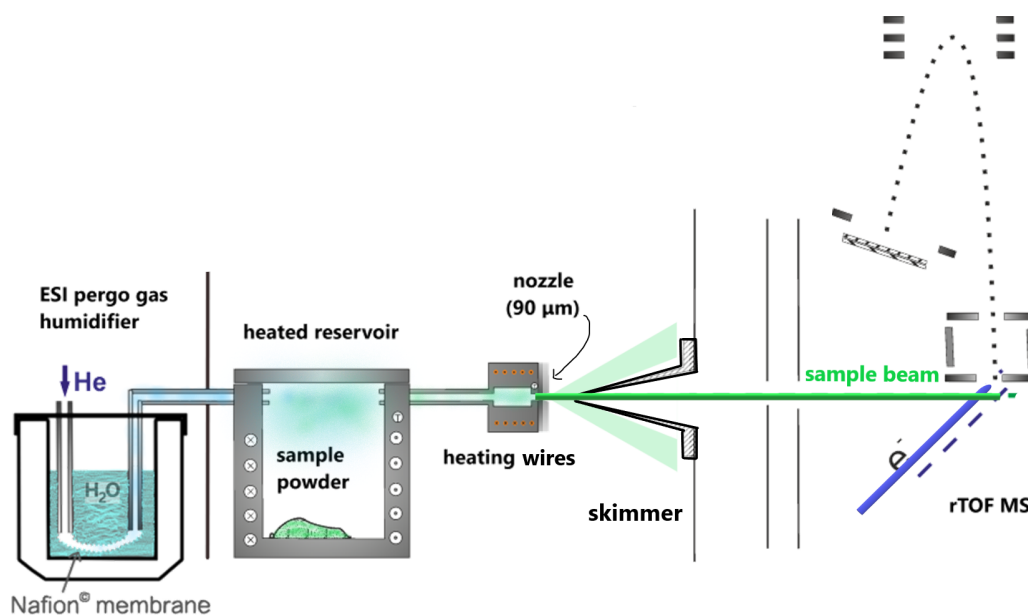


Figure 2.2: Detailed schematic drawing of inner experimental layout in the CLUB apparatus.

The principle of experimental equipment

CLUB, the experimental device, starts with vacuum chamber OK1, where the inlet system is located (figures 2.3, 2.4), as well as the cluster source. The inlet system contains a metal or glass vessel for the sample located in a reservoir. Then, a sample in liquid/solid form is evaporated/sublimated in the reservoir. In the gas phase in the reservoir under atmospheric pressure, molecules move with velocities according to the wide Maxwell-Boltzmann distribution. They collide but are in an equilibrium state, and the rectified flow is low. The molecules create a mixture with a carrier gas (possibly also enriched with solvent molecules) coming through the upper part of the reservoir. Under the room temperature (273,15 K) and the pressure of 1 bar, the mean free paths of helium, neon and argon were calculated as 2100 nm, 433 nm, resp. 53 nm.

When the molecular beam passes through the conical nozzle with a diameter of 90 μm into the vacuum, and when it exits the nozzle, supersonic expansion occurs. The velocities of all molecules in a supersonic beam, i.e. the velocity of a rectified flow, is several times higher than the speed of sound. Forming a vertical shock wave, the so-called Mach disk, and overall many shock waves, the so-called Barrel shock. A skimmer at a suitable distance from the nozzle (cca 6.7 cm), which has the shape of a cone with a hole in its tip, is used to select only those which fly to the reaction chamber -that is, those that fly directly to the centre through the hole in the skimmer.

In the reaction chamber, the molecular beam of selected compounds crosses with an electron beam under the right angle of 90°. As a result of a collision, the ions are formed and then extracted to the reflectron time-of-flight spectrometer (rTOF). In the rTOF, the formed ions are analyzed based on their different time of flight. After

that, ions are detected. The device enables the measurement in two possible modes, negative and positive, for detecting negative resp. positive ions, and obtaining negative resp. positive mass spectra. An essential part of measurement is the detection of the background. It is possible to measure the background of the whole device; for this, the chopper is located just behind the nozzle. The chopper plays the role of the disk barrier, which, in its appropriate position, prevents the passage of the always-used continuous molecular beam from passing through. The background is measured when the chopper is in the correct position, and the molecular beam is not passing.

Inlet system of sample and preparation of cluster

The inlet system for a sample is a removable component of the vacuum chamber, and its picture can be seen from the top in the Fig. 2.3 and from the profile in the Fig. 2.4. The main component of the inlet system is a metal vessel for a sample, which is located in the middle of the system. In some cases, a glass vessel can be used to prevent the interaction of the heated sample with metal inlet components in a system under higher temperatures required for the sublimation of the sample. Before heating the sample, it is essential to determine whether the molecule is temperature-stable or at what temperature it degrades, and only then a suitable temperatures can be chosen. Two thermometers to measure temperature are installed on the inlet system in two different locations. The first type, K, was installed outside the metal vessel. Thus, it shows a higher temperature than the actual one inside the reservoir with the sample. These temperatures are only for guidance because of the constant flow of carrier gas at room temperature and an outside location of temperature sensors. The second thermometer indicates the temperature in the nozzle block.

The next part of an inlet system is used to study the effect of the solvent environment on the reaction. This system is graphically represented on the left side of Fig 2.2. The system contains a reservoir with the solvent. The carrier gas such as helium, neon or argon passes through the Nafion tube, absorbing solvent molecules from the reservoir through the membrane. This mixture flows into the heated reservoir, picks up the sample molecules, and carries them to the nozzle. The level of solvation can be regulated directly by setting carrier gas pressure using a pressure gauge on the cylinder with carrier gas. When the aim is to study only isolated molecules without any solvent effect, the tube with carrier gas is not immersed in a solvent-filled reservoir.

Measurement with solid samples typically requires a particular cleaning procedure for a metal sample-inlet system. First, the inlet system must be removed from the vacuum chamber OK1. The second step is cleaning when the nozzle, sealing pad, and glass bowl are removed from the inlet system. A glass vessel with a nozzle is washed in water and then in acetone in an ultrasonic bath. The metal inlet system is flushed with acetone. Finally, the nozzle has to be checked with a microscope in case of suspicion of its blockage. Sometimes, removing a skimmer and subjecting it to a cleaning procedure using acetone is necessary. However, the handling of the skimmer must be cautious, as the cone with a through-millimetre hole is made of fragile sheet metal, which could be easily deformed by improper handling in the dry conditions

and by pressure in the solution, where it should remain in a vertical position all the time. Using a deformed skimmer would violate the concept of creating the molecular beam.

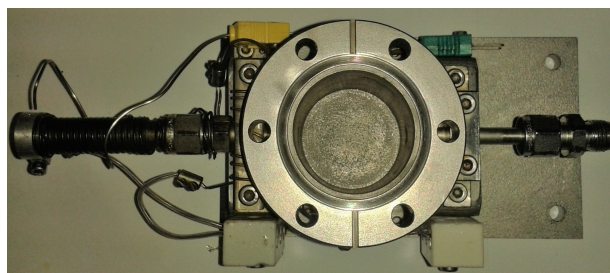


Figure 2.3: Top view of the inlet system for sample removed from the vacuum chamber of experimental device CLUB.



Figure 2.4: Profil view of the inlet system for sample removed from the vacuum chamber of experimental device CLUB.

Mass spectrometer rTOF

Reflectron time of flight mass spectrometer (mass spectrometer rTOF) is a pulsed (10kHz) mass analyser. Firstly, ions are extracted from the reaction chamber by a voltage pulse, and after that, they are accelerated to an energy of 8 keV. They fly through space without an electric field in a tube with a length of 0.5 m to the reflectron, which aims to balance the kinetic energies of flying ions with the same m/z and thus increase the mass resolution of the spectrometer. The different kinetic energies of ions with the same m/z are caused by ionisation when the ions acquire a kinetic energy with a particular distribution, which results in a broadening of their peaks and, thus, a deterioration of the resolution. Such an undesired phenomenon can be remedied by the way that ions with higher kinetic energies penetrate deeper into the electron field of the reflectron because penetration depth depends on the kinetic energy of the flying ion according to the equation below:

$$\mathbf{F} = m \cdot \mathbf{a} = q \cdot \mathbf{E} \quad (2.1)$$

Where \mathbf{F} is an electrostatic force acting on a charged particle, m is the particle's mass, \mathbf{a} is its acceleration, q is the particle's charge, and \mathbf{E} is the electric field of a flying particle.

It delays ions with a higher kinetic energy, so ions with the same m/z gain the same speed, path, and time of flight on the way to the detector. Reflected ions from the deflector fly through a 0.5 m long tube until they hit a detector. Using an rTOF, isolated molecules or their cluster forms can be measured in two opposite modes. Measurements in positive mode allow the detection of cations, while measurements in negative mode provide measurements of anions.

2.1.2 Calibration of energy scale using CO_2

Measurements of energy-dependent ion yields in the negative ion mode require calibration of the energy scale of the incident electrons. Calibration of energy scale was performed using a molecule CO_2 having a characteristic peak in the negative ion yield with a maximum at 4.3 eV [105] in reaction:

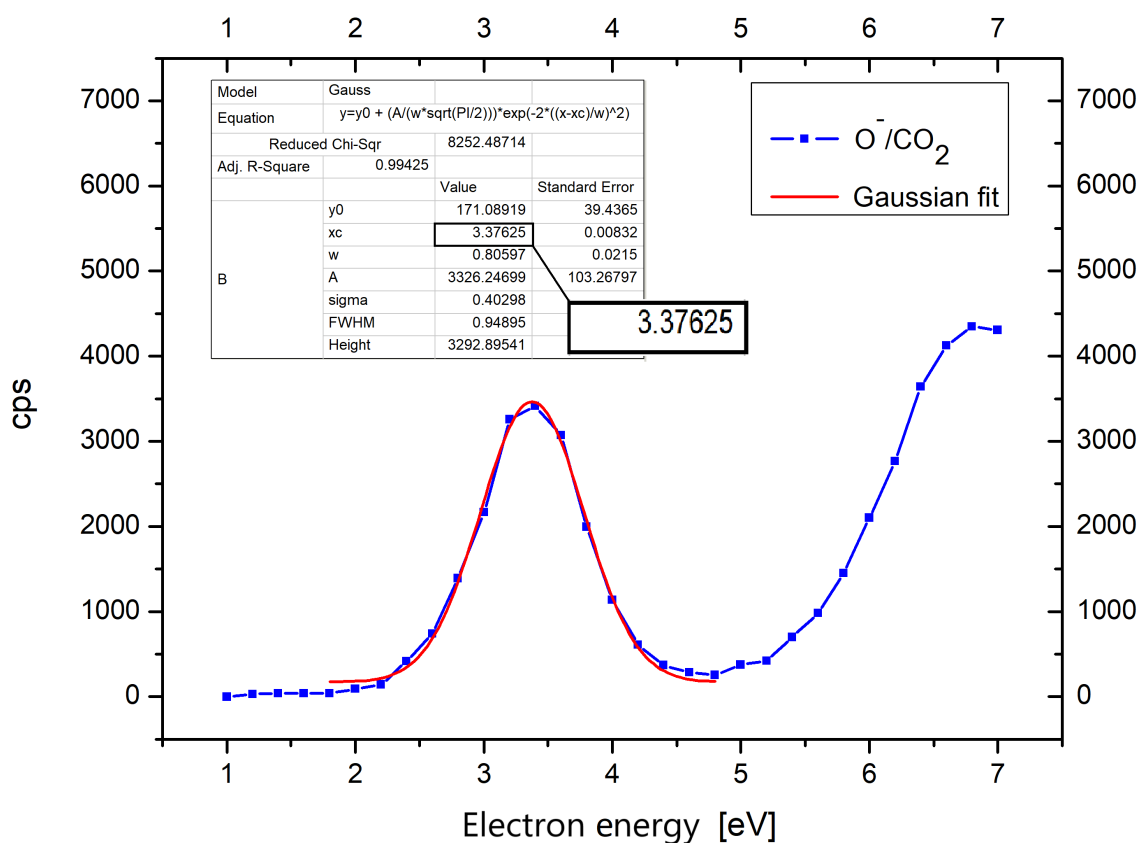


Figure 2.5: Calibration of energy scale using molecules of CO_2 .

Calibration aims to convert values of the accelerating voltage of electrons to the actual electron energy in eV. The signal of anion O^- coming from molecule CO_2 depending on accelerated voltage was measured. The obtained dependency was compared with the already-known dependency for this decay. Our data were interpolated with a Gaussian function, and a shift of the actual energy scale from the original voltage scale was estimated.

Illustrative calibration can be seen in the figure 2.5. A curve in the graph in this figure consists of two peaks/ resonances. The first peak around 3.4 eV is determinative for this calibration and was thus interpolated with the Gaussian function. The maximum resonance was detected at approximately 3.4 eV. Due to our measured value of electron energy, it was necessary to shift our energy scale by approximately 0.9 eV in the direction of higher energies.

Experimental conditions for measurement of favipiravir and RRx-001

Electron attachment to favipiravir was carried out in both negative and positive modes. The preparation of the molecular target was based on the co-expansion of He buffer gas and vapours of favipiravir through a conical nozzle with a diameter of 90 μm into the vacuum. Clusters of micro-hydrated molecules were prepared using a micro-hydration technique developed in our laboratory, which was established by adding a low quantity of water into the buffer gas through the Nafion membrane. During all experiments, the sublimation of the sample occurred at a temperature around 85 $^{\circ}\text{C}$. To examine the thermal stability of the favipiravir, the sample was heated up to 118 $^{\circ}\text{C}$. For all these experiments, a sample of favipiravir in the form of white crystalline powder was ordered from Santiago Labs with the following parameters of sample: ($\text{C}_5\text{H}_4\text{FN}_3\text{O}_2$, $M_r = 157.10$ g/mol, 99%, Santiago Labs).

For measurement of the RRx-001 molecule, the sample in the form of white crystalline powder was inserted into a metal vessel localized in a removable inlet system and sublimed at a temperature of approximately 110 $^{\circ}\text{C}$. Then, vapours of RRx-001 were co-expanded in the flow of Ne as a carrier gas into the conical 90 μm nozzle into the vacuum. The unique approach was applied to the gradually increasing level of micro-ethanol solvation for each subsequent measurement. Mass and electron energy dependence spectra of negative ions were measured after electron attachment to RRx-001 in the gas phase under various levels of solvation. Mass spectra measurements under various levels of ethanol solvation are based on using only electrons with an energy of 1.5 eV, and temperatures in the nozzle/reservoir were 130 $^{\circ}\text{C}$, resp. 110 $^{\circ}\text{C}$. A molecule of RRx-001 ($\text{C}_5\text{H}_6\text{BrN}_3\text{O}_5$) was purchased from AmBeed with a declared purity of 95.00%.

2.2 Electron attachment spectrometer

2.2.1 Experimental device

This experimental device uses an electron beam from a trochoidal electron monochromator (TEM) that intersects with a target molecular beam in a gas phase in an electron attachment spectrometer. Forming anions are then detected by a quadrupole mass spectrometer. The TEM and the mass spectrometer are located inside the vacuum chamber, where the pressure is 10^{-7} mbar. This arrangement allows for the performance of two types of experiments. Either the mass spectra can be measured at constant energy of the electron, and the individual DEA reaction channels can be identified for this energy, or electron energy dependence spectra can be measured for particular generated ions (of a given mass-to-charge ratio, m/z) and thus cross-sections of specific reaction can be achieved. The schematic drawing of the electron attachment spectrometer is shown in the Figure 2.6. The components of this experimental device, which offer the collision-free transport of electrons into the reaction chamber and the transport of formed ions into the quadrupole mass detector, will be described in more detail in this chapter.

Trochoidal electron monochromator

The function of the TEM is to select electrons with the same energy, which leads to an increase in the resolution of the quadrupole mass spectrometer. This monochromator is a design copy of the original designed by Professor M. Allan [106] in whose laboratory it was also built. The TEM is made of molybdenum, but the other parts of the electron attachment spectrometer are made of stainless non-magnetic steel suitable for high vacuum. In principle, at first, electrons are emitted from a heated iridium fiber (with an yttrium surface treatment) which is deviated by 1.6 mm from the axis of symmetry of the monochromator. Electrons are emitted from a fiber heated to a temperature of ~ 2500 K. The electron-energy distribution is characterized by a Gaussian distribution, and a value of full width at half maximum (FWHM) of the peak is ~ 0.7 eV. The movement of electrons is directed by a system of three electrodes and a parallel magnetic field. Coils generate the magnetic field in a vacuum in the Helmholtz configuration. The vacuum can be found in the monochromator, an area with a crossed electric field (figure 2.6 - marked in green colour). Here, the motion of electrons is indicated by two components: cycloidal ($\mathbf{v} \times \mathbf{B}$) and drift ($\mathbf{E} \times \mathbf{B}$). The composition of these two components results in a trochoidal electron trajectory; thus, the monochromator is referred to as a trochoidal monochromator. After passing through the monochromator, the electrons are guided further in the direction of the axis of the monochromator. Only electrons with a total drift deviation of $\mathbf{E} \times \mathbf{B}$ equal to 1.6 mm are selected in the monochromator. The total deflection depends on the input energy of the electron and on the time the electron needs to pass through the monochromator. In principle, this is how electron-energy distribution is reduced behind the monochromator. [107] In the case of the monochromator described here, the decrease of the original width in the electron energy distribution is ≈ 0.7 eV FWHM to ≈ 0.1 eV FWHM. Subsequently,

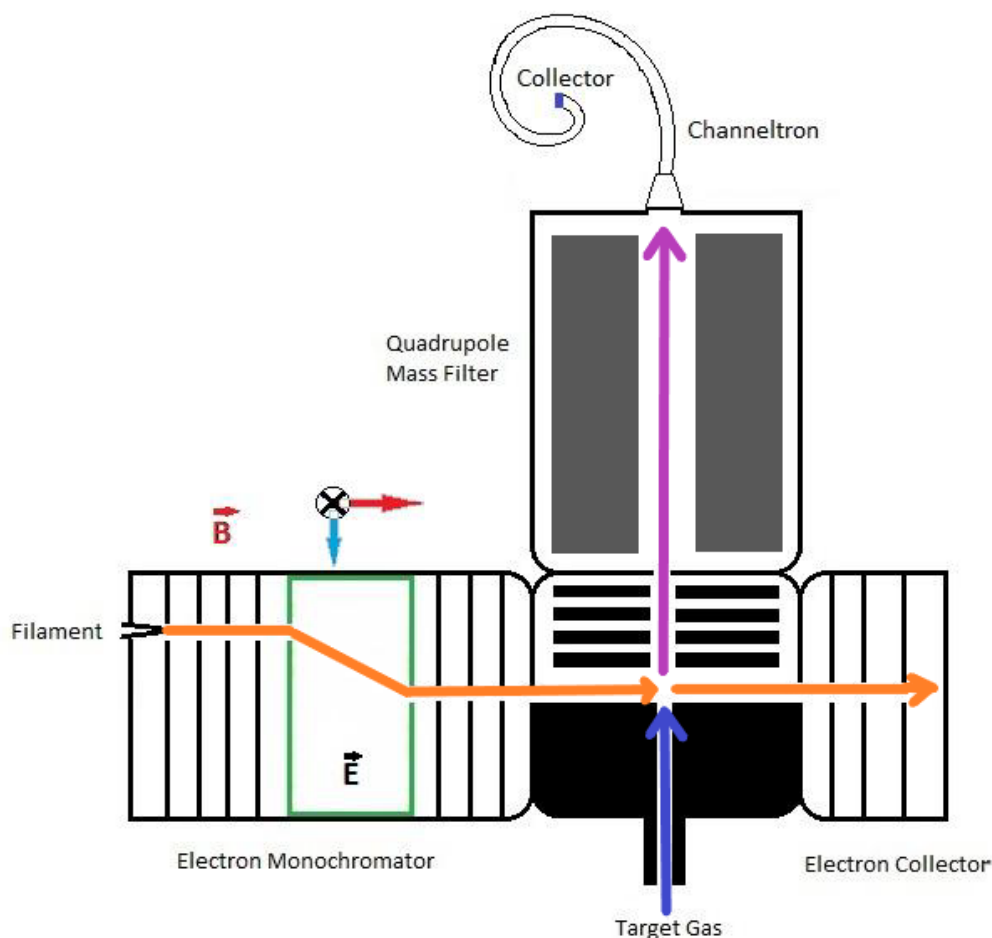


Figure 2.6: Schematic drawing of the electron attachment spectrometer.

the electrons are accelerated in the electrode system to such energies that accelerated electrons can immediately interact with our selected molecules in the reaction chamber. After the passing of electrons through the reaction chamber, electrons are detected in a Faraday cylinder, which consists of a system of three electrodes and monitors the electron current during the measurement. [106]

Quadrupole mass spectrometer

Ions are formed in the reaction chamber, then extracted by a weak electric field and accelerated by a set of parallel electrodes up to the entrance of the quadrupole mass filter. Selected ions with a specific mass-to-charge ratio m/z are then accelerated to the channeltron by a voltage of 1 kV. This voltage is sufficient to eject an electron from the surface of the channeltron. The ejected electrons are accelerated to a final voltage of 3.7 kV and collide with the internal surface of the channeltron. Thereby, additional electrons are ejected from this surface. An electron avalanche is formed, producing a charge amplification of 10^9 . Then, the multiplied pulses are separated from the high-voltage output of the multiplier by a capacitor. Then, they are amplified, processed by the counting electronics, and transferred to a computer. Data

acquisition and the actual experiment control using the ELS program were developed in the Department of Dynamics of Molecules and Clusters laboratory at the JH IPC. The quadrupole mass spectrometer is one of the analyzers with low resolution. In our measurements, the typical value of the resolution was $m/\Delta m = 100$, as described more in subchapter 2.3.

2.2.2 Calibration of electron-energy scale using SF₆

As in the case of measurements on the CLUB apparatus, it is also necessary for electron attachment spectroscopy to convert the energies of the accelerating voltage of the electrons into their actual kinetic energy. In the case of experiments with favipiravir, the focus was on low-energy resonances, and therefore, an energy scale was calibrated using a molecule of sulfur hexafluoride SF₆. These molecules are characterized by one of the most effective cross-sections for electron attachment. In this type of reaction, the maximum effective cross-section is achieved at zero electron energy when the parent anion forms.

We measured the dependence of the ion signal for the anion SF₆⁻ from the molecule SF₆ on the accelerating voltage. Thus, a calibration was performed, and a shift of the voltage scale was obtained in relation to the actual energy scale. The shift of the energy scale is given by the maximum of the peak SF₆ concerning the characteristic zero value. In this experiment, the gained shift equals -193 meV relative to the characteristic value of 0 eV.

The illustration calibration of the energy scale is shown in the graph in the figure 2.7. From this graph, it is possible to determine the maximum of the measured peak at the value of electron energy of -193 meV. Since the width of 0 eV resonance is of the order of meV, it is possible to use the measured FWHM as the value of energy resolution. In the graph 2.7, the Gaussian function can be seen; thus, it was possible to determine the value of energy resolution (interpolated highest peak in the middle of its height). In our case, an energy resolution value reached about 150 meV, which was, with the calibrated energy scale, a valid parameter for all DEA measurements performed on favipiravir.

Experimental conditions for measurement of favipiravir

An electron attachment spectrometer was used to study favipiravir in its isolated form. Sample powder was put into a glass bulb and placed at the end of the probe, which was positioned in a heated copper cylinder (the temperature was constant at 340 K). Molecules were sublimed and then effused into the reaction chamber through a capillary with a length of 1 cm. Measurements were carried out with an electron-energy resolution of around 150 meV. For all these experiments, a sample of favipiravir in the form of white crystalline powder was ordered from Santiago Labs with the following parameters of sample: (C₅H₄FN₃O₂, M_r = 157.10 g/mol, 99%, Santiago Labs)

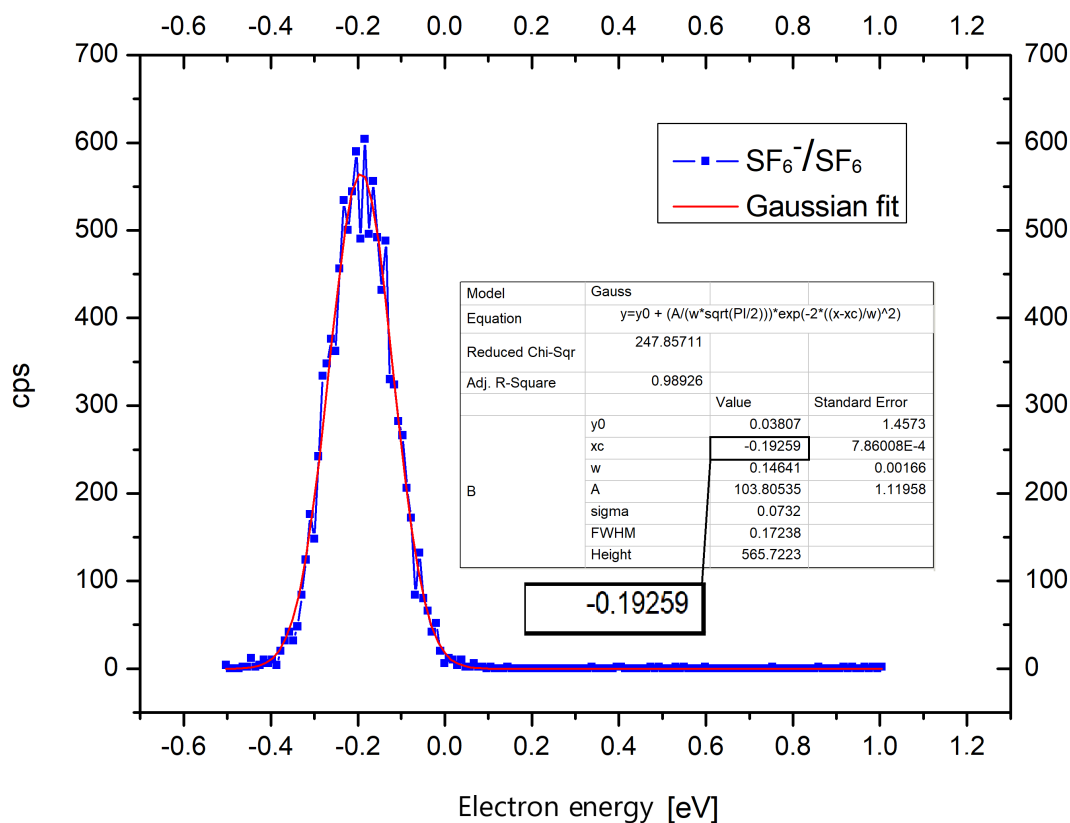


Figure 2.7: Calibration of energy scale using a molecule of SF₆.

2.3 Mass resolution of mass spectrometers

The experiments were measured on two types of mass spectrometers. The resolution R of the spectrometer is defined by:

$$R = \frac{M}{\Delta M} \quad (2.3)$$

where M represents the mass of the detected ion, and ΔM symbolizes either the full width of the peak at half of its maximum or the difference between the measured mass and its nearest mass, which is distinguishable from it in the spectrum.

The rTOF spectrometer has a mass resolution of more than 1000, which is favourable for studying large clusters. Most measurements in the negative mode were performed with a lower mass resolution of around 700 (bin = 16 x 250 ps). However, in some cases, high resolution is essential and, therefore, can be measured with a spectrometer resolution of about 1500 (bin = 2 x 250 ps). Common resolutions (bin = 8 x 250 ps) were used to measure mass spectra in the positive mode.

The electron attachment spectrometer contains a quadrupole mass spectrometer that measures a single mass over a long period. It measures dissociative electron attachment with high energy resolution and good measurement statistics for isolated molecules. A quadrupole mass spectrometer is characterized by better energy resolution than mass resolution. The mass resolution R is around 100, which is also the maximum value of the resolution R that can be achieved using this mass analyzer.

2.4 Experimental ELYSE platform

ELYSE platform is an experimental platform that can perform electron pulse radiolysis experiments. The pulse radiolysis method belongs to classical pump-probe spectroscopy techniques, where the light probe stays, but the light excitation pulse is exchanged for the electron excitation pulse. A basic graphical representation of this experimental platform is shown in the Figure 2.8. The measuring platform is a main part of The fast kinetic centre for experimental pulse radiolysis with picosecond temporal resolution, which was opened in 2001 as the first in Europe then. The ELYSE platform is located in the Institut de Chimie Physique, UMR8000 (ICP, Orsay, France), which is a part of both Université Paris-Saclay (Orsay, France) and the French National Centre for Scientific Research (CNRS, Paris, France). ELYSE platform is also a part of EMIR&A, the French national network of accelerators for irradiation and analysis of molecules and materials. This section is dedicated primarily to describing the experimental ELYSE platform for pulse radiolysis experiments. [108]

2.4.1 Experimental device

This pulse radiolysis platform contains a core and two experimental parts, which allow measurements in two different time-scales provided by two different setups. From the point of view of the time-scale of detection, experiments can be divided into picosecond pump-probe experiments (direct line, VD) and nanosecond to millisecond time-scale experiments (bend line, VD2).

The experimental ELYSE platform (figure 2.8) contains a laser producing ultra-short pulses @780nm, ~ 110 fs. A 50% of energy is used on the VD line for supercontinuum generation and as a pump for OPA. The rest is used for the third harmonic generation of approximately 260nm. This UV light is utilized to extract electrons from the photocathode (figure 2.9). The source of ionizing radiation in the form of high-energy electrons is an electron accelerator (2.10). The accelerated electrons are pumped along a direct line (picosecond pulse radiolysis experiments) or the bend line (nanosecond to millisecond time-scale experiments) to irradiate a liquid sample located in a cell in a sample holder (figures 2.11, 2.12). The electron pulse causes radiolysis of a sample solution, followed by a large number of ultrafast reactions and the formation of a high-reactive transient species such as radicals, secondary electrons and others, which can react with a sample. The detection allows for directly studying these transient species and their ultrafast reactions with a sample. Detection for picosecond pulse radiolysis is based on white light with a delay mechanism and a spectrometer with a CCD camera. In comparison, nanosecond to millisecond time-scale experiments uses for the detection a white light from the Xe-lamp and a streak-camera with a spectrograph.

The laser and laser chain

A cornerstone of the ELYSE platform is formed by a femtosecond fibre oscillator (composed of C-fiber 780 and femtosecond Erbium laser) and a broadband stretcher.

The laser operates at 80 MHz and is a source of extremely short photon pulses with a pulse frequency from 0.1 to 50 Hz; the maximal frequency used with the accelerator and for pulse radiolysis experiments is 10 Hz. The energy of one pulse is 2 mJ, the wavelength is 780 nm, and it has a 150 fs broad continuum. 50% of this photon beam is used as a reference path for a picosecond pulse radiolysis detection, and these pulses are synchronized with the electron accelerator. Another 50% of a photon beam continues for a radiolysis purpose to a tripler, where the third harmonic is generated, and the parameters of a beam are changing. The changed photon beam is then used to extract electrons from a photocathode in an accelerator. [109]

[108, 109]

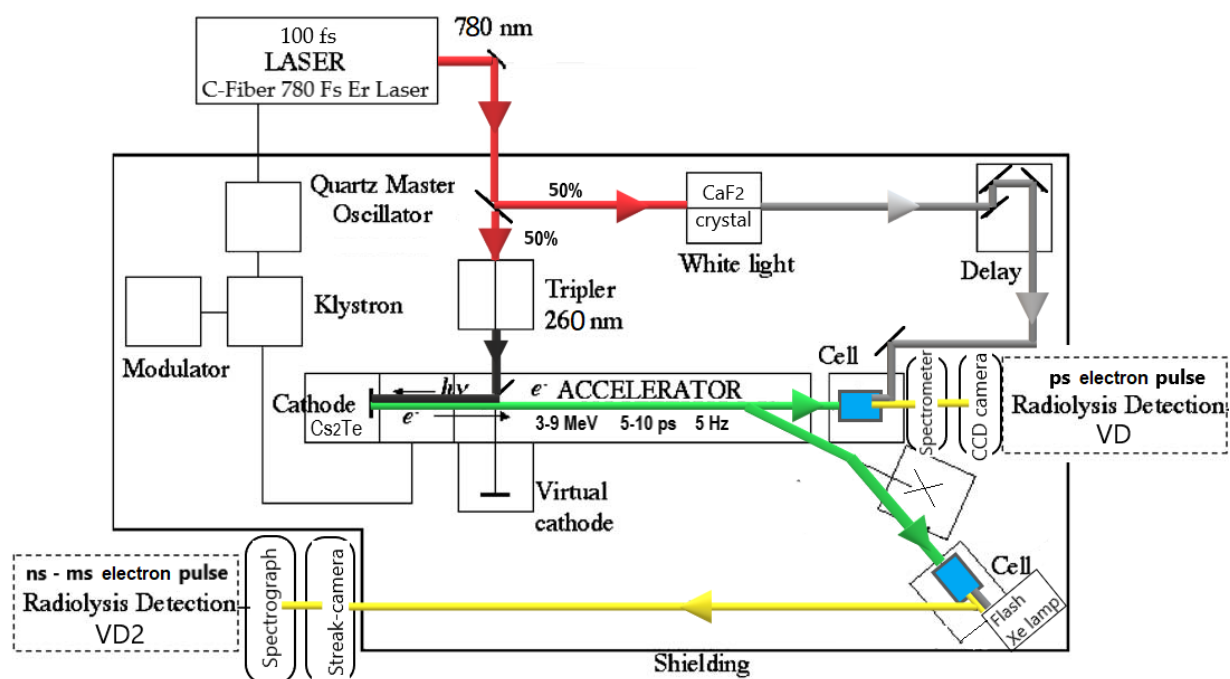


Figure 2.8: Graphical representation of the experimental ELYSE platform. ([109], modified)

The photocathode

The ELYSE photocathode is a Cs_2Te photocathode with a quantum efficiency of 1%, a lifetime of 2 years at maximum. It is prepared in situ and made of copper substrate with deposits of Tellurium and Caesium Chromate (Cs_2CrO_4). Then, the Caesium Telluride (Cs_2Te) is formed. The photocathode produces electron pulses with final energy after acceleration equals to 7.8 MeV, a standard half-width of 7 ps, and a repetition rate from 5 Hz to 10 Hz. [108, 109]

The electron accelerator

The electron accelerator that can be seen in the figure 2.10 offers two possible ways. The direct line VD for the pump-probe experiments and the bend line VD2 are determined for conducting absorption spectroscopy experiments with the streak camera. The electron accelerator can produce electrons with energies from 3 to 9 MeV and with a charge from 0.1 to 7 nC. Electrons are delivered as pulses with a

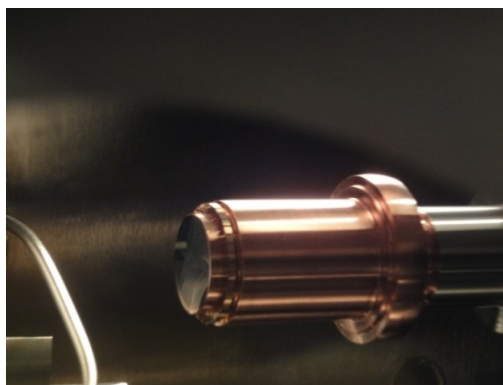


Figure 2.9: A photo of a Cs₂Te photocathode [108].

duration from 5 to 10 ps (at half height) and repetition frequency from 0.1 to 10 Hz (but usually 5 Hz). The beam diameter can be at least 3 mm with a 1% energy dispersion, but its maximum size could be much bigger. [108, 109]

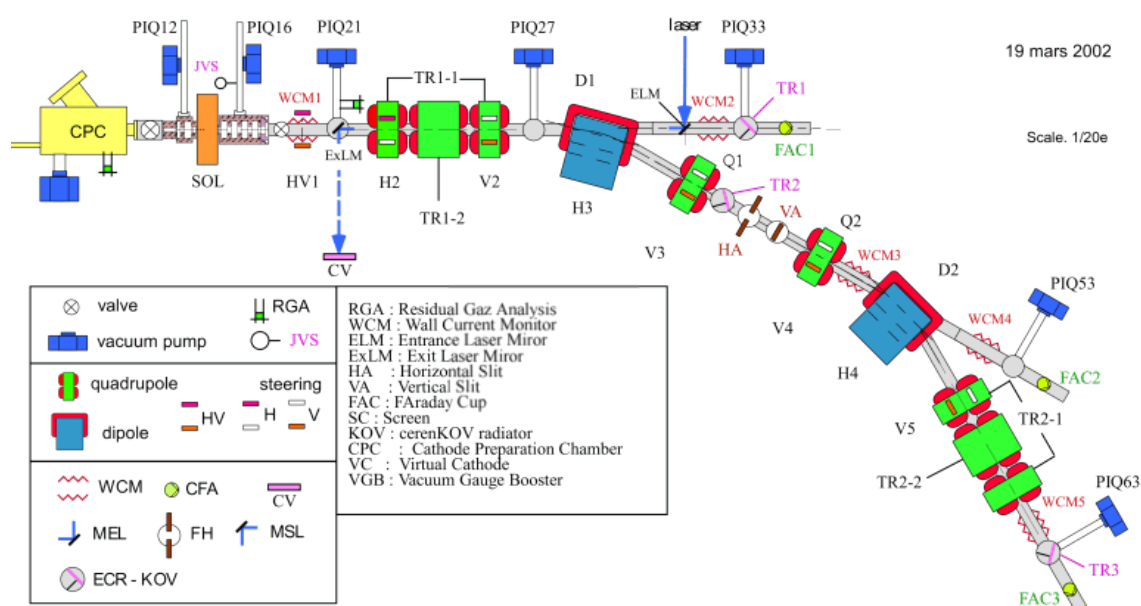


Figure 2.10: Graphical representation of the electron accelerator [108].

Picosecond pump-probe experiments

Picosecond pulse radiolysis experiments are performed on the direct line (VD) with the transient absorption pulse-probe setup. This pump-probe spectroscopy setup allows stroboscopic optical detection. That detection is based on time-monitoring of changes that appear in optical absorption spectra. The spectral changes can be detected with changes in the time delay of the arrival of the light probe, considering the constant arrival of the electron pulse from the pump. The time delay can be achieved with a mechanical delay stage when light is forced to travel longer distances. This experimental device works with four delay paths, and every length is 1 m; therefore, the final delay can be 11.5 ns. The broadband super-continuum from 360 nm to 700 nm is generated by focusing a minor part of the 780 nm laser into a CaF₂

crystal (probe/reference paths are divided into 60/40). Reference and probe paths are merged into optical fibres, conducted to a spectrometer and scattered on a CCD camera. The time window ranges from 0 ns to 11.5 ns. A spectral window offers light wavelengths between 360 nm and 700 nm, and a temporal resolution is 150 fs. The uniqueness of the ELYSE platform, in the case of pump-probe experiments, is based on the synchronization of the electron source and the photon source used, which allows to identify a transient species and study their ultrafast reactions directly. A picosecond pump-probe carries many benefits including an ultra-short time-window, a wider spectral window and an excellent resolution. [108, 109]

Nanosecond to millisecond time-scale experiments

Nanosecond to millisecond time-scale experiments are carried out on the bend line (VD2). Besides the core described above, it contains the detection part, which includes a home made flash xenon lamp as a source of light for analysis. A light passing through the irradiated solution goes to the highly dynamic streak-camera (Hamamatsu C7700-01) in connection with a spectrograph for detection (AndorKymera 328i). There is a time window between electron and reference pulses from 1 ns to 1 ms. The spectral window ranges between 350 and 600 nm and a temporal resolution is 50 ps (for the 1 ns time window). [108, 109]

2.4.2 Sample preparation and sample inlet

Samples can be measured using a method of pulse radiolysis in their liquid form. Solid samples need to be dissolved in the appropriate solvent at first. However, solvents with aromatic character are unfavourable when detecting secondary low-energy electrons due to radiolysis. These electrons tend to react especially with benzene rings in aromatic solvents and thus cause their excitation into triplet states. This reaction occurs at the expense of electron scavenging by a studied compound in solution. For measurements, liquid samples are located in a static cell or the cell with sample circulation, which enables the maintenance of the homogeneous solution. Evaluation of pulse radiolysis measurements is based on comparing the results for a sample in solution and a reference solution containing only that solvent.

The static cells for the pump-probe experiments are made of synthetic fused silica and have an optical path length of 0.5 cm. The optical window thickness is 200 μm to prevent the detection of transient species generated by the electron pulse in quartz. In the non-static cells, the sample flows at approximately 20 cm^3/min . For the pressure of 75 bar inside the cell, 1 mm-input window and 5 mm-output window are sufficient. Then, both types of cells are fixed in the sample holder, illustrated in the figure 2.11. The photo in the figure 2.12 shows the whole system of cells in a cell holder. During the measurement, the sample reacts with an electron beam followed by radiolysis of a solution with a sample; many highly reactive transient species are formed, and many reactions occur. The evolution of formed transient species during the measurement is explored by probe pulses from the broadband white light. [109, 108]

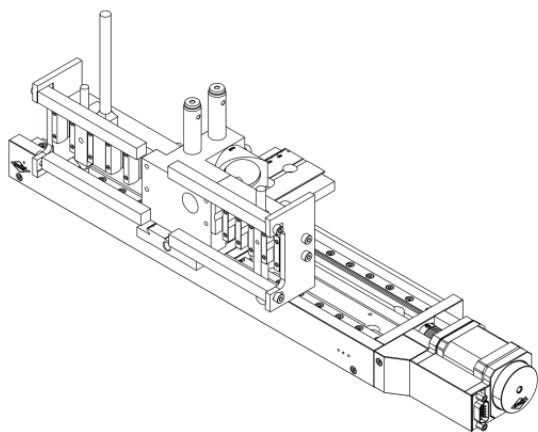


Figure 2.11: A sketch of a sample holder [108].

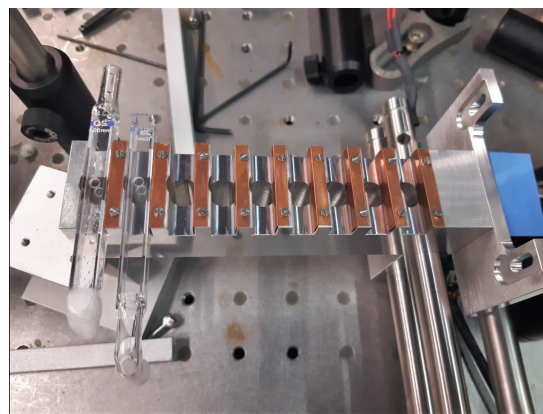


Figure 2.12: A photo of cells in a sample holder.

Data output and evaluation with a focus on quasi-free/solvated electrons

As a result of measurements, data in the matrix form are gained. It contains three types of information: static x- and y-axes represent wavelength and time, and z-axis is intended for measuring the intensities of optical density of transient species present at a specific point at a time and a certain wavelength. Such a type of matrix can be used in further data analysis to obtain both absorption spectra/kinetics for selected detected transient species. To study the interaction of the investigated molecule with quasi-free and solvated electrons in solution, two tools for characterization of the interaction of these intermediates are presented. Both tools use kinetics data for solvated electrons, for quasi-free electrons cannot be detected directly because of the time range for measurements and resolution. Kinetics show the evolution of optical density in solution at a specific wavelength in time (for solvated electrons, it is 600 nm, at which they absorb). Kinetics is recorded in time, which can be divided into three periods: time before irradiation (several ps/ns), zero time at the time of irradiation and time after irradiation (several ps/ns). The kinetics of solvated electrons generally follow. Before irradiation of solution, optical density is at zero value. Immediately after irradiation, the concentration of released solvated electrons increases very strongly (so as measured optical density) and reaches a maximum at picoseconds. Then these values decrease with time, meaning that solvated electrons are scavenged by studied molecules of scavenger in solution and thus become invisible for measurements.

In the case of quasi-free electrons, an indirect characterization of their interaction with studied molecules can be used based on the concept of C_{37} . The C_{37} is the concentration of a scavenger in solution at which the initial amount of solvated electrons present in the solution is 37% ($1/e$). This value, therefore, indirectly speaks about the interaction of the scavenger with quasi-free electrons, since 63% [$1-(1/e)$] of all quasi-free electrons had to interact with the scavenger before. [110, 111]

Solvated electrons and their behaviour in the sense of kinetics, interactions and decay in the solution can be detected directly at a wavelength around 600 nm and at a time in order of ps. The scavenging of solvated electrons in solution depends on the molar concentration of the molecule as its scavenger in solution. With increasing concentration of scavengers, scavenging will be faster, and the kinetics of solvated electrons in solution will be steeper in time. For each molar concentration of scavenger, the absolute rate constant for interaction with solvated electrons can be calculated.

This process leading to calculation can be described as follows. From kinetics, specifically from the curve for select concentration, the time at half of amplitude $T_{1/2}$ must be determined. In the units of seconds, this value will be inserted into the following formula:

$$k = \ln(2)/T_{1/2}, \quad (2. 1)$$

where k is the absolute rate constant [-], $\ln(2)$ is the natural logarithm of 2 and $T_{1/2}$ is the time when the concentration of solvated electron reaches its half-value. Then, the absolute rate constants for selected concentrations are plotted in dependence on these molar concentrations c [mol/l, M] and are fitted with a linear fit to gain slope value, which represents the normalized rate constant.

Experimental conditions for measurement of RRx-001 and fullerenes

Measurements of RRx-001 in ethanol solutions were carried out using both picosecond pulse radiolysis (VD) and nanosecond to millisecond time-scale pulse radiolysis (VD2). Both static cell (2.5 ml of solution) and cell with constant circulation (25 ml of solution) were used to prevent overdosing of irradiated volume or provide a homogeneous concentration in case of approaching the solubility limit. Circulation in the cell was achieved using a closed tube loop with a solution and a home-made pump under the electromagnetic control. The circulation can reach a rate of around 20 cm³/min - the molecule of RRx-001 was purchased from AmBeed with a declared purity of 95.00%.

In case of experiments with fullerenes, three samples were used: buckminsterfullerene C₆₀ in form of dark crystals powder (C₆₀, $M_r = 720.64$ g/mol, sublimed, 99.9%), C₆₀ pyrrolidine tris-acid (C₆₀-PTA) in form of dark powder (C₆₆O₆NH₇, $M_r = 909.76$ g/mol, 97%), and fullerenols in form of yellow powder (C₆₀(OH)_{*n*}·*m*H₂O (*n*>40, *m*>8), $M_r \geq 1545.076$ g/mol). All samples were ordered from Sigma Aldrich. Molecules of fullerenols are soluble in water with a declared mass concentration of up to 50 mg/ml. Nevertheless, our highest reached mass concentration was 6 mg/ml. Measurements were performed on both VD and VD2 lines.

Measurements on ELYSE were conducted using electron pulses from the accelerator with an energy of 7.8 MeV, a repetition rate of 5 or 10 Hz, a half-width between 5 and 7 ps, and a charge of 6nC.

2.5 Microtron MT25

Microtron MT25 (Nuclear Physics Institute, CAS, Prague) is a ring electron accelerator with a Kapitz resonator. Electrons are accelerated by a high-frequency electric field with constant amplitude and frequency in a homogeneous magnetic field. In a vacuum chamber, electrons move along circular paths with a common tangent point, where a cavity resonator is located and is powered by microwave radiation. The frequency of the incoming microwaves is timed so that the length of the electron orbit around the circle is a multiple of its wavelength. Thanks to this, additional energy is repeatedly transferred to the electrons in each orbit, which causes them to move to a higher orbit with a larger circle radius. The maximum energy is 25 MeV; the energy can differ in 1 MeV steps from 12 to 25 MeV or in 0.5 MeV steps from 6 to 15 MeV. The pulse length is 3.5 μs , the standard repetition rate is 423 Hz, and the mean maximum current is about 30 μA depending on the electron energy. In this work, the electron energy of 16.5 MeV was applied. [112]

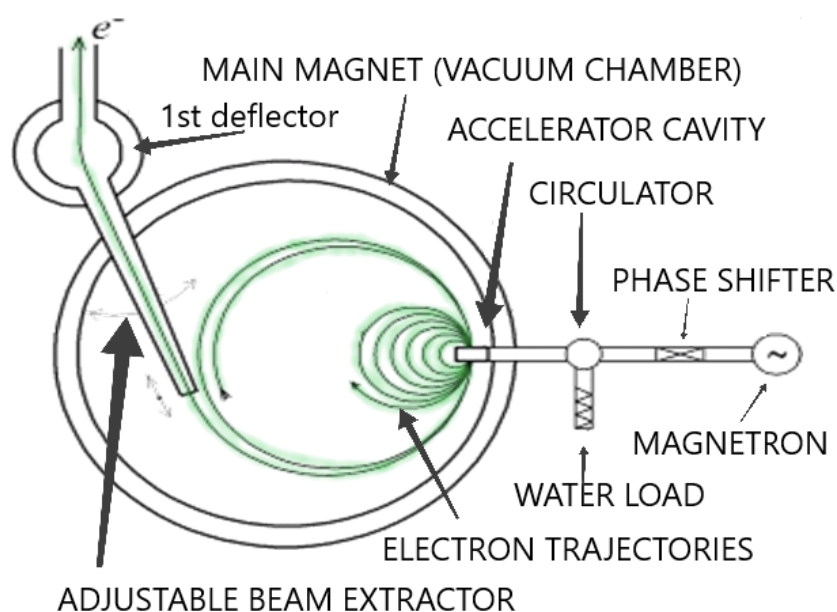


Figure 2.13: Graphical representation of the microtron MT25 ([112], modified).

Experimental conditions for irradiation of RRx-001 molecules

RRx-001, usually in ethanol solutions, was irradiated in 15 ml tubes on a constantly rotating mat that enabled equal irradiation of all tubes during one irradiation. Solutions were usually 12 ml or 4 ml. In most cases, the solvent was ethanol, once methanol, and once deuterated methanol, all ordered from Sigma Aldrich. The molecule of RRx-001 was purchased from AmBeed with a declared purity of 95.00%.

2.6 *Ab initio* calculations using Gaussian software

The idea of predicting the radiosensitizing properties of molecules without any experimental studies became a driving force to incorporate quantum-mechanical calculations into this work. In order to study the reductive properties of selected compounds based on their electron affinities, the Gaussian 16 software was selected for *ab initio* calculations. For the plotting of structures, Chemcraft and Avogadro software were used.

Gaussian 16, the latest version of the Gaussian programs, enables the performance of state-of-the-art electronic structure modelling in a wide range of various scientific sectors. It can be used to study real chemical problems of all levels of complexity. This program is based on fundamental quantum-mechanics laws and offers many applications. Gaussian 16 presents a wide range of methods. Among them are Hartree-Fock methods (HF), density functional (DFT) methods, excited-state methods, high-accuracy energy models, and many others. [113]

This work operates, in particular, with density functional methods, Hartree-Fock methods, and high-accuracy energy models.

The DFT method is a computational modelling method based on quantum mechanics that uses functionals of electron density, which is spatially dependent. DFT calculations build on the first and significant part of calculations coming from the Hartree-Fock (HF) method. The method of DFT only adds a final computational step, which consists of numerical integration of the functional. Thus, the accuracy of DFT calculations depends on the errors arising during Hartree-Fock calculations and the number of points utilized for numerical integration. The DFT method works with several DFT models. It is one of the most applied methods in the field of computational chemistry and physics, as well as physics dealing with condensed matter. The DFT methods exploit numerous hybrid functionals that result from a correlated mixture of Hartree-Fock exchange with DFT exchange. They can be divided into several groups: Becke Three-Parameter Hybrid Functionals (B3LYP, B3P86, B3PW91, O3LYP) Functionals Including Dispersion (APFD, APF, wB97XD) Long-Range-Corrected Functionals (LC-wHPBE, CAM-B3LYP, wB97XD), and others. *Ab initio* calculations in this research work use B3LYP and M062x as a hybrid functional. [113]

High-accuracy energy models, also called Gn Methods, are used to compute very accurate energies, and four types of G1-G4 are recognized. The calculations presented in this work benefited directly from using the G3 method, specifically G3MP2. [113]

***Ab initio* calculations of reductive properties of favipiravir**

Ab initio calculations on favipiravir were performed to calculate energies of neutral and anions, adiabatic electron affinities, energetic thresholds for reaction channels of DEA to favipiravir and vertical attachment energies for modelling of favipiravir HOMO/LUMO virtual orbitals.

1) *Calculations of energies for neutral and anionic favipiravir*

The neutral molecules of favipiravir (2 conformers and their two keto-tautomers) and their corresponding anionic forms were pre-optimized first at the B3LYP/6-31(d) level of theory and then at the B3LYP/aug-cc-pVTZ levels of theory. In the next step, energies obtained from these calculations were verified by calculations using the G3MP2 method. Errors originating from re-optimizing B3LYP structures were checked by M062x, which is functional with the same aug-cc-pVTZ basis set.

2) *Calculations of adiabatic electron affinities*

A molecule of favipiravir is characterized by two conformers (which differ in two orientations of CONH₂ group) and their two keto-tautomers. Electron adiabatic affinities were obtained as a difference of the neutral energy and anion energy in the optimized geometry.

3) *Calculations of energetic thresholds for DEA reaction channels*

To confirm the experimental results, energetic thresholds for reaction channels of the DEA reaction to favipiravir were computed via the B3LYP/aug-cc-pVTZ level of theory. Threshold energies can be gained from the equation:

$$E_{\text{Th}} = E_{(\text{M}_a)^-} + E_{\text{M}_b} + E_{\text{M}} \quad (3.1.2 \text{ a})$$

where $E_{(\text{M}_a)^-}$ and E_{M_b} are energies of anion, resp. all neutral fragments which are formed in the individual reaction channel. E_{M} represents the energy belonging to the neutral parent molecule. Method errors were determined by recalculating values using the M062x/aug-cc-pVTZ level of theory.

3

Overview of results & discussion

This chapter summarizes all the results achieved using various combinations of experiments and calculations. The chapter is divided into three subchapters, each belonging to one of three studied molecules and their interactions with (secondary) LEEs.

The first examined molecule is an antiviral - a molecule of favipiravir. In that case, a study is presented combining electron attachment spectroscopy of isolated and micro-hydrated molecules with *ab initio* calculations to reveal favipiravir's stability upon single electron reduction (JH INST, Prague, Czech Republic). Based on these results, the article has been published [62] and is enclosed in the attachment of the dissertation. Therefore, the subchapter dedicated to favipiravir and its study intentionally contains only a short description, which aims to introduce the already published results.

The second molecule type is an epigenetic agent with proven chemotherapeutic and radiosensitizing properties - RRx-001. At this point, experimental results that were obtained from combining electron attachment spectroscopy of isolated and micro-hydrated molecules (JH INST, Prague), pulse radiolysis with both picosecond and nanosecond to millisecond time-scales (ICP, UMR8000, Orsay), and irradiation on microtron followed by NMR spectroscopy (Prague) for analysis of irradiated samples. These results will be published after the submission of the present doctoral thesis. However, this molecule was first studied in a dominant collaboration with the University of Innsbruck, specifically with Prof. Stephan Denifl and Prof. Milan Ončák. That joint work relates their theoretical calculations of RRx-001 with the experimental results achieved during measurements at the CLUB experimental device (JH INST, Prague) in which I participated. The results of this collaboration have already been published and attached in the form of an article. Therefore, it is only marginally mentioned in the thesis and finally discussed concerning the current results.

The third and last type of studied molecules are fullerenes, specifically water-soluble fullereneols. Based on the theoretical proposal of the radiosensitizing mechanism of the π - π complex simultaneously allowing the EPR effect, a series of studies were performed in Innsbruck as well as in the home laboratory, and using pulse radiolysis in solution on the ELYSE platform (ICP, UMR8000, Orsay), and relevant discussion on this topic.

3.1 Studies on the molecule of favipiravir

The present study aimed to examine the behaviour of favipiravir in reactions with LEEs [60] using electron attachment spectroscopy (EAS). Favipiravir was investigated in its isolated and micro-hydrated forms in the gas phase, as well as the effect of the water environment on the reaction. Two experimental devices were used for measurements. An electron attachment spectrometer with better energy resolution (about 150 meV) was used to measure electron-energy dependent yields of main fragments from EA to isolated favipiravir in the gas phase. At the same time, a CLUB apparatus was used to measure the mass spectra of favipiravir undergoing EA in its various hydrated forms. Investigating clusters of favipiravir with attached water molecules allows for studying the environmental effect on EA reaction. Experimental data were supported by *ab initio* calculations. [62]

As a result of measurements using an electron attachment spectrometer, dependencies of ion yields on electron energy were obtained for main fragments formed in EA reaction to favipiravir. The primary reaction channel is associative electron attachment (reaction 1.3. a), forming a negative parent ion ($m/z = 157$) with a main resonance peak around 2 eV. Other fragments formed in the reaction of DEA had at least a hundred times lower intensities. The second most intense fragment is $[M-CONH_3]^-$, showing two peaks in the spectrum at around 2 and 4 eV. As the *ab initio* calculations revealed, the fragmentation is subject to hydrogen transfer from hydroxyl to the amino group with a significant reaction barrier. The second most intense peak indicates a hydrogen removal with electron energies higher than 2 eV. The third most intensively forming fragment is $[OCN]^-$; because of its high electron affinity, it is a common product of DEA to many bio-molecules [114, 115]. [62]

Experiments on CLUB studying the effect of the water environment on EA to favipiravir in the gas phase with electron energies from 0 - 9 eV confirm that dry conditions give rise to favipiravir parent anion primarily via AEA reaction. The fragmentation in CLUB experiments was suppressed, which can be mainly explained by the detection time of a dozen microseconds, which is roughly ten times shorter than the detection time of TEM-QMS. Therefore, there is less time for auto-detachment or dissociative electron attachment processes during CLUB experiments. The temperature of precursor molecules is another parameter that affects fragmentation. The molecular beam in CLUB has a lower temperature than the effusive beam in the TEM-QMS. Measurements with various levels of hydration show that EA to hydrated favipiravir followed by ionisation of favipiravir leads to that energy being transferred to the solvent (at the level of several electron volts), and thus neutral water molecules being evaporated from water-favipiravir clusters, and the fragmentation of favipiravir is suppressed. It has been postulated [69] that such energy transfer could increase the value of linear energy transfer (LET) after interaction with ionising radiation, providing an alternative for the radiosensitising action of electron affine molecules.

Based on *ab initio* calculations of energy in the ground state, it was revealed that its enol-form is the most stable form of favipiravir. Next, adiabatic electron affinities and dipole moments were calculated. Also, threshold energies were calculated for individual reaction channels of dissociative electron attachment to favipiravir, shown in our already published article [62]. The threshold energies were used to interpret the experimentally obtained fragmentation patterns.

Final discussion and conclusion of experiments with favipiravir

Investigation of the favipiravir molecule, an important biochemical compound with promising radiosensitising properties, shows that the main reaction is AEA when a long-living parent ion forms. In contrast, only a minor part of transient parent ions decays via DEA. The high stability of parent ions is an exciting property for transport and radiosensitising purposes because it can allow multiple electron reductions. The main fragmentation occurs via DEA reaction on the CONH₂ group. EA to hydrated favipiravir Fav.(H₂O)_n leads to the dissipation of available energy into the solvent after the EA reaction. The energy released from a reduced form of favipiravir in the process of EA could also increase the LET in the presence of favipiravir and cause the radiosensitizing effect. These findings gained based on the investigation of interaction with LEEs strongly support the radiosensitising potential of favipiravir and its future investigation as a candidate for radiosensitisers. [62]

3.2 Studies on the molecule of RRx-001

This subchapter is dedicated to results obtained by studying the behaviour of RRx-001 in reactions with LEEs [60]. The study used electron attachment spectroscopy (EAS) in the gas phase and picosecond pulse radiolysis in ethanol solution to describe short-lived species. Stable products of studied reactions were detected using a nuclear magnetic resonance spectroscopy applied to ethanol solutions of RRx-001 irradiated with highly accelerated electrons on the microtron. The molecule of RRx-001 was investigated first in dominant cooperation with colleagues from the University of Innsbruck, and this study was completed with a publication. Therefore, this study is first summarized in short. After that, a more detailed description of the following work is provided, which is the subject of a publication under preparation. For greater clarity due to the several experimental approaches used, the most important findings are summarised in bullet points at the end of each subchapter devoted to one experimental method and its results.

3.2.1 Studies on the molecule of RRx-001 in cooperation with University of Innsbruck

The study of the RRx-001 molecule was initiated by Prof. Stefan Denifl based on their pilot experiments with the isolated molecule sublimed directly to the reaction zone of the electron attachment spectrometer. These were complemented by our measurements of isolated molecules in molecular beam experiments at CLUB setup and the computational modelling of Prof. M. Ončák. The study of reductive

properties of RRx-001 combines an experimental approach with theoretical calculations, specifically electron attachment spectroscopy and mass spectrometry in the gas phase (CLUB, Prague) with single and multi-reference calculation support using Gaussian and MolPro software. The attachment of free LEEs to RRx-001 leads to the formation of electronically excited transient negative ions (TNI) at the femtosecond time via a fast electronic transition process. This study aimed to follow the relaxation pathways at different time-scales, which are several of them and present insight into the radiation chemistry of RRx-001. The work shows a significant interaction of RRx-001 with LEEs. Depending on the initial state, the molecule can undergo direct dissociation into Br^- or NO_2^- channels, or the reaction proceeds via the formation of long-lived transient Br^- complexes. We have also observed the formation of similar complexes in our study of bromothiophenol [116]. Therefore, these complexes may also play an important role in the radiation chemistry of the solution. After EA to RRx-001, the most abundant fragment were Br^- , NO_2^- . The calculations revealed the raising anionic complex $\text{Br}^-(\text{RRx-HNOO}_2)$. Experiments of electron attachment indicate the formation of nitrous acid, nitrogen dioxide, and nitrite, which can be followed by reactions interesting for radiosensitizing effects such as electron transfer, addition reactions, or abstraction reactions. Their consequence can be the expansion of blood vessels and increased blood flow. It can also lead to the formation of OH groups, which leads to oxidative stress, and in hypoxic cells, reoxygenation would occur, making the cells more sensitive to radiation.

3.2.2 SHORT TIME-SCALE: Intermediates

Short-lived species forming after the interaction of RRx-001 with LEEs were studied using electron attachment spectrometry in the gas phase and pulse radiolysis in an ethanol solution.

3.2.2.1 Electron attachment to RRx-001 in gas phase (CLUB)

This part of the study is dedicated to the reaction of EA to RRx-001. A reaction of EA is characterized by the capture of a low-energy electron on a studied molecule (RRx-001) and the formation of a transient parent ion $(\text{RRx-001}^-)^*$. The transient parent ion $(\text{RRx-001}^-)^*$ can stabilize via forming a stable anion (associative attachment- eq. 1.3. a) or, due to excessive energy, can decompose into fragments A^- and B (dissociative electron attachment- eq. 1.3. c)

The third possibility, when the transient ion decays via an electron separation (autodetachment - 1.3. b), is not detectable with our experimental method. Nevertheless, this third reaction channel does not seem attractive for the possible radiosensitizing potential of the molecule and the mechanism which could be one of the sources of synergism.

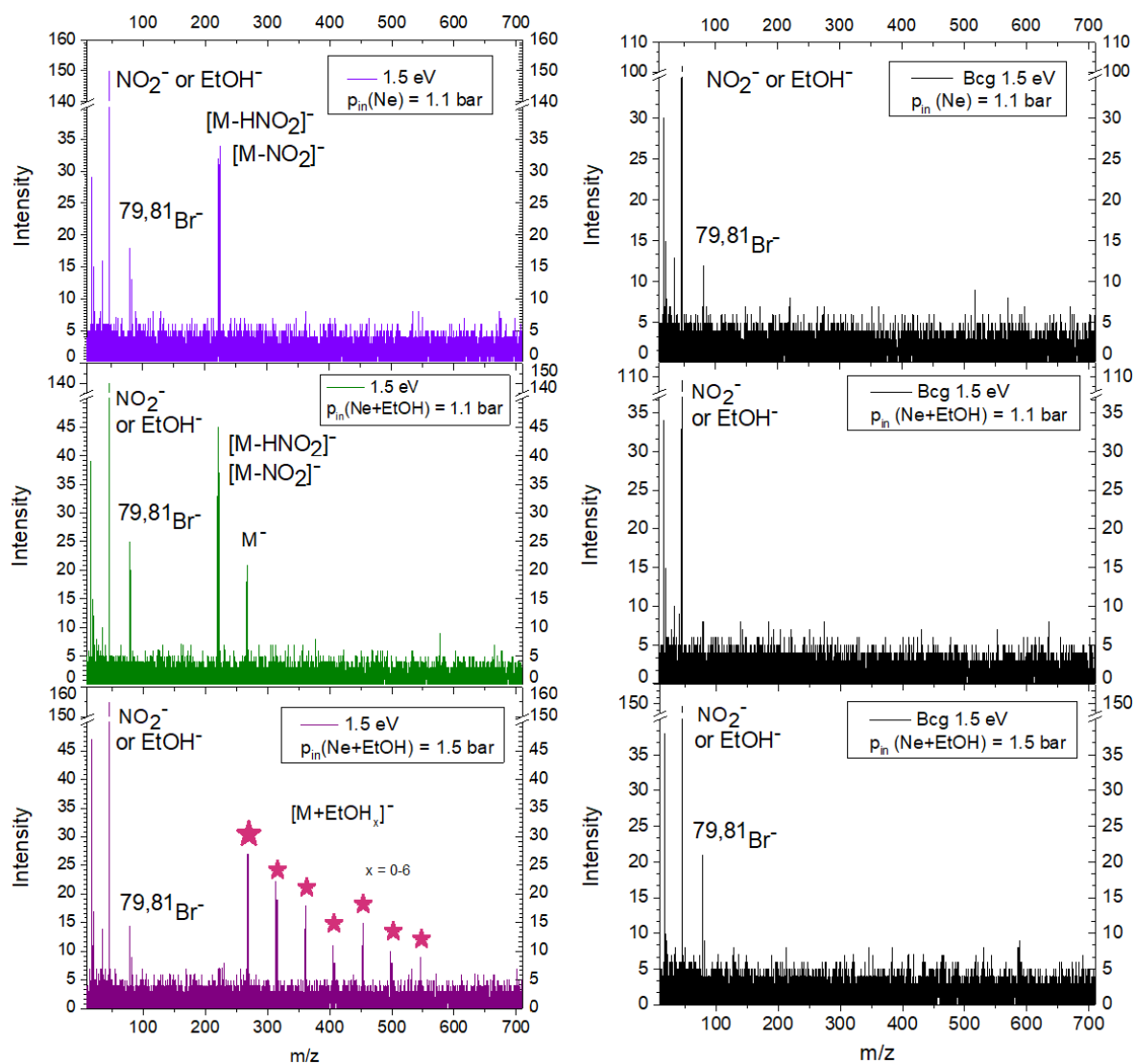


Figure 3.1: Negative mass spectra for electron attachment to RRx-001 in the gas phase for electron energies 0 - 12 eV and with increasing level of EtOH-micro solvation. From the top to the bottom: 1.1 bar (without EtOH), 1.1 bar (with EtOH), and 1.5 bar (with EtOH). Negative background spectra measured before each measurement are plotted next to each sample measurement.

Firstly, I investigated the effect of increasing levels of ethanol solvation on the reaction of electron attachment to RRx-001. Ethanol as a solvent was selected to reproduce the conditions in the pulse radiolysis experiments, which will be discussed later. As a main result, three mass spectra are presented with appropriate backgrounds. The pressures of carrier gas indicating the level of ethanol solvation were chosen as follows: 1.1 bar (dry, without EtOH), 1.1 bar (micro-solvated with EtOH), and 1.5 bar (micro-solvated with EtOH).

The resulting negative mass spectra are shown in the Figure 3.1. The graph in the top left corner shows data for EA to isolate molecule RRx-001 with the pressure of carrier gas of 1.1 bar without ethanol molecules. From this graph, significant peaks for forming anions can be observed, and they were assigned to NO_2^- , Br^- , and $[\text{M}-\text{NO}_2]^-$. The graph in the middle on the left side represents the outcome for RRx-001 with the lowest level of ethanol solvation (1.1 bar). In this case, the parent anion M^- is also detected. The graph at the bottom with the maximal level of ethanol solvation (1.5 bar) exhibits the most intense signal of parent ion $\text{M}(\text{EtOH})_n^-$ within ethanol clusters, indicating RRx-001 anion stabilization, possibly via caging. Based on these mass spectra, the effect of ethanol solvation on the evolution of reaction channels can be summarized.

The evolution of significant reaction channels for forming negative anions is depicted in the Figure 3.2. Generally, it is observed that the increasing solvation leads to the parent anion stabilization and closing of all fragmentation channels as Br^- , NO_2^- , $\text{M}-\text{HNO}_2^-$, and $\text{M}-\text{NO}_2^-$. It must be noted that the signal of the isolated parent anion also decreases with increasing levels of solvation. However, the total signal for the negative parent ion increases after increasing the amount of EtOH clusters in its surroundings. Under solvated conditions, the fragmentation is further suppressed by energy transfer to the solvent. It has been postulated [69] that such energy transfer could increase the value of LET after interaction with ionizing radiation, providing an alternative for the radiosensitizing action of electron affine molecules.

The most intense peak with a mass around $m/z = 46$, clearly seen in each of the graphs with negative mass spectra, could belong to two anions. The first one is NO_2^- anion; the second one could be the parent anion of ethanol. The masses are: $m/z (\text{NO}_2^-) = 45.99$ and $m/z (\text{EtOH}^-) = 46.04$, which should be possible to resolve in our mass spectrometer with a measured resolution of better than 1400. However, two peaks or any shoulder cannot be seen, so the peak was assigned to NO_2^- . The peak around $m/z = 46$ decreases with increasing levels of EtOH-micro-solvation.

The electron-energy dependence spectrum for the formation of the anion with m/z around 46 is shown in the graph in the Figure 3.3. Unfortunately, NO_2^- DEA resonance cannot be resolved here either. Therefore, it cannot be concluded that the dissociation channel is closing purely via caging and M^- formation or also due to decay into neutral products (e.g. $\text{M}-\text{NO}_2$ neutral).

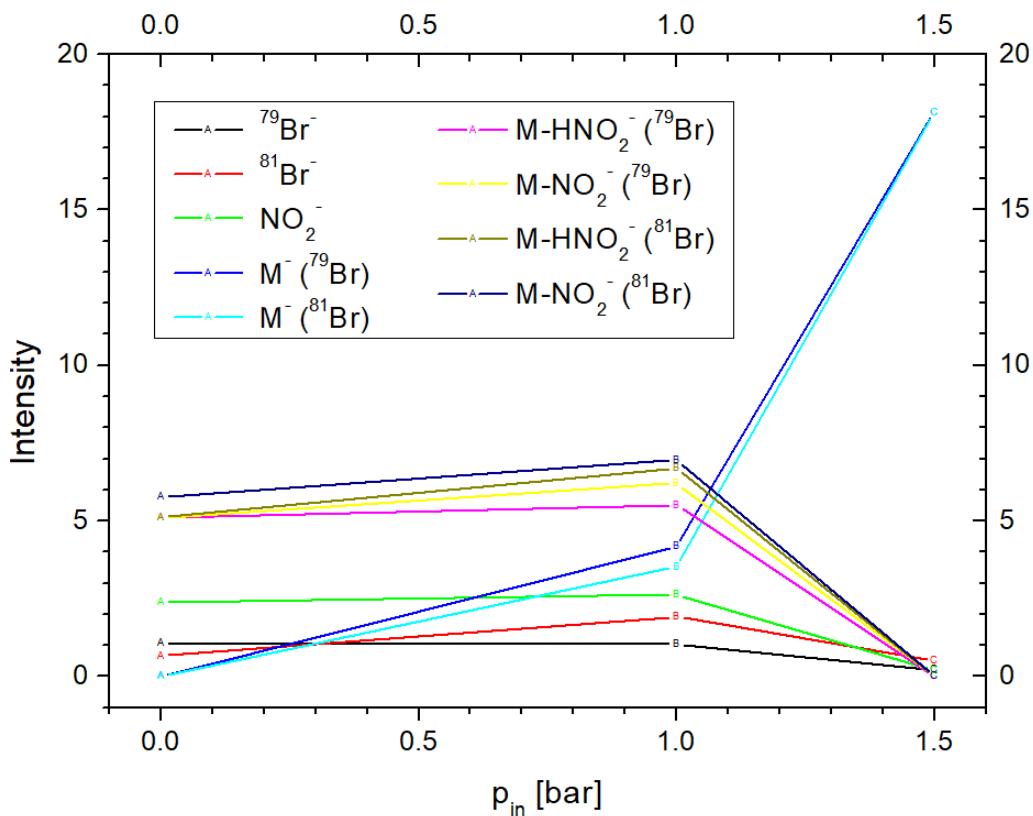


Figure 3.2: Total intensities of the different product ions under various EtOH micro-solvation levels.

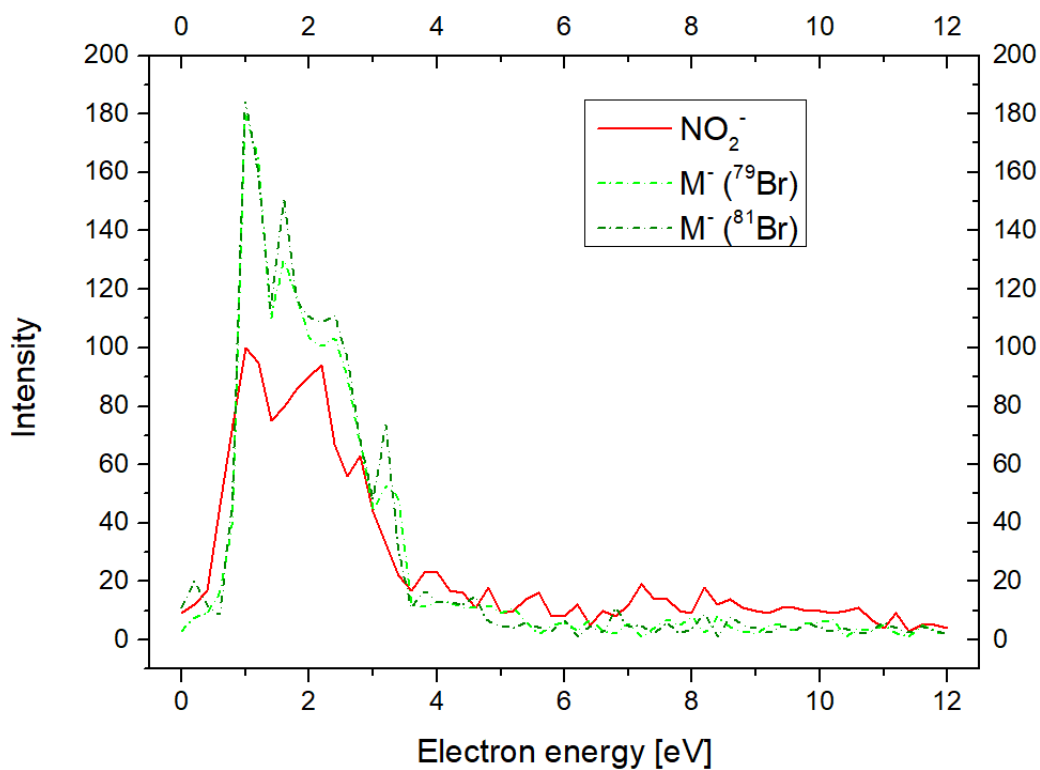


Figure 3.3: Electron-energy dependence spectra for the formation of the parent anion M^- and NO_2^- with $m/z = 46$.

Secondly, I additionally examined the effect of temperature on the reaction of EA to RRx-001. The aim was to investigate if the molecule remains stable at higher temperatures used in our microsolvation studies. The temperature of the nozzle was increased to (130 °C - 160 °C) and the sample reservoir (110 °C - 140 °C) with a 10 °C step. The resulting mass spectra of negative ions are plotted in the Figure 3.4. The same type of species was observed compared to the previous case, where the solvation effect was studied. The dependence of the signal intensity on the temperature is shown in the Figure 3.5.

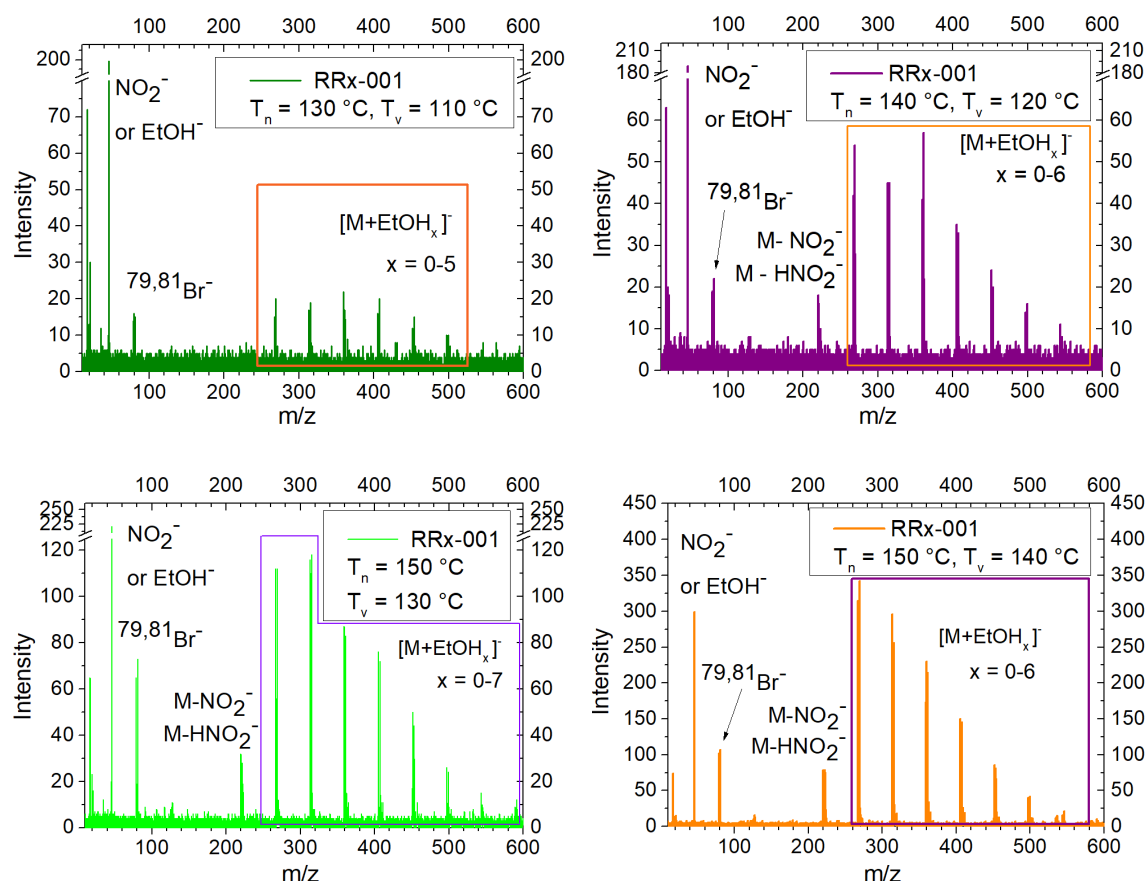


Figure 3.4: Negative mass spectra for electron attachment to RRx-001 in the gas phase for electron energies 0 - 12 eV and with increasing temperature.

With the increasing temperature in the reservoir, the amount of the studied molecule in the molecular beam will increase and, consequently, with the detected anion signal. If there is thermal decomposition, the signal of fragments resulting from such a process will exhibit different temperature dependence than the parent anion. Increasing the temperature is one way to increase the signal of the molecule, but it also depends on the proper setup of the experimental system. The graph of the evolution of the signal intensities after the subtraction of background signals shows that intensities increase with increasing temperature. The chosen temperature setting for the previous study of the solvation effect is adequate to see clearly the development of the studied peaks with increasing pressure of neon.

The electron attachment experiments indicate that fragmentation channels are clos-

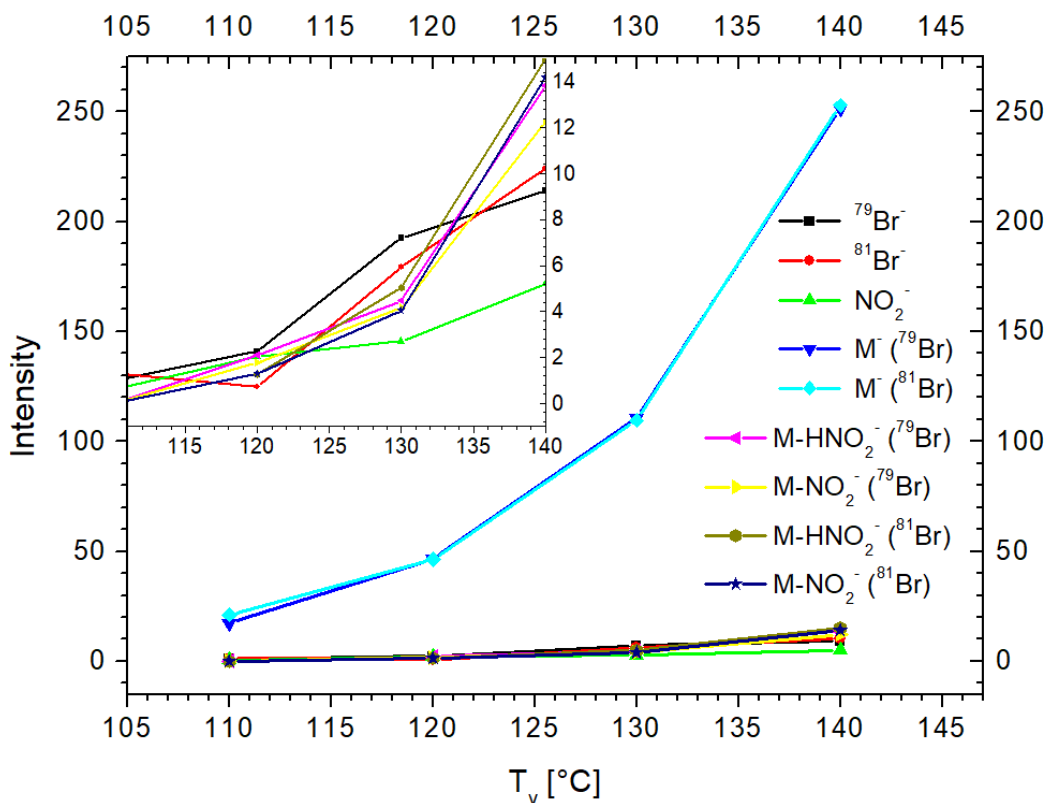


Figure 3.5: Total counts of the different product ions under the increasing temperature of the nozzle and sample reservoir.

ing with increasing levels of ethanol solvation because of the stabilization of parent ion in the solvent environment and formation of M^- . However, there exists a probability that M^- formation is not the only existing channel, and the anion decays into NO_2^- anion and neutral $M-NO_2$.

Key insights gained about the RRx-001 based on EAS

- Electron attachment to RRx-001 in dry conditions leads to formation of fragments: NO_2^- , Br^- , and $[M-NO_2]^-$.
 - With increasing ethanol solvation, the negative parent ion is more stabilized; the fragmentation is suppressed by energy transfer to the solvent.
 - Stabilized negative parent ion can serve as a potential source of multiple electron reductions. Energy transfer could increase LET of ionizing radiation in irradiated volume. Both observed effects provide an alternative for the radiosensitizing action of electron affine molecules.
-

3.2.2.2 Picosecond pulse radiolysis of RRx-001 in ethanol

The molecule of RRx-001 in ethanol solution was studied using picosecond pulse radiolysis to describe its interactions with secondary LEEs in the form of quasi-free and solvated electrons.

First, ethanol solutions of molecule RRx-001 with various molar concentrations (10, 25, 50, 70 and 80 mM) were studied in static cells (except for 70 mM solution, measured in a cell with circulation later) with a volume of solutions around 3 ml. As a result of this measurement, the kinetics for solvated electrons were gained and are plotted in the graphs in the Figures 3.6 and 3.7. The kinetics of solvated electrons in ethanol is plotted by the black curve, and in the ethanol solutions of RRx-001 with various concentrations by the reddish curves. The graph with a time-scale of only 30 ps shows that the amount of solvated electrons in ethanol solution is lower than in water at zero time. With the increasing concentration of RRx-001 in ethanol, the amount is further decreased. It is observed because these electrons have already reacted in the form of quasi-free electrons with RRx-001.

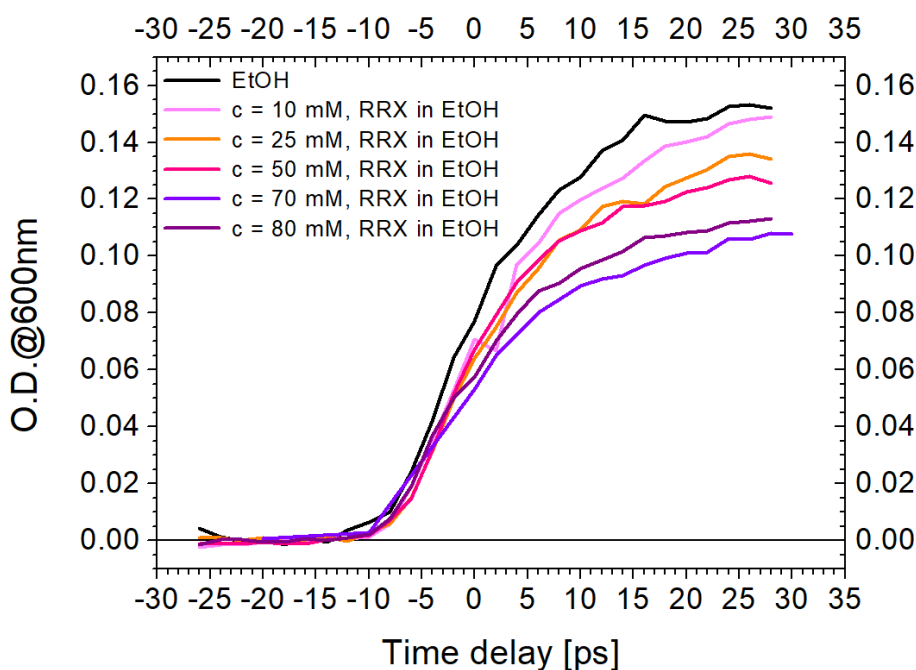


Figure 3.6: Kinetics of solvated electrons up to 30 ps after absorption of a 5 ps electron pulse by a sample of ethanol (black curve) and RRx-001 in ethanol solutions with various concentrations (reddish curves).

The graph, with a time range of up to 10 ns, shows faster decay of solvated electrons with increasing concentrations of RRx-001 in EtOH. That is proof of the interaction of solvated electrons with RRx-001. Thus, the molecule of RRx-001 interacts with both quasi-free and solvated electrons. It can be seen that decay in a 70 mM solution is steeper than in an 80 mM solution. This could be for several reasons. These concentrations are approaching the maximum achievable concentration of 83 mM declared by the supplier. Therefore, the samples with a concentration approaching the highest declared value may have been more difficult to dissolve. Moreover, a 70 mM solution was measured in a cell with circulation.

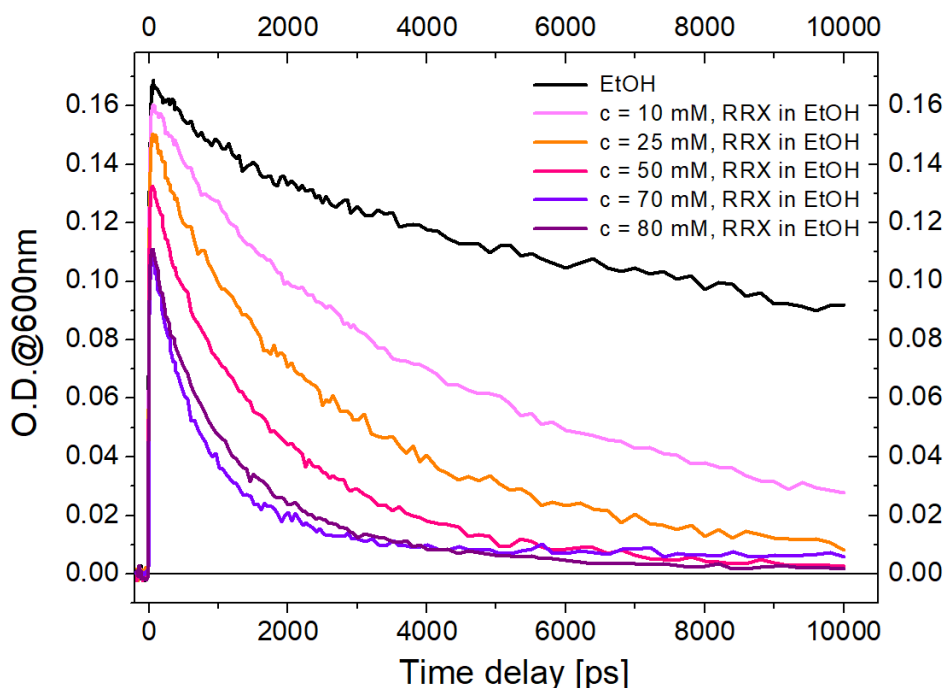


Figure 3.7: Kinetics of solvated electrons up to 10 ns after absorption of a 5 ps electron pulse by a sample of ethanol (black curve), and RRx-001 in ethanol solutions with various concentrations (reddish curves). The graph points to the interaction with solvated electrons.

c_{mass} [mg/mL]	c_{mol} [mol/L]	Y	$Y_{1/2}$	$T_{1/2}$ [s]	k_{abs} [s^{-1}]
0	0	0.169	0.084	11E-09	6.3E+07
21.4	0.010	0.158	0.079	3.2E-09	2.2E+08
13.4	0.025	0.150	0.075	1.8E-09	3.8E+08
6.7	0.050	0.134	0.067	1.2E-09	5.7E+08
2.7	0.080	0.117	0.058	8.2E-10	8.4E+08

Table 3.1: Table including data for determining the normalized rate constant describing the reaction of solvated electrons with RRx-001 revealed in the graph in the Figure 3.7, from which the data originate. The columns of c_{mass} [mg/ml] and c_{mol} [mol/l] show mass concentration and molar concentration, respectively, of four measured ethanol solvation of RRx-001, Y is a maximal reached optical density at 600 nm for solvated electrons in solution after its irradiation, $Y_{1/2}$ is half of the amplitude, $T_{1/2}$ [s] is the time when $Y_{1/2}$ is reached, and k_{abs} [s^{-1}] is the absolute rate constant belonging to a specific concentration of RRx-001 in ethanol solution.

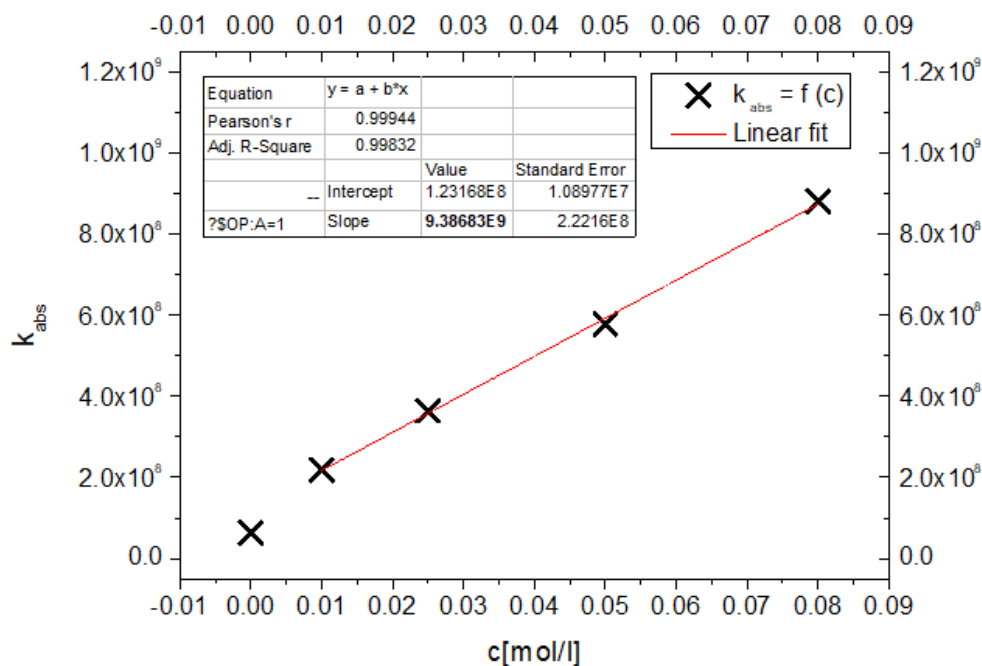


Figure 3.8: Dependencies of absolute rate constant on the molar concentration of RRx-001 in ethanol. As a result, 5 points are plotted and 4 are fitted with a linear fit in order to gain the normalized rate constant.

Based on the graph in the Figure 3.7, a table shown in the Figure 3.1 was prepared to determine the normalized rate constant for the interaction of solvated electrons with RRx-001, points belonging to a solution containing RRx-001 were linearly fitted. Only data for the measurement of 70 mM solution were not included because they were obtained on different days. The normalized rate constant does not depend on the concentration of RRx-001 in the solution. For its determination, it was necessary at first to calculate the absolute rate constant for each measured concentration of RRx-001. For this purpose, values from " $T_{1/2}$ [s]" for each concentration shown in the column " c_{mol} [mol/l]" were used in the formula:

$$k_{\text{abs}} = \ln(2)/T_{1/2}, \quad (3.1)$$

where k_{abs} [s^{-1}] is the absolute rate constant for selected molar concentration, $\ln(2)$ is a natural logarithm of 2, and $T_{1/2}$ is the time when signal decreases to half of its maximal value. The calculated absolute rate constants are in the last column of the Table.

The dependence of absolute rate constants on molar concentration of RRx-001 in ethanol is plotted in the Figure 3.8. Finally, the normalized rate constant for the interaction of RRx-001 with solvated electrons equals the slope value after linear fitting of plotted dependence. The value of the normalized rate constant based on fit parameters is:

$$k_{\text{normalized}}^{\text{RRx-001}} = 9.4 \times 10^9 \text{ dm}^3 \text{ mol}^{-1} \text{ s}^{-1} \quad (3.2)$$

The previously discussed results were further confirmed by our second campaign, which used ELYSE to measure RRx-001 in ethanol. The RRx-001 sample of molar concentration 70 mM was put into a cell with the circulation. The obtained experimental results show a significantly better signal-to-noise ratio due to a higher laser stability. The result is shown in the Figure 3.9. The graph contains the kinetics of solvated electrons measured up to 10 ns in ethanol (black curve) and RRx-001 (70 mM) in ethanol (orange curve). The data confirm interactions between RRx-001 and solvated electrons.

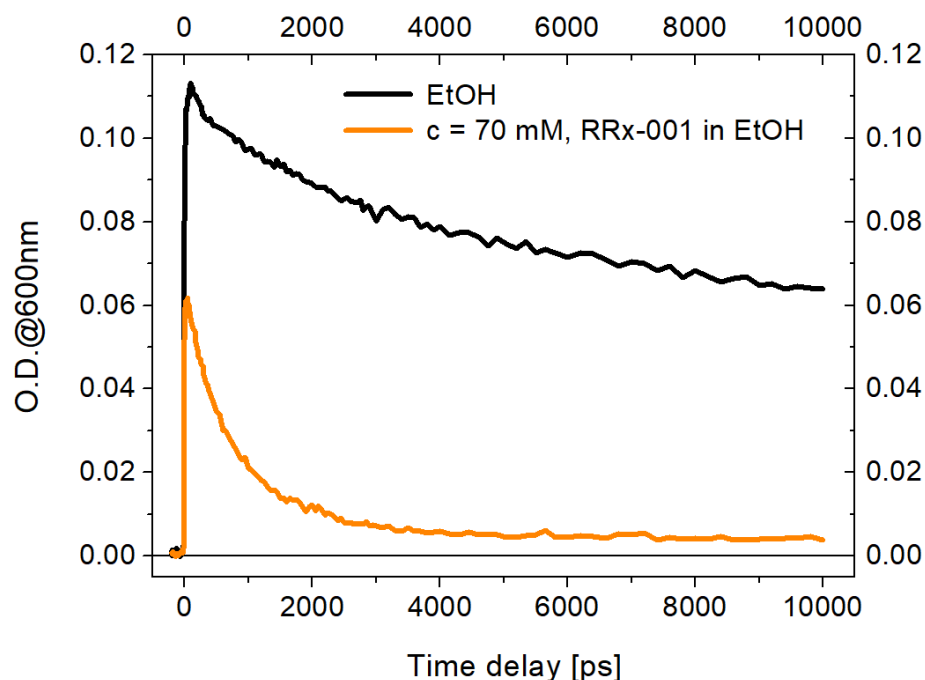


Figure 3.9: Kinetics of solvated electrons measured up to 10 ns after absorption of a 5 ps electron pulse by a sample of ethanol (black curve), and RRx-001 in ethanol solution with a molar concentration of 70 mM (orange curve). These kinetics were measured with higher laser stability. The graph points to interaction with solvated electrons.

Based on this measurement of RRx-001 (70 mM), the data analysis was performed using the software SK-Ana, which allows the deconvolution of the measured spectrokinetics data. [117].

The obtained absorption spectra and kinetics for solvated electrons and a new species formed during radiolysis are shown in the Figure 3.10. The solvated electrons show a short lifetime, leading to their zero signal within 3 ns, which is caused by their interaction with a molecule of RRx-001. However, the product of such interaction was not detected because it apparently does not absorb at a visible range of wavelengths. The newly formed species originate from interactions of quasi-free electrons with RRx-001 because its kinetics do not correlate with the measured kinetics of solvated electrons. It was revealed that this unknown species has a broad absorption spectrum with a maximum of 520 nm. The intermediates form at 7 ps and are stable at least over 10 ns in 70 mM ethanol solution of RRx-001.

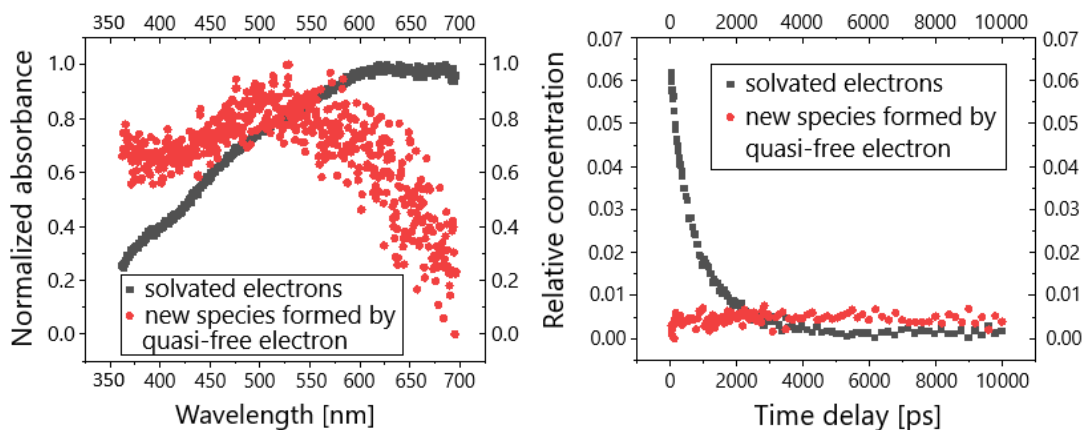


Figure 3.10: Absorption spectra (left side) and kinetics (right side) of solvated electrons and newly formed transient species during radiolysis of 70 mM ethanol solution of RRx-001. Data marked in black is dedicated to solvated electrons, and the newly formed species are shown in red. Radiolysis data from ELYSE were analyzed using the software SK-Ana [117].

Another output from SK-Ana [117] is shown in the Figure 3.11. It is the extracted absorption spectrum of a transient species formed after the interaction of a quasi-free electron with the RRx-001 molecule.

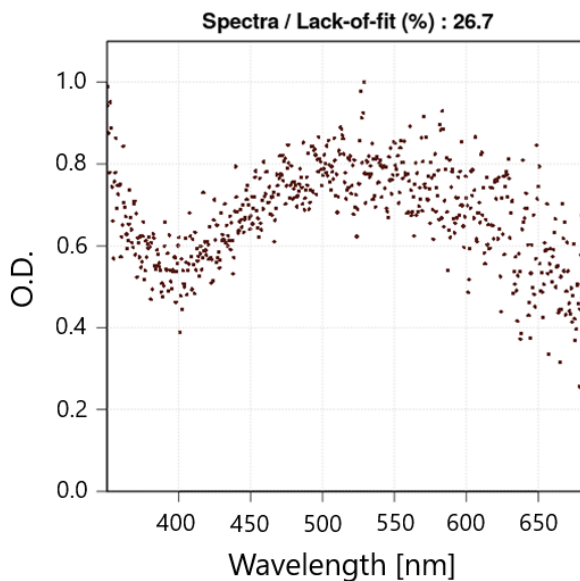


Figure 3.11: Absorption spectrum of intermediate forming after interaction of RRx-001 with quasi-free electron during radiolysis of RRx-001 (70 mM) in ethanol solution. Radiolysis data from ELYSE were analyzed using the software SK-Ana [117] (provided by Prof. Mehran Mostafavi).

Considering that I detected the interaction of the RRx-001 molecule with quasi-free and solvated electrons, and the picosecond pulse radiolysis measurement revealed the product of the interaction with the quasi-free electron, the question remains: Why

the product arising after the interaction of the solvated electron was not detected? It is possible that this product does not absorb in the visible region but in the UV region, which is below the measurement limit in picosecond pulsed radiolysis on the VD path. Therefore, I decided to conduct additional experiments on the VD2 path (nanosecond to millisecond time-scale experiments), extending slightly into the UV region, as its wavelength detection band ranges between 350 and 450 nm.

The measurements on VD2 were carried out for RRx-001 in ethanol solutions with molar concentrations of 2 and 70 mM. Moreover, to compare the effect of the argon atmosphere on the radiolysis results, two 2 mM solutions were prepared. The first one was measured under an argon atmosphere, while the second one was under air. As interesting results of these measurements, I present here four figures. For simplification, a transient particle arising after the interaction of quasi-free resp. solvated electron with RRx-001 will be marked X, resp. Y.

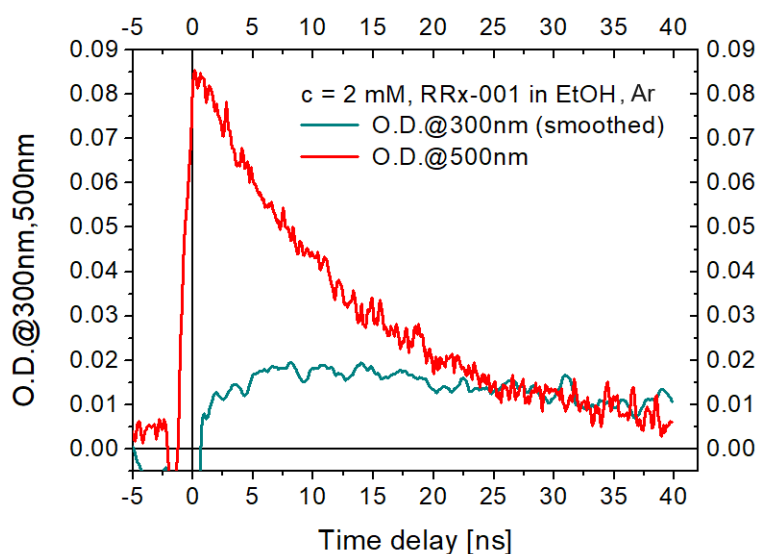


Figure 3.12: Kinetics of forming intermediates X (at 500 nm, red curve) and Y (at 300 nm, teal blue curve) measured up to 40 ns after absorption of a 5 ps electron pulse by a two mM ethanol solution of RRx-001.

The figure 3.12 shows a graph with clear kinetics of both transient species X and Y up to 40 ns after irradiation (VD2) of 2 mM ethanol solutions of RRx-001 under argon atmosphere. Kinetics of X was gained after focusing on wavelengths of 500 nm), while the kinetics of Y was obtained after extraction of data for 300 nm. Data for X are plotted in red colour. It can be observed that the intermediates forming in 2 mM solution after interaction of RRx-001 with quasi-free electron are forming at the very beginning after irradiation of solution (in order of ps); however, they gradually decay/interact, and their signal decreases in the spectrum, it almost disappears at the end of the measurement. While the product of the interaction of RRx-001 with solvated electron arises in solution in the order of ns and then seems stable at least to the end of measurement at 40 ns, it is necessary to take into account that the absorption spectrum for product X is very broad and it is difficult to separate it entirely from the absorption spectrum for the solvated electron at 600 nm. In the

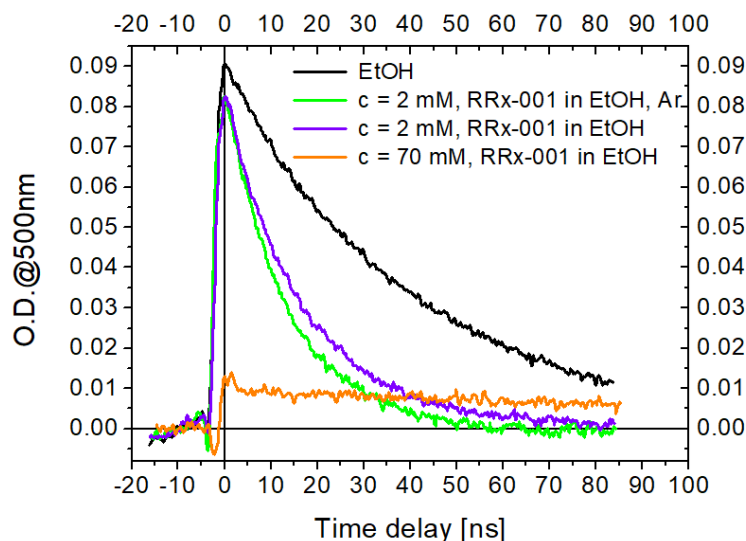


Figure 3.13: Kinetics of forming intermediates X (at 500 nm, red curve) measured up to 85 ns after absorption of a 5 ps electron pulse by two mM and one 70 mM ethanol solutions of RRx-001. The first two mM solution was measured under an argon atmosphere.

case that I extracted kinetic data for 500 nm from the row data in the form of a measured 3D spectrum (wavelength, time, intensity) in the Origin program, it cannot be completely sure that these data belong purely to species X. Still there is a possibility that the information about the solvated electron may have partially interfered there and the result must be judged in the light of this circumstance.

The graph in the Figure 3.13 finally shows the kinetics of X in ethanol (black curve) in both two mM RRx-001 solutions (green and violet curves) and 70 mM solution (orange curve). This graph also points to the effect of argon atmosphere because two two mM solutions were irradiated and measured - the first with an argon atmosphere and the second with air. It is clearly seen that the argon atmosphere has a slightly positive effect in the sense that the molecule of RRx-001 scavenges with slightly greater efficiency. The reason is that the radiolysis under the atmosphere allows the interaction of secondary low-energy electrons with the oxygen in the atmosphere and the solution. The graph also clearly demonstrates the difference between 2 and 70 mM solutions with regard to the ratio of scavenging of quasi-free and solvated electrons. The orange curve for 70 mM shows that RRx-001 interacts effectively with quasi-free electrons, and the residual solvated electrons are very quickly scavenged.

The following Figure 3.14 with seven graphs demonstrates the time evolution of signals for both Y and X/solvated electrons presented in a time-scale from 5 ns to 75 ns after irradiation of solutions. Each graph contains absorption spectra for two mM and 70 mM ethanol solution of RRx-001. Within this time-scale, it can be observed that the dominant signal of X/solvated electrons in a 2 mM solution of RRx-001 gradually decreases; thus, it can be assumed that solvated electrons are totally scavenged, while the dominant signal for Y remains almost the same in a 70 mM solution.

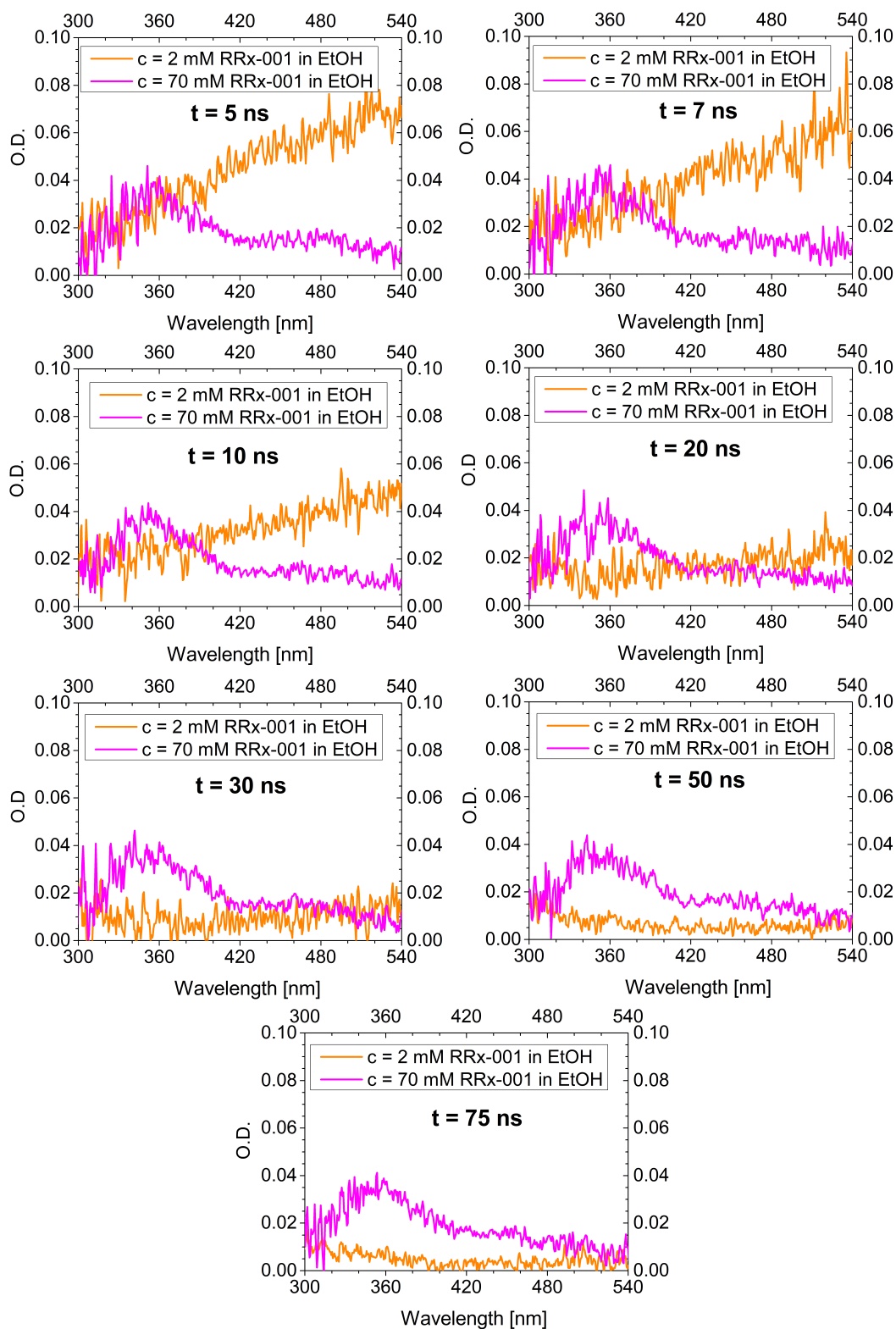


Figure 3.14: Absorption spectra of X and Y at various times (5 ns - 75 ns) after irradiation (VD2) of two ethanol solutions of RRx-001 with molar concentrations of 2 and 70 mM. Each graph shows the development (formation/disappearing) of both transient species in two solutions. In the case of X, its evolution in solution is unclear, as its absorbance around 520 nm cannot be distinguished from the absorbance of a solvated electron around 600 nm.

As a significant result of these measurements on VD2 and shown in the Figure 3.15, I extracted the absorption spectrum of transient species Y forming after the reaction of RRx-001 with solvated electrons. The species absorbs around 350 nm. However, 350 nm is also a lower limit of detection. Thus, measured absorption values at lower wavelengths than 350 nm may not accurately reflect the reality in the experiment, and the real maximum peak could be located lower than 350 nm.

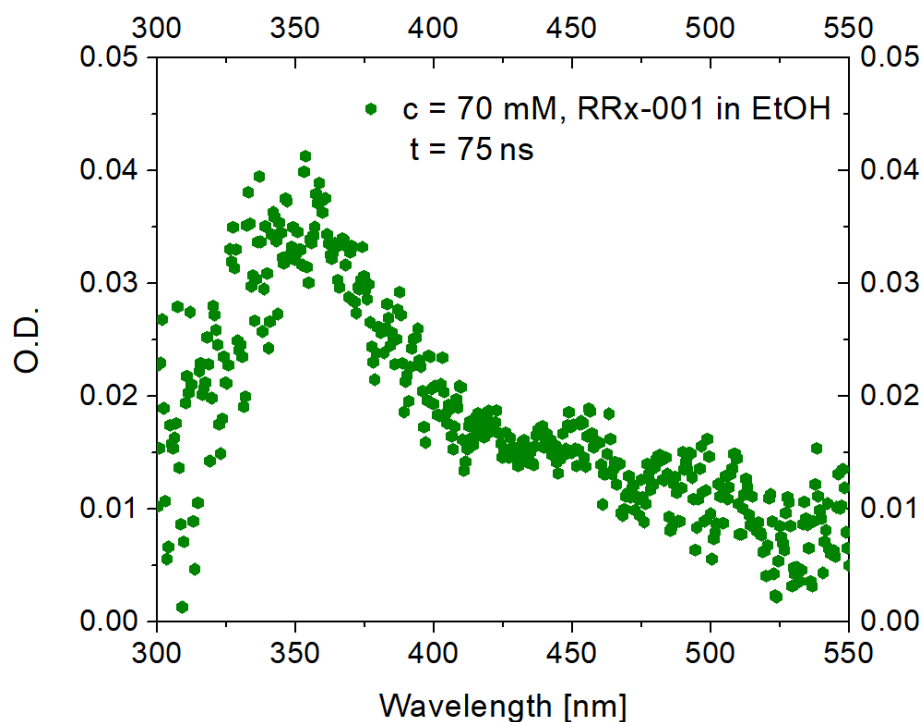


Figure 3.15: Absorption spectrum of Y in time of 75 ns after irradiation (VD2) of 70 mM ethanol solution of RRx-001.

Key insights gained about the RRx-001 based on PR

- Molecule of RRx-001 significantly scavenges both quasi-free and solvated electrons
 - Interaction of RRx-001 with quasi-free electrons results in the formation of new transient species absorbing around 520 nm, which is stable at least to 10 ns.
 - Molecule of RRx-001 interacts with solvated electrons with high value of the normalized rate constant $9.4 \times 10^9 \text{ dm}^3 \text{ mol}^{-1} \text{ s}^{-1}$. The newly formed intermediates absorb between 350 and 450 nm.
-

3.2.3 LONG TIME-SCALE: Products of radiolysis

A study of stable products coming from radiolysis is built on the combination of irradiating a solution with accelerated electrons on a microtron and subsequent subjection of irradiated solutions to NMR spectroscopy.

3.2.3.1 Radiolysis of RRx-001 in ethanol solution on microtron

In order to study stable products of interactions of secondary LEEs with RRx-001 in an ethanol solution, the ethanol solutions of RRx-001 (each of 12 ml) were irradiated on a microtron with highly accelerated electrons of energies around 16.5 MeV. Two types of experiments were done: Firstly, I examined the effect of radiation dose on forming stable products. Secondly, I irradiated RRx-001 in three solvents - ethanol, methanol, and fully deuterated methanol. Irradiated solvents were then investigated by nuclear magnetic resonance spectroscopy (in collaboration with Mgr. Jiří Pinkas, PhD. from JH IPC) in order to reveal the product of interactions of secondary LEEs with RRx-001 in solution.

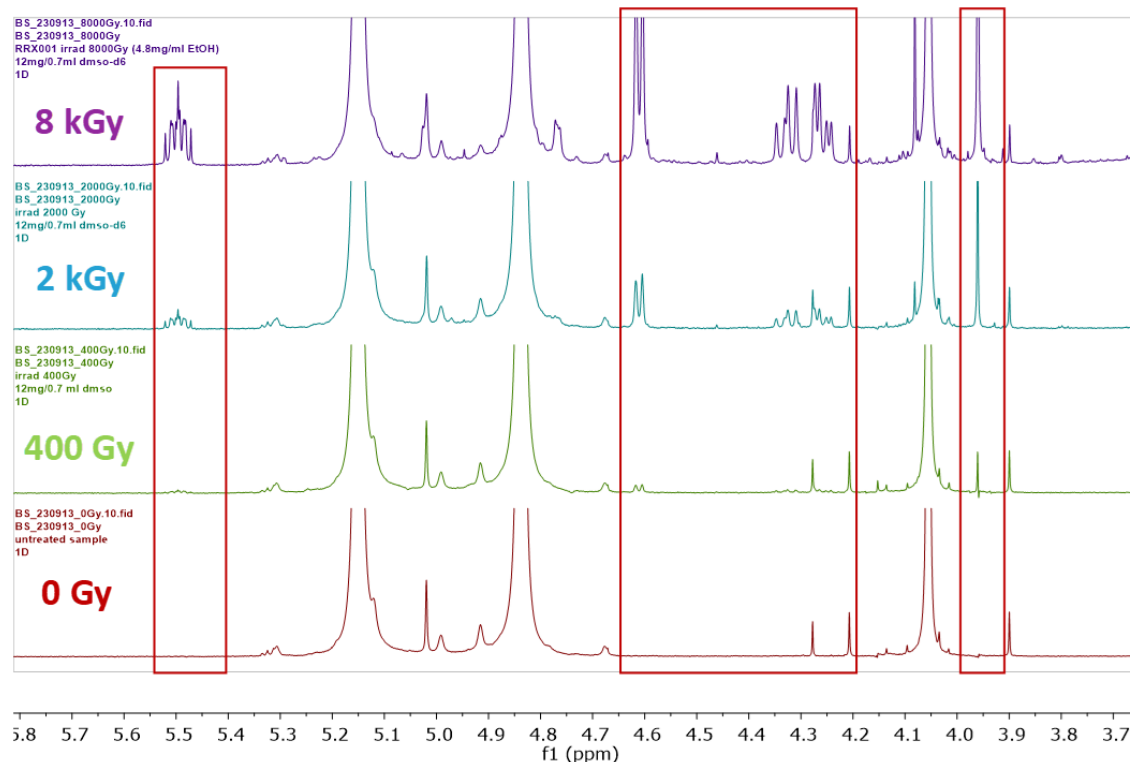


Figure 3.16: ¹H nuclear magnetic resonance spectra measured in DMSO-d₆ for identical prepared ethanol solution of RRx-001 after irradiation of different doses of ionizing radiation (0, 400, 2 000, and 8 000 Gy). The red-marked area points to the formation of a product whose intensity increases with the dose. (In collaboration with Mgr. Jiří Pinkas, PhD.)

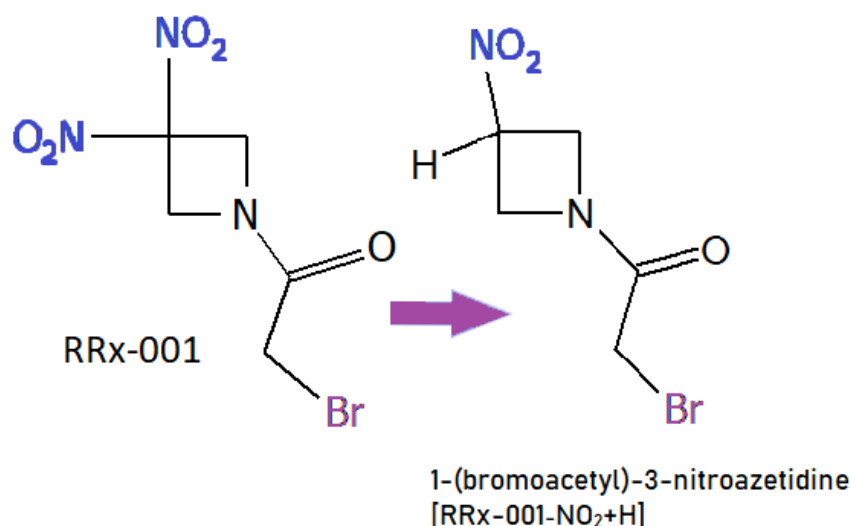


Figure 3.17: Structural pattern of RRx-001 and product formed after radiolysis of RRx-001 in ethanol solution.

The first experiment consisted of irradiating the solutions of RRx-001 in ethanol with different doses (0, 400, 2000, and 8000 Gy). Each solution had a volume of 12 ml and a molar concentration of 17.909 mM (4.8 mg/ml). Nuclear magnetic resonance spectra were measured for all irradiated solutions, and the results can be seen in the Figure 3.16. A new signal appears in red-marked areas with the increasing dose. The signal was assigned to neutral molecule 1-(bromoacetyl)-3-nitroazetidine shown in the Figure 3.17. It is a derivative of RRx-001 with hydrogen instead of the NO₂ group. Spectra have characteristic signals for the methine group at 5.46-5.53/71.7 ppm ($\delta\text{H}/\delta\text{C}$). Conversion of RRx-001 to newly formed product was <1%, 4%, and 13% at 400, 2000, and 8000Gy doses, respectively.

Revealed neutral product [M-NO₂+H] by NMR spectroscopy is significantly similar to one of the negative fragments [M-NO₂]⁻ detected by me after the electron attachment to RRx-001 in the gas phase. These two species differ in the presence of hydrogen and the charge. The question remains: What is the source of incoming hydrogen?

The ethanol solvent appears as the most probable source of hydrogen. For this reason, the RRx-001 was irradiated in three different solvents: ethanol, methanol, and fully deuterated methanol CD₃OD with the same concentration of RRx-001. The mass concentration of 4.8 mg/ml remains the same as in the previous measurement. The NMR spectra after irradiation are shown in the Figure 3.18. In the case of methanol solvent, I observed the same neutral product [M-NO₂+H] as in ethanol. However, irradiation in deuterated methanol leads to a different spectrum, and D incorporation was not observed.

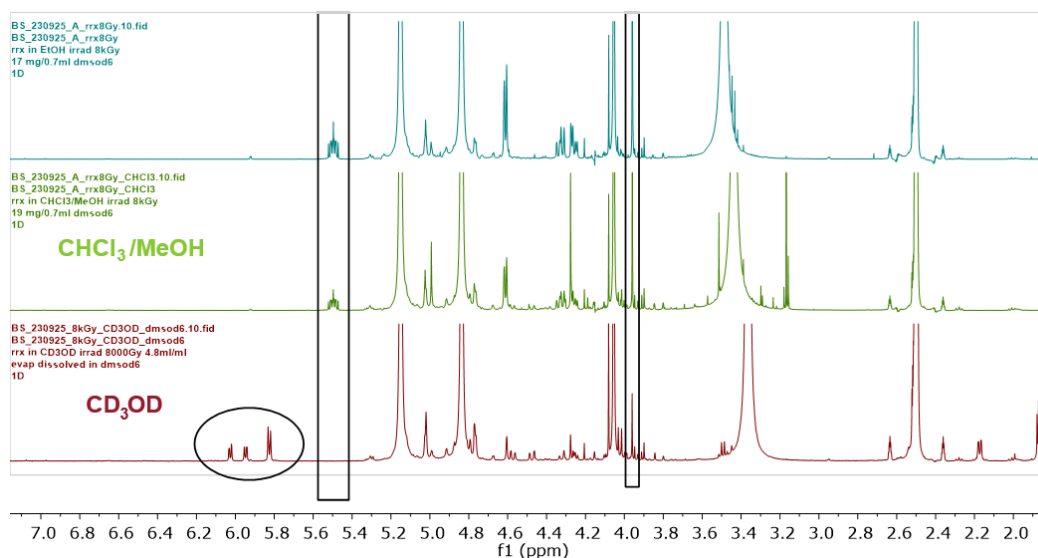


Figure 3.18: Examination of origin of H in a product [M-NO₂+H]. ¹H nuclear magnetic resonance spectra measured in DMSO-d₆ for samely concentrated RRx-001 (17.809 mM/ 4.8 mg/ml) in ethanol (data on the top), in methanol (in the middle), and the deuterated methanol CD₃OD (data at the bottom). (In collaboration with Mgr. Jiří Pinkas, PhD.)

Further, I investigated the possible role of a dose rate on the radiolysis of RRx-001 in an ethanol solution because this effect is known and is possible. For this reason, I prepared four solutions of RRx-001 of the same mass concentration (4.8 mg/ml), and I let them be exposed to highly accelerated electrons for varying lengths of time so that the final dose was the same 8 kGy, but the dose rate was therefore different. The first sample was a reference solution without irradiation. The other three samples were irradiated for 5 min, 20 min, and 40 min, corresponding to the dose rates of 26.7 Gy/s; 6.7 Gy/s; resp. 3.3 Gy/s. ¹H NMR spectra measured for these four solutions are plotted in the Figure 3.19. From the graphs, it can be concluded that the ¹H NMR profiles of irradiated solutions are the same and do not depend on the dose rate.

In the next step, I wanted to investigate the effect of the type of atmosphere on radiolysis. For this reason, it was necessary to select the best concentration from already used concentrations to see the apparent effect of the atmosphere on NMR spectra. Therefore, I prepared three solutions with a mass concentration of 4.8 mg/ml, three with a mass concentration of 9.6 mg/ml and three with mass concentrations of 16.8 mg/ml. Then, each concentration was irradiated with three different doses (2, 8, and 20 kGy). Finally, ¹H NMR spectra were measured for each irradiated solution, and results are plotted in the Figures: 3.20, 3.21, and 3.22. Each figure contains three graphs) represents one concentration irradiated with three different doses. After comparing the dose effect for each concentration, it can be summarized that the most visible effect is seen for the lowest mass concentration, 4.8 mg/ml.

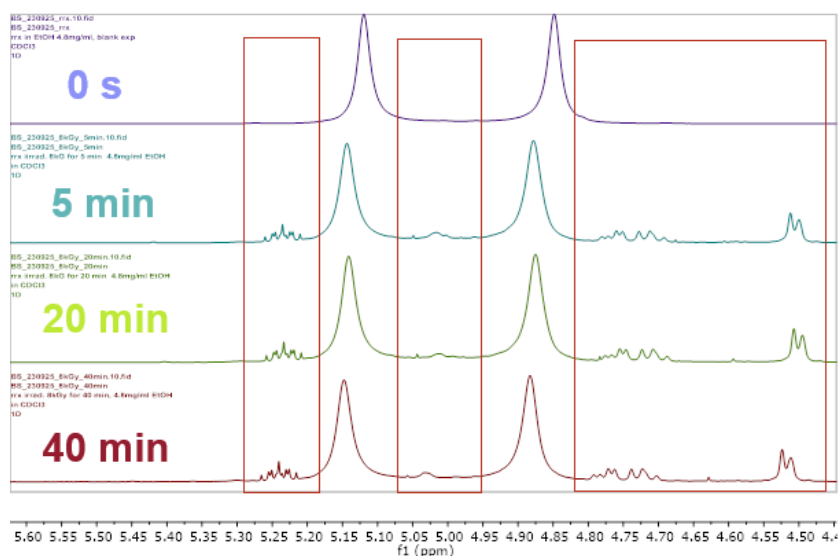


Figure 3.19: Effect of dose rate on radiolysis. ^1H NMR spectra of the chemical residues after evaporation after dissolution in CDCl_3 . The chemical residues were gained after evaporation of each of the same concentrated RRx-001 (4.8 mg/ml) in ethanol solution irradiated with a dose of 8 kGy, however with different dose rates (irradiation times were 0, 5, 20, and 40 min). (In collaboration with Mgr. Jiří Pinkas, PhD.)

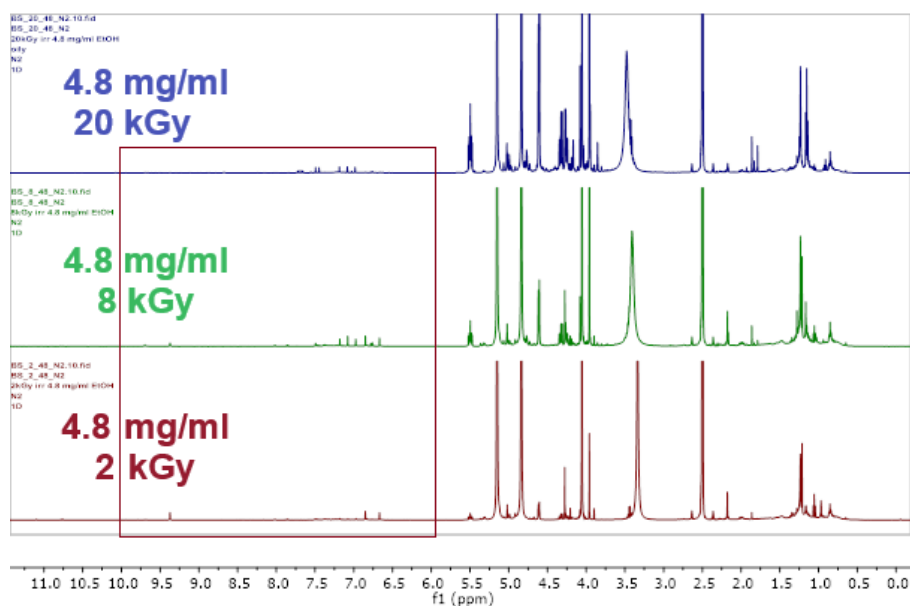


Figure 3.20: Study of the dose effect at a certain concentration. ^1H nuclear magnetic resonance spectra were measured for RRx-001 in ethanol solutions with the same concentrations (17.809 mM/ 4.8 mg/ml) irradiated under the nitrogen atmosphere with different radiation doses (2, 8, and 20 kGy). (In collaboration with Mgr. Jiří Pinkas, PhD.)

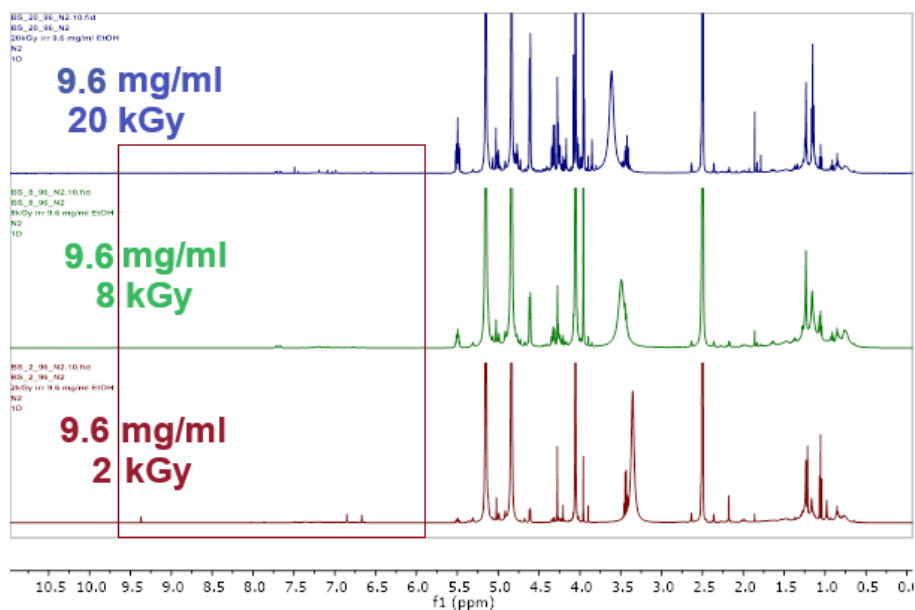


Figure 3.21: Study of the dose effect at a certain concentration. ¹H nuclear magnetic resonance spectra measured for RRx-001 in ethanol solutions with the same mass concentrations (9.6 mg/ml) irradiated under the nitrogen atmosphere with different radiation doses (2, 8, and 20 kGy). (In collaboration with Mgr. Jiří Pinkas, PhD.)

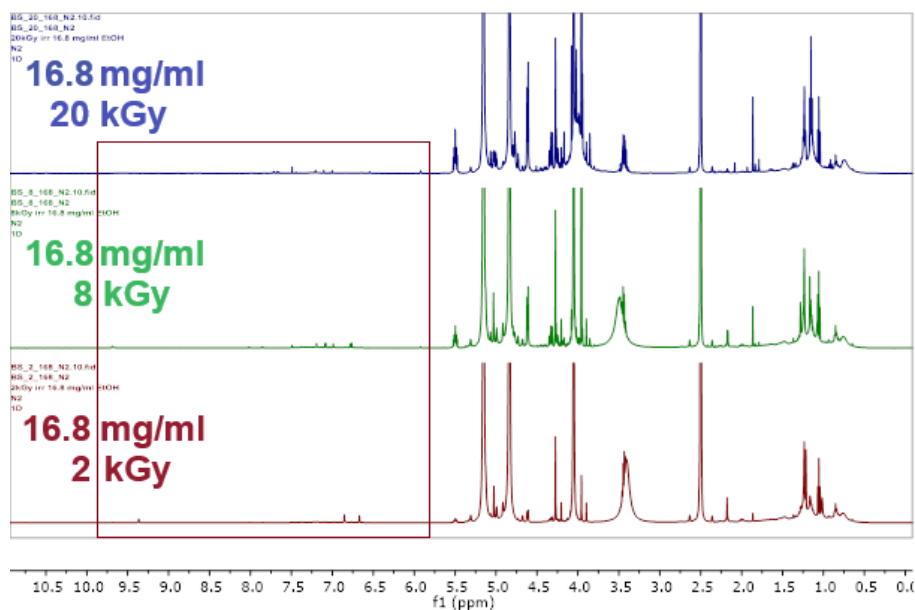


Figure 3.22: Study of the dose effect at a certain concentration. ¹H nuclear magnetic resonance spectra measured for RRx-001 in ethanol solutions with the same mass concentrations (16.8 mg/ml) irradiated under the nitrogen atmosphere with different radiation doses (2, 8, and 20 kGy). (In collaboration with Mgr. Jiří Pinkas, PhD.)

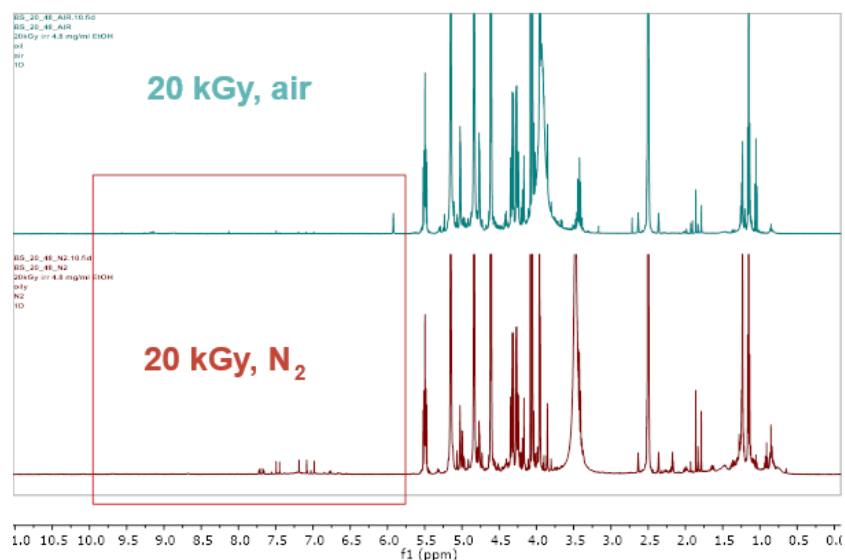


Figure 3.23: Study of the effect of the atmosphere on radiolysis. ^1H nuclear magnetic resonance spectra measured for RRx-001 in ethanol solutions with the same concentration (17.809 mM/ 4.8 mg/ml) irradiated under the air/ nitrogen atmosphere with the dose of 20 kGy. (In collaboration with Mgr. Jiří Pinkas, PhD.)

Based on this finding, the final experiment was dedicated to investigate the effect of air/ N_2 atmosphere on the radiolysis of RRx-001 in ethanol solution with a mass concentration of 4.8 mg/ml. One solution was in the air, and the second was under N_2 atmosphere. Both were irradiated with the radiation dose of 20 kGy to see maximal intensities. Results in the form of later measured NMR spectra for both solutions are presented in the Figures. 3.23. These two ^1H NMR spectra revealed that radiolysis under N_2 atmosphere leads to a higher fraction of the product than radiolysis in the air. Oxygen is a strong electron scavenger; therefore, the present result, replacing the air with N_2 , indicates that the final product $[\text{M}-\text{NO}_2+\text{H}]$ observed using NMR spectroscopy may primarily arise from the interaction of RRx-001 with secondary low-energy electrons. It is the same conclusion as in the case of measurement under an inert argon atmosphere when irradiating 2 mM solution of RRx-001 on the ELYSE platform, VD2.

Key insights: the RRx-001 after irradiation on microtron

- Stable product of radiolysis of RRx-001 in ethanol was identified as neutral molecule $[\text{M}-\text{NO}_2+\text{H}]$.
 - Molecule of RRx-001 shows its radiation resistance with lower doses. The first significant effect is observed with the dose of 400 Gy (note: the lower applied dose was 200 Gy).
 - The effect of the dose rate on the radiolysis of RRx-001 in ethanol was not observed.
 - Radiolysis of ethanol solution of RRx-001 under N_2 atmosphere leads to a higher fraction of the product than radiolysis in the air, probably due to the oxygen as a strong electron scavenger.
-

3.2.4 Final discussion and conclusion of the experiments with RRx-001

Experiments of electron attachment to molecule RRx-001 in the gas phase show the trend of stabilisation of parent anion with increasing ethanol solvation. Simultaneously, the fragmentation channels are closing. EA experiments were focused on conditions with a single RRx-001 molecule per cluster. As the molecule is very stable up to high sublimation temperatures, dimers can also be explored in the future.

From the point of view of picosecond pulse radiolysis experiments, the interaction of RRx-001 in ethanol solution with both quasi-free and solvated electrons was confirmed in case of solvated electron with the normalised rate constant with high value of $9.4 \times 10^9 \text{ dm}^3 \text{ mol}^{-1} \text{ s}^{-1}$ indicating strong interaction. Reaction with quasi-free electrons with RRx-001 leads to the formation of a product X with a broad absorption band around 520 nm. This reaction is very fast and occurs within a few fs. In fact, the lifetime of the quasi-free electron is very short, but it is a very delocalised electron that can react very quickly with a solute. The result of the interaction of RRx-001 with solvated electrons is transient species Y with a maximum absorption band of around 350 nm.

To confirm our suggested origin of the new transient species detected during pulse radiolysis, the absorption spectra for potential candidates were calculated (by Prof. Milan Ončák, PhD. from the University of Innsbruck). These calculated absorption spectra are shown in the Figure 3.24.

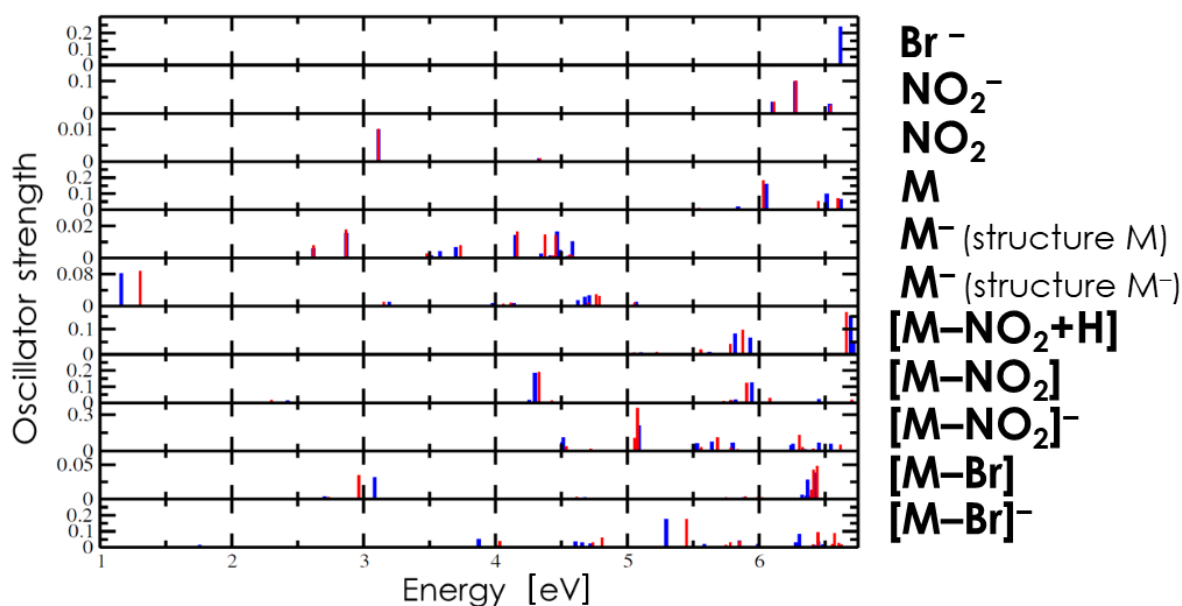


Figure 3.24: Calculated absorption spectra of anion and neutrals: M^- , and M^- in geometry of neutral, M , Br^- , NO_2^- , NO_2 , $[M-NO_2+H]$, $[M-NO_2]$, $[M-NO_2]^-$, $[M-Br]$, and $[M-Br]^-$ in gas phase, resp. in ethanol solution (peaks in black, resp. red colours).

In the Figures 3.25, resp. 3.26, the calculated absorption spectra were compared with two absorption peaks for two unknown transient species forming arising in solution after interaction of RRx-001 with quasi-free resp. solvated electrons were observed using pulse radiolysis. The areas in the graph are assigned to the absorption areas of the candidates for the observed species. It can be seen that in neither of the cases, there is no reaction product directly fitting to the band.

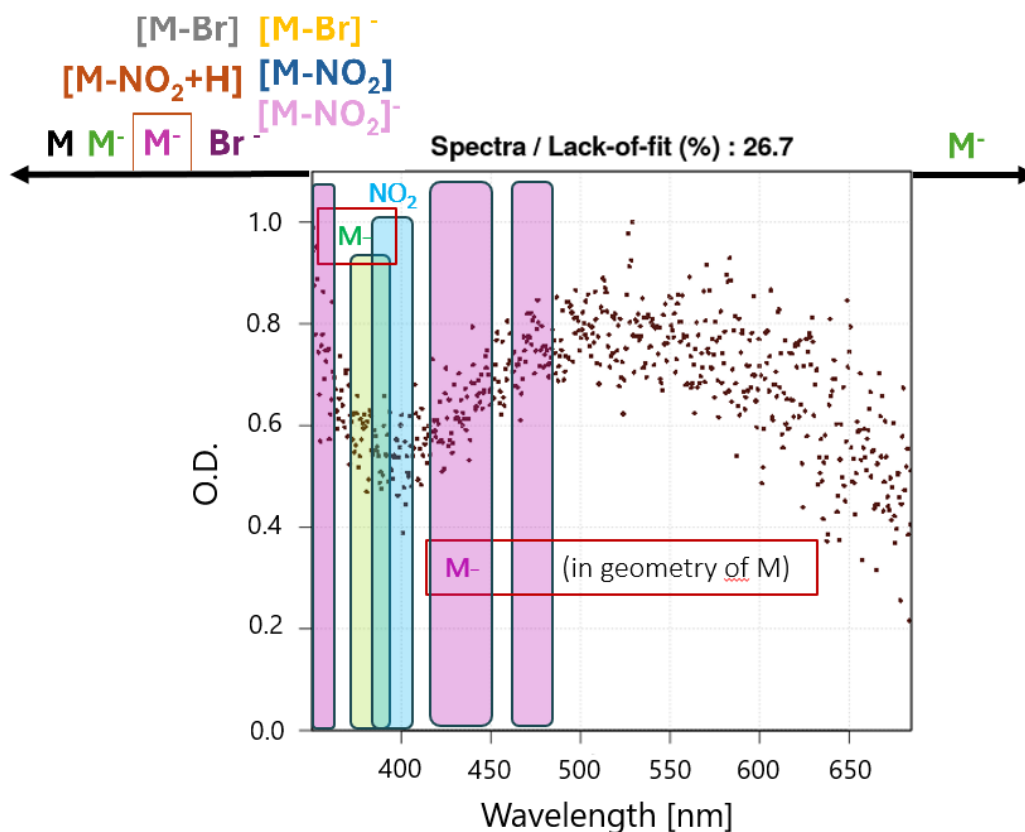


Figure 3.25: Absorption spectrum of unknown species with broad absorption band with a maximum around 520 nm, observed using of picosecond pulse radiolysis on VD and after application of software, SK-Ana [117]. An additional graphic was created based on the calculation shown above, which approximately represents wavelength regions where the potentially forming species could absorb.

In the case of X (Fig.3.25), forming after interaction of the quasi-free electron with RRx-001, it absorbs at a broad band between 400 nm and 690 nm and a maximum around 520 nm. The wide wavelength range corresponds to energies from 1.8 eV to 3.1 eV. Considering the comparison, a first assumption might be that the new species is most probably the negative ion of RRx-001 in its specific geometry after electron capturing. However, this assumption is rejected upon revealing that the newly formed species is stable at least up to a time of 10 ns, which does not quite point to the short-lived excited parent ion in any of its geometry. Still, it is most probable that it is RRx-001^- . The further hypothesis is that the absorption band might originate from an anion in some specific form formed via dissociation of RRx-001^- - possibly its dimer $(\text{RRx-001})_2^-$.

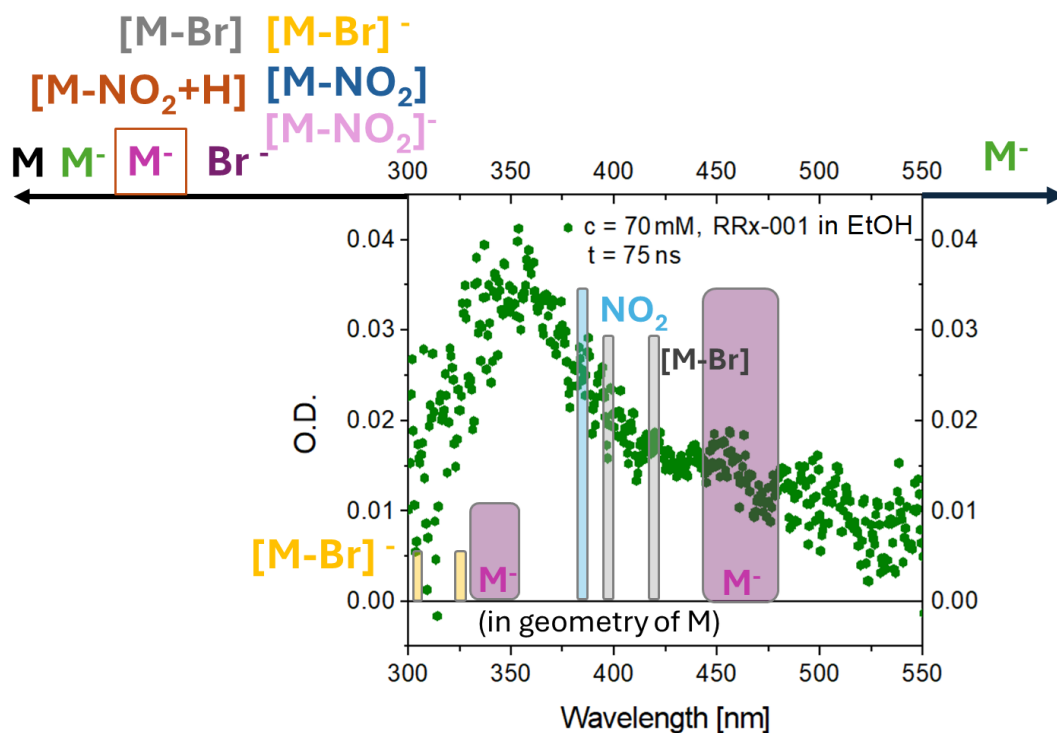


Figure 3.26: Absorption spectrum of unknown species with broad absorption band with a maximum around 350 nm, observed using pulse radiolysis with ns-ms time-scale on VD2 and after application of Origin program. An additional graphic was created based on the calculation shown above, which approximately represents wavelength regions where the potentially forming species could absorb.

In the case of Y (Fig.3.26), forming after interaction of the solvated electron with RRx-001 demonstrates the crucial absorption band between 320 nm and 450 nm with a maximum of around 350 nm. However, because of the detection limit of around 350 nm, it is not clear how reliable the signal is. The range corresponds to the energy range from 3.10 eV to 3.87 eV. It may be RRx-001^- or/and neutral NO_2 as is shown in the graphical representation.

Experiments on microtron revealed a product of radiolysis, which also seems stable with radiation dose because, at 400 Gy, no product is observed yet. In this study, the product was detected at higher doses at (2 kGy). The product was identified as neutral $[\text{M-NO}_2+\text{H}]$, a protonated fragment of RRx-001. This neutral product is formed under very high irradiation doses of 8 kGy. NO_2 loss is in good agreement with gas phase studies; neutralization of anion by proton transfer seems reasonable. The question arises if this product is forming as a result of the interaction of LEEs. If that is the case, the reaction intermediate exists (in the form of a predissociated anion, dimer, etc.), which can be linked to pulse radiolysis species with an absorption band around 520 nm. It is improbable that anion directly transforms to neutral without any intermediate from the point of view of results coming from the picosecond pulse radiolysis. It was also discovered that this product does not change its intensity with the dose rate and that the atmosphere has some effect on radiolysis, when the inert atmosphere causes higher product yields than the air environment.

3.3 Studies on fullerenes considering π - π complex

This result section presents a study on fullerenes considered for the concept of π - π complex. First, for the experimental study, fullerenes as buckminsterfullerene C_{60} and its water-soluble derivatives C_{60} pyrrolidine tris-acid and fullerenols were selected, which were subsequently subjected to preliminary study using a pulse radiolysis method with an nanosecond to millisecond time-scale on the bend line (VD2) of the ELYSE platform during my stay at the ICP in Orsay. This section also brings a discussion when describing a selective route for choosing a suitable derivative for more profound studies using pulse radiolysis. After the selection, I focused on only one type of molecule: fullerenols. Therefore, primarily, in the remainder of this study, the results from pulse radiolysis experiments on fullerenols are presented. Beyond the scope of my aim, I also marginally dealt with the method of detecting the π - π complex. For that, I selected a method of fluorescence spectroscopy performed in Prague at JH IPC, and this short study is discussed in the last part of this chapter. Subsequently, all the outputs that this study has brought are discussed.

A crucial property of the studied molecule resulting from our bio-motivation is its solubility in water or bio-medium. For the radiosensitizing purpose of the molecule, it is essential to insert it into the living tissue and be able to move to the destination in a tumour cell without any difficulties. Nevertheless, a pure molecule of C_{60} is not soluble in water. The best solvents for C_{60} are aromatic solvents, especially 1-chloronaphthalene (51 mg/ml) or 1-phenylnaphthalene (50 mg/ml). All solvents suitable for this molecule are listed in table 3.2. Based on the non-water solubility of pure C_{60} , it was highly demanded to find its water-soluble derivatives. Molecules of C_{60} pyrrolidine tris-acid and fullerenols are soluble in water with the declared highest mass concentration of 0.5 mg/ml, resp. 50 mg/ml. Further requirements on the studied molecules were supposed to be met by the experimental technique, which is discussed in the next paragraph.

The time-resolved pulse radiolysis experiment has high requirements on the sample concentration in solution and, at the same time, special requirements on the solvent, which does not interfere with the spectroscopic signatures of studied systems such as quasi-free or solvated electrons. According to my literature research on the best solvents for studied compounds, three solutions were prepared. The first solution was the solution of pure C_{60} in 1,4-dimethylbenzene, which was available in a chemical laboratory at the ICP, UMR8000. The highest declared solubility was found with a value of 5.9 mg/ml [118]. The second solution was a water solution of C_{60} pyrrolidine tris-acid with the addition of NaOH for increasing pH to ~ 13 when C_{60} -PTA is the most soluble in water. The highest solubility value for this case is 0.5 mg/ml according to the Sigma-Aldrich [89]. However, despite heating and stirring, I prepared a solution with pH ~ 13 and a mass concentration of only 0.025 mg/ml. The third solution was a water solution of fullerenols with a stated mass concentration higher than 50 mg/ml. However, as in a previous case, I could prepare the solution with a maximum mass concentration of only 6 mg/ml.

Solubility of C ₆₀ molecule in solvents		
solvent	c_{mass} [mg/ml]	c_{mol} [mmol/l]
1-chloronaphthalene	51 [119]	70.77
1-phenylnaphthalene	50 [119]	69.38
dimethylnaphthalene	36 [119]	49.96
1-bromo-2-methylnaphthalene	34.8 [118]	48.29
1-methylnaphthalene	33.2 [118]	46.07
1, 2-dichlorobenzene	24.6 [118]	34.14
1, 2, 3, 5-tetramethylbenzene	20.8 [118]	28.86
1, 2, 4-trimethylbenzene	17.9 [118]	24.84
(+)-trans-1,2- dibromocyclohexane	14.28 [120]	19.82
1, 2-dibromobenzene	13.8 [118]	19.15
1, 3-dibromobenzene	13.8 [118]	19.15
1, 2, 4-trichlorobenzene	10.4 [118]	14.43
1, 2, 3-tribromopropane	8.31 [120]	11.53
cyclohexyl iodide	8.06 [120]	11.18
CS ₂	7.9 [119]	10.96
quinoline	7.2 [118]	9.99
1, 5, 9-cyclododecatrien	7.14 [120]	9.91
chlorobenzene	7 [119]	9.71
thiophenol	6.91 [120]	9.59
2-methylthiophene	6.8 [119]	9.44
1, 4-dimethylbenzene	5.9 [118]	8.19
1, 2, 3, 4-tetramethylbenzene	5.8 [118]	8.05
bromoform	5.64 [120]	7.83
methoxybenzene	5.6 [119]	7.77
1, 1, 2, 2-tetrachloroethane	5.3 [119]	7.35

Table 3.2: Research on solubility of C₆₀ molecule in best solvents stated in mass concentrations c_{mass} [mg/ml] and converted to molar concentrations c_{mol} [mmol/l], solubility are valid for solutions at room temperature and are listed with decreasing value.

Molecules of C_{60} and its water-soluble derivatives were studied in a static cell configuration of the ELYSE VD2 line. Every cell with the sample belonged to a reference cell containing only a pure solvent. C_{60} was measured in 1,4-dimethyl benzene, and water-soluble fullerenes were measured in water. Thus, it was necessary to use two reference cells. The first contained 1,4-dimethyl benzene, and the second was filled with water.

3.3.1 Pulse radiolysis experiments on fullerenes

In the next step, 2 ml of each prepared solution was poured into a measuring cell and placed in the cell holder. Then, first experiments of pulse radiolysis were carried out on VD2. Three preliminary results were obtained, and the three main conclusions were reached based on them.

It was shown that the first solution of C_{60} in 1,4-dimethylbenzene does not scavenge solvated electrons by a molecule of C_{60} . Instead, LEEs react with the aromatic ring in 1,4-dimethylbenzene and cause its excitation into the triplet state. It could also explain why the aromatic solvents are generally not used at the pulse radiolysis experiments.

The second solution of C_{60} -PTA in water and pH ~ 13 exhibited very low scavenging of solvated electrons during pulse radiolysis experiments. Nevertheless, the very low solubility of C_{60} -PTA led only to detecting a very low, non-significant signal, which could not be a sufficient quality basis for further experiments. For this reason, a molecule of C_{60} -PTA for measurements with the pulse radiolysis method was inconvenient.

Measurement with the third solution of fullerenols in the water finally brought positive results. The measurement output is a graph shown in the figure 3.27. It is the main result that I obtained during measurements on the bend line of the ELYSE platform: The figure 3.27 shows an absorbance decay of the solvated electrons at 600 nm in water solution (shown with the black curve) and in a water solution of fullerenol (illustrated with the red curve). This kinetics was measured within a few nanosecond time range and after a 5 ps electron pulse.

A more detailed background of the meaning of the chart is as follows. A high-energy radiolysis beam (7.8 MeV electrons) from the accelerator irradiates a solution with a sample in a cell. Radiolysis of a solution occurs, and one of the secondary species formed after irradiation in a solution is secondary electrons. They gradually slow down and become solvated electrons by turning water dipoles in their surroundings. The energy needed for the solvated electron to become free is about 2 eV, corresponding to the excitation band in the detected absorption spectrum. The time evolution of such a band is then presented in the Figure 3.27. A steep increase to 20 ns time delay characterizes the quantity of secondary LEEs formed in a solution as a secondary species after irradiation. On the contrary, a decrease symbolizes the quantity of free secondary electrons, the rest of the electrons scavenged in a studied molecule. After comparing the scavenging of secondary LEEs in the water solution of a sample and pure water, it can be seen that secondary LEEs significantly react with fullerenols.

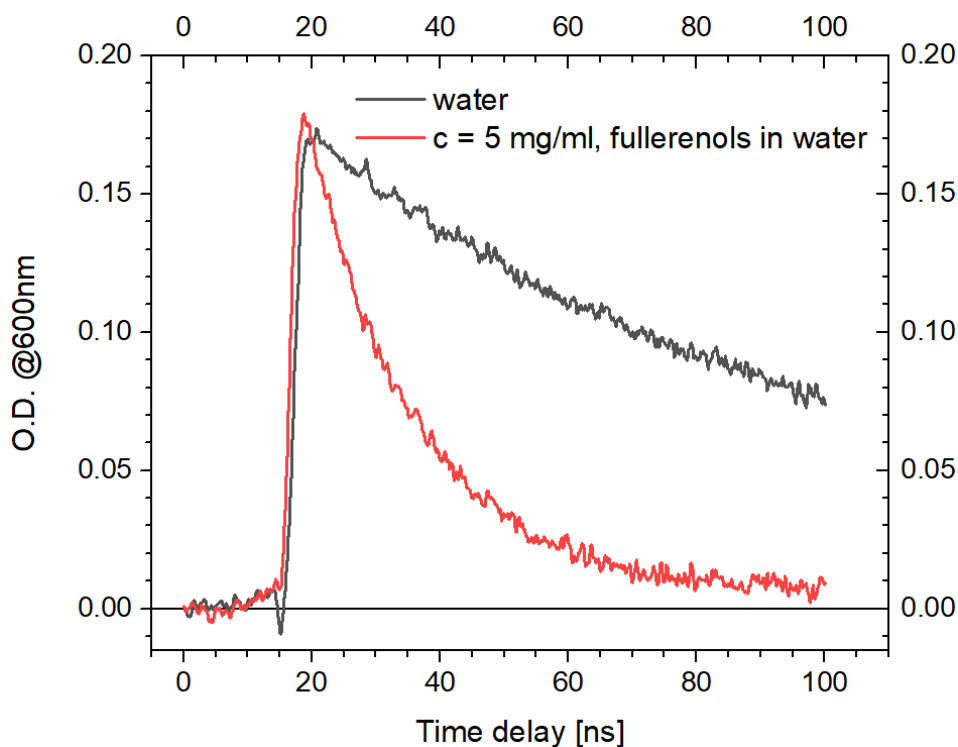


Figure 3.27: Absorption decay of solvated electrons in pure water solution in a static reference cell (black curve) and water solution fullerenols with mass concentration 5 mg/ml in static cell (red curve). Kinetics were measured after 5 ps electron pulse in solutions on VD2.

3.3.2 Picosecond pulse radiolysis experiments on fullerenols

Molecules of fullerenols in water solutions were studied in a static cell configuration of the ELYSE VD line. The results were compared to the reference cell containing only a pure solvent.

First, I performed picosecond pulse radiolysis on fullerenols in a water solution with a mass concentration of 6 mg/ml. I examined the interaction of both quasi-free and solvated electrons with fullerenols. As a result of this measurement, the kinetics for solvated electrons were gained and are plotted in the Figures 3.28,3.29. The kinetics of solvated electrons in the water solution of fullereneol is represented by the red curve; in pure water, it is represented by the blue and black curves. From the top graph with a time-scale up to 30 ps, it is visible that the amount of solvated electrons in water is at the same level as in the case of water solution of fullerenols. The reason is that quasi-free electrons did not react with fullerenols and gradually became solvated, which could be detected. Thus, the interaction of quasi-free electrons with fullerenols of that concentration and in water solution was not observed. The bottom graph measured up to 10 ns shows that the concentration of solvated electrons decreases faster in the presence of fullerenols in water compared to pure water. It indicates an interaction of the solvated electron with fullerenols. In summary, fullerenols interact under these conditions (concentration, solvent) only with solvated electrons.

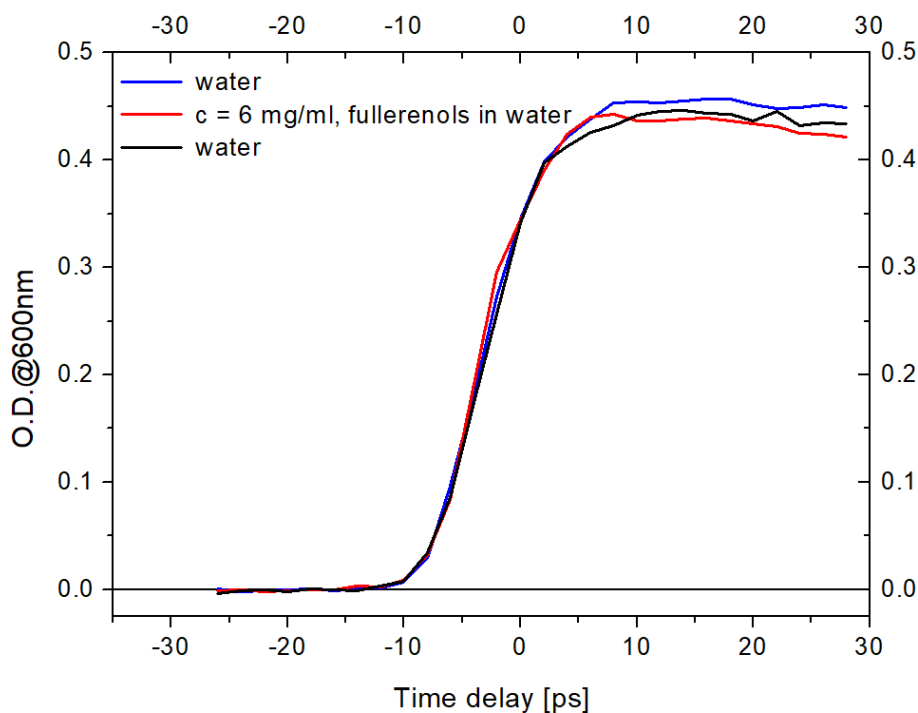


Figure 3.28: Kinetics of solvated electrons up to 30 ps after absorption of a 5 ps electron pulse by a sample of water (blue and black curves), and fullerenols in water solution (red curve) on VD.

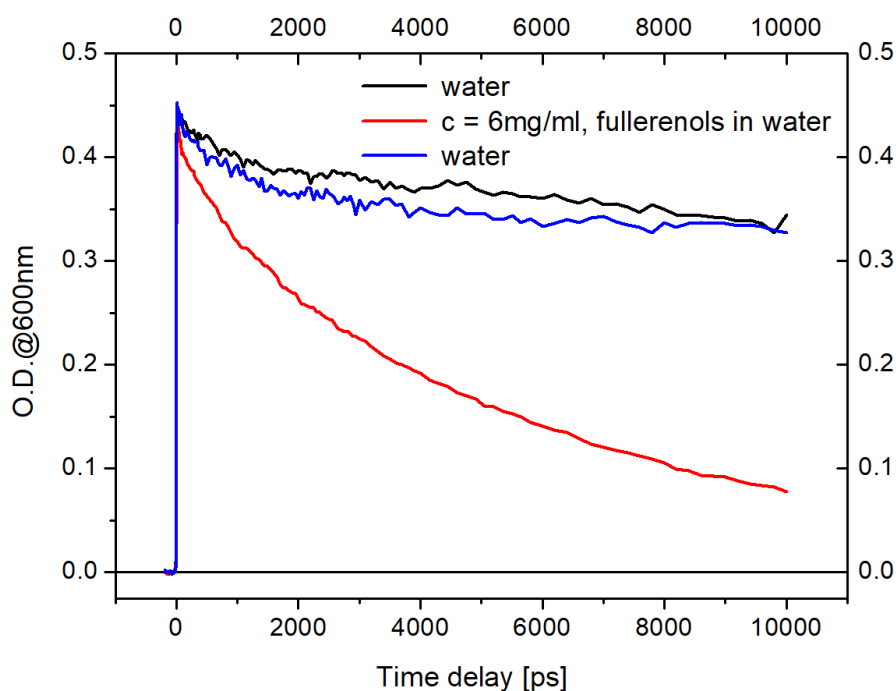


Figure 3.29: Kinetics of solvated electrons up to 10 ns after absorption of a 5 ps electron pulse by a sample of water (blue and black curves), and fullerenols in water solution (red curve) on VD. The graph points to interaction with solvated electrons.

Further, I focused more on the interaction of fullerenols with solvated electrons to study the dependency of scavenging on the concentration of fullerenols. Therefore, I investigated aqueous solutions of fullerenols with various mass concentrations (2, 3, 4, 5, and 6 mg/ml) using picosecond pulse radiolysis in a static cell with a volume of 3 ml. The kinetics of solvated electrons measured up to 10 ns is shown in the Figure 3.30. The kinetics of solvated electrons in water is represented by the blue curve, in water solutions of fullerenols (various concentrations) by the other curves. The amount of solvated electrons decreases with the increasing concentration of fullerenols in water. It is an explicit confirmation of the interaction between fullerenols and solvated electrons.

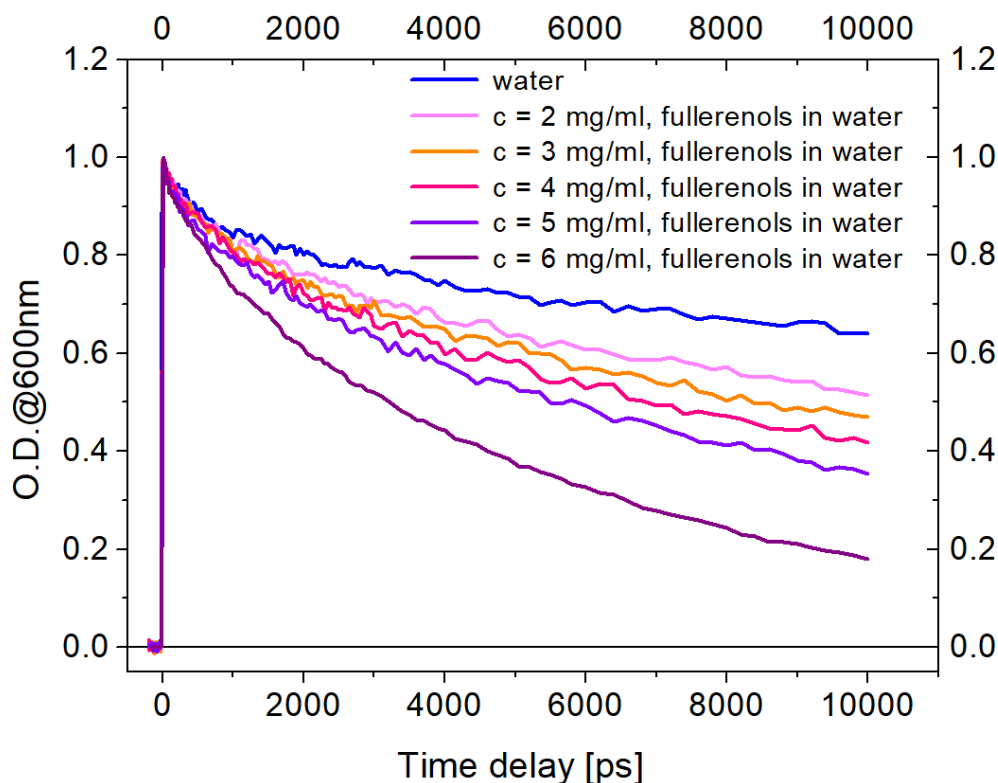


Figure 3.30: Kinetics of solvated electrons up to 10 ns after absorption of a 5 ps electron pulse by a sample of water (blue curve), and water solution of fullerenols with various concentrations (other curves). The graph reveals interaction with solvated electrons.

The kinetics for solvated electrons in solution with a concentration of 6 mg/ml dramatically decrease compared to other decreases when the mass concentration of fullerenols is increased by 1 mg/ml. Moreover, 6 mg/ml is the value of mass concentration equal to my maximum attainable solubility. Therefore, the result of this measurement does not have to be reproducible.

As in the case of molecule RRx-001, based on the previous graph in the Figure 3.30, a table with data was prepared to determine the normalized rate constant for the interaction of solvated electrons with fullerenols (Table 3.3). Only the data from the measurement of 6 mg/ml solution of fullerenols were not included for two reasons:

they were measured on different days, the mass concentration of 6 mg/ml was on the edge of the achievable solubility with regard to my existing experimental experience. Firstly, based on column " $T_{1/2}$ [s]" in the table, absolute rate constants were calculated for each concentration of measured water solutions of fullerenols. The last column of the table belongs to calculated absolute rate constants.

c_{mass} [mg/mL]	c_{mol} [mol/L]	Y	$Y_{1/2}$	$T_{1/2}$ [s]	k_{abs} [s ⁻¹]
0	0	1.0	0.50	30E-09	2.3E+07
2.0	0.0013	1.0	0.50	11E-09	6.3E+07
3.0	0.002	1.0	0.50	8.6E-09	8.0E+07
4.0	0.0027	1.0	0.50	7.1E-09	9.8E+07
5.0	0.0033	1.0	0.50	5.9E-09	1.2E+08

Table 3.3: The table includes data significant for determining the normalized rate constant describing the reaction of solvated electrons with fullerenols demonstrated on the graph in the Figure 3.30, from which the data originate. The table does not include the data for the 6mg/ml solution. The columns of c_{mass} [mg/ml] and c_{mol} [mol/l] show mass concentrations and molar concentrations, respectively, of four measured water solutions of fullerenols, Y is the amplitude - a maximal reached optical density at 600 nm for solvated electrons in solution after its irradiation, $Y_{1/2}$ is half of the amplitude, $T_{1/2}$ [s] is the time when $Y_{1/2}$ is reached, and k_{abs} [s⁻¹] is the absolute rate constant belonging to a specific concentration of fullerenols in water solution.

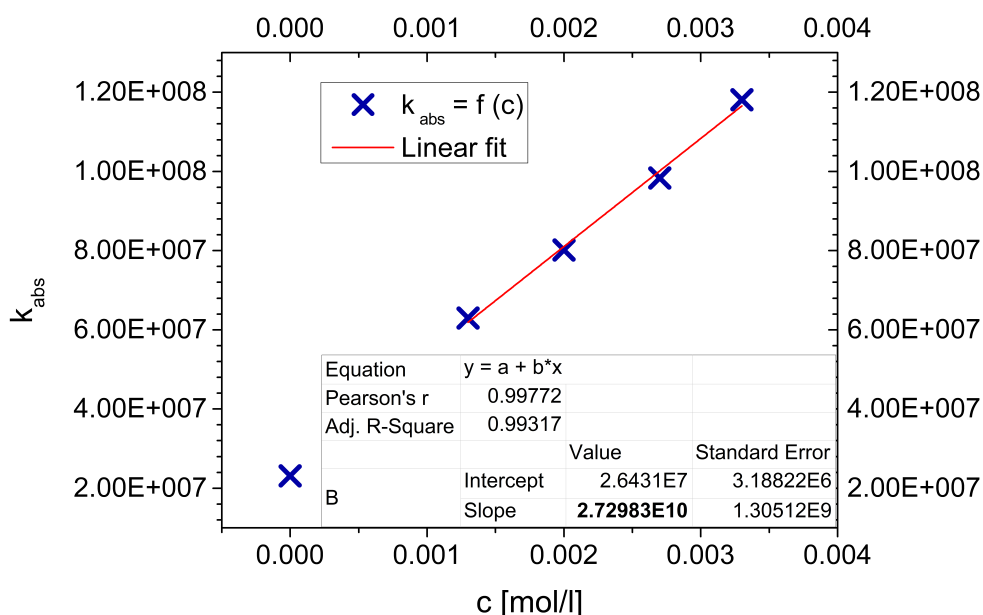


Figure 3.31: Figure shows dependencies of absolute rate constant on the concentration of fullerenols in water. As a result, 5 points are plotted and fitted with a linear fit to gain the normalized rate constant.

Then, the dependence of absolute rate constants on molar concentration c [mol/l] of fullerenols in water was plotted in the graph in the Figure 3.31. Finally, the normalized rate constant for the interaction of fullerenols with solvated electrons was determined as slope value after linear fitting of plotted dependence.

The value of the normalized rate constant based on fit parameters is:

$$k_{\text{normalized}}^{\text{full}} = 2.7 \times 10^{10} \text{ dm}^3 \text{ mol}^{-1} \text{ s}^{-1} \quad (3.3)$$

The determined normalized rate constant is of high value. These experiments confirmed strong scavenging of solvated electrons with fullerenols.

Beyond the framework of work significantly limited by time, I moved the work forward within the design of the $\pi - \pi$ complex. Specifically, I designed a method for detecting the π - π complex in an aqueous solution.

Key insights gained about the fullerenes based on PR

- C_{60} is not soluble in water. Measurement of C_{60} in aromatic solvent was unsuccessful due to aromatic solvent, which appeared as unsuitable solvents for pulse radiolysis because electrons react with the aromatic core.
 - C_{60} pyrrolidine tris-acid is unsuitable for pulse radiolysis because of its very low solubility in water as a primary solvent.
 - Interaction of fullerenols with quasi-free electrons was not observed. However, it could also be caused by their lower solubility, around 5mg/ml.
 - Fullerenols highly efficiently scavenge solvated electrons with a high value of the rate constant; $k = 2.7 \times 10^{10} \text{ dm}^3 \text{ mol}^{-1} \text{ s}^{-1}$.
-

3.3.3 Fluorescence spectroscopy for 2-aminopurine in water

At a further level, the π - π complex consists of fullerenols, and a second molecule needs to be created and its existence verified so as its π - π character. I aim to confirm the existence of the complex in an aqueous solution based on fluorescence spectroscopy. The condition is that at least one of two molecules has to be fluorescent. After the formation of a complex, it is assumed that the binding molecule will influence the fluorescence spectrum of the molecule, and such a change in fluorescence will be detected by fluorescence spectroscopy. 2-aminopurine, with well-known fluorescent properties, was chosen as the second molecule to pair with fullerenols. Therefore, this part presents the preliminary results of a fluorescence spectroscopic study on 2-aminopurine as a second part of the π - π complex. 2-aminopurine was ordered from Sigma Aldrich in the form of white powder ($C_5H_5N_5$), $M_r = 135.13 \text{ g/mol}$, 99%, Sigma Aldrich). The fluorescence spectroscopic study was performed in Prague at JH IPC. Unfortunately, the fluorometer enables the excitation of the sample with only four possible wavelengths, and the fluorescence intensity is provided in 4 regions (UV, Blue, Green, and Red). Thus, further investigations would be needed to verify the π - π character of the complex.

Here, the preliminary fluorescence spectroscopic experiments are presented for 2-aminopurine in water solution.

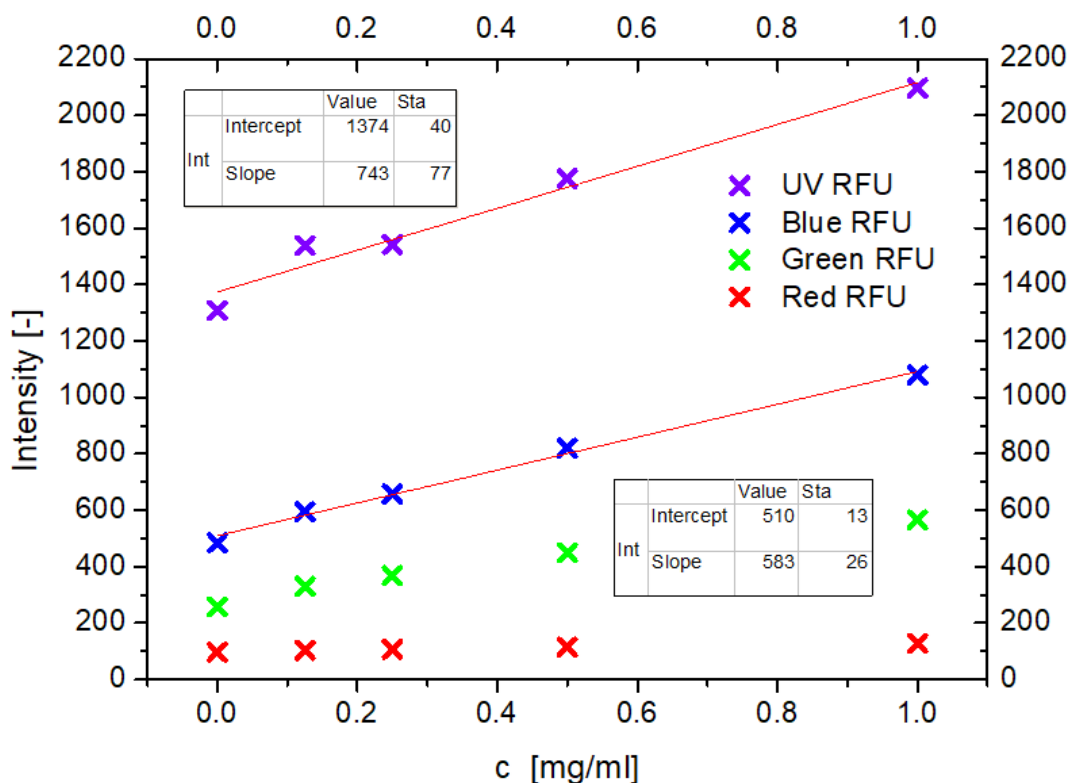


Figure 3.32: Dependencies of fluorescence intensities on the concentration of 2-aminopurine in water at an excitation wavelength of 375 nm. Each colour of points belongs to a specific wavelength region.

The fluorescent properties of 2-aminopurine were measured for various mass concentrations of 2-aminopurine in water (0.125, 0.25, 0.5, and 1 mg/ml), and the results are shown in the Figure 3.32. The excitation wavelength was 375 nm. However, the closest absorbance maximum of 2-aminopurine is at 305 nm. The graph shows the dependence of the fluorescence intensities at measured wavelength regions on the concentration of 2-aminopurine. Similar dependencies were also measured for fullerenols and a mixture of fullerenols and 2-aminopurine and are not presented here. Nevertheless, further experiments would be necessary to obtain full emission spectra and use excitation wavelength closer to the absorption maximum of 2-aminopurine to discuss the presence of the π - π complex.

To conclude, the fluorescence of both compounds appears to be a powerful tool for revealing the existence of their complex.

3.3.4 Final discussion and conclusion of fullerenes study

The measurements of pulse radiolysis on fullerenes aimed to carry out the experiments of pulse radiolysis with C_{60} and its water-soluble derivatives more appropriate for bio-utilization in living tissue. Based on the measurements, only the fullerenols remained suitable for this type of experiment. It maintained the potential for subsequent experimental examination due to its water solubility and positive interaction with secondary LEEs. Further experimental steps led to the examination of this molecule with both picosecond and nanosecond to millisecond time-scale pulse radiolysis to confirm their interaction with solvated electrons and investigate a dependency of LEEs scavenging on an increasing concentration of fullerenols in a water solution. It determined the normalized rate constant for the reaction of fullerenols with solvated electrons, which reached a high value.

As the conclusion is that fullerenols behave like efficient scavengers of electrons with energies of the environment, and it supports the radiosensitizing potential. Simultaneously, their nanosize could allow better targeting delivery in the living tissue due to the EPR effect, and they are already a part of targeted therapy models and complexes for photodynamic therapy [100]. Moreover, theoretical calculations show that molecules based on C_{60} core should be able to create π - π stack complexes with appropriate molecules [104]. All these facts strongly support the idea of the design of such a π - π complex. This work only aimed to examine the LEEs-scavenging properties of fullerenols and, from this perspective, their radiosensitizing potential simultaneously, e.g., for their specific role in radiosensitizing $\pi - \pi$ complex with good targeting properties, and it seems that the fullerenol molecule has potential for such use.

Since the presented work was limited in time, it was unrealistic to go significantly further in this intention and design such a complex. It would require finding a suitable secondary molecule with radiosensitizing potential and the ability to form a $\pi - \pi$ complex with fullerenol. It would be necessary to carry out a comprehensive study of the reducing properties of the proposed molecule, using electron attachment spectroscopy in the gas phase and pulse radiolysis in solution. It could be further supported by *ab initio* calculations of the electron affinities of the molecule and its fragments.

Conclusion

The present work aimed to reveal new information for the rational design of novel radiosensitizers for more efficient and less toxic chemoradiotherapy of cancer treatment. I focused on studying the radiosensitizing potential of selected compounds from the point of view of LEEs-induced chemistry, even considering strategy of targeted drug delivery.

As described in Chapter 1.4, this research work is built on two parts. The first part includes the theoretical and experimental investigation of reductive properties of selected compounds for their use as radiosensitizers in chemoradiotherapy. The second part of the present work deals with studying electron-scavenging properties of fullerenes chosen for exploring their potential to be a part of the $\pi - \pi$ complex with good radiosensitizing and targeted drug delivery properties for chemoradiotherapy.

In the frame of primary research, I conducted extensive research of existing literature on concomitant chemoradiotherapy and radiosensitizers from the group of cytostatics. Then, I focused on the groups as modified DNA components, organometallics and nitroimidazoles, and this review was already published in the article "Interaction of low-energy electrons with radiosensitizers" in journal *Phys. Chem. Chem. Phys.* [8]. Based on the literature research, I gained an overview of the field that led to selecting a particularly interesting molecule for repurposing in radiosensitization - the antiviral favipiravir.

I performed a detailed study of favipiravir's interaction with LEEs as a prerequisite of its radiosensitizing potential. This study combined electron attachment experiments in the gas phase on two experimental devices with opportunity to examine the environment effect on the reaction. I also performed *ab initio* calculations of the electron affinities for the selected molecules. The results of the study, already published in the article "Electron attachment to isolated and microhydrated favipiravir" in journal *Phys. Chem. Chem. Phys.* [62], revealed that interactions of LEEs with highly electron-affine favipiravir support the formation of negative parent ions in micro-hydration conditions, so as a releasing of energy to the environment. These can be crucial mechanisms of action involved in reaction strategies leading to possible synergism in chemoradiotherapy. Based on this study focused on interaction with LEEs, a molecule of favipiravir is a promising candidate for a radiosensitizer and, thus, should be suggested for experimental assays on cells.

The molecule of RRx-001 was my second target molecule, now successfully tested as a chemotherapeutics and radiosensitizer in phase 3 clinical trials. Here, the goal was to examine whether the radiosensitizing potential of this molecule can result from its interaction with secondary LEEs and, if so, to describe such a mechanism. In this

study, I combined the gas-phase electron attachment spectroscopy and pulse radiolysis in solution with temporal range from picosecond to millisecond to study the intermediates formed after the interaction of RRx-001 with LEEs. To study the final product of radiolysis of RRx-001 in ethanol solution, I irradiated the solutions with high-energy electrons on a microtron, and then they were evaluated using NMR spectroscopy. This second study showed that the RRx-001 molecule with electron-affine groups is a very efficient scavenger of LEEs and brought interesting spectroscopic and dynamics information about the formed intermediates. As in the previous study, I observed the stabilization of negative parent ions with increasing solvation and the release of energy into the environment. These key observations could be involved in radiosensitizing processes, which give a chance to result in a synergistic effect within chemoradiotherapy. The initial gas-phase study was already accepted for publication in "Dissociative Electron Attachment Dynamics of a Promising Cancer Drug Indicates Its Radiosensitizing Potential", in journal *Angew. Chem.* [121]. A more complex publication, "Anion formation and neutral dissociation upon the interaction of secondary low-energy electrons with radio-modifying substance RRx-001", is under preparation. After conducting all the experiments, I cooperated with Prof. Milan Ončák from the University of Innsbruck to apply his *ab initio* calculations to interpret the complex experimental data.

In a minor part focused on fullerenes, I mainly studied the fullerlenols and their radiosensitizing potential for prospective role in a complex with radiosensitizing and good targeted drug delivery properties in living tissue within chemoradiotherapy. I attended a one-week internship at the University of Innsbruck, Austria, under the supervision of Prof. Paul Scheier, where I tried to study fullerlenols using spectroscopy of helium nanodroplets. Unfortunately, it turned out that fullerlenols cannot be studied isolated in the gas phase, nor the helium droplets, since they thermally decompose before the sublimation. Consequently, I examined this molecule by pulse radiolysis in an aqueous solution within my one-year stay in ICP, Orsay, where the significant scavenging of solvated electrons by fullerlenols was revealed. That provides an important starting point for further research, e.g., in the direction of designing a carrier platform as a radiosensitizing π - π complex with targeted drug delivery properties where a molecule of fullerlenols is bound with electron affine molecule via π - π stack; it can be supposed that fullerlenols will scavenge solvated electrons, which could then be attracted by higher electron-affinity of the second molecule and transfer there via electron transfer. It could potentially result in several postirradiation pathways. Due to the very stable fullerlenol sphere, the pathways could involve mainly the second molecule, e.g., its detachment from the complex, breaking bonds, conformation changes, and releasing energy to the surrounding. All these potential pathways seem promising in light of requiring a radiosensitizing effect.

To conclude, all three molecules investigated in this work demonstrated their radiosensitizing potential from the point of view of interaction with LEEs and are highly recommended for further investigation. I believe investigating the mechanisms leading to the radiosensitizing effect is a critical task for the more accessible and elegant rational design of radiosensitizers for chemoradiotherapy. This ultimate goal could be achieved using complex experimental approaches accompanied by *ab initio* calculations and modelling of postirradiation processes.

Bibliography

- [1] E. E. Vokes, M. S. Kies, D. J. Haraf, K. Stenson, M. List, R. Humerickhouse, M. E. Dolan, H. Pelzer, L. Sulzen, M. E. Witt, Y.-C. Hsieh, B. B. Mittal, and R. R. Weichselbaum, “Concomitant chemoradiotherapy as primary therapy for locoregionally advanced head and neck cancer,” *Journal of Clinical Oncology*, vol. 18, no. 8, pp. 1652–1661, 2000, pMID: 10764425. [Online]. Available: <https://doi.org/10.1200/JCO.2000.18.8.1652>
- [2] P. Šlampa, R. Soumarová, and I. Kocáková, *Konkomitantní chemoradioterapie solidních nádorů*. Galén, 2005, první vydání.
- [3] M. C. Joiner and A. V. D. Kogel, *Basic Clinical Radiobiology*. Taylor & Francis Ltd, 2018, vol. 8.
- [4] A. Tewabe, A. Abate, M. Tamrie, A. Seyfu, and S. E. Abdela, “Targeted drug delivery - from magic bullet to nanomedicine: Principles, challenges, and future perspectives,” *J Multidiscip Healthc.*, vol. 14, p. 1711—1724, 2021.
- [5] Y. Dong, Y. Wang, P. Zhuang, X. Fu, Y. Zheng, and L. Sanche, “Role of transient anions in chemoradiation therapy: Base modifications, cross-links, and cluster damages induced to cisplatin-DNA complexes by 1–20 eV electrons,” *The Journal of Physical Chemistry B*, vol. 124, no. 16, pp. 3315–3325, 2020, pMID: 32233508. [Online]. Available: <https://doi.org/10.1021/acs.jpcc.0c00946>
- [6] M. Khosravifarsani, S. Ait-Mohand, B. Paquette, L. Sanche, and B. Guérin, “Design, synthesis, and cytotoxicity assessment of [64Cu]Cu-NOTA-Terpyridine platinum conjugate: A novel chemoradiotherapeutic agent with flexible linker,” *Nanomaterials*, vol. 11, no. 9, 2021. [Online]. Available: <https://www.mdpi.com/2079-4991/11/9/2154>
- [7] L. Sanche, “Role of secondary low-energy electrons in radiobiology and chemoradiation therapy of cancer,” *Chemical Physics Letters*, vol. 474, no. 1, pp. 1–6, 2009. [Online]. Available: <https://www.sciencedirect.com/science/article/pii/S0009261409003078>
- [8] B. Sedmidubská and J. Kočišek, “Interaction of low-energy electrons with radiosensitizers,” *Phys. Chem. Chem. Phys.*, vol. 26, pp. 9112–9136, 2024. [Online]. Available: <http://dx.doi.org/10.1039/D3CP06003A>

- [9] The American Cancer Society, Medical and editorial content team. The history of cancer. [Online]. Available: <https://www.cancer.org/cancer/cancer-basics/history-of-cancer.html>
- [10] E. C. Halperin, D. E. Wazer, C. A. Perez, and L. W. Brady, *Principles and practice of radiation oncology*. Philadelphia: Lippincot Williams & Wilkins, 2004, 4th edition.
- [11] R. B. Mokhtari, T. S. Homayouni, N. Baluch, E. Morgatskaya, S. Kumar, B. Das, and H. Yeger, “Combination therapy in combating cancer,” *Oncotarget*, vol. 8, no. 23, pp. 38 022–38 043, 2017. [Online]. Available: <https://www.oncotarget.com/article/16723/>
- [12] H. Wang and Y. Huang, “Combination therapy based on nano codelivery for overcoming cancer drug resistance,” *Medicine in Drug Discovery*, vol. 6, p. 100024, 2020. [Online]. Available: <https://www.sciencedirect.com/science/article/pii/S2590098620300117>
- [13] N. M. Ayoub, “Editorial: Novel combination therapies for the treatment of solid cancers,” *Frontiers in Oncology*, vol. 11, 2021. [Online]. Available: <https://www.frontiersin.org/article/10.3389/fonc.2021.708943>
- [14] A. Inciura and E. Juozaityte, “Concomitant chemo-radiation treatment of malignant tumors: biological bases.” *Medicina*, vol. 3810, pp. 1042–9; quiz 1051, 2002.
- [15] E. E. Vokes, M. S. Kies, D. J. Haraf, K. Stenson, M. List, R. Humerickhouse, M. E. Dolan, H. Pelzer, L. Sulzen, M. E. Witt, Y.-C. Hsieh, B. B. Mittal, and R. R. Weichselbaum, “Concomitant chemoradiotherapy as primary therapy for locoregionally advanced head and neck cancer,” *Journal of Clinical Oncology*, vol. 18, no. 8, pp. 1652–1661, 2000, pMID: 10764425. [Online]. Available: <https://doi.org/10.1200/JCO.2000.18.8.1652>
- [16] J. S. Cooper, T. F. Pajak, A. A. Forastiere, J. Jacobs, B. H. Campbell, S. B. Saxman, J. A. Kish, H. E. Kim, A. J. Cmelak, M. Rotman, M. Machtay, J. F. Ensley, K. C. Chao, C. J. Schultz, N. Lee, and K. K. Fu, “Postoperative concurrent radiotherapy and chemotherapy for high-risk squamous-cell carcinoma of the head and neck,” *New England Journal of Medicine*, vol. 350, no. 19, pp. 1937–1944, 2004, pMID: 15128893. [Online]. Available: <https://doi.org/10.1056/NEJMoa032646>
- [17] E. E. Vokes and R. R. Weichselbaum, “Concomitant chemoradiotherapy: rationale and clinical experience in patients with solid tumors.” *Journal of Clinical Oncology*, vol. 8, no. 5, pp. 911–934, 1990, pMID: 2185342. [Online]. Available: <https://doi.org/10.1200/JCO.1990.8.5.911>
- [18] E. J. Hall and A. J. Giaccia, *Radiobiology for the Radiologist*. Wolters Kluwer Health, 2018, vol. 8.

- [19] T. Y. Seiwert, J. K. Salama, and E. E. Vokes, “The concurrent chemoradiation paradigm general principles,” *Nature Clinical Practice Oncology*, vol. 4, no. 2, pp. 86–100, 2007. [Online]. Available: <https://doi.org/10.1038/ncponc0714>
- [20] G. G. Steel, T. J. McMillan, and J. H. Peacock, “The 5Rs of radiobiology,” *International journal of radiation biology*, vol. 56 6, pp. 1045–8, 1989.
- [21] National Cancer Institute at the National Institutes of Health, “Cytostatic agent,” [cit. 10.7.2024]. [Online]. Available: <https://www.cancer.gov/publications/dictionaries/cancer-terms/def/cytostatic-agent>
- [22] National Cancer Institute at the National Institutes of Health, “Radiosensitizing agent,” [cit. 11.7.2024]. [Online]. Available: <https://www.cancer.gov/publications/dictionaries/cancer-terms/def/radiosensitizing-agent>
- [23] S. Hynie, *Farmakologie v kostce*. Karolinum, 1998, 2th edition.
- [24] J. Vorlíček, Z. Adam, L. Volková, and H. Vorlíčková, “Chemoterapie a vy rady pro nemocné léčené chemoterapií,” Brochure, 2013, 5th edition, revised. [Online]. Available: http://www.telespazio.it/docs/brodoc/GCC_eng.pdf
- [25] “Livertox: Clinical and research information on drug-induced liver injury: Alkylating agents,” 2012, [cit. 2.2.2022]. [Online]. Available: <https://www.ncbi.nlm.nih.gov/books/NBK547849>
- [26] C. Avendaño and J. C. Menéndez, “Chapter 5 - DNA alkylating agents,” in *Medicinal Chemistry of Anticancer Drugs*, 2nd ed. Boston: Elsevier, 2015, pp. 197–241. [Online]. Available: <https://www.sciencedirect.com/science/article/pii/B9780444626493000053>
- [27] C. Avendaño and J. C. Menéndez, “Chapter 2 - Antimetabolites that interfere with nucleic acid biosynthesis,” in *Medicinal Chemistry of Anticancer Drugs*, 2nd ed. Boston: Elsevier, 2015, pp. 23–79. [Online]. Available: <https://www.sciencedirect.com/science/article/pii/B9780444626493000028>
- [28] T. S. Lawrence, A. Blackstock, and C. McGinn, “The mechanism of action of radiosensitization of conventional chemotherapeutic agents,” *Seminars in Radiation Oncology*, vol. 13, no. 1, pp. 13–21, 2003. [Online]. Available: <https://www.sciencedirect.com/science/article/pii/S1053429603500042>
- [29] J. Raviraj, V. Bokkasam, v. s. Kumar, U. Reddy, and V. Suman, “Radiosensitizers, radioprotectors, and radiation mitigators,” *Indian Journal of Dental Research: official publication of Indian Society for Dental Research*, vol. 25, pp. 83–90, 2014.
- [30] Y. Dong, L.-M. Zhou, Q. Tian, y. Zheng, and L. Sanche, “Chemoradiation cancer therapy: Molecular mechanisms of cisplatin radiosensitization,” *The Journal of Physical Chemistry C*, vol. 121, 2017.
- [31] Q. Bao, Y. Chen, y. Zheng, and L. Sanche, “Cisplatin radiosensitization of DNA irradiated with 2–20 eV electrons: Role of transient anions,” *The Journal of Physical Chemistry C*, vol. 118, pp. 15 516–15 524, 2014.

- [32] B. Behmand, J.-L. Marignier, M. Mostafavi, J. Wagner, D. Hunting, and L. Sanche, "Radiosensitization of DNA by cisplatin adducts results from an increase in the rate constant for the reaction with hydrated electrons and formation of PtI," *The journal of physical chemistry. B*, vol. 119, pp. 9496–9500, 2015.
- [33] S. Dasari and P. Bernard Tchounwou, "Cisplatin in cancer therapy: Molecular mechanisms of action," *European Journal of Pharmacology*, vol. 740, pp. 364–378, 2014. [Online]. Available: <https://www.sciencedirect.com/science/article/pii/S0014299914005627>
- [34] R. Doijad, F. Manvi, D. Godhwani, R. Joseph, and N. Deshmukh, "Formulation and targeting efficiency of cisplatin engineered solid lipid nanoparticles," *Indian Journal of Pharmaceutical Sciences*, vol. 70, pp. 203–7, 2008.
- [35] A. El-Sheikh and Z. Khired, "Interactions of Analgesics with Cisplatin: Modulation of Anticancer Efficacy and Potential Organ Toxicity," *Medicina*, vol. 58, no. 1, 2022. [Online]. Available: <https://www.mdpi.com/1648-9144/58/1/46>
- [36] T. Luo, J. Yu, J. Nguyen, C.-R. Wang, R. G. Bristow, D. A. Jaffray, X. Z. Zhou, K. P. Lu, and Q.-B. Lu, "Electron transfer-based combination therapy of cisplatin with tetramethyl-p-phenylenediamine for ovarian, cervical, and lung cancers," *Proceedings of the National Academy of Sciences*, vol. 109, no. 26, pp. 10 175–10 180, 2012. [Online]. Available: <https://www.pnas.org/content/109/26/10175>
- [37] Q. Zhang and Q. Lu, "New combination chemotherapy of cisplatin with an electron-donating compound for treatment of multiple cancers." *Scientific Reports*, vol. 11, p. 788, 2021.
- [38] M. Al-Sarraf, T. F. Pajak, V. A. Marcial, P. Mowry, J. S. Cooper, J. Stetz, J. F. Ensley, and E. Velez-Garcia, "Concurrent radiotherapy and chemotherapy with cisplatin in inoperable squamous cell carcinoma of the head and neck. an rtog study," *Cancer*, vol. 59, no. 2, pp. 259–265, 1987. [Online]. Available: <https://acsjournals.onlinelibrary.wiley.com/doi/abs/10.1002/1097-0142>
- [39] A. A. Forastiere, "Chemotherapy in the treatment of locally advanced head and neck cancer," *Journal of Surgical Oncology*, vol. 97, no. 8, pp. 701–707, 2008. [Online]. Available: <https://onlinelibrary.wiley.com/doi/abs/10.1002/jso.21012>
- [40] N. Zhang, Y. Yin, S.-J. Xu, and W.-S. Chen, "5-fluorouracil: Mechanisms of resistance and reversal strategies," *Molecules*, vol. 13, no. 8, pp. 1551–1569, 2008. [Online]. Available: <https://www.mdpi.com/1420-3049/13/8/1551>
- [41] J. Byfield, "5-fluorouracil radiation sensitization — a brief review," *Invest New Drugs*, vol. 7, p. 111–116, 4 1989.
- [42] D. Longley, D. Harkin, and P. Johnston, "5-fluorouracil: mechanisms of action and clinical strategies," *Nat Rev Cancer*, vol. 9, p. 330–338, 5 2003.

- [43] A. Singh and Y.-J. Xu, “The cell killing mechanisms of hydroxyurea,” *Genes*, vol. 7, no. 11, 2016. [Online]. Available: <https://www.mdpi.com/2073-4425/7/11/99>
- [44] B. Pauwels, A. E. Korst, G. G. Pattyn, H. A. Lambrechts, D. R. Van Bockstaele, K. Vermeulen, M. Lenjou, C. M. de Pooter, J. B. Vermorcken, and F. Lardon, “Cell cycle effect of gemcitabine and its role in the radiosensitizing mechanism in vitro,” *International Journal of Radiation Oncology-Biology-Physics*, vol. 57, no. 4, pp. 1075–1083, 2003. [Online]. Available: <https://www.sciencedirect.com/science/article/pii/S0360301603014433>
- [45] C. Liu, F. Liu, L. Feng, M. Li, J. Zhang, and N. Zhang, “The targeted co-delivery of DNA and doxorubicin to tumor cells via multifunctional PEI-PEG based nanoparticles,” *Biomaterials*, vol. 34, 01 2013.
- [46] H. Ijäs, B. Shen, A. Heuer-Jungemann, A. Keller, M. Kostianen, T. Liedl, J. Ihalainen, and V. Linko, “Unraveling the interaction between doxorubicin and DNA origami nanostructures for customizable chemotherapeutic drug release,” *Nucleic Acids Research*, vol. 49, 02 2021.
- [47] Q. Zhang, Q. Jiang, N. Li, L. Dai, Q. Liu, L. Song, J. Wang, Y. Li, J. Tian, B. Ding, and Y. Du, “DNA origami as an in vivo drug delivery vehicle for cancer therapy,” *ACS nano*, vol. 8, 06 2014.
- [48] D. Agudelo, P. Bourassa, G. Bérubé, and H. Tajmir-Riahi, “Review on the binding of anticancer drug doxorubicin with DNA and tRNA: Structural models and antitumor activity,” *Journal of Photochemistry and Photobiology B: Biology*, vol. 158, pp. 274–279, 2016. [Online]. Available: <https://www.sciencedirect.com/science/article/pii/S1011134416300240>
- [49] D. Agudelo, P. Bourassa, M. Beauregard, G. Bérubé, and H.-A. Tajmir-Riahi, “tRNA binding to antitumor drug doxorubicin and its analogue,” *PLOS ONE*, vol. 8, no. 7, pp. 1–8, 07 2013. [Online]. Available: <https://doi.org/10.1371/journal.pone.0069248>
- [50] E. Arthur-Baidoo, K. Falkiewicz, L. Chomicz-Mańka, A. Czaja, S. Demkowicz, K. Biernacki, W. Kozak, J. Rak, and S. Denifl, “Electron-induced decomposition of uracil-5-yl o-(n,n-dimethylsulfamate): Role of methylation in molecular stability,” *International Journal of Molecular Sciences*, vol. 22, no. 5, 2021. [Online]. Available: <https://www.mdpi.com/1422-0067/22/5/2344>
- [51] R. Meißner, S. Makurat, W. Kozak, P. Limão-Vieira, J. Rak, and S. Denifl, “Electron-induced dissociation of the potential radiosensitizer 5-selenocyanato-2'-deoxyuridine,” *The Journal of Physical Chemistry B*, vol. 123, 2019.
- [52] T. F. M. Luxford, S. A. Pshenichnyuk, N. L. Asfandiarov, T. Perečko, M. Falk, and J. Kočíšek, “5-nitro-2,4-dichloropyrimidine as an universal model for low-energy electron processes relevant for radiosensitization,” *International Journal of Molecular Sciences*, vol. 21, no. 21, 2020. [Online]. Available: <https://www.mdpi.com/1422-0067/21/21/8173>

- [53] R. Meißner, J. Kočíšek, L. Feketeová, J. Fedor, M. Fárník, P. Limáo-Vieira, E. Illenberger, and S. Denifl, “Low-energy electrons transform the nimorazole molecule into a radiosensitiser,” *Nature Communications*, vol. 10, no. 1, p. 2388, 2019. [Online]. Available: <https://doi.org/10.1038/s41467-019-10340-8>
- [54] E. Arthur-Baidoo, K. Falkiewicz, L. Chomicz-Mańka, A. Czaja, S. Demkowicz, K. Biernacki, W. Kozak, J. Rak, and S. Denifl, “Electron-induced decomposition of uracil-5-yl o-(n,n-dimethylsulfamate): Role of methylation in molecular stability,” *International Journal of Molecular Sciences*, vol. 22, no. 5, p. 2344, 2021. [Online]. Available: <https://doi.org/10.3390>
- [55] B. Sedmidubská, *Interakce nízkoenergetických elektronů s izolovanými a hydratovanými biomolekulami*. FJFI ČVUT v Praze, 2020, diplomová práce.
- [56] E. Britannica, “Range-particle-radiation,” July 1998, [cit. 7.8.2024]. [Online]. Available: <https://www.britannica.com/science/range-particle-radiation>
- [57] S. Pimblott and J. A. LaVerne, “Production of low-energy electrons by ionizing radiation,” *Radiation Physics and Chemistry*, vol. 76, pp. 1244–1247, 2007.
- [58] M. Dingfelder, A. Travia, R. A. McLawhorn, J. L. Shinpaugh, and L. H. Toburen, “Electron emission from foils and biological materials after proton impact.” *Radiation Physics and Chemistry*, vol. 77, pp. 1213–1217, 2008.
- [59] A. Motl, *Úvod do radiační chemie*. Vydavatelství ČVUT, 2004, novel edition.
- [60] E. Alizadeh and L. Sanche, “Precursors of solvated electrons in radiobiological physics and chemistry,” *Chemical Reviews*, vol. 112, 2012.
- [61] M. Rezaee, R. P. Hill, and D. A. Jaffray, “The Exploitation of Low-Energy Electrons in Cancer Treatment,” *Radiation Research*, vol. 188, no. 2, pp. 123–143, 2017. [Online]. Available: <https://doi.org/10.1667/RR14727.1>
- [62] B. Sedmidubská, T. F. Luxford, and J. Kočíšek, “Electron attachment to isolated and microhydrated favipiravir,” *Physical Chemistry Chemical Physics*, vol. 23, no. 38, pp. 21 501–21 511, 2021.
- [63] R. Schürmann, S. Vogel, K. Ebel, and I. Bald, “Frontispiece: The physico-chemical basis of DNA radiosensitization: Implications for cancer radiation therapy,” *Chemistry - A European Journal*, vol. 24, no. 41, pp. 10 271–10 279, 2018.
- [64] J. Gorfinkiel and S. Ptasinska, “Electron scattering from molecules and molecular aggregates of biological relevance,” *Journal of Physics B: Atomic, Molecular and Optical Physics*, vol. 50, no. 18, p. 182001, sep 2017.
- [65] S. M. Pimblott and J. A. LaVerne, “Production of low-energy electrons by ionizing radiation,” *Radiation Physics and Chemistry*, vol. 76, no. 8, pp. 1244–1247, 2007, proceedings of the 11th Tihany Symposium on Radiation Chemistry. [Online]. Available: <https://www.sciencedirect.com/science/article/pii/S0969806X07000448>

- [66] P. Wardman, “Chemical radiosensitizers for use in radiotherapy,” *Clinical oncology (Royal College of Radiologists (Great Britain))*, vol. 19, pp. 397–417, 2007.
- [67] L. Chomicz, M. Zdrowowicz, F. Kasprzykowski, J. Rak, A. Buonaugurio, Y. Wang, and K. H. Bowen, “How to find out whether a 5-substituted uracil could be a potential DNA radiosensitizer,” *The Journal of Physical Chemistry Letters*, vol. 4, no. 17, pp. 2853–2857, 2013. [Online]. Available: <https://doi.org/10.1021/jz401358w>
- [68] J. Rak, L. Chomicz-Mańka, J. Wiczak, K. Westphal, M. Zdrowowicz, P. Wityk, M. Żyndul, S. Makurat, and Ł. Golon, “Mechanisms of damage to DNA labeled with electrophilic nucleobases induced by ionizing or UV radiation,” *The Journal of Physical Chemistry B*, vol. 119, pp. 8227–8238, 2015.
- [69] J. Poštulka, P. Slavíček, J. Fedor, M. Fárník, and J. Kočíšek, “Energy transfer in microhydrated uracil, 5-fluorouracil and 5-bromouracil,” *The Journal of Physical Chemistry B*, vol. 121, p. 8965–8974, 2017.
- [70] D. Reimitz, M. Davídková, O. Mestek, J. Pinkas, and J. Kočíšek, “Radiomodifying effects of RAPTA C and CDDP on DNA strand break induction,” *Radiation Physics and Chemistry*, vol. 141, pp. 229–234, 2017.
- [71] J. Rackwitz, M. Ranković, A. Milosavljevic, and I. Bald, “A novel setup for the determination of absolute cross sections for low-energy electron induced strand breaks in oligonucleotides – the effect of the radiosensitizer 5-fluorouracil*,” *The European Physical Journal D*, vol. 71, pp. 397–417, 2017.
- [72] P. Spisz, M. Zdrowowicz, W. Kozak, L. Chomicz-Mańka, K. Falkiewicz, S. Makurat, A. Sikorski, D. Wyrzykowski, J. Rak, E. Arthur-Baidoo, P. Ziegler, M. Costa, and S. Denifl, “Uracil-5-yl o-sulfamate – an illusive radiosensitizer. on the pitfalls in modeling the radiosensitizing derivatives of nucleobases,” *The Journal of Physical Chemistry B*, vol. 124, no. 27, pp. 5600–5613, 2020. [Online]. Available: <https://doi.org/10.1021/acs.jpcc.0c03844>
- [73] S. Pushpakom, F. Iorio, P. Eyers, K. Escott, S. Hopper, A. Wells, A. Doig, T. Guilliams, J. Latimer, C. McNamee, A. Norris, P. Sanseau, D. Cavalla, and M. Pirmohamed, “Drug repurposing: progress, challenges and recommendations,” *Nature reviews. Drug discovery*, vol. 18, pp. 41–58, 2018.
- [74] P. Pantziarka, L. Meheus, K. Rombauts, L. Vandeborne, and G. Bouche, “Chapter 1 - drug repurposing for cancer therapy—an introduction,” in *Drug Repurposing in Cancer Therapy*, K. K. To and W. C. Cho, Eds. Academic Press, 2020, pp. 1–14. [Online]. Available: <https://www.sciencedirect.com/science/article/pii/B9780128196687000014>
- [75] A. Talevi, “Drug repurposing,” in *Reference Module in Biomedical Sciences*. Elsevier, 2021. [Online]. Available: <https://www.sciencedirect.com/science/article/pii/B9780128204726001080>

- [76] Z. Zhang, L. Zhou, N. Xie, E. Nice, T. Zhang, Y. Cui, and C. Huang, "Overcoming cancer therapeutic bottleneck by drug repurposing," *Signal Transduction and Targeted Therapy*, vol. 5, p. 113, 2020.
- [77] L. Sleire, H. E. Førde, I. A. Netland, L. Leiss, B. S. Skeie, and P. Øyvind Enger, "Drug repurposing in cancer," *Pharmacological Research*, vol. 124, pp. 74–91, 2017. [Online]. Available: <https://www.sciencedirect.com/science/article/pii/S1043661817308538>
- [78] D. Bai, Y. Tian, K. Chen, X. Zhang, F. Wang, Y. Cheng, X. Zheng, K. Xiao, and X. Dong, "Novel 6F-Iridium(III) complexes as potent theranostic agents: Hypoxia probing, radiosensitization and antiviral functionalities," *Dyes and Pigments*, vol. 182, p. 108635, 2020. [Online]. Available: <https://www.sciencedirect.com/science/article/pii/S0143720820313322>
- [79] H. M. Temin, "How do viruses cause cancer?" *Radiology*, vol. 92, no. 5, pp. 931–938, 1969, pMID: 4306170. [Online]. Available: <https://doi.org/10.1148/92.5.931>
- [80] B. Oronsky, J. Scicinski, S. Ning, D. Peehl, A. Oronsky, P. Cabrales, M. Bednarski, and S. Knox, "RRx-001, a novel dinitroazetidide radiosensitizer," *Investigational New Drugs*, vol. 34, pp. 371–377, 6 2016.
- [81] B. Oronsky, X. Guo, X. Wang, P. Cabrales, D. Sher, L. Cannizzo, B. Wardle, N. Abrouk, M. Lybeck, S. Caroén, A. Oronsky, and T. R. Reid, "Discovery of RRx-001, a Myc and CD47 downregulating small molecule with tumor targeted cytotoxicity and healthy tissue cytoprotective properties in clinical development," *Journal of Medicinal Chemistry*, vol. 64, pp. 7261–7271, 6 2021.
- [82] S. Ning, M. Bednarski, B. Oronsky, J. Scicinski, G. Saul, and S. J. Knox, "Dinitroazetidines are a novel class of anticancer agents and hypoxia-activated radiation sensitizers developed from highly energetic materials," *Cancer Research*, vol. 72, pp. 2600–2608, 5 2012.
- [83] J. Fang, H. Nakamura, and H. Maeda, "The EPR effect: Unique features of tumor blood vessels for drug delivery, factors involved, and limitations and augmentation of the effect," *Advanced drug delivery reviews*, vol. 63, pp. 136–151, 2010.
- [84] D. Rosenblum, N. Joshi, W. Tao, J. Karp, and D. Peer, "Progress and challenges towards targeted delivery of cancer therapeutics," *Nature Communications*, vol. 9, 2018.
- [85] Y. Wang and D. Kohane, "External triggering and triggered targeting strategies for drug delivery," *Nature Reviews Materials*, vol. 2, p. 17020, 2017.
- [86] B. Murugan, S. Sagadevan, I. Fatimah, W.-C. Oh, M. A. M. Hossain, and M. R. Johan, "Smart stimuli-responsive nanocarriers for the cancer therapy nanomedicine," *Nanotechnology Reviews*, vol. 10, no. 1, pp. 933–953, 2021. [Online]. Available: <https://doi.org/10.1515/ntrev-2021-0067>

- [87] X. Xie, Y. Zhang, F. Li, T. Lv, Z. Li, H. Chen, L. Jia, and Y. Gao, “Challenges and opportunities from basic cancer biology for nanomedicine for targeted drug delivery,” *Current Cancer Drug Targets*, vol. 18, 2018.
- [88] T. Jaffke, E. Illenberger, M. Lezius, S. Matejcik, D. Smith, and T. D. Märk, “Formation of C_{60}^- and C_{70}^- by free electron capture. activation energy and effect of the internal energy on lifetime,” *Chemical Physics Letters*, vol. 226, no. 1, pp. 213–218, 1994. [Online]. Available: <https://www.sciencedirect.com/science/article/pii/0009261494007047>
- [89] Sigma-Aldrich, [cit. 3.3.2022]. [Online]. Available: <https://www.sigmaaldrich.com/CZ/en/product/aldrich/709085>
- [90] Sigma-Aldrich, “Polyhydroxylated fullerenes, water soluble,” [cit. 30.8.2024]. [Online]. Available: <https://www.sigmaaldrich.com/CZ/en/product/aldrich/793248>
- [91] M. Orlova, “Perspectives of fullerene derivatives in PDT and radiotherapy of cancers,” *British Journal of Medicine and Medical Research*, vol. 3, no. 4, p. 1731–1756, 2013.
- [92] Z. Chen, L. Ma, Y. Liu, and C. Chen, “Applications of functionalized fullerenes in tumor theranostics,” *Theranostics*, vol. 2, pp. 238–250, 2012. [Online]. Available: <https://www.thno.org/v02p0238.htm>
- [93] M. D. Tzirakis and M. Orfanopoulos, “Radical reactions of fullerenes: From synthetic organic chemistry to materials science and biology,” *Chemical Reviews*, vol. 113, no. 7, pp. 5262–5321, 2013, PMID: 23570603. [Online]. Available: <https://doi.org/10.1021/cr300475r>
- [94] Sigma-Aldrich, “Fullerene-c60,” [cit. 30.8.2024]. [Online]. Available: <https://www.sigmaaldrich.com/CZ/en/product/aldrich/572500>
- [95] Y. I. Prylutsky, V. I. Petrenko, O. I. Ivankov, O. A. Kyzyma, L. A. Bulavin, O. O. Litsis, M. P. Evstigneev, V. V. Cherepanov, A. G. Naumovets, and U. Ritter, “On the origin of C_{60} fullerene solubility in aqueous solution,” *Langmuir*, vol. 30, no. 14, pp. 3967–3970, 2014, PMID: 24660846. [Online]. Available: <https://doi.org/10.1021/la404976k>
- [96] A. Djorđević and G. Bogdanović, “Fullerenol: A new nanopharmaceutic?” *Archive of Oncology*, vol. 16, no. 3-4, pp. 42–45, 2008.
- [97] S. Goodarzi, T. Da Ros, J. Conde, F. Sefat, and M. Mozafari, “Fullerene: biomedical engineers get to revisit an old friend,” *Materials Today*, vol. 20, no. 8, pp. 460–480, 2017. [Online]. Available: <https://www.sciencedirect.com/science/article/pii/S1369702116301808>
- [98] S. Augustine, J. Singh, M. Srivastava, M. Sharma, A. Das, and B. D. Malhotra, “Recent advances in carbon based nanosystems for cancer theranostics,” *Biomater. Sci.*, vol. 5, pp. 901–952, 2017. [Online]. Available: <http://dx.doi.org/10.1039/C7BM00008A>

- [99] H. Kazemzadeh and M. Mozafari, “Fullerene-based delivery systems,” *Drug Discovery Today*, vol. 24, no. 3, pp. 898–905, 2019. [Online]. Available: <https://www.sciencedirect.com/science/article/pii/S1359644618302964>
- [100] S. K. Sharma, L. Y. Chiang, and M. R. Hamblin, “Photodynamic therapy with fullerenes in vivo: reality or a dream?” *Nanomedicine*, vol. 6, no. 10, pp. 1813–1825, 2011, pMID: 22122587. [Online]. Available: <https://doi.org/10.2217/nnm.11.144>
- [101] S. Prylutska, R. Panchuk, G. Golunski, L. Skivka, Y. Prylutsky, V. Hurmach, N. Skorohyd, A. Borowik, A. Woziwodzka, J. Piosik, O. Kyzyma, V. Garamus, L. Bulavin, M. Evstigneev, A. Buchelnikov, R. Stoika, W. Berger, U. Ritter, and P. Scharff, “C₆₀ fullerene enhances cisplatin anticancer activity and overcomes tumor cell drug resistance,” *Nano Research*, vol. 10, no. 2, pp. 652–671, 2017. [Online]. Available: <https://doi.org/10.1007/s12274-016-1324-2>
- [102] M. Raoof, Y. Mackeyev, M. A. Cheney, L. J. Wilson, and S. A. Curley, “Internalization of C₆₀ fullerenes into cancer cells with accumulation in the nucleus via the nuclear pore complex,” *Biomaterials*, vol. 33, no. 10, pp. 2952–2960, 2012. [Online]. Available: <https://www.sciencedirect.com/science/article/pii/S0142961211015262>
- [103] R. R. Panchuk, S. V. Prylutska, V. V. Chumak, N. R. Skorokhyd, L. V. Lehka, M. P. Evstigneev, Y. I. Prylutsky, W. Berger, P. Heffeter, P. Scharff, U. Ritter, and R. S. Stoika, “Application of C₆₀ fullerene-doxorubicin complex for tumor cell treatment in vitro and in vivo,” *Journal of Biomedical Nanotechnology*, vol. 11, no. 7, pp. 1139–1152, 2015. [Online]. Available: <https://www.ingentaconnect.com/content/asp/jbn/2015/00000011/00000007/art00003>
- [104] N. Obernikhina, M. Zhuravlova, O. Kachkovsky, O. Kobzar, V. Brovarets, O. Pavlenko, M. Kulish, and O. Dmytrenko, “Stability of fullerene complexes with oxazoles as biologically active compounds,” *Applied Nanoscience*, vol. 10, no. 4, pp. 1345–1353, 2019. [Online]. Available: <https://doi.org/10.1007/s13204-019-01225-9>
- [105] R. Dressler and M. Allan, “Energy partitioning in the O⁻/CO₂ dissociative attachment,” *Chemical Physics*, vol. 92, pp. 449–455, 1985.
- [106] M. Allan, “Study of triplet states and short-lived negative ions by means of electron impact spectroscopy,” *Journal of Electron Spectroscopy and Related Phenomena*, vol. 48, pp. 219–351, 1989.
- [107] A. Stamatovic and G. J. Schulz, “Characteristics of the trochoidal electron monochromator,” *Review of Scientific Instruments*, vol. 41, pp. 423 – 427, 1970.
- [108] S. Denisov. Elyse platform. [cit. 3.3.2022]. [Online]. Available: <https://elyse-platform.academy/>

- [109] J. Belloni, H. Monard, F. Gobert, J.-P. Larbre, A. Demarque, V. De Waele, I. Lampre, J.-L. Marignier, M. Mostafavi, J. Bourdon, M. Bernard, H. Borie, T. Garvey, B. Jacquemard, B. Leblond, P. Lepercq, M. Omeich, M. Roch, J. Rodier, and R. Roux, “Elyse—a picosecond electron accelerator for pulse radiolysis research,” *Nuclear Instruments and Methods in Physics Research Section A: Accelerators, Spectrometers, Detectors and Associated Equipment*, vol. 539, no. 3, pp. 527–539, 2005. [Online]. Available: <https://www.sciencedirect.com/science/article/pii/S0168900204023575>
- [110] K. Iwamatsu, G. Holmbeck, R. Gakhar, P. Halstenberg, B. Layne, S. Pimblott, and J. Wishart, “Radiation-induced reaction kinetics of Zn_2^+ with e_s^- and Cl_2^- in Molten LiCl-KCl eutectic at 400 - 600 °C,” *Physical Chemistry Chemical Physics*, vol. 24, pp. 25 088–25 098, 07 2022. [Online]. Available: <http://dx.doi.org/10.1039/D2CP01194H>
- [111] D. Dobrovolskii, M. Mostafavi, and S. Denisov, “Reactivity of presolvated electrons with supercritical CO_2 in water,” *Physical Chemistry Chemical Physics*, vol. 25, pp. 15 916–15 919, 01 2023. [Online]. Available: <http://dx.doi.org/10.1039/D3CP01535A>
- [112] Nuclear Physics Institute of the CAS, “Microtron MT25,” [cit. 10.3.2023]. [Online]. Available: <http://www.ujf.cas.cz/cs/oddeleni/oddeleni-urychlovacu/microtron/>
- [113] “Gaussian 16,” [cit. 4.3.2022]. [Online]. Available: <https://gaussian.com/g16main/>
- [114] C. Koenig-Lehmann, J. Kopyra, I. Dabkowska, J. Kočíšek, and E. Illenberger, “Excision of CN^- and OCN^- from acetamide and some amide derivatives triggered by low energy electrons,” *Physical Chemistry Chemical Physics*, vol. 10, pp. 6954–61, 2009.
- [115] T. Hamann, A. Edtbauer, F. Ferreira da Silva, S. Denifl, P. Scheier, and P. Swiderek, “Dissociative electron attachment to gas-phase formamide,” *Physical Chemistry Chemical Physics*, vol. 13, pp. 12 305–12 313, 2011.
- [116] L. Sala, B. Sedmidubská, I. Vinklárek, M. Fárník, R. Schürmann, I. Bald, J. Med, P. Slavicek, and J. Kočíšek, “Electron attachment to microhydrated 4-nitro- and 4-bromo-thiophenol,” *Physical Chemistry Chemical Physics*, vol. 23, pp. 18 173–18 181, 09 2021. [Online]. Available: <http://dx.doi.org/10.1039/D1CP02019F>
- [117] P. Pernott, “SK-Ana: Analysis of spectro-kinetic data (version v3.4),” 2018, [cit. 7.8.2024]. [Online]. Available: <https://doi.org/10.5281/zenodo.1064370>
- [118] W. A. Scrivens and J. M. Tour, “Potent solvents for C_{60} and their utility for the rapid acquisition of ^{13}C NMR data for fullerenes,” *J. Chem. Soc., Chem. Commun.*, pp. 1207–1209, 1993. [Online]. Available: <http://dx.doi.org/10.1039/C39930001207>

- [119] R. S. Ruoff, D. S. Tse, R. Malhotra, and D. C. Lorents, “Solubility of fullerene C_{60} in a variety of solvents,” *The Journal of Physical Chemistry*, vol. 97, no. 13, pp. 3379–3383, 1993. [Online]. Available: <https://doi.org/10.1021/j100115a049>
- [120] M. T. Beck and G. Mándi, “Solubility of C_{60} ,” *Fullerene Science and Technology*, vol. 5, no. 2, pp. 291–310, 1997. [Online]. Available: <https://doi.org/10.1080/15363839708011993>
- [121] F. Izadi, T. Luxford, B. Sedmidubská, E. Arthur-Baidoo, J. Kočíšek, M. Ončák, and S. Denifl, “Dissociative electron attachment dynamics of a promising cancer drug indicates its radiosensitizing potential,” *Angewandte Chemie (International ed. in English)*, p. e202407469, 07 2024.

List of author 's publications

During my doctoral studies, I have published three articles; the fourth publication has already been accepted, and another is being prepared for submission. Two published and one accepted articles are directly part of this work: The first article brings theoretical insight into finding radiosensitizing molecules based on their interactions with LEEs. The second article summarizes a study of electron attachment to favipiravir. The third article deals with electron attachment to the RRx-001 molecule. The article under preparation outlines a radiochemistry study of RRx-001.

Related to the scope of the dissertation

1. B. Sedmidubská and J. Kočíšek, "Interaction of low-energy electrons with radiosensitizers," *Phys. Chem. Chem. Phys.*, vol. 26, pp. 9112–9136, 2024. [Online]. Available: <http://dx.doi.org/10.1039/D3CP06003A>
2. B. Sedmidubská, T. F. Luxford, and J. Kočíšek, "Electron attachment to isolated and microhydrated favipiravir", *Phys. Chem. Chem. Phys.*, vol. 23, no. 38, pp. 21 501–21 511, 2021, DOI: 10.1039/d1cp02686k
3. F. Izadi et al., "Dissociative electron attachment dynamics of a promising cancer drug indicates its radiosensitizing potential," *Angewandte Chemie (International ed. in English)*, 07 2024, accepted (28.6. 2024).

Other publication

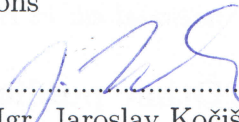
4. L. Sala et al. "Electron attachment to microhydrated 4- nitro- and 4-bromothiophenol," *Phys. Chem. Chem. Phys.*, vol. 23, no. 33, pp. 18 173–18 181, 2021, DOI: 10.1039/D1CP02019F

Author contribution statement

The original scientific results of the present dissertation are based on publications [1], [2], and [3]. Since these works were prepared in collaboration with other authors, the following statement declares the specific contribution of the student who is simultaneously the author of the present work.

- [1] Student carried out extensive theoretical research as a basis for the manuscript, in the preparation of which the student participated.
- [2] Student participated in the experimental part that included preparation of the sample, measurements on both experimental devices, data acquisition and evaluation. The student also performed several theoretical calculations and participated in the preparation of the manuscript.
- [3] Student participated in the measurement on the experimental device CLUB, specifically sample preparation, own measurements, data acquisition and evaluation. The student also participated in the preparation of the manuscript.

This statement is confirmed by Mgr. Jaroslav Kočíšek, Ph.D., the scientific supervisor of the research team that prepared the publications


.....
Mgr. Jaroslav Kočíšek, Ph.D.

Author's publications

1.

Interaction of low-energy electrons with
radiosensitizers



Cite this: *Phys. Chem. Chem. Phys.*,
2024, 26, 9112

Interaction of low-energy electrons with radiosensitizers

Barbora Sedmidubská ^{abc} and Jaroslav Kočíšek ^{*a}

We provide an experimentalist's perspective on the present state-of-the-art in the studies of low-energy electron interactions with common radiosensitizers, including compounds used in combined chemo-radiation therapy and their model systems. Low-energy electrons are important secondary species formed during the interaction of ionizing radiation with matter. Their role in the radiation chemistry of living organisms has become an important topic for more than 20 years. With the increasing number of works and reviews in the field, we would like to focus here on a very narrow area of compounds that have been shown to have radio-sensitizing properties on the one hand, and high reactivity towards low-energy electrons on the other hand. Gas phase experiments studying electron attachment to isolated molecules and environmental effects on reaction dynamics are reviewed for modified DNA components, nitroimidazoles, and organometallics. In the end, we provide a perspective on the future directions that may be important for transferring the fundamental knowledge about the processes induced by low-energy electrons into practice in the field of rational design of agents for concomitant chemo-radiation therapy.

Received 10th December 2023,
Accepted 12th February 2024

DOI: 10.1039/d3cp06003a

rsc.li/pccp

1 Introduction

The motivation for studying interactions of low-energy electrons (LEEs) with radiosensitizers results from the possible role of such interactions in chemoradiation synergism. Identification of major processes contributing to the synergism may open the direct way for the efficient design of chemoradiation drugs. The hypothesis that LEEs are actively involved in the synergism during concomitant chemo-radiation therapy is rationalized by two main facts. The first is a high amount of secondary low-energy electrons produced during the passage of high-energy ionizing radiation particles through biological matter. The second fact is that many chemo-radiotherapeutics exhibit strong reactivity with LEE due to the high electron affinity of the molecule or its components. In the introduction, we will zoom in on these two facts as well as better define the scope of the present perspective article.

Ionization is a process of removing an electron from the molecular orbital. Depending on the mechanism, electrons with different energies are ejected into the environment. These initial electrons can induce further ionization in the $e-2e$

avalanche process or slow down by electronic excitations. The histogram of the processes contributing to the electron slow-down in the medium is known as the electron degradation spectrum. A good introduction to the initial processes during the physicochemical stage of radiation interaction with living tissue can be found in the book of Bednar¹ or reviews on the topic.^{2,3} Determination of electron degradation spectrum in living tissue is an extremely complicated issue due to the large number of molecules present at different densities and polymeric forms. The number of available experimental cross-sections for electron scattering on the constituents of living tissue is rather low (*e.g.* ref. 4 and 5), and therefore the electron transport is typically approximated based on theoretical models.^{6,7} Important in the present content is that the LEEs, in contrast to other secondary species, can be distributed far, several tens of nm from the ionization track of the primary particle.⁸ Since electron ionization is the lowest energetically accessible process resulting in the multiplication of the number of free electrons in the medium, it is clear that the main component of the electron energy degradation spectrum is formed by electrons with energies below the ionization threshold of the medium.⁹ Processes induced by such LEEs with sub-ionization energies are of the primary focus in the present perspective.

1.1 LEE-induced processes in isolated molecules

In Fig. 1 we show the main interactions of LEEs with isolated molecules depending on the energy of the incident electron

^a *J. Heyrovský Institute of Physical Chemistry of the CAS, Dolejškova 3, 182223 Prague, Czech Republic. E-mail: kocisek@jh-inst.cas.cz*

^b *Department of Nuclear Chemistry, Faculty of Nuclear Sciences and Physical Engineering, Břehová 7, 11519 Prague, Czech Republic*

^c *Institut de Chimie Physique, UMR 8000 CNRS and Faculté des sciences d'Orsay, Université Paris Saclay, F-91405 Orsay Cedex, France*



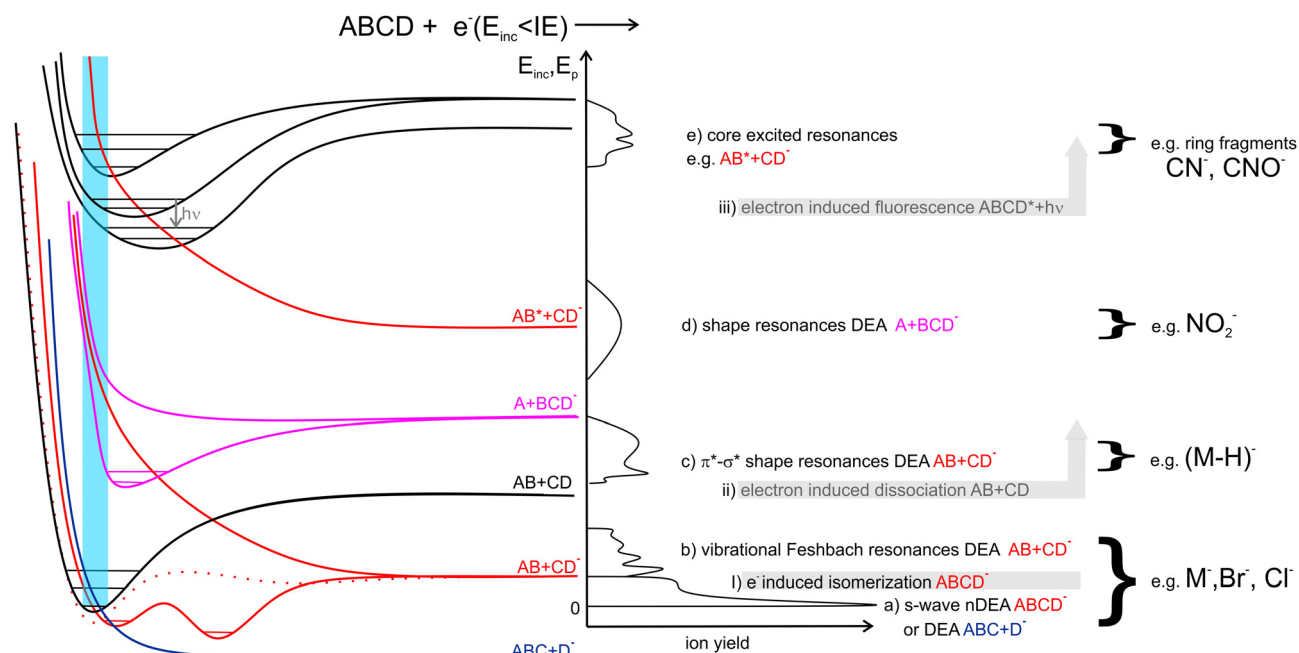


Fig. 1 Common LEE interactions with radiosensitizers discussed in the present work. Gas phase experiments focus mainly on the reactions leading to stable anion formation (a)–(e) via electron attachment EA. Scattering processes leading to neutral products I–III are less explored. The left side of the image provides an example of potential energy curves that can be associated with the processes listed on the right side together with some typical products of LEE interactions with radiosensitizers after the parentheses. The central line provides an example of the corresponding anion yield as a function of the energy of the incident electron that can be expected in a typical electron attachment spectroscopy experiment.

and examples of the relevant potential energy curves. Scattering processes, including elastic and inelastic scattering of electrons (I), electron-induced dissociation (II) and electron-induced fluorescence (III), can occur by simple collision of the incident electron with a molecular system, without the need for the formation of a transient negative ion (TNI). Even though, these processes may be strongly enhanced when LEE interaction time is prolonged by the formation of TNI. Examples are resonant features in vibrational excitation curves¹⁰ or LEE-catalysed dissociation.^{11,12}

Electron attachment processes in Fig. 1(a)–(e), require the formation of TNI, which means that the electron is attached to the molecule on the timescales longer than the typical period for vibrational motion. TNI can be stabilized via intramolecular vibrational energy redistribution (IVR)^{13,14} or anion isomerization^{15,16} to form parent molecular anion. Another means of anion stabilization represents the emission of photons, which is closely related to IVR and recently explored mainly for anions of astrophysical relevance.^{17,18} Alternatively, the TNI can fragment via dissociative electron attachment (DEA), when an anion and a neutral co-products are formed. DEA is interesting from the point of view of reaction enthalpy. Formation of an anion fragment is accompanied by energy surplus due to the fragment electron affinity, significantly lowering the dissociation energy in comparison to the dissociation into neutral fragments.

EA can occur via different scenarios. If the anion's potential energy surface crosses that of the ground state of the neutral and electron attachment is exothermic (Fig. 1a), the

cross-section at energies of the incident electron close to 0 eV diverges, theoretically exceeding the values of the elastic scattering cross-section.¹⁹

In the range of energies corresponding to the vibrational excitation of the ground state neutral, attachment via (dipole supported) vibrational Feshbach resonances (VFRs) occur (Fig. 1b). VFRs are initiated by the overlap of the neutral and anion vibrational energy levels caused by nuclear displacement, a consequence of the long-range interaction of the incident electron with the molecular dipole.²⁰ As shown by Fabrikant, Hotop, and Allan,²¹ as well as the more recent experiments,^{22–24} not only the permanent dipole moment,²⁵ but molecular polarizability as well plays an important role in the formation of dipole bound states. In systems with low-lying electronic excited states such as pyrazolide, the VFR may occur also via a core-excited (two-particle one-hole) process.²⁶ The structure of the dipole-bound anions is very close to that of the neutral²⁷ and therefore, VFRs can be understood only as a doorway mechanism for the formation of energetically lower-lying valence-bound anions.²⁸ However, this is not always the case. In molecules with low or slightly negative electron affinities, the dipole-bound state can lay energetically under that of the valence-bound state.^{29,30} Moreover, the anion rearrangement from dipole to valence state may require additional energy input forming energetic barriers for the transformation.^{31,32}

In the energy range between vibrational and electronic excitation levels shape resonances (Fig. 1d) are usually observed. These are formed by electron attachment to the unoccupied molecular orbitals LUMO+n of the molecule



(virtual orbitals). The energies of these virtual states are directly related to the energies of molecular orbitals of the neutral precursor molecule (see *e.g.* ref. 33). Theoretically, electrons cannot be attached to the orbitals having zero angular momentum (σ) as they do not provide a barrier against autodetachment. In molecules, however, short-lived Sigma resonances can be detected in the vibrational excitation spectra, usually not resulting in DEA (short lifetime) and having only limited contribution to the total elastic cross section (large width).^{34–36} Even though the direct DEA mechanism of these resonances has a low probability, the σ and π molecular orbitals in complex biomolecules are often mixed allowing for rich fragmentation dynamics of TNIs. Examples are biomolecules in which hydrogens are displaced off the symmetry axis in CN–H and possibly also CO–H subunits. There, the low-lying shape resonances can have mixed $\sigma^*-\text{H}^*$ character (Fig. 1c), *e.g.* ref. 37–39.

Finally, at energies of electronically excited states (Fig. 1(e)), core excited resonances can be detected. These are naturally of Feshbach's character (formation of TNI is stabilizing the system). Core-excited shape resonances are typically observed at significantly higher energies than the ones corresponding to the excitation of the neutral molecule.³⁴ More details on the individual LEE processes can be found in specialized reviews^{40,41} or books on the topic.^{42–44}

1.2 LEE interactions in solvent

The wavelength of LEE is already larger than molecular dimensions, implying that the cross-section for the molecular interaction can be larger than the geometrical cross-section of a molecule. This is reflected in the high LEE reaction cross-sections measured in the gas phase experiments, discussed in the previous section. On the other hand, in solvent media, the same long-range electron–dipole interaction results in the fast orientation of the neighboring molecules forming so-called solvated electrons. Water, with its large dipole moment, is one of the fastest traps for electrons with the transition to the aqueous state represented by a potential well of ~ 3.5 eV⁴⁵ at the timescale well below a picosecond.^{46–48}

In contrast to LEEs, the reactivity of solvated electrons is low. The fact that LEEs in biological media are only transient species limits their studies in realistic environments to state-of-the-art time-resolved experiments.^{49,50} On the other side, electrons of controlled energy can be also produced artificially in a vacuum, where molecular dynamics approaches can be applied to explore their interactions with model systems of various complexity.⁵¹ The present perspective focuses, but is not limited to these gas-phase experimental studies.

The advantage of the gas phase studies with model systems is that they can separate various effects of the environment on the dynamics of TNIs. Reviewing the present state-of-the-art, the four main effects on the reaction dynamics of LEEs in the environment can be identified, which are sketched in Fig. 2. The primary effect of the environment is an energy sink Fig. 2(a). As we discussed previously, electron affinity makes many of the LEE-induced processes exothermic. This energy gain, which induces fragmentation *via* DEA in the isolated molecules, is

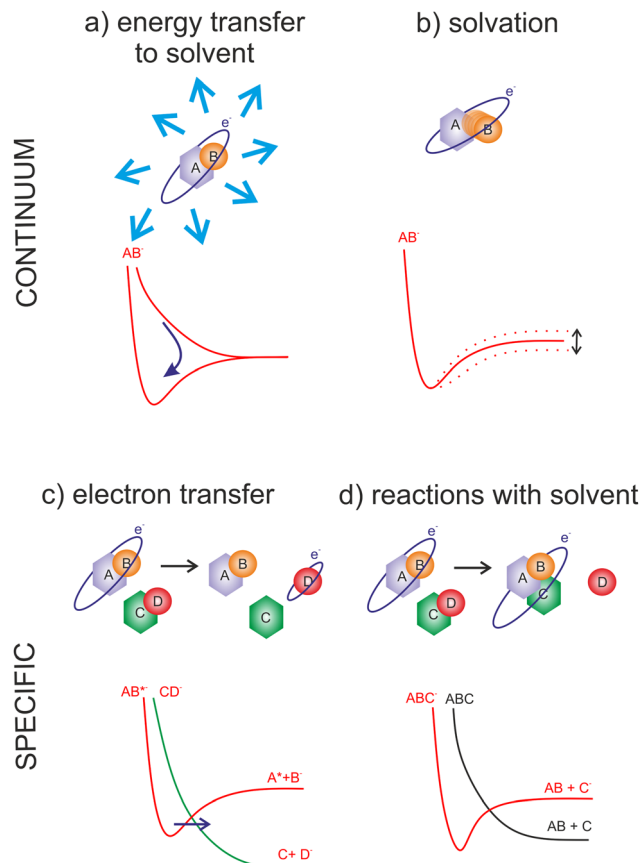


Fig. 2 Commonly observed solvent effects on the dynamics of transient negative ions. (a) Energy transfer to the solvent can prevent molecular fragmentation as well as lead to significant heating of the environment; (b) solvation can prevent as well as promote dissociation or isomerization of TNI; (c) the process studied as self-scavenging in small clusters or electron transfer in gas phase experiments results in the formation of TNIs of one molecule *via* resonant electron attachment to another, in systems with many types of molecules such as in tissue this practically transfers very narrow resonant electron attachment processes into threshold processes operative over a wide range of electron energies; (d) the reactions TNI with solvent molecules can change the final product of electron attachment reaction. Important is also the catalytic role of an electron, in promoting the reactions that could not be possible in between neutrals.

often dissipated to the environment. If the solvent molecules are different from the interacting molecule, the most probable mechanism is intermolecular vibrational energy redistribution *via* momentum transfer of the moving nuclei.^{52–54} In the case of overlapping energetic levels, such as in the case of molecules of the same type, this process may become more effective *via* resonant energy transfer.¹⁴

The second effect is the effect of solvation Fig. 2(b) when the neutral or anion geometry is distorted with respect to the gas phase geometry. A good example is the transformation of valence-bound anions of nucleobases with negative electron affinities into positive electron affinities in the solvent (stabilization of valence-bound anions).^{55,56} Another example is anion predissociation, typical *e.g.* for halogen-substituted molecules.⁵⁷



The third effect is electron transfer Fig. 2(c).^{58,59} In contrast to isolated molecules in the gas phase, in bulk, the molecules are in permanent interaction allowing for the fast electron transfer to the energetically favorable sites. There are many electron transfer sequences known at the cellular level from electron transfer through DNA, through protein-mediated electron transfer chains to cell respiration and metabolism. Free LEEs can enter these sequences at any stage and influence their function. Identification of LEE reactions involved in these cellular mechanisms is one of the important tasks that will require close collaboration of molecular physicists and biophysicists.⁶⁰ Considering the radiosensitization, the electron attractive centers in DNA are thymine bases⁶¹ that may act as an electron transfer terminus in nonsensitized strands. Follow-up electron transfer processes within nucleotides and nucleotide pairs can result in DNA strand breaks.^{62,63} The radiosensitizers may act as additional electron gain centers allowing for the enhancement of these processes.

The second important fact associated with electron transfer is the energy range under which a particular reaction occurs. As we discussed, the attachment of an electron is always possible only at a specific resonant energy. Therefore, from the wide energy distribution of LEEs, only a small part can interact *via* a particular DEA channel. This “bond and site selectivity” is an important characteristic of DEA.^{64–67} In the environment, one molecule can act as an electron scavenger and another can be dissociated upon electron transfer. This way the region of the reaction energies is significantly widened by all possible attachment-transfer sequences. This process is well known in cluster physics as a self- or auto-scavenging.^{68–71}

Finally, reactions with solvent often occur. A good example is the reactivity of nucleotide TNI. McAllister *et al.* suggested that within the nucleotide, electron attachment to the DNA base will result in fast protonation of the base followed by C–N glycosidic bond cleavage.⁷² Such description is consistent with experimentally observed fragmentation of microhydrated 2-deoxycytidine-5-monophosphate upon interaction with LEEs.⁷³ It is worth mentioning that electron-induced glycosidic bond cleavage in nucleotide was observed also using transient absorption spectroscopy in the bulk.⁷⁴

Another good example related to the radiosensitizing molecules is the 5-nitro-2,4-dichloropyrimidine,⁷⁵ where the DEA channel resulting in the release of the Cl neutral is accompanied by hydroxylation of the formed anion.

1.3 Why radiosensitizers?

Many molecules used in the concomitant chemo-radiation therapy have high electron affinities or bare electron affine groups. Typical examples are halogens or nitro groups. The electron affinity represents a negative (exothermic) contribution to the reaction enthalpy, often in the range of electron-volts. The presence of electron affine groups therefore significantly increases reactivity with LEEs as well as their ability to induce molecular transformations in the medium. This fact has attracted attention, since the fundamental mechanisms of chemo-radiation synergism are not fully understood. LEEs react

during the physico-chemical stage of the radiation interaction with tissue and therefore only a tiny enhancement of reactivity towards LEEs can have significant consequences in further stages of radiation interaction with living tissue.³

Several LEE-based mechanisms have been suggested so far to contribute to radio-sensitization and synergism. Simple attachment of an electron by a molecule can lead to the release of the energy equivalent to electron affinity into the environment. Considering the high number of LEEs forming around the ionization track, the addition to the linear energy transfer to the tissue can be significant.⁵² Another contribution of the non-dissociative electron attachment can be enhanced transport through the cellular membranes or accumulation in the cells.⁷⁶ Except for the enhanced transport, in realistic environments the electron attachment is an important prerequisite of multiple electron reduction, which should be better explored, as will be discussed in the perspectives section. Electron affinity is also reflected in the dissociative processes induced by LEEs. LEEs can induce bond breaking at energies significantly below that required by sole energy input into the systems, such as photoexcitation. Already a single LEE can induce the formation of double-strand breaks in cisplatin-sensitized DNA strands.^{77,78} Many more DNA intercalating molecules have been suggested as possible radiosensitizers based on their DEA (*e.g.* ref. 79). However, the DEA to unbound molecules in the cellular medium can produce reactive radicals leading to cell stress and death.^{80,81} An interesting suggestion is also that the presence of heavy metal atoms, such as Pt can locally enhance the production of reactive LEEs.⁸²

All these processes will be discussed on examples of particular molecules from three main groups of radiosensitizers studied during the last years: modified DNA components, nitroimidazoles and organometallics. In the end, we provide a perspective section focused on future directions that should be addressed to enable some real impact in the field of rational design of radiosensitizers and chemo-radiotherapeutics.

2 DNA components

The most studied derivatives of DNA components concerning the LEE-induced chemistry are halogenated pyrimidine bases, nucleosides and nucleotides (Fig. 3). The primary mechanism of action of these compounds in cancer chemotherapy is pyrimidine antagonism. Their presence inhibits the repair and formation of the DNA *via* replacing the pyrimidine bases in the DNA or *via* saturating the nucleotide synthesis proteins. Reduction in the DNA damage site repairs is an important source of combined and synergistic effects of these molecules with radiation.

Additionally to the suppression of repair, the molecules can also act as DNA radiosensitizers, increasing the susceptibility of DNA to damage. When incorporated into DNA, mispairings and DNA mutations are formed influencing the DNA secondary structure as well as increasing the number of accessible sites for radicals and LEEs.⁸³ Indeed, the works with



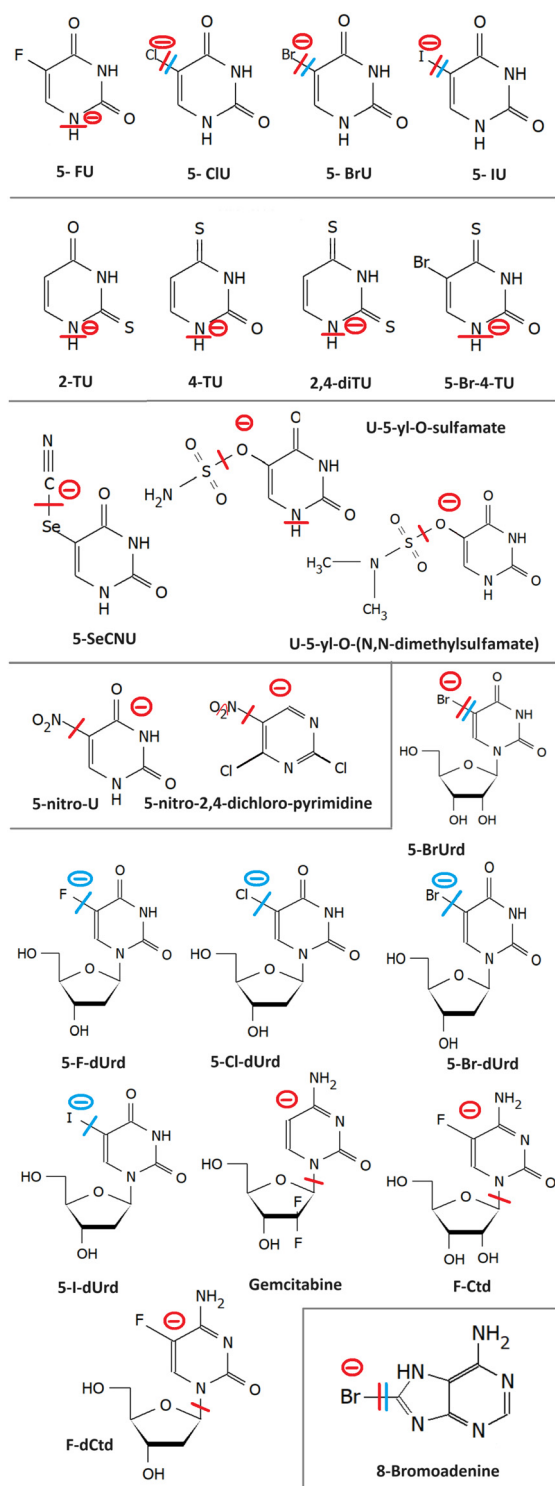


Fig. 3 Radiosensitizers from the group of modified DNA components and their model compounds, whose reactivity with LEEs is discussed in the text. From top to bottom halouracils (2.1); thiouracils (2.2); 5-selenocyanatouracil (2.3), uracil-5-yl-O-sulfamate and uracil-5-yl-O-(N,N-dimethylsulfamate) (2.4); 5-nitrouracil (2.5) and 5-nitro-2,4-dichloropyrimidine (2.6); modified nucleosides (2.8) and 8-bromoadenine (2.7). The red line marks the bond broken in the most intense DEA reaction of the molecule identified for the isolated molecule, and the blue line the dissociation for a solvated molecule. The minus sign marks the anionic DEA fragment.

oligonucleotides⁸⁴ as well as short DNA segments^{85,86} demonstrate enhancement of DNA strand breaks by low-energy electrons due to the presence of halogen-modified nucleosides. The enhancement can be direct, when more single-strand breaks are produced or due to the formation of reactive radicals, enhancing the clustered and double-strand damages.⁸⁷ The direct and electron transfer mechanisms induced by LEEs are well-reviewed in the works of Von Sonntag,⁸⁸ Rak *et al.*⁸⁹ or Kumar.⁶³ Poorly explored are the effects of mutations on the DNA secondary structure that can lead to better access of reactive species to the DNA components and enhanced damages during irradiation.^{86,90} Another unexplored field is the effect on hydrogen bonding of DNA bases important in protein interactions and during the DNA repair process.⁹¹ In this direction, there is only a handful of studies directed at non-modified DNA bases (*e.g.* ref. 92–95). An important benchmark to the computational models can be acquired in precisely designed experiments on DNA origami platforms⁹⁶ but also using various clustering techniques.^{51,97,98}

Generally, pyrimidines are considered better radiosensitizers than purines, which can be related to their higher electron affinities.⁹⁹ Except for electron affinity, also the DEA was considered an important prerequisite of radio-sensitizing properties of pyrimidine substitutes. Systematic studies on the topic were performed mainly in the J. Rak group. Fig. 5 shows a set of substituted uracils with the main DEA reaction channels identified in the work of Makurat.⁸⁹ The DFT-based study sorted the studied uracils into three groups according to their DEA fragmentation pattern resulting in the stabilization of parent anions in group A, fragmentation of substituent group B, and formation of reactive oxygen radical anion in group C. Based on the high stability of the parent anion, group A was excluded as not having radiosensitizing potential. However, based on recent studies with different radiosensitizers, DEA is not a necessary condition for radiosensitizing properties. Single electron reduction can result in several sensitizing mechanisms already discussed, such as enhanced linear energy transfer, better transport of the radiosensitizer within the biological system, or an increase in electron transfer and multiple electron reduction rates. *In vitro*, experimental studies with complexity similar to the DFT study of Makurat would give us much better insight into the undergoing mechanisms. Systematic *in vitro* studies with model molecular systems are, however, complicated due to a large number of parameters that have to be considered when moving from gas phase experiments to biological buffers.^{75,100,101}

2.1 Halouracils

We will start with probably the most studied systems, 5-halo uracils. Three energy regions for the interaction with LEEs can be identified.

In the first region, at energies of the incident electron below 1 eV the electron is attached by the molecular dipole moment into VFRs.^{102,103} Resulting anion in the vibrationally excited state allows for very different dissociation dynamics of that of ground or electronically excited anion.^{104–106} The cross section



at these low energies has a shape of discrete vibrational bands, whose threshold and intensity depend on the reaction enthalpy for the particular DEA channel. DEA at these energies proceeds *via* carbon-to-halogen bond breakage resulting in halogen or U-yl anions products. The enthalpy depends on the electron affinity of the fragment anion and bond dissociation energy. Carbon-to-halogen bond dissociation energies in organic molecules decrease from around 5 eV for C–F to around 2.5 eV for C–I.¹⁰⁷ Electron affinities of all F to I halogens are higher than 3 eV^{108,109} while that of 5-U-yl radical is 2.34 eV.¹¹⁰ Simply subtracting the bond dissociation energy and electron affinity can give us energy surplus for some halogen uracils while shortage for others. In gas phase experiments, however, all but FU efficiently fragment *via* DEA at the energy of incident electron 0 eV, while the calculated reaction enthalpies are typically positive in the 0–1 eV range. This behavior was assigned to the high sensitivity of the vibrational Feshbach resonances to temperature.¹¹¹ The experiments with isolated molecules are performed *via* sublimation of the molecules into the gas phase, which requires high temperatures in the order of hundreds of degrees Celsius. Even though only the tail of the Boltzmann distribution may allow for dissociation, the electron interaction probability at near 0 eV diverges, as we already mentioned, and therefore the molecules from this very tail of the thermal distribution can be enough to produce significant DEA ion signals. This is also in agreement with different distributions of the most intense bands in the cross sections from different experiments.^{104–106}

On the other hand, TNI allows also for hydrogen and proton mobility¹¹² or complex rearrangements.¹¹³ By way of example, simple hydrogen migration upon electron attachment can result in the formation of N1 U-yl radical with an electron affinity of 3.4810 ± 0.0006 eV.¹¹⁴ instead of simple bond cleavages and 5-U-yl radical formation. Such change can explain several previously puzzling 0 eV DEA peaks. However, the rearrangement barriers will need to be explored in detail, recently done *e.g.* for 5-bromo-4-thio-uracil.¹¹⁵ An additional explanation for the observed dissociation near 0 eV can be the creation of stable neutral HX molecules during the TNI lifetime, where X is halogen, which was suggested in the mentioned study of 5-bromo-4-thio-uracil as well as several other TNIs.^{116–118}

In the second region of incident electron energies between 1 eV and 4 eV, electrons are attached *via* shape resonances into the three lowest-lying unoccupied π orbitals. Even though their coupling to the dissociative σ^* state still plays an important role in the dissociation process.^{102,119} The fragmentation spectra at low energies below 4 eV are dominated by halogen or U-yl anions being highly reactive. Formation of these species was observed in early photolysis experiments.^{120,121} They were also suggested to play an important role in the evolution of other reactive species such as OH radicals.¹²²

In the third energy region, core excited resonances result in complex multiple bond cleavages including the ring breakage and formation of anions such as OCN^- , $\text{H}_2\text{C}_3\text{NO}^-$,¹²³ HC_2N^- , C_3NO^- and others.¹¹⁷

When halouracils are submerged in solvent, their dissociation efficiency at low energies is reduced. Studies with microhydrated molecules in clusters demonstrate that while FU doesn't dissociate, BrU and ClU anions can dissociate even when fully surrounded by water molecules.⁵² In contrast to *e.g.* thiophenols⁵⁷ no halogen-water clusters were observed in the fragmentation spectrum of microhydrated uracils. This indicates either a fast dissociation, without the formation of intermediate products, or neutral HBr formation, similar to recently reported HF from fluorouracil.¹¹⁷ Such neutral products, which cannot be detected using mass spectrometry, can be one of the reasons for a significant decrease in the fragmentation signal upon solvation. However, a similar trend of decreasing fragmentation from intense IdU decay to non-decaying FdU was observed also in the pulsed radiolysis study in bulk.¹²⁴ Further suppression of LEE-induced fragmentation can be expected in biological buffers, as demonstrated by Beach, Fuciarelli, and Zimbrick.¹²⁵

The suppression of fragmentation in the environment does not necessarily mean the inactivation of LEE-induced radiosensitization. These studies actually demonstrate that even in the solvent conditions, LEE will effectively attach to halogenated DNA bases. When incorporated in the DNA, electrons can be transferred into the backbone,^{126,127} or negative ions may become attractive for proton transfer from the backbone,^{128,129} which are both efficient ways for DNA strand breaks. Except for chemical ways of radiosensitization, there are also physical consequences of high electron attachment rate in the solution. The energy gained by the system due to the electron affinity of halogen-modified nucleobases can efficiently dissipate into the solvent as demonstrated in Fig. 4 from the work of Poštulka

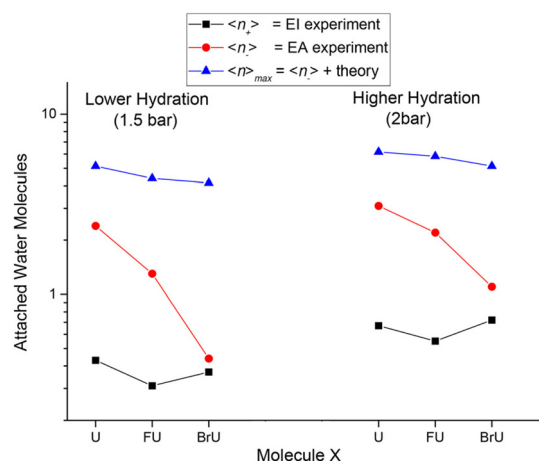


Fig. 4 The image from the work of Poštulka *et al.* showing that theory predicted increase in the energy transfer to solvent due to the electron affinity of the microhydrated halo uracils can reproduce well the fragmentation of their TNIs. For uracil (U), bromouracil (BrU) and fluorouracil (FU) shown on the x-axis the y-axis shows the detected mean size of ionic clusters upon electron attachment (red) and electron ionization (black). The blue points are mean values of neutral cluster sizes estimated based on electron affinities and under the assumption that all energy transferred to solvent leads to the evaporation of water molecules from the cluster. Reproduced from ref. 52 with permission from American Chemical Society, copyright 2017.



et al. In other words, electron affinity represents a positive contribution to the linear energy transfer (LET).

Except for the water solvent, other environmental effects have been studied for halogenated bases, particularly the effect of base pairing.¹³⁰ Pairing of halogenated bases results in a decrease in their adiabatic electron affinity. Therefore, the mutations in the double strands may be less sensitive to LEEs in comparison to the single strand form, *e.g.* during repair and replication processes.

2.2 Thiouracils

Electron attachment to 2-TU in the gas phase was studied using electron attachment spectroscopy and *ab initio* calculations. Low-energy VFRs lead to efficient hydrogen abstraction from nitrogen, with a possible contribution from low-lying π^* resonances at the high energy tail of the observed signal. At energies

above 4 eV, DEA is proceeding *via* core excited resonances of the CS bond in a mechanism similar to CS₂.¹³¹ The most intense DEA channels opening at this energy are leading to S⁻ and (TU-S)⁻. However, the ion yield of the second most intense decomposition product of the molecule SCN⁻ is slightly shifted towards lower energy, which can be a result of the contribution from the high π^* shape resonance to this DEA channel.¹³² Dependency of the anion signal on temperature has shown only a little effect in comparison to the usual behavior of VFRs.¹³³

TU is a nice example demonstrating how reactivity with the solvent (Fig. 2) can change the reaction output of LEE interaction. Prasanthkumar *et al.*¹³⁴ studied TU and TC using pulsed radiolysis in solution. Changing buffer solution composition, two modes of interaction were reached dominated by reactions with solvated electrons or CO₂⁻ ions. In the first case, the electron attachment and formation of TNI is accompanied by a fast proton transfer from the solvent resulting in the formation of protonated radical. While EA in the gas phase discussed in the previous paragraph, results mainly in hydrogen abstraction, in solution it is the opposite. When CO₂⁻ is introduced in solution, it can abstract hydrogens from the molecules, but the formed radicals interact with each other to form sulfur-to-sulfur bound dimers.

More recently, 5-bromo-4-thio-uracil was studied showing strong effects of intramolecular proton transfer on reaction dynamics, partially stabilizing the parent anion and allowing for HBr formation and release during the TNI decay.¹¹⁵ It is worth repeating that the formation of hydrohalic acids seems to be an important process upon LEE interaction with many halogenated molecules^{116,118,135} however, the biological consequences of this process are not well explored.

Other thiouracils were explored theoretically. The electron affinities were calculated to rise from 2-TU with EA of 0.26 eV to 4-TU (0.61 eV) and 2,4-diTU (0.87 eV). Therefore, observation of stable parent anions should be possible, particularly for di-substituted thiophenols¹³⁶

2.3 5-Selenocyanatouracil

Based on the already mentioned systematic work of Makurat,⁸⁹ 5-SeCNU was selected for further experimental studies. Isolated 5-SeCNU is more sensitive to EA than BrU and efficiently releases CN⁻. However, this mechanism does not transfer into a solution, where the U-Se radical stabilizes *via* the formation of two stable products: dimer U-Se-Se-U and an adduct of radical *tert*-Bu to radical U-Se (=U-Se-*tert*-Bu) due to the used *tert*-butanol [*t*BuOH] scavenger in the buffer solution.¹³⁷ It is worth mentioning that dimer formation was observed also upon 2-TU and 2-TC radiolysis in solution, but their occurrence was buffer dependent.¹³⁴ Actually, the composition of buffer solutions to separate LEE-induced processes is one of the major issues complicating the experiments as will be mentioned on several places in the present perspective.

2.4 Uracil-5-yl-O-sulfamate and uracil-5-yl-O-(*N,N*-dimethylsulfamate)

LEE interaction with isolated uracil-5-yl-O-sulfamate results in complex fragmentation already at near 0 eV energies of the

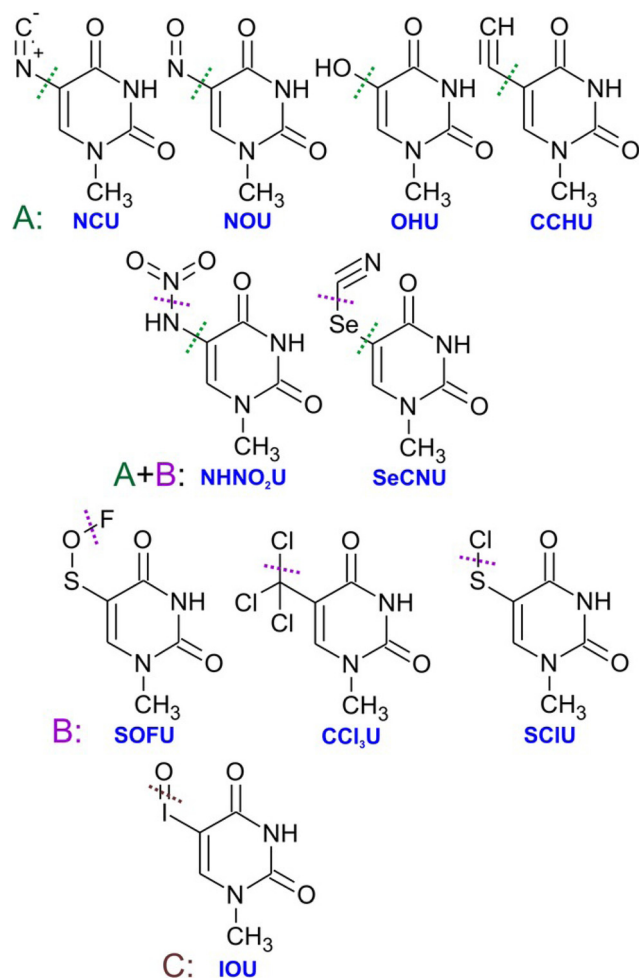


Fig. 5 Substituted uracils from the systematic DFT study of Makurat *et al.* with dotted lines showing main sites of fragmentation *via* dissociative electron attachment induced by LEEs in solution modelled by polarizable continuum model. Electron attachment to the group A molecules was predicted to result in stable negative ions, while B type ions will fragment by dissociation of the substituent group and IOU by the formation of reactive oxygen radical anion. Reproduced from ref. 89 with permission from John Wiley and Sons, copyright 2016.



electrons. The main product results from the S–O bond cleavage and neutral NH_2SO_2 radical release. The other intense fragmentation channels observed at low energies are associated with sulfamate dissociation, particularly the strong SNO^- . This is understandable based on the large electron affinity of this fragment¹³⁸ in comparison to other anions that are commonly observed from sulfoxy compounds, such as SO_2^- and SO_3^- , detected with only minor intensity. Upon solvation, DEA channels seem to be closed as demonstrated by radiolysis of the solutions with *t*-BuOH as a radical scavenger.¹³⁹ For uracil-5-yl-*O*-(*N,N*-dimethylsulfamate), the LEE-induced fragmentation of the isolated molecule is analogous to uracil-5-yl *O*-sulfamate, only intensities differ because of methylation. *e.g.* the intensities of 5-U-yl fragments were under the detection limits.¹³⁵

2.5 5-Nitro-uracil

The electron affinity of the nitrogen dioxide is 2.273 ± 0.005 eV,¹⁰⁸ close to that of the U-yl radical. While the C–N bond is one of the strongest, in the nitro compounds it has a single bond character with bond dissociation energy values ranging from 2.5 eV to 3 eV.^{112,140} As a result, DEA *via* release of neutral NO_2 , which is the most intense channel, is endothermic. The occurrence of intense 0 eV VFRs in the DEA cross section for this channel is therefore surprising.¹⁴⁰ As discussed in the case of halouracils, the exothermicity can be enabled by hydrogen migration over the radical, internal vibrational energy of the neutral, as well as more complex rearrangements during the TNI lifetime. The similar electron affinities of the co-products allowing for charge migration between NO_2 and U-yl and suggested rearrangement before the dissociation probably contribute to the long lifetime of the parent anion of 5-nitro-uracil that was also experimentally observed with high intensities.¹⁴¹

2.6 5-Nitro-2,4-dichloropyrimidine

5-Nitro-2,4-dichloropyrimidine is a model compound containing two halogen atoms and a nitro group connected to the pyrimidine ring. The molecule has exceptionally high electron affinity and anion lifetime. DEA proceeds *via* the release of neutral NO and NO_2 radicals at near 0 eV energies and Cl^- at energies above 2 eV. The reaction channels are suppressed by hydration but NO_2 release channel remains open in the solvent, which is not common *e.g.* for nitroimidazoles that will be discussed further in the perspective. Additionally, reactivity with solvent results in the halogen replacement reaction, where Cl atom is replaced by OH forming a $\text{C}_4\text{H}_2\text{Cl}_2\text{N}_3\text{O}_3$ anion.⁷⁵

2.7 8-Bromoadenine

8-Bromoadenosine incorporation into DNA enhances its susceptibility for single and consequently double-strand breaks upon irradiation.⁸⁷ It has been shown in the experiments on hot electron transfer through DNA vires that strong dehalogenation occurs on the 8BrA-modified sequences, presumably *via* the DEA mechanism.¹⁴² Similar strong dehalogenation was observed also for 8-bromoadenine¹⁴³ and 8-bromoguanine, directly bound to plasmonic nanoparticles.¹⁴⁴

Dehalogenation is also a primary channel for DEA to the isolated 8-bromoadenine in the gas phase resulting in both Br^- and $(\text{M}-\text{Br})^-$ anions in approximately 6 to 1 ratio. DEA seems to proceed *via* VFRs at energies close to 0 eV and a shape resonance peaking around 1.3 eV. The minor $(\text{M}-\text{H})^-$ channel demonstrates typical behavior of $\sigma^*-\pi^*$ mixing with the sharp onset of the signal, which may be temperature dependent. An intense signal upon electron attachment was observed also for the parent anion. The anion has a structure of pre-dissociated Br^- relatively far from the polarized adenine core. This type of non-covalent anion structure was recently identified for several cyclic halocarbons (*e.g.* ref. 145–147) and may be crucial for understanding also the evolution of cyclic hydrocarbon TNIs in the solution.^{57,99,148}

2.8 Halogenated nucleosides

Halogenated nucleosides are generally more soluble in aqueous solutions than bare DNA bases. As discussed by Falkiewicz *et al.*¹⁴⁹ it is the OH group at the 2nd position in ribose and its electronic and steric effects determining the solubility. Nucleosides are, however also more thermally labile. Therefore, the number of their studies in the gas phase is significantly lower than that for the DNA bases, while there are more studies in bulk.

The most studied nucleoside is 5-bromouridine. DEA to isolated molecule leads to the release of Br^- anion and 5-BrU-yl anion with high cross sections of 2×10^{-14} cm² and (9×10^{-16} cm²), respectively.¹⁵⁰ Other dissociation channels, including uracil fragmentation are much less intense.¹⁵¹ In water, pulsed radiolysis was employed to demonstrate Br^- release by LEEs.¹⁵² The mechanism was further confirmed by a more recent study in diethylene glycol.¹⁵³ A pulsed radiolysis study with F to I deoxyuridines in water then demonstrated a decreasing trend from strongly decaying IdU to practically non-decaying FdU in LEE-induced halogen release reactions.¹²⁴

Even more effective dissociation upon electron attachment than in 5 substituted species can occur in 6-substituted uridines. However, as demonstrated for 6-iodo-2-deoxyuridine,¹⁴⁹ the bond dissociation energies may allow dissociation in solvents before electron attachment. The environmental effects such as solubility and buffer reactivity will be critical for the transfer of further halogen-based radiosensitizers into applications such as 5-iodo-4-thio-2-deoxyuridine¹⁵⁴ or 5-bromo-4-thio-deoxyuridine.¹¹⁵

An important difference in comparison to DNA bases is that nucleosides can be modified also on the sugar moiety. A well-known sugar-modified molecule already in use in clinical practice is gemcitabine.¹⁵⁵ Comparative experimental study of gemcitabine and fluorocytidine demonstrated that the binding site of the electron affine atom changes the outcome of DEA significantly. The π system of the DNA base is highly attractive for the electron and halogenation of the ring enhances the cross-section for hydrogen loss $(\text{Cyt}-\text{H})^-$ channel 5.5 times. Fluorine on the sugar moiety still enhances the $(\text{Cyt}-\text{H})^-$ formation, but only 2.8 times, indicating that overall the gemcitabine is probably a weaker electron scavenger.¹⁵⁶



The recent study of 2'-deoxy-2'-fluorocytidine, as a model compound, and 8-bromoadenosine modified DNA studied on a model DNA nanostructure supports⁸⁷ demonstrated that the DEA intensity may not be the sole difference between sugar and base halogenated radiosensitizers. While 8-bromoadenosine modified strands show an increase in the total number of lesions and consequently in double-strand breaks with respect to the random sequence, the 2'-deoxy-2'-fluorocytidine modified strands show only an increase in the number of double-strand breaks but no enhancement in the total number of lesions. 2'-Deoxy-2'-fluorocytidine is therefore enhancing the probability for double-strand break in the case that single-strand break occurs. Such enhancement was tentatively assigned to forming reactive sugar-based radicals in the modified strands inducing clustered damages.¹⁵⁷

The role of LEEs in the formation of sugar-based radicals in radiosensitizer-modified DNA is not sufficiently explored. Tentatively, the mechanism can copy that explored for unmodified DNA using ESR,^{63,158} where dehydrogenated base radicals can be formed by hydrogen abstraction followed by proton extraction from the sugar moiety. The scenario may be, however, influenced by the environment. While phosphate counter ions have only minor effects on electron affinities¹⁵⁹ or electron transfer,⁹⁴ proton transfer from the solvent may play an important role in the dissociation dynamics (see *e.g.* ref. 160) and lead to the formation of sugar moiety anions as demonstrated for microhydrated deoxycytidine monophosphate.^{72,73}

Another mechanism is the direct electron attachment to the sugar moiety. For unmodified DNA it was demonstrated already in the seminal work of Boudaiffa.¹⁶¹ Ptasinska and co-workers then showed high electron attachment cross sections for isolated ribose, a model compound of more complex sugars.¹⁶² Sugar-based radicals and anions were reported also upon electron attachment to softly desorbed *D*-ribose-5-phosphate.¹⁶³ We therefore believe that there should be more focus on the formation of sugar-based radicals and anions upon the interaction of modified DNA with LEEs.

3 Nitroimidazoles

Mostazole-based cancer chemotherapeutics (Fig. 6) are antimetabolites, mainly involved in the folate cycle. Folic acid is required to build and repair DNA, and in many types of cancer, the folate receptors are overexpressed. Azoles are also biomimetic to amide bonds and therefore they are known to interact with proteins¹⁶⁴ strongly. This fact is only poorly explored concerning the DNA repair mechanisms upon irradiation. Research of the LEE community is mainly focused on nitroimidazoles due to their radiosensitizing potential dependence on electron affinity, which was realized in the 1970s already.^{165,166} The first works focused on the direct incorporation of nitroazoles into DNA and electron scavenging. Later, many other mechanisms appeared ranging from NO_x effects,¹⁶⁷ particularly the DNA repair enzyme inhibition,^{168,169} vasodilation effects, fixation of organic radicals, enzyme-catalyzed

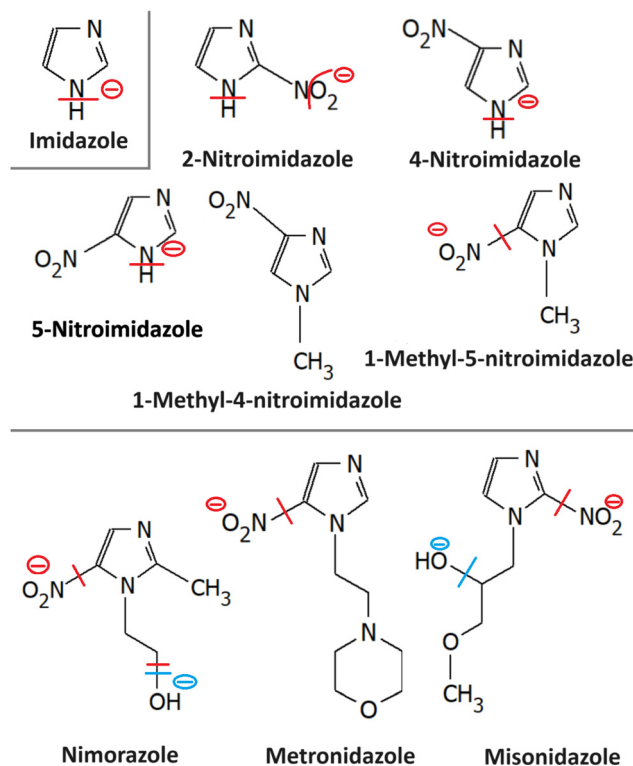


Fig. 6 Radiosensitizers from the group of nitroimidazoles and their model compounds, whose reactivity with LEEs is discussed in the text. From top to bottom imidazole (3.1) and nitroimidazoles (3.2); nimorazole (3.4); metronidazole (3.3) and misonidazole (3.5). The red line marks the bond broken in the most intense DEA reaction of the molecule identified for the isolated molecule, and the blue line the dissociation for a solvated molecule. The minus sign marks the anionic DEA fragment.

depletion of nucleophiles, formation of toxic products, and interference with recombination reactions.¹⁷⁰

Nitroimidazoles are efficient under hypoxic conditions, which further support their bioactivation mechanisms by single electron reduction, a process in strong competition with oxygen reduction under normoxic conditions (see Fig. 7).¹⁷¹ The single electron reduction may be induced by electron transfer¹⁷² in applications such as antibiotics or antiparasitics, while direct attachment of LEEs may be responsible for their activation during radiotherapy.⁷⁶ The genotoxicity can be then induced by the nitro anions, reactive oxygen species or redox reaction intermediates. The remaining problem is that the most important mechanisms of genotoxicity have not been identified yet, despite very systematic studies on a range of compounds.^{173,174} Only a full understanding of the nature and reactivity of nitro anions formed after LEE interaction will enable rational design of new radiosensitizers and possibly also more efficient antibiotics.

3.1 Imidazole

Similar to pyrimidine bases, imidazole contains N–H bonds prone to dissociation upon low-energy electron attachment. In the unsubstituted imidazole, the N–H bond strength is high and therefore DEA can occur only at energies above 1 eV *via* π^*



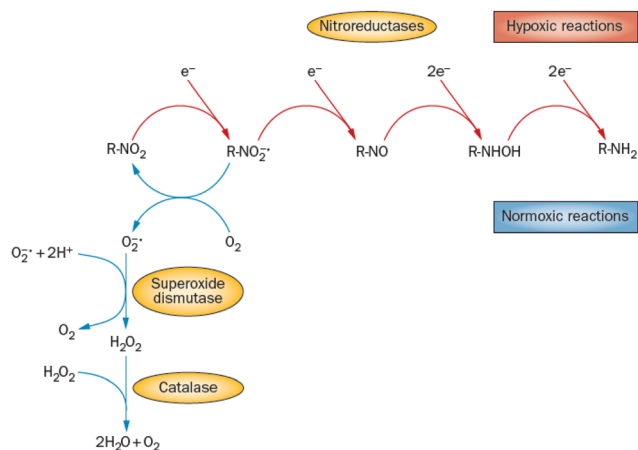


Fig. 7 Different radiation chemistry of nitro group under hypoxia and normoxia. While under normoxic conditions single electron reduction is in strong competition with the reduction of oxygen, under hypoxia multiple electron reduction occurs leading to a variety of reactive radical species. Reproduced from ref. 171 with permission from Springer Nature, copyright 2012.

resonances. Electron attachment, however, can occur also *via* low-lying VFRs due to the high dipole moments of azoles (*e.g.* 3.67(5)D for imidazole).¹⁷⁵ Such attachment is also discernible from the electron transmission spectroscopy.¹⁷⁶ Competition between electron auto detachment, DEA, and valence anion stabilization for these VFRs is then controlled by the functional groups attached to the ring as will be discussed for particular derivatives. Another important similarity to pyrimidines is in the strong coupling of σ^* and π^* states,¹⁷⁷ which is an important characteristic of the CN–H moiety.³⁸

Imidazole loses hydrogen *via* shape resonances in 1.5–4 eV range,^{176,178} presumably upon electron attachment to the LUMO and LUMO+2 orbitals.^{177,179,180} In isoxazole additionally, O–N bond can be cleaved at energies as low as 1.5 eV leading to the ring opening.^{181,182} At higher energies, core excited resonances can be identified in the 6–11 eV range also leading to the N–O bond cleavages and ring opening in imidazole¹⁷⁶ or isoxazole.¹⁸¹ An important process observed is multiple hydrogen cleavage at low energies that must be accompanied by hydrogen molecule formation.^{176,178} The fundamental electron attachment properties of the imidazole ring, its propensity to be opened or fast hydrogen migration across the ring all transform to the LEE-induced chemistry of more complex models of imidazole-based radiosensitizers.

3.2 Nitroimidazole

A range of nitroimidazoles has been studied as model compounds for electron-affinic radiosensitizers. In the systematic DFT exploration and electrospray experiments of Feketeová *et al.*¹⁸³ eight derivatives were studied. For all the studied compounds, the most stable anion structure has the additional electron localized on the nitroimidazole with only negligible effect from the other functional groups. Fig. 8. The SOMO energies are influenced only by the nitro group position on

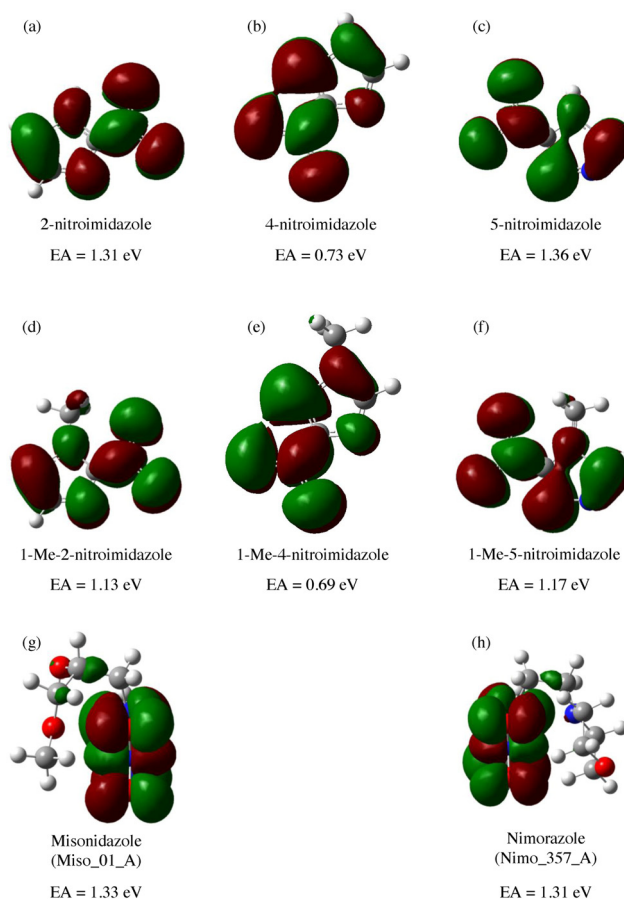


Fig. 8 M062x/6-311+G(d,p) optimized structures of radical anions and their SOMOs reproduced from the work of Feketeová *et al.*¹⁸³ with permissions from Elsevier, copyright 2014. We can see that in these compounds, the electron is always localized over the imidazole ring and while the nitro group position shifts the SOMO energy levels, the other substituents have practically no influence. Single occupied molecular orbital SOMO, forms upon electron attachment into the lowest unoccupied orbital (LUMO) of the neutral precursor molecule. The effects of the substituents can be expected for attachment at higher energies due to the often observed additive effect of electron attachment.^{184,185}

the ring. As a result, the adiabatic electron affinity of 4- and 5-nitroimidazole have values around 1.3 eV, while that of 2-nitroimidazole is more than 0.6 eV lower. Despite that, fragmentation induced by LEEs to 2-nitroimidazoles is richer than that of the 4- and 5-nitroimidazoles.

In all nitroimidazoles, the most intense DEA channel is the release of neutral OH. The second, still exothermic, channel is NO release and the third is hydrogen release. The nitro group is strongly bound to the ring and therefore cross section for the nitro C–N bond cleavage *via* both NO_2^- or $(\text{M}-\text{NO}_2)^-$ channels is observed in a shape resonance around 3 eV. An additional fragment appears in 2-nitroimidazole due to the release of a neutral water molecule. The calculated reaction barriers for this process are practically isoenergetic for 5- and 2-nitroimidazoles,¹⁸⁶ and therefore exclusive observation of this channel for 2-nitroimidazole is quite surprising. Either the channel is closed in 5-nitro derivative due to the dynamical



restraints or the anion product may differ from that predicted by calculation. In the first case, one can imagine a two-step process. In 2-nitroimidazole oxygen interacts with hydrogen at position 1 and position 2 to form water, in 5 nitroimidazoles, upon the interaction with hydrogen at position 1, the formed OH and hydrogen at position 4 will be separated by the remaining NO group at position 5 of the molecule preventing the fragmentation. In the second case, *e.g.* ring opening isomerization of the formed anion may be energetically more favorable upon 1,5 dehydrogenation in contrast to 1,4 dehydrogenation, which can influence the reaction enthalpy as well as the lifetime of the formed anion with respect to the autodetachment.

Another interesting observation for nitroimidazoles is that methylation of N1 hydrogen suppresses the fragmentation of molecules below 2 eV.^{187,188} Methylation of hydrogen sites is quite a common approach used in fragmentation studies to assign dissociation sites.^{189–191} In the case of nitroimidazoles, however, the methylation on the N1 position closed all fragmentation at energies below 2 eV.¹⁸⁷ This is clear for channels relying on N1–H dissociation such as OH release, but the influence on the NO or NO₂[−] release is not straightforward. 2 processes have to be separated at these energies.

The first is π^* resonance, identified theoretically.¹⁹² The lifetime of the resonance with respect to autodetachment is significantly lower upon methylation at the N1 site. The result is the disappearance of the resonance from fragmentation but also from the parent anion spectra. Autodetachment is faster than anion detection.

The second region of energies is below 1 eV, where strong VFRs result in the release of NO. This channel is closed upon methylation and a stable anion is formed, which can have several explanations. The first is the change in the molecular dipole moment and the size of the dipole-bound state. These effects on dipole-supported states were explained by Desfrancois and co-workers.¹⁹³ A decrease of the dipole moment due to the methylation can result in a lowering of the affinity for the VFR.¹⁹⁴ For small molecules important effect can have also an increase in the molecular size. For larger molecules, the molecular core potential is better shielded and the probability of electron attachment is lower. On the other side, the polarizability, also influencing the VFR formation, can be larger, and therefore, the interplay of these effects on VFRs should be carefully explored from one case to another. In the discussed case of methyl-4-nitroimidazole the dipole moment is huge, larger than that of the bare 4-nitroimidazole 8.50 D *vs.* 7.78 D and the molecules are relatively large, the addition of the methyl does not have a significant effect on molecular size. Probability for the formation of VFRs is therefore not influenced what is reflected in a strong signal of the molecular parent anion at near 0 eV energy.

The nitro group fragmentation *via* VFRs therefore must be influenced on the side of the outgoing – dissociative channel. Either it is the hydrogen migration upon DEA and NO release that can result in the formation of hydroxyl form of (M–NO)[−] anion instead of carboxyl form in 4-nitroimidazole but not in

the methyl-4-nitroimidazole or methylation stabilizes the parent anion by a different mechanism, such as the ring opening. Additionally, all these molecules are studied upon sublimation. At such conditions, different propensities of molecules for dimerization can result in a surprising parent ion stabilization, particularly in the case of VFRs. This was observed *e.g.* in the case of pyruvic acid.¹⁹⁵

Nitroimidazoles efficiently attach electrons also in the energy region of core excited resonances above 6 eV. However, practically no DEA fragmentation is observed at these high energies. In the study of a model compound 1-methyl-5-nitroimidazole, it was suggested that dissociation into two neutral fragments may occur at these energies, pointing out the importance of the studies of neutral dissociation products upon electron attachment.⁸⁰ The total scattering cross section at low energies was complemented by differential and DEA as well as ionization cross sections in the follow-up publication.¹⁹⁶ We would like to add that in complex environments the core excited resonances may play an important role irrespective of the dissociation as they can act as doorways for electron transfer (Fig. 2c) discussed in the introduction.

3.3 Metronidazole

The formation of negative ion intermediates of metronidazole during pulsed radiolysis was already identified in the 1970s by the ESR study of Willson.¹⁹⁷ The fundamentals of LEE interactions with the molecule isolated in the gas phase and in the microhydrated environment were, however, explored only recently.¹⁹⁸ Electron attachment spectroscopy of isolated and microhydrated molecules shows that irrespective of the environment the molecule forms a stable parent anion in agreement with the early pulsed radiolysis studies. Main DEA reaction channels include the release of NO₂[−] and OH[−]. While the first channel is strongly quenched in the water environment, OH[−] may be still observed as a minor channel upon hydration.

3.4 Nimorazole

Nimorazole interacts with low-energy electrons in two main energy ranges. Strong near 0 eV resonance results in the formation of a stable parent anion. Nimorazole has a large adiabatic as well as vertical electron affinities of 1.31 eV and 0.82 eV, respectively.¹⁸³ The reported cross section of 3×10^{-18} cm² indicates S-wave electron attachment. However, the bump at 0.2 eV in the parent anion yield measured in the same work and structure corresponding to the negative electron affinity of 0.4 eV in the electron transmission spectrum in collisions with K⁺ ions¹⁹⁹ indicate that also VFRs are present, in line with the VFR feature in the electron transmission spectrum of imidazole.¹⁷⁶ The adiabatic electron affinity is still not enough for imidazole ring opening or significant molecular rearrangement and the anion is primarily stabilized by intramolecular energy redistribution in the gas phase or intermolecular energy transfer in the solvent.⁷⁶ At higher energies a rich fragmentation pattern can be observed *via* shape resonances in



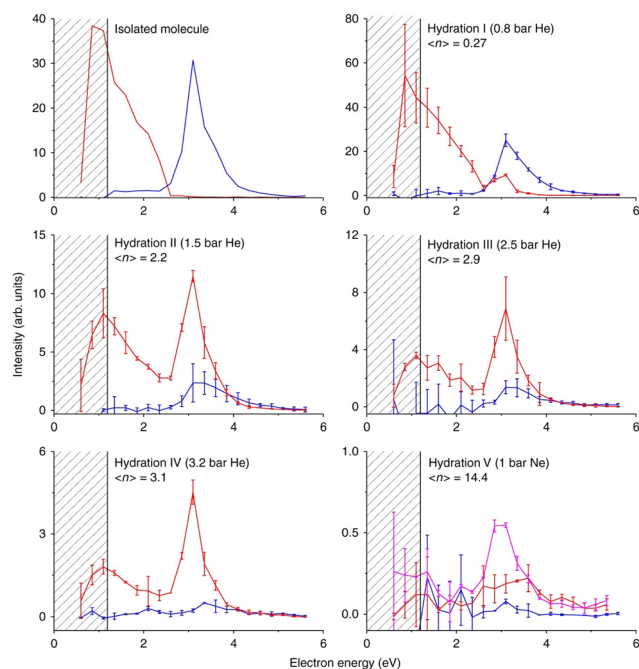


Fig. 9 Caging of DEA fragments of nimorazole studied in the molecular beam of microhydrated molecules. Hydration (average number of water molecules attached to nimorazole neutral precursor) rises from top to bottom and from left to right. The red curve represents the ion yield of the parent anion M^- , blue curve represents the ion yield of NO_2^- after the cluster interaction with LEEs at energies shown on the x-axis. Increasing hydration, the peak of NO_2^- at ~ 3 eV disappears, while the M^- signal appears at the same energy demonstrating the "caging effect" of the environment on the DEA reaction. A drop of the near 0 eV signal of the parent anion is caused by the fact that at higher hydration, the energy gained in the electron attachment is not enough to evaporate all water molecules from the cluster and $M^-(H_2O)_n$ cluster anions are produced instead of M^- . Reproduced from ref. 76 with permission from Springer Nature, copyright 2019.

the 2 eV to 4 eV energy range. The only significant signal is, however, observed for NO_2^- anion.²⁰⁰

The work of Meißner *et al.*⁷⁶ is particularly important for demonstrating the caging effect of the environment on the DEA. In microhydrated water clusters, electron attaches to the same resonances of the nimorazole as in the isolated system. However, these resonances are no longer dissociative but lead to the formation of stable parent anions as shown in Fig. 9. With the rising number of water molecules, covering the nimorazole in the neutral precursor cluster, nimorazole parent and heterogeneous nimorazole-water cluster anions were reported for the same electron incident energies as observed for the dissociative shape resonances in the gas phase.

The stabilization of the nimorazole parent anion upon single electron reduction was recently confirmed by cyclic voltammetry in bulk water.²⁰¹ However, also 4 electron reduction was reported resulting in the hydroxylamine derivative formation at specific conditions. Except for the confirmation of the relevance of cluster studies for the LEE-induced chemistry in the bulk, the work also expresses the need for extending the studies with microhydrated molecules to other

solvents as well as towards the multiple electron reduction experiments.

3.5 Misonidazole

Pulsed radiolysis studies of misonidazole were performed in 1980's reporting a high rate constant for interaction with solvated electrons $2.5 \times 10^{10} M^{-1} s^{-1}$.²⁰² The products of such interaction as well as the interactions with LEE electrons in the (0–10 eV) can be understood based on the experiments in the gas phase²⁰³ and the microhydrated environment.²⁰⁴ Similar to imidazole, two energy ranges for electron attachment have been identified, where the 0 eV attachment leads to the formation of parent anion while 2–4 eV shape resonances lead to the variety of the fragment anions dominated by the NO_2 bond cleavage. In contrast to nimorazole, MISO fragmentation upon interaction with LEEs seems not to be fully suppressed by hydration, but OH^- channel remains open. This may be caused by the preferred hydration of the MISO over the hydroxyl group and predissociation as supported by theoretical calculations in the work.²⁰⁴ Computational modeling also reveals that TNI fragmentation *via* OH loss can be accompanied by significant rearrangement of the neutral counterpart forming ring structures and increasing the exothermicity of the process in solution.

4 Organometallics

Most of the organometallic cancer chemotherapeutics (Fig. 10) are designed to bind covalently to the DNA or intercalate, resulting in inter- and intrastrand crosslinks or secondary structure distortions. The most studied organometallics concerning chemo-radiation therapy are platinum compounds²⁰⁵ due to the initial success of cisplatin (CDDP). CDDP releases Cl atoms in a water environment becoming reactive towards DNA where it forms preferentially guanine adducts²⁰⁶ and intra-strand crosslinks with high susceptibility for further reaction to form DNA-protein²⁰⁷ or guanine-cytosine crosslinks.²⁰⁸ These interactions strongly interfere with the DNA repair mechanisms that are accepted as one of the leading explanations of the CDDP mechanism of action.²⁰⁹

Concerning the low-energy electrons, the most interest is in synergism observed for the CDDP and radiation therapy. The synergism can also be caused by the CDDP involvement in the DNA repair pathways in the biological stage of the tissue interaction with ionizing radiation. However, if the synergism occurs already during the physicochemical stage of the interaction, the tiny effects may result in significant radiosensitization on the biological timescales.³ Therefore, the fundamental reactivity of low-energy electrons towards CDDP and its DNA adducts has been under investigation for more than 15 years. The first suggestions on the LEE involvement in CDDP synergism came from the works of Q. B. Lu and coworkers, demonstrating fast electron transfer from guanine base to CDDP within its single covalently bound DNA adduct. Such transfer can result in Cl^- release having two possible



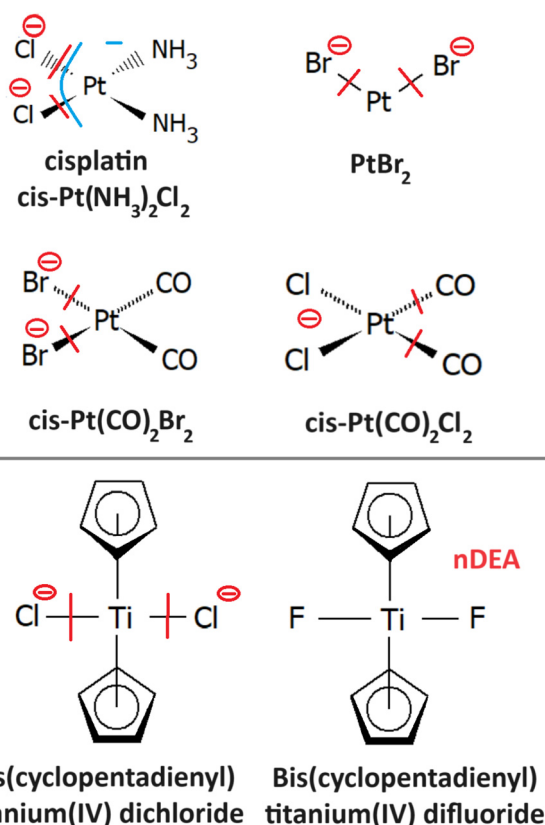


Fig. 10 Radiosensitizers from the group of organometallics and model compounds, whose reactivity with LEEs is discussed in the text: cisplatin (4.1), PtBr_2 (4.2); $\text{PtBr}_2(\text{CO})_2$ (4.3); titanocenes (4.4). The red line marks the bond broken in the most intense DEA reaction of the molecule identified for the isolated molecule, and the blue line the dissociation for a solvated molecule. The minus sign marks the anionic DEA fragment.

sensitizing effects, increasing cross-linking efficiency for the Pt adduct and reactivity of the formed Cl^- anion.²¹⁰ Several follow-up works in the Q. B. Lu group were devoted to these mechanisms including suggestions for novel chemo-radio therapy combinations.^{210–212} In the L. Sanche group, the direct action of LEEs was investigated mainly in the drug-loaded DNA thin films in the surface experiments with ballistic low-energy electrons in vacuum⁷⁷ and in the simulated environment.²¹³ However, also a series of studies was performed in realistic conditions of plasmid DNA in buffer solutions, where the electron effects were disentangled by the suppression of the radical chemistry by scavengers. (e.g. ref. 214 and 215).

4.1 Cisplatin

The only gas phase study of electron attachment to isolated cisplatin is that of Kopyra.²¹⁶ CDDP strongly attaches near 0 eV electrons resulting in a range of products in decreasing probability order Cl^- , $[\text{Pt}(\text{NH}_3)_2\text{Cl}]^-$, $[\text{Pt}(\text{NH}_3)_2]^-$, Cl_2^- , and NH_2^- . Particularly the fact that a single electron can induce dissociation of both Cl to Pt bonds and form a reactive cross-linking intermediate $[\text{Pt}(\text{NH}_3)_2]^-$. The mechanism of multiple bond cleavages can be operative also in cases when CDDP is already bound to the DNA. Additionally, the single dehalogenated

fragment $[\text{Pt}(\text{NH}_3)_2\text{Cl}]^-$, which is formed in the second most intense channel of DEA, is highly reactive towards DNA.²¹⁷

Most of the later studies focus on creating the links between LEE-induced processes and chemo-radiation therapy by studies of cisplatin-modified DNA. For example in the study of Bao *et al.*, five monolayer DNA films were irradiated with and without cisplatin showing approximately doubling of the damage in the 3 eV to 19 eV range. Most important is the observation of a single electron induced double-strand breaks in the incoming electron energy range of 1.6 to 3.6 eV, which was not present in the unmodified DNA.²¹⁸ The work of Rezaee shifts the LEE damage limit much lower, to 0.5 eV energies causing both single and double-strand breaks and enhancing the formation of DNA lesions.²¹⁹ In a later work, absolute cross sections for the damages were determined for 5 monolayers of DNA irradiated in vacuum at resonance energies 4.6 eV and 9.6 eV. At 4.6 eV, $244 \pm 42 \times 10^{-15}$ damages per electron and molecule were reported, while at 9.6 eV, $359 \pm 44 \times 10^{-15}$ damages per electron and molecule.²²⁰ Clustered damages in DNA were reported in 5.6 eV to 10 eV range, while no clustered lesions are observed at LEE energies below 5 eV.²²¹ This energy dependence, also shown at Fig. 11, demonstrates how important is to know the details of LEE interaction including the initial state of the TNI related to the energy of the incident electron as well as the evolution of the TNI.

An important set of experiments was performed also on DNA oligomers by Behmand and co-workers. In the first work,²²² TTTTGTGTTT and TTTTTTGTTT oligomers loaded with CDDP were irradiated by gamma rays in solutions with EDTA, scavenging the OH radicals and enhancing the effects of solvated electrons. The work demonstrated the solvated electron damage at the CDDP site. In the follow-up work,²²³ HPLC MS was employed to elucidate more details on the mechanism of the damage. The process was described as an initial electron attachment to thymine followed by electron transfer to CDDP and base or cisplatin release. The same approach was used also in the third work on the topic,²²⁴ studying shorter GTG sequence demonstrating the catalytic effect of cisplatin on the reactivity with solvated electrons. CDDP presence increased the rate constant for interaction with solvated electrons from $(7.4 \times 10^9 \text{ mol}^{-1} \text{ L s}^{-1})$ for bare GTG oligomer to $(2.23 \times 10^{10} \text{ mol}^{-1} \text{ L s}^{-1})$ for GTG-CDDP complex. Similarly, a strong enhancement was observed also for double-stranded oligomers showing an increase of the reaction rate from $2 \times 10^9 \text{ mol}^{-1} \text{ L s}^{-1}$ to $7 \times 10^9 \text{ mol}^{-1} \text{ L s}^{-1}$. Additionally, the transformations of intra- to interstrand crosslinks were identified for CDDP-modified strands using gel electrophoresis.²²⁵

Despite a high number of studies in solution, the gas phase studies with Pt-based organometallics are scarce. The reason behind this is the weight of the Pt atom and the low decomposition temperature of organic ligands. If the molecule is not directly designed for sublimation, there is a high probability that it will thermally decompose before sublimation. Therefore, the gas phase experiments with these compounds are very complicated and as most of the experiments focus on the anion products, it is also hard to identify, if the attachment occurred



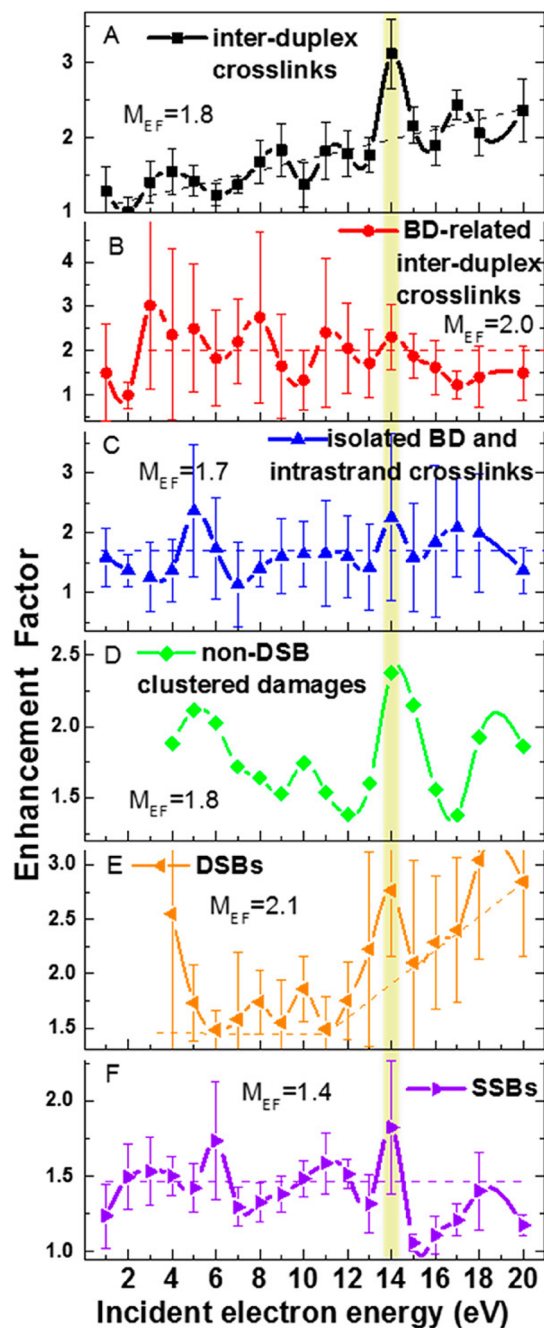


Fig. 11 Enhancement factors for different types of DNA damages from the ratios of damages for cisplatin–DNA to those of unmodified DNA as a function of the energy of incident electron reproduced from the work of Dong *et al.*²²¹ with permission from American Chemical Society, copyright 2020. We can see that cisplatin enhances all types of damages at all studied energies showing that there is a constant enhancement component introduced by cisplatin such as enhancement of LEE scavenging, enhancement of access sites or enhancement of the deposited energy. At the same time, we can see that at some energies the enhancements are more pronounced, demonstrating also resonant – LEE related contribution.

to the parent anion or a part of the molecule formed during thermal decomposition. This requires either detailed studies of temperature dependencies or detection of neutral by-products

as already mentioned several times, ideally in the coincidence regime. Few other organometallic compounds were therefore studied to better understand the chemistry of CDDP as well as the details of the chemo-radiation synergism. The examples are.

4.2 PtBr₂

Radiosensitizing potential of this compound was identified in the work of Śmialek *et al.*,²²⁶ by evaluating damage enhancement in plasmid DNA upon X-ray irradiation. The DEA reaction results exclusively in the formation of Br[−] anions.²²⁷ Three resonances were observed in the spectrum. The most intense signal at 0.4 eV was assigned to the impurity of HBr as a possible product of PtBr₂ reactions with residual water in the inlet system since the strong temperature dependence of its signal did not correlate with the other observed features in the spectrum. It is worth noting that such behavior of near 0 eV cross section is not uncommon,²²⁸ even though the impurities are a significant issue in the electron attachment spectroscopy of halocarbons.²²⁹ Based on DFT calculations of reaction enthalpies, the signal peaking at 1.2 eV and 7 eV was assigned to DEA reactions leading to PtBr and Pt+Br neutral co-products.

4.3 Pt(CO)₂Br₂, Pt(CO)₂Cl₂

Modification of organometallics by carbonyl groups represents a common way of increasing sublimation efficiency, mainly for applications in charged particle beam-induced deposition. The present study demonstrates that such modification can significantly influence also the DEA dynamics. For previously discussed PtBr₂ and CDDP, the primary DEA channel is leading to the formation of halogen anion. Both carbonyls Pt(CO)₂Br₂²³⁰ and Pt(CO)₂Cl₂²³¹ lose primary the CO ligands, despite the exothermicity of halogen anion formation channel. The provided explanation is based on the different orbitals available for electron attachment. While the LUMO of CDDP or PtBr₂ has σ* antibonding character LUMO of the carbonyl compounds have π* character that additionally do not allow energy flow to the Pt-halogen vibration due to the symmetry restrictions. CO ligands can provide an effective energy sink *via* C–O stretches as shown for Fe(CO)₅, prolonging TNI lifetime over several vibrational periods. As a result the PtBr₂ and CDDP fastly dissociate in a direct non-ergodic process, while the dissociation of carbonyl molecules will be probably more ergodic. It would be interesting to theoretically explore the interplay using time-dependent molecular dynamics approaches.

These studies of seemingly unrelated compounds bearing carbonyl ligands provide an important insight into the fundamental mechanisms of CDDP dissociation with possible consequences for the design of CDDP analogs. Most of the CDDP successor compounds suggested so far are complex molecules, where the direct dissociation upon single electron reduction can be quenched by energy dissipation into internal degrees of freedom. In other words, a significant portion of energy available upon single electron reduction is consumed by heating of the molecule rather than its fragmentation. Pt molecules, where such energy dissipation is minimized and direct bond



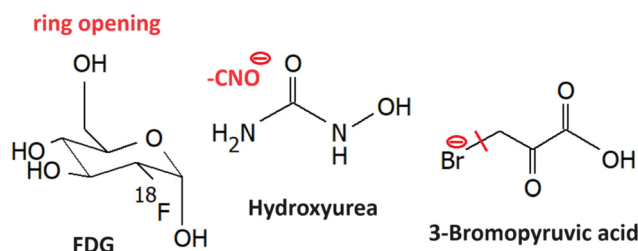


Fig. 12 Other small molecule radiosensitizers discussed in the text: fluorodeoxyglucose (5.1), hydroxyurea₂ (5.2) and 3-bromopyruvic acid (5.3). The red line marks the bond broken in the most intense DEA reaction of the molecule identified for the isolated molecule, and the blue line the dissociation for a solvated molecule. The minus sign marks the anionic DEA fragment.

cleavage is possible may be promising radiosensitizers. Indeed the high radiosensitizing potential of PtBr₂ reported by Śmiałek and co-workers²²⁶ supports this hypothesis.

4.4 Bis(pentamethylcyclopentadienyl) titanium(IV) dichloride and difluoride

The idea behind the study²³² is to separate LEE processes from ionization processes in realistic conditions by designing selective probes for such processes. Out of the two molecules, the dichloride efficiently dissociates by the release of Cl⁻ while the difluoride anion signal upon electron attachment is dominated by the parent anion. At the same time, the ionization cross section is controlled by huge pentamethylcyclopentadienyl rings and it is similar for both molecules. Upon distribution into the environment, Cl⁻ formation can be used as a selective probe for electron attachment and therefore contribute to the evaluation of absolute numbers for the reactions of secondary LEEs in radiation chemistry and chemo-radiation synergism.

5 Other small molecules

LEE reactions of several other small molecule radiosensitizers were explored, such as the ones shown in Fig. 12.

5.1 Fluorodeoxyglucose

Fluorodeoxyglucose, which is commonly used in tumor imaging in its F18 form is an example of a sugar with high reactivity towards LEEs. Electrons lower than 2 eV can cause the decomposition of FDG and it leads to 7 anions out of them, C₃H₃O₂⁻ has the highest yield. Dissociation of HF is less energetic demanding than dissociation of F⁻. Therefore, F⁻ is forming only a minor DEA channel. However, the formed TNIs can decompose *via* a large number of dissociating channels including ring opening and reactions leading to the formation of neutral molecules, such as H₂O, H₂, HF.²³³

5.2 Hydroxyurea

Upon administration in living organisms, hydroxyurea efficiently creates nitric oxide in a set of one to three electron redox reactions.²³⁴ Nitric oxide inhibits ribonucleotide reductase enzyme, as discussed for nitroimidazoles, which is believed to

be the primary mechanism of action.²³⁵ However, other reactive species can also be formed such as hydroxylamine or hydrogen peroxide, which are genotoxic.²³⁶ The need to understand multiple electron reduction as well as the involvement of electron affinic radiosensitizers in DNA repair was already mentioned in several places within the review.

Hydroxyurea has a large dipole and therefore it can attach electrons *via* VFRs.²³⁷ However, the parent anion is unstable and fragments due to the high electron affinity of its components. The most intense anion reported is NCO⁻. The electron attachment spectrum shows three peaks at 0 eV, 0.1 eV, and 0.4 eV, which is not typical for the vibrational structure that should be in this region distributed approximately equidistantly. On the other side, Therefore an explanation for the structure was based on the possible attachment of the electron into three different conformers of the molecule that could be present in the gas phase. The process discussed *e.g.* for amino acid serine.²³⁸ Other fragments are produced *via* shape resonance peaking at ~2 eV ((M-H)⁻, (M-OH)⁻, (M-H₂O)⁻, CN⁻) and core excited resonance ~6 eV ((M-H₂O)⁻, NH₂⁻, OH⁻, CN⁻). No hydroxylamine was observed upon LEE. It will be definitely interesting to explore how hydration changes the hydroxyurea reaction dynamics.

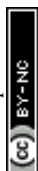
5.3 3-Bromopyruvic acid

3-Bromopyruvic acid is similar to the discussed nitroimidazoles active in hypoxic cells. The believed mechanism is *via* inhibition of glycolytic pathway enzymes.²³⁹ These are more pronounced in tumors due to hypoxia. Under normoxia, the energy is gained *via* ATP phosphorylation. It is worth mentioning that electron transfer reactions play an important role in both hypoxic and normoxic glycolysis,²⁴⁰ which may have consequences for the secondary LEE effects on the cell viability. Electron attachment 3Br pyruvic acid is dominated by strong Br⁻ ion yield at near 0 eV energies,²⁴¹ which corresponds to the s-wave attachment and exothermic dissociation (ref. (Fig. 1a)). This is in strong contrast to pyruvic acid, where VFRs are observed with only a short lifetime with respect to autodetachment and therefore they are detected only upon anion stabilization in a three-body process.¹⁹⁵ This strong enhancement of the electron attachment cross-section by Br substituent was proposed as one of the possible mechanisms of radiosensitization by 3-bromopyruvic acid.

Another important observation is a strong shift in the electronic excited states of the anion due to the presence of bromine. While in pyruvic acid, the core excited resonances peak above ~6 eV, in 3-bromopyruvic acid it is at under 5 eV.

6 Conclusions and perspective

A large number of radiosensitizing molecules has been studied concerning LEE interactions during recent years. Studies for DNA base components, nitroimidazoles, and organometallics already demonstrated the variety of interaction regimes with LEEs and suggested some important mechanisms that can



contribute to the high efficiency of these compounds in concomitant chemo-radiotherapy. While DNA bases or platinum compounds decompose exothermically in processes that often cannot be prevented by energy transfer to the environment, nitro-azole decomposition is more energetically neutral and their anions often stabilize in the environment. DEA therefore does not provide the only explanation of the fundamental radiosensitizing mechanism by electron affinic radiosensitizers. The overview of so far suggested mechanisms is in Fig. 13 To provide real societal impact, these mechanisms need to be evaluated on more complex biophysical models.

For example, in the molecular physics community, enormous focus is given to DNA interactions and damage. This is natural since DNA damage is the most lethal form of cellular damage. On the other hand, life evolved in an environment with a relatively high radiation background, and therefore, various mechanisms exist in living organisms to mitigate radiation damage to DNA.²⁴² Instead of focusing on DNA damage, as something expected by the organism, we should focus on the less expected changes in the cellular environment. When exploring the effects of the three types of molecules reviewed here, each of them is actively influencing the DNA repair processes. The role of LEEs in the repair process is practically unexplored. For that, a crucial point will be to involve the repair enzymes in more complex studies in a realistic environment. On the level of DNA in bulk solution,

one can use time-resolved absorption spectroscopy²⁴³ or state-of-the-art X-ray crystallography.^{244,245} Another approach is to design complex architectures for single-molecule experiments.²⁴⁶ One such architecture, the DNA origami frame developed by Endo *et al.* was already demonstrated to be suitable for enzyme interaction studies.^{(e.g. ref. 247).}

Further directions of complex biological pathways that may be explored concerning the evolution of the negative ions and radicals produced by secondary LEEs on chemical and biological timescales of radiation interaction with radiosensitizing compounds are shown in the red box of the Fig. 13. Except for the mentioned DNA repair processes these include effects on the cellular membrane or metabolism that are practically unexplored and will require *in vitro* biophysical and biochemistry studies.²⁴⁸ Another direction is the higher-order structure of DNA. In this direction, the telomeric sequences are in the focus at the moment.^{249,250}

The suggested studies of biological consequences can provide guidelines for selecting relevant targets for LEE interactions on the molecular level. Only systematic experimental studies on the molecular level, which can be well complemented by computational modeling, can provide the level of understanding required for reaching the ultimate objective of all these efforts – providing the base for the rational design of novel chemo-radiotherapy agents. The basic needs that we identified are visualized in Fig. 14 and in this section, we will describe them in more detail.

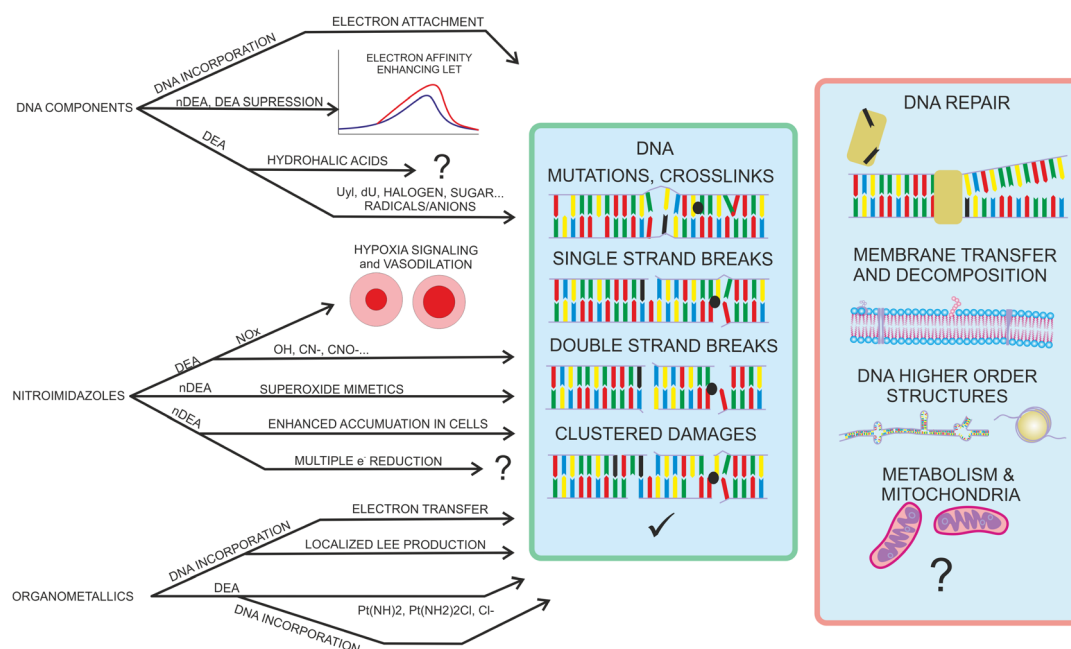


Fig. 13 Different mechanisms proposed for radiosensitising and synergistic effects of LEEs with derivatives of DNA components, nitro azoles and organometallics. So far the research has focused on direct DNA sensitization towards the LEEs by enhancement of base excision, mutations, crosslinks, single and double-strand breaks, or clustered damages as depicted in the central green box of the image. The combined action of LEEs and the radiosensitizers on the other cellular mechanisms is practically unexplored. LEE based radiosensitizers can form negative parent ions or reactive species that can influence repair enzymes, electron transfer chains through cellular membranes, interact with membrane lipids and proteins, modify the higher order structure of DNA or enter into mitochondrial and other cell metabolism processes. Exploration of these processes will require further extension of molecular physics experiments towards biochemistry and biophysics.



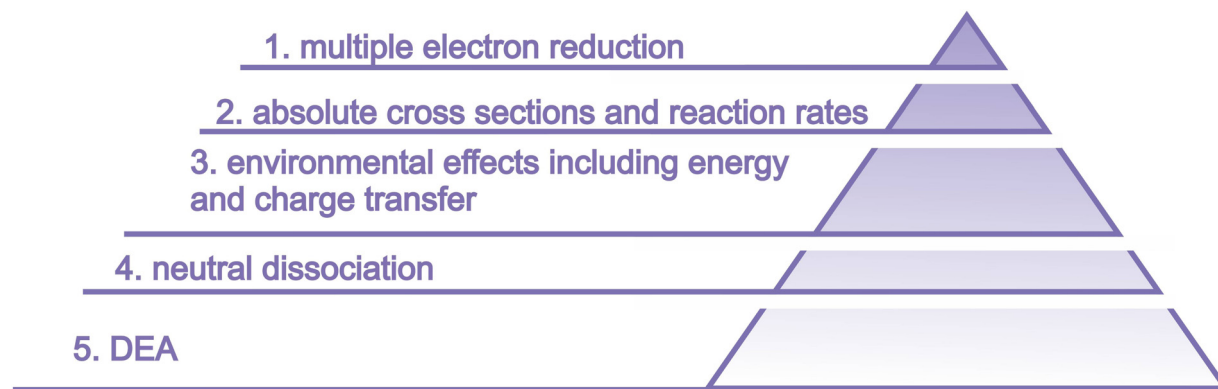


Fig. 14 Suggested experimental research directions for exploration of LEE interactions with model radiosensitizers. Interplay between the needs and current state of the art can be visualized by a pyramid, where the importance decreases from the top to the bottom of the pyramid, while the present number of the studies is represented by the area of the corresponding level of the pyramid.

6.1 Multiple electron reduction

Studies with isolated molecules or clusters are performed for singly charged species. Complex molecules can undergo multiple electron reductions, particularly in an environment, where the singly charged TNI can be stabilized by energy transfer to solvent. Multiply-charged anions in the gas phase attracted significant interest in 1990s and 2000s.^{251–254} Their preparation using the electrospray or sputtering technique is straightforward and state of the art time resolved photoelectron spectroscopy can already reveal intriguing details of state to state, oxidation or dissociation dynamics of these species.^{255–257}

Here we suggest that in addition to studies of these stable species, the field will profit from studies mimicking the multiple electron reduction and therefore performing step-by-step electron attachment, ideally in a time-resolved manner. While some information about the process can be revealed from voltametry²⁰¹ the details of the dynamics can be revealed only by performing step-by-step attachment of electrons, similar to the pioneering experiment with C_{84} of Compton and coworkers.²⁵⁸

6.2 Absolute numbers for LEE formation and reaction rates

The number of works studying absolute numbers for LEE-induced reactions in complex biomolecular systems is low (see *e.g.* ref. 259) and the number of studies including radiosensitizers is even lower. Examples include surface experiments on DNA origami templates in vacuum,^{85,260,261} in controlled environment,^{213,220} or bulk.²²⁵ While the measurements of absolute cross sections for LEE interactions of isolated molecules is straightforward, the number of parameters influencing the reactivity in the more complex environment is high and needs to be carefully analysed.²⁶²

The most promising approach seems to be pulsed radiolysis, where, however, the LEE reactions are generally induced by high-energy radiation. The disentangling of LEE contribution is not straightforward. Either the laser-induced electron transfer has to be used as in the seminal works of Q. B. Lu, or the environment has to be precisely controlled by modifying

electron scavenger (such as oxygen), or radical scavenger (such as tris) content. (*e.g.* ref. 134, 222, 263 and 264). However, the experiments must be performed with care about the the LEE-induced chemistry of buffer components to avoid misinterpretations.^{101,265,266}

Another possible approach can be quantitative electron-induced fluorescence.²⁶⁷ A properly designed fluorescent probe requiring singlet to triplet excitation by LEEs to induce fluorescence can be irradiated by LEEs in realistic environments *e.g.* in liquid jets.^{265,268}

Two approaches to LEE-induced processes come from the field of aerosol research. In the first approach, a photoelectron is produced inside homogeneous or heterogeneous aerosol by a tunable wavelength light source and escapes the aerosol.^{269,270} Combination of this approach with biomolecular doping and advanced anion detection techniques may provide new insight into transient anion formation as well as dynamics. The second approach already significantly contributed to establish the links between the radiation chemistry in bulk and the formation of transient negative ions. In the experiment, a high-energy ionizing particle interacts with aerosols containing molecules of interest, and negative ions are analyzed using mass spectrometry.²⁷¹ The technique was already applied to several biomolecular targets.^{272–274} Adaptation of these techniques for absolute data measurements would be beneficial.

The methods to prepare and study LEE-induced processes at biologically relevant conditions are the subject of recent reviews of Gao and co-workers²⁷⁵ or that of Alizadeh and Ptasinska.²⁷⁶

6.3 Environmental effects

The reviewed experiments are on a limited set of molecular systems that cannot reproduce the complex radiation chemistry in biological buffers. We need to experimentally explore a much larger amount of solvent, counter ions, or cellular components, such as DNA-peptide or lipid TNI formation, and their dynamics in various solvents.

There is an ongoing discussion about shifts of the electron attachment resonances in the presence of a solvent.^{277–279} For some systems, the shifts can be identified using photoelectron



spectroscopy.^{280,281} However, as reviewed here for radiosensitizers, the anions often undergo DEA, TNIs are pre-dissociated or they undergo isomerizations. In such cases, the stable anion states, which can be used for photoelectron spectroscopy, do not correspond to that of the anion forming in the vertical attachment process. For some systems, this can be solved by electron transfer photoelectron spectroscopy.³¹ However, the most straightforward approach to probe the energetics of the initial electron attachment states will be a combination of the state-of-the-art sources of neutral cluster beams with electron sources having high energy resolution.

Another important issue is the stability of the molecular anions in the solvent. The cluster experiments, with relatively large water clusters, demonstrated that the initial resonant states correspond to that of individual solvated molecules rather than to the electron attachment to the water cluster *via* polarization interaction (*e.g.* Fig. 9).⁷⁶ However, there exists a theoretical prediction that in some systems the attachment or transfer of the electron to the solvent^{282–284} may be very effective. Except for the energy sink, the environment can provide an electron sink. In cluster beam experiments, we can probably explore the limits of the cluster size, at which the interaction with solvated molecules is completely shielded. Such information can be compared with the minimal molecular concentrations required to observe LEE effects in realistic environments. Important is to understand that while electron affinity is a characteristic of a single molecule, the potential well that traps the solvated electron requires the rearrangement of several molecules, and therefore even the adiabatically exothermic processes are often not barrierless. Anion lifetime and charge transfer to solvent studies using state of the art spectroscopy in gas phase or bulk can provide better insight into this interesting topic.

6.4 Neutral detection

The need for the studies of LEE processes in biologically relevant molecules was already well defined by Ptasinska *et al.*²⁸⁵ The detection of neutrals is important for the process of neutral dissociation upon electron impact as well as for dissociative electron attachment.¹ In the first case, various techniques were developed historically from electron energy loss-based approaches used mainly for diatomics to electron-induced fluorescence measurements performing well at higher energies, where electronically excited fragments are forming.^{286–288} Interesting can be a combination of the fluorescence technique with coincidence measurement of the outgoing electron, since the outgoing electron will provide information about the initial dissociative state while photons the final state of the dissociated fragment.

In the case of DEA process, except for the detection of neutral itself, as performed in the current state-of-the-art experiments,^{289–291} it will be beneficial to have the option to perform a detailed analysis of the neutral products. Only in such a way the complex rearrangement (*e.g.* ref. 204 or neutral molecule¹¹⁷) formation mechanisms could be unambiguously identified. Considering the low densities of the products

formed upon DEA, this will probably require sensitive laser based techniques such as the resonance-enhanced multiphoton ionization, as employed *e.g.* in the electron-induced desorption studies of Lane and Orlando.²⁹²

6.5 DEA

The number of DEA studies with radiosensitizers is significant and some general trends in the dynamics were already over-viewed in the present perspective. However, we are still missing systematic studies on larger sets of molecules.

Particularly interesting could be studies of azole derivatives. While the field focuses on imidazoles, there are also other molecules with azole ring having radiosensitizing potential.²⁹³ They form specific stacking interactions and they are intensely used in the drug design due to their biomimetic nature as well as because azoles are the product of several click chemistry reactions²⁹⁴ widely used in the modern drug design.²⁹⁵ Except for the better understanding of the radiosensitizing properties and possibly giving guidelines for the rational design of chemo-radiotherapeutics, the ring opening attachment can provide a way for selective modification of bonds created by click chemistry.

Another possible field of interest are organometallic complexes. Practically, the only thoroughly explored molecule is CDDP, few attempts for resembling LEE processes in solution exist for the CDDP analogs.^{77,213,296} However, there are many other organometallic molecules with promising radiotherapy applications,²⁹⁷ particularly these are ruthenium arene complexes.^{263,298}

The suggestions described in this part can be summarized in three directions. The first is the absolute numbers for the LEE-induced reactions that will allow unambiguous identification of the most relevant processes in chemo-radiation synergism. The second is the evolution of the TNI to understand not only the energetics of the processes but also the final products of LEE interaction in realistic environments upon electron transfer and multiple electron reduction. The third direction should focus on establishing more rigid connections between the initial LEE-induced processes occurring in the physico-chemical stage of ionizing radiation interaction and their biological consequences. For that, more active collaborations between physical chemists, biophysicists, and/or biochemists will be required.

Conflicts of interest

In accordance with our policy on. There are no conflicts to declare.

Acknowledgements

We would like to thank Juraj Fedor and Leo Sala for reading the manuscript and providing valuable feedback. The work was supported by Czech Science Foundation project number 21-26601X (EXPRO) and COST Action CA18212 – Molecular



Dynamics in the GAS phase (MD-GAS), supported by COST (European Cooperation in Science and Technology).

Notes and references

- J. Bednar, *Theoretical foundations of radiation chemistry*, 1990.
- E. Alizadeh and L. Sanche, *Chem. Rev.*, 2012, **112**, 5578–5602.
- R. Schurmann, S. Vogel, K. Ebel and I. Bald, *Chem. – Eur. J.*, 2018, **24**, 10271–10279.
- C. Szymtkowski and P. Mozejko, *Eur. Phys. J. D*, 2020, **74**, 90.
- R. D. White, D. Cocks, G. Boyle, M. Casey, N. Garland, D. Kononov, B. Philippa, P. Stokes, J. de Urquijo, O. González-Magaña, R. P. McEachran, S. J. Buckman, M. J. Brunger, G. Garcia, S. Dujko and Z. L. Petrovic, *Plasma Sources Sci. Technol.*, 2018, **27**, 053001.
- H. Nikjoo, D. Emfietzoglou, T. Liamsuwan, R. Taleei, D. Liljequist and S. Uehara, *Rep. Prog. Phys.*, 2016, **79**, 116601.
- S. A. Zein, M.-C. Bordage, Z. Francis, G. Macetti, A. Genoni, C. Dal Cappello, W.-G. Shin and S. Incerti, *Nucl. Instrum. Methods Phys. Res., Sect. B*, 2021, **488**, 70–82.
- T. Kai, A. Yokoya, M. Ukai, K. Fujii, T. Toigawa and R. Watanabe, *Phys. Chem. Chem. Phys.*, 2018, **20**, 2838–2844.
- S. M. Pimblott and J. A. LaVerne, *Radiat. Phys. Chem.*, 2007, **76**, 1244–1247.
- T. P. R. Kumar, J. Kočišek, K. Bravaya and J. Fedor, *Phys. Chem. Chem. Phys.*, 2020, **22**, 518–524.
- D. Davis, V. P. Vysotskiy, Y. Sajejev and L. S. Cederbaum, *Angew. Chem., Int. Ed.*, 2011, **50**, 4119–4122.
- D. Davis, V. P. Vysotskiy, Y. Sajejev and L. S. Cederbaum, *Angew. Chem., Int. Ed.*, 2012, **51**, 8003–8007.
- C. S. Anstöter, G. Mensa-Bonsu, P. Nag, M. C. V. Ranković, T. P. R. Kumar, A. N. Boichenko, A. V. Bochenkova, J. Fedor and J. R. R. Verlet, *Phys. Rev. Lett.*, 2020, **124**, 203401.
- J. Med, t Sršeň, P. Slavíček, A. Domaracka, S. Indrajith, P. Rousseau, M. Fárník, J. Fedor and J. Kočišek, *J. Phys. Chem. Lett.*, 2020, **11**, 2482–2489.
- T. Sommerfeld and M. C. Davis, *J. Chem. Phys.*, 2018, **149**, 084305.
- T. F. M. Luxford, J. Fedor and J. Kočišek, *J. Chem. Phys.*, 2021, **154**, 214303.
- J. Forer, V. Kokoouline and T. Stoecklin, *Phys. Rev. A*, 2023, **107**, 043117.
- V. Chandrasekaran, A. Prabhakaran, B. Kafle, H. Rubinstein, O. Heber, M. Rappaport, Y. Toker and D. Zajfman, *J. Chem. Phys.*, 2017, **146**, 094302.
- I. I. Fabrikant and H. Hotop, *Phys. Rev. A: At., Mol., Opt. Phys.*, 2001, **63**, 022706.
- K. D. Jordan and F. Wang, *Ann. Rev. Phys. Chem.*, 2003, **54**, 367–396.
- I. I. Fabrikant, H. Hotop and M. Allan, *Phys. Rev. A: At., Mol., Opt. Phys.*, 2005, **71**, 022712.
- M. Allan, M. Lacko, P. Papp, Š. Matejčík, M. Zlatar, I. I. Fabrikant, J. Kočišek and J. Fedor, *Phys. Chem. Chem. Phys.*, 2018, **20**, 11692–11701.
- Y.-R. Zhang, D.-F. Yuan, C.-H. Qian, G.-Z. Zhu and L.-S. Wang, *J. Am. Chem. Soc.*, 2023, **145**, 14952–14962.
- D.-F. Yuan, Y. Liu, Y.-R. Zhang and L.-S. Wang, *J. Am. Chem. Soc.*, 2023, **145**, 5512–5522.
- C.-H. Qian, G.-Z. Zhu and L.-S. Wang, *J. Phys. Chem. Lett.*, 2019, **10**, 6472–6477.
- Y.-R. Zhang, D.-F. Yuan and L.-S. Wang, *J. Phys. Chem. Lett.*, 2022, **13**, 2124–2129.
- C. Desfrancois, H. Abdoul-Carime and J.-P. Schermann, *Int. J. Mod. Phys. B*, 1996, **10**, 1339–1395.
- D. H. Kang, J. Kim, H. J. Eun and S. K. Kim, *J. Am. Chem. Soc.*, 2022, **144**, 16077–16085.
- T. Sommerfeld, *J. Phys. Chem. A*, 2004, **108**, 9150–9154.
- J. H. Hendricks, S. A. Lyapustina, H. L. de Clercq, J. T. Snodgrass and K. H. Bowen, *J. Chem. Phys.*, 1996, **104**, 7788–7791.
- A. Kunin and D. M. Neumark, *Phys. Chem. Chem. Phys.*, 2019, **21**, 7239–7255.
- X. Li, K. H. Bowen, M. Haranczyk, R. A. Bachorz, K. Mazurkiewicz, J. Rak and M. Gutowski, *J. Chem. Phys.*, 2007, **127**, 174309.
- D. Chen and G. A. Gallup, *J. Chem. Phys.*, 1990, **93**, 8893–8901.
- G. J. Schulz, *Rev. Mod. Phys.*, 1973, **45**, 423–486.
- J. N. Bardsley, A. Herzenberg and F. Mandl, *Proc. Phys. Soc.*, 1966, **89**, 321.
- T. P. Ragesh Kumar, P. Nag, M. Ranković, T. F. M. Luxford, J. Kočišek, Z. Mašin and J. Fedor, *J. Phys. Chem. Lett.*, 2022, **13**, 11136–11142.
- E. M. de Oliveira, M. A. P. Lima, M. H. F. Bettega, S. D. Sanchez, R. F. da Costa and M. T. D. N. Varella, *J. Chem. Phys.*, 2010, **132**, 204301.
- M. Zawadzki, M. Čížek, K. Houfek, R. Čurík, M. Ferus, S. Civiš, J. Kočišek and J. Fedor, *Phys. Rev. Lett.*, 2018, **121**, 143402.
- P. Nag, M. Tarana and J. Fedor, *Phys. Rev. A*, 2021, **103**, 032830.
- I. I. Fabrikant, S. Eden, N. J. Mason and J. Fedor, *Recent Progress in Dissociative Electron Attachment: From Diatomics to Biomolecules*, Academic Press, 2017, vol. **66**, pp. 545–657.
- S. A. Pshenichnyuk, N. L. Asfandiarov, A. S. Vorobev and Š. Matejčík, *Physics-Uspekhi*, 2022, **65**, 163.
- O. Ingolfsson, *Low-Energy Electrons Fundamentals and Applications*, Taylor and Francis, 2019, **434**.
- L. Christophorou and J. Olthoff, *Fundamental Electron Interactions with Plasma Processing Gases, Fundamental Electron Interactions with Plasma Processing Gases*, 2003.
- E. Illenberger and J. Momigny, *Electron Attachment Spectroscopy*, Steinkopff, Heidelberg, 1992, pp. 264–298.
- J. M. Herbert and M. P. Coons, *Ann. Rev. Phys. Chem.*, 2017, **68**, 447–472.
- A. E. Bragg, J. R. R. Verlet, A. Kammrath, O. Cheshnovsky and D. M. Neumark, *Science*, 2004, **306**, 669–671.



- 47 V. Svoboda, R. Michiels, A. C. LaForge, J. Med, F. Stienkemeier, P. Slavíček and H. J. Wörner, *Sci. Adv.*, 2020, **6**, eaaz0385.
- 48 F. Novelli, K. Chen, A. Buchmann, T. Ockelmann, C. Hoberg, T. Head-Gordon and M. Havenith, *Proc. Natl. Acad. Sci. U. S. A.*, 2023, **120**, e2216480120.
- 49 J. Belloni, M. Mostafavi, T. Douki and M. Spothem-Maurizot, *Radiation chemistry from basics to applications in material and life sciences*, Editions EDP Sciences, Les Ulis (France), France, 2008.
- 50 Q.-B. Lu, *Mutat. Res.*, 2010, **704**, 190–199.
- 51 H. Zettergren, A. Domaracka, T. Schlathölder, P. Bolognesi, S. Díaz-Tendero, M. Abuda, S. Tosic, S. Maclot, P. Johnsson, A. Steber, D. Tikhonov, M. C. Castrovilli, L. Avaldi, S. Bari, A. R. Milosavljević, A. Palacios, S. Faraji, D. G. Piekarski, P. Rousseau, D. Ascenzi, C. Romanzin, E. Erdmann, M. Alcamí, J. Kopyra, P. Limão-Vieira, J. Kočišek, J. Fedor, S. Albertini, M. Gatchell, H. Cederquist, H. T. Schmidt, E. Gruber, L. H. Andersen, O. Heber, Y. Toker, K. Hansen, J. A. Noble, C. Juvet, C. Kjær, S. B. Nielsen, E. Carrascosa, J. Bull, A. Candian and A. Petrigiani, *Eur. Phys. J. D*, 2021, **75**, 152.
- 52 J. Poštulka, P. Slavíček, J. Fedor, M. Fárník and J. Kočišek, *J. Phys. Chem. B*, 2017, **121**, 8965–8974.
- 53 J. Kočišek, A. Pysanenko, M. Fárník and J. Fedor, *J. Phys. Chem. Lett.*, 2016, **7**, 3401–3405.
- 54 M. McAllister, N. Kazemigazestane, L. T. Henry, B. Gu, I. Fabrikant, G. A. Tribello and J. Kohanoff, *J. Phys. Chem. B*, 2019, **123**, 1537–1544.
- 55 J. Schiedt, R. Weinkauff, D. Neumark and E. Schlag, *Chem. Phys.*, 1998, **239**, 511–524.
- 56 J. H. Hendricks, S. A. Lyapustina, H. L. de Clercq and K. H. Bowen, *J. Chem. Phys.*, 1998, **108**, 8–11.
- 57 L. Sala, B. Sedmidubská, I. Vinklárek, M. Fárník, R. Schürmann, I. Bald, J. Med, P. Slavíček and J. Kocisek, *Phys. Chem. Chem. Phys.*, 2021, **23**, 18173–18181.
- 58 M. J. Brunger, *Int. Rev. Phys. Chem.*, 2017, **36**, 333–376.
- 59 P. Limão-Vieira, F. F. da Silva and G. G. Gómez-Tejedor, in *Electron Transfer-Induced Fragmentation in (Bio)Molecules by Atom-Molecule Collisions*, ed. G. García Gómez-Tejedor and M. C. Fuss, Springer Netherlands, Dordrecht, 2012, pp. 59–70.
- 60 A. M. Stanislav, A. Pshenichnyuk and A. S. Komolov, *Int. Rev. Phys. Chem.*, 2018, **37**, 125–170.
- 61 P. M. Callis, G. D. D. Jones, M. C. R. Symons and J. S. Lea, *Nature*, 1987, **330**, 773–774.
- 62 J. Simons, *Acc. Chem. Res.*, 2006, **39**, 772–779.
- 63 A. Kumar, D. Becker, A. Adhikary and M. D. Sevilla, *Int. J. Mol. Sci.*, 2019, **20**, 3998.
- 64 S. Ptasíńska, S. Denifl, B. Mróz, M. Probst, V. Grill, E. Illenberger, P. Scheier and T. D. Märk, *J. Chem. Phys.*, 2005, **123**, 124302.
- 65 M. Orzol, I. Martin, J. Kocisek, I. Dabkowska, J. Langer and E. Illenberger, *Phys. Chem. Chem. Phys.*, 2007, **9**, 3424–3431.
- 66 D. S. Slaughter, T. Weber, A. Belkacem, C. S. Trevisan, R. R. Lucchese, C. W. McCurdy and T. N. Rescigno, *Phys. Chem. Chem. Phys.*, 2020, **22**, 13893–13902.
- 67 V. Tadsare, S. Das, S. Gokhale, E. Krishnakumar and V. S. S. Prabhudesai, *Atoms*, 2022, **10**, 98.
- 68 O. Ingólfsson, F. Weik and E. Illenberger, *Int. J. Mass Spectrom. Ion Processes*, 1996, **155**, 1–68.
- 69 H. Hotop, M.-W. Ruf, M. Allan and I. Fabrikant, *Resonance and threshold phenomena in low-energy electron collisions with molecules and clusters*, Academic Press, 2003, vol. **49**, pp. 85–216.
- 70 J. Lengyel, J. Kočišek, M. Fárník and J. Fedor, *J. Phys. Chem. C*, 2016, **120**, 7397–7402.
- 71 D. Mészáros, P. Papp and Š. Matejíček, *Eur. Phys. J. D*, 2023, **77**, 62.
- 72 M. McAllister, M. Smyth, B. Gu, G. A. Tribello and J. Kohanoff, *J. Phys. Chem. Lett.*, 2015, **6**, 3091–3097.
- 73 J. Kočišek, B. Sedmidubská, S. Indrajith, M. Fárník and J. Fedor, *J. Phys. Chem. B*, 2018, **122**, 5212–5217.
- 74 J. Ma, A. Kumar, Y. Muroya, S. Yamashita, T. Sakurai, S. A. Denisov, M. D. Sevilla, A. Adhikary, S. Seki and M. Mostafavi, *Nat. Commun.*, 2019, **10**, 102.
- 75 T. F. M. Luxford, S. A. Pshenichnyuk, N. L. Asfandiarov, T. Perečko, M. Falk and J. Kočišek, *Int. J. Mol. Sci.*, 2020, **21**, 8173.
- 76 R. Meißner, J. Kočišek, L. Feketeová, J. Fedor, M. Fárník, P. Limão-Vieira, E. Illenberger and S. Denifl, *Nat. Commun.*, 2019, **10**, 2388.
- 77 M. Rezaee, D. J. Hunting and L. Sanche, *Int. J. Radiat. Oncol., Biol., Phys.*, 2013, **87**, 847–853.
- 78 S. Zhao and R.-b Zhang, *RSC Adv.*, 2016, **6**, 83053–83059.
- 79 L. Chomicz-Mañka, M. Zdrochowicz, F. Kasprzykowski, J. Rak, A. Zeigler, Y. Wang and K. Bowen, *J. Phys. Chem. Lett.*, 2013, **4**, 2853–2857.
- 80 A. I. Lozano, F. Kossoski, F. Blanco, P. Limão-Vieira, M. T. N. Varella and G. García, *J. Phys. Chem. Lett.*, 2022, **13**, 7001–7008.
- 81 D. Nandi, E. Krishnakumar, A. Rosa, W. Schmidt and E. Illenberger, *Chem. Phys. Lett.*, 2003, **373**, 454–459.
- 82 F. Xiao, X. Luo, X. Fu and Y. Zheng, *J. Phys. Chem. B*, 2013, **117**, 4893–4900.
- 83 N. Bhagavan and C.-E. Ha, *Essentials of Medical Biochemistry*, Academic Press, San Diego, 2nd edn, 2015, pp. 381–400.
- 84 Z. Li, P. Cloutier, L. Sanche and J. R. Wagner, *J. Phys. Chem. B*, 2011, **115**, 13668–13673.
- 85 J. Rackwitz, M. Ranković, A. Milosavljevic and I. Bald, *Eur. Phys. J. D*, 2017, **71**, 32.
- 86 T. Kimura, K. Kawai, S. Tojo and T. Majima, *J. Org. Chem.*, 2004, **69**, 1169–1173.
- 87 L. Sala, H. Lyschchuk, J. Šachová, D. Chvátíl and J. Kočišek, *J. Phys. Chem. Lett.*, 2022, **13**, 3922–3928.
- 88 C. von Sonntag, *The Chemical Basis of Radiation Biology: Radiobiology*, Taylor Francis, London, 1987.
- 89 S. Makurat, L. Chomicz-Mañka and J. Rak, *ChemPhysChem*, 2016, 2572–2578.
- 90 M.-E. Dextraze, J. R. Wagner and D. J. Hunting, *Biochemistry*, 2007, **46**, 9089–9097.
- 91 H. Yang and M. W. Wong, *J. Am. Chem. Soc.*, 2013, **135**, 5808–5818.



- 92 I. Dabkowska, J. Rak, M. Gutowski, J. M. Nilles, S. T. Stokes, D. Radisic and K. H. Bowen Jr., *Phys. Chem. Chem. Phys.*, 2004, **6**, 4351–4357.
- 93 B. Gu, M. Smyth and J. Kohanoff, *Phys. Chem. Chem. Phys.*, 2014, **16**, 24350–24358.
- 94 X. Wang, H. Liao, W. Liu, Y. Shao, Y. Zheng and L. Sanche, *J. Phys. Chem. Lett.*, 2023, **14**, 5674–5680.
- 95 P. Verma, J. Narayanan S J and A. K. Dutta, *J. Phys. Chem. A*, 2023, **127**, 2215–2227.
- 96 J. Huang, A. Suma, M. Cui, G. Grundmeier, V. Carnevale, Y. Zhang, C. Kielar and A. Keller, *Small Struct.*, 2020, **1**, 2000038.
- 97 E. Gloaguen, M. Mons, K. Schwing and M. Gerhards, *Chem. Rev.*, 2020, **120**, 12490–12562.
- 98 M. Ahmed and O. Kostko, *Phys. Chem. Chem. Phys.*, 2020, **22**, 2713–2737.
- 99 M. Wiczór, P. Wityk, J. Czub, L. Chomicz and J. Rak, *Chem. Phys. Lett.*, 2014, **595–596**, 133–137.
- 100 P. Spisz, M. Zdrowowicz, W. Kozak, L. Chomicz-Mańka, K. Falkiewicz, S. Makurat, A. Sikorski, D. Wyrzykowski, J. Rak, E. Arthur-Baidoo, P. Ziegler, M. Costa and S. Denifl, *J. Phys. Chem. B*, 2020, 5600–5613.
- 101 A. Ribar, S. E. Huber, M. A. Śmiałek, K. Tanzer, M. Neustetter, R. Schürmann, I. Bald and S. Denifl, *Phys. Chem. Chem. Phys.*, 2018, **20**, 5578–5585.
- 102 F. Kossoski and M. T. N. Varella, *Phys. Chem. Chem. Phys.*, 2015, **17**, 17271–17278.
- 103 P. Storoniak, H. Wang, Y. J. Ko, X. Li, S. T. Stokes, S. Eustis, K. H. Bowen and J. Rak, in *Valence Anions of DNA-Related Systems in the Gas Phase: Computational and Anion Photoelectron Spectroscopy Studies*, ed. J. Leszczynski and M. K. Shukla, Springer US, Boston, MA, 2014, pp. 323–392.
- 104 R. Abouaf, J. Pommier and H. Dunet, *Int. J. Mass Spectrom.*, 2003, **226**, 397–403.
- 105 R. Abouaf, J. Pommier and H. Dunet, *Chem. Phys. Lett.*, 2003, **381**, 486–494.
- 106 A. M. Scheer, K. Aflatoon, G. A. Gallup and P. D. Burrow, *Phys. Rev. Lett.*, 2004, **92**, 068102.
- 107 S. J. Blanksby and G. B. Ellison, *Acc. Chem. Res.*, 2003, **36**, 255–263.
- 108 J. C. Rienstra-Kiracofe, G. S. Tschumper, H. F. Schaefer, S. Nandi and G. B. Ellison, *Chem. Rev.*, 2002, **102**, 231–282.
- 109 C. Ning and Y. Lu, *J. Phys. Chem. Ref. Data*, 2022, **51**, 021502.
- 110 X. Li, L. Sanche and M. D. Sevilla, *J. Phys. Chem. A*, 2002, **106**, 11248–11253.
- 111 S. Denifl, S. Matejcik, B. Gstir, G. Hanel, M. Probst, P. Scheier and T. D. Märk, *J. Chem. Phys.*, 2003, **118**, 4107–4114.
- 112 W. Wang, M. Marshall, E. Collins, S. Marquez, C. Mu, K. H. Bowen and X. Zhang, *Nat. Commun.*, 2019, **10**, 1170.
- 113 S. Klaiman and L. S. Cederbaum, *Angew. Chem., Int. Ed.*, 2015, **54**, 10470–10473.
- 114 H.-T. Liu, C.-G. Ning, D.-L. Huang and L.-S. Wang, *Angew. Chem., Int. Ed.*, 2014, **53**, 2464–2468.
- 115 F. Izadi, A. Szczyrba, M. Datta, O. Ciupak, S. Demkowicz, J. Rak and S. Denifl, *Int. J. Mol. Sci.*, 2023, **24**, 8706.
- 116 B. Ómarsson, E. H. Bjarnason, O. Ingólfsson, S. Haughey and T. A. Field, *Chem. Phys. Lett.*, 2012, **539–540**, 7–10.
- 117 E. Arthur-Baidoo, G. Schöpfer, M. Ončák, L. Chomicz-Mańka, J. Rak and S. Denifl, *Int. J. Mol. Sci.*, 2022, **23**, 8325.
- 118 M. Cipriani and O. Ingólfsson, *Radiat. Phys. Chem.*, 2023, **202**, 110544.
- 119 L. M. Cornetta, T. J. Martinez and M. T. N. Varella, *Phys. Chem. Chem. Phys.*, 2022, **24**, 6845–6855.
- 120 J. W. J. D. Zimbrick and L. Myers, *Int. J. Radiat. Oncol. Biol. Phys.*, 1969, **16**, 505–523.
- 121 J. D. Zimbrick, J. F. Ward and L. S. Myers, Jr, *Int. J. Radiat. Biol.*, 1969, **16**, 525–534.
- 122 K. Westphal, J. Wicz, J. Miloch, G. Kciuk, K. Bobrowski and J. Rak, *Org. Biomol. Chem.*, 2015, **13**, 10362–10369.
- 123 H. Abdoul-Carime, S. Gohlke and E. Illenberger, *Phys. Chem. Chem. Phys.*, 2004, **6**, 161–164.
- 124 C.-R. Wang and Q.-B. Lu, *Angew. Chem., Int. Ed.*, 2007, **46**, 6316–6320.
- 125 C. Beach, A. F. Fuciarelli and J. D. Zimbrick, *Radiat. Res.*, 1994, **137**, 385–393.
- 126 J. Narayanan S J, D. Tripathi, P. Verma, A. Adhikary and A. K. Dutta, *ACS Omega*, 2023, **8**, 10669–10689.
- 127 L. Cupellini, P. Wityk, B. Mennucci and J. Rak, *Phys. Chem. Chem. Phys.*, 2019, **21**, 4387–4393.
- 128 P. Schyman, R. B. Zhang, L. A. Eriksson and A. Laaksonen, *Phys. Chem. Chem. Phys.*, 2007, **9**, 5975–5979.
- 129 J. Rak, L. Chomicz-Mańka, J. Wicz, K. Westphal, M. Zdrowowicz, P. Wityk, M. Żyndul, S. Makurat and Ł. Golon, *J. Phys. Chem. B*, 2015, **119**, 8227–8238.
- 130 X. Li, M. D. Sevilla and L. Sanche, *J. Am. Chem. Soc.*, 2003, **125**, 8916–8920.
- 131 A. Paul and D. Nandi, *Phys. Chem. Chem. Phys.*, 2022, **24**, 21020–21029.
- 132 J. Kopyra, H. Abdoul-Carime, F. Kossoski and M. T. N. Varella, *Phys. Chem. Chem. Phys.*, 2014, **16**, 25054–25061.
- 133 J. Kopyra and H. Abdoul-Carime, *J. Chem. Phys.*, 2016, **144**, 034306.
- 134 K. P. Prasanthkumar, J. R. Alvarez-Idaboy, P. V. Kumar, B. G. Singh and K. I. Priyadarsini, *Phys. Chem. Chem. Phys.*, 2016, **18**, 28781–28790.
- 135 E. Arthur-baidoo, K. Falkiewicz, L. Chomicz-Mańka, A. Czaja, S. Demkowicz, K. Biernacki, W. Kozak, J. Rak and S. Denifl, *Int. J. Mol. Sci.*, 2021, **22**, 1–13.
- 136 F. Meng, *J. Mol. Struct.: THEOCHEM*, 2007, **806**, 159–164.
- 137 M. Sosnowska, S. Makurat, M. Zdrowowicz and J. Rak, *J. Phys. Chem. B*, 2017, **121**, 6139–6147.
- 138 T. Trabelsi, O. Yazidi, J. S. Francisco, R. Linguerrri and M. Hochlaf, *J. Chem. Phys.*, 2015, **143**, 164301.
- 139 P. Spisz, M. Zdrowowicz, W. Kozak, L. Chomicz-Mańka, K. Falkiewicz, S. Makurat, A. Sikorski, D. Wyrzykowski, J. Rak, E. Arthur-Baidoo, P. Ziegler, M. S. Rodrigues Costa and S. Denifl, *J. Phys. Chem. B*, 2020, **124**, 5600–5613.
- 140 R. Abouaf, S. Ptasinska and D. Teillet-Billy, *Chem. Phys. Lett.*, 2008, **455**, 169–173.



- 141 S. Ptasinska, E. Alizadeh, P. Sulzer, R. Abouaf, N. J. Mason, T. D. Märk and P. Scheier, *Int. J. Mass Spectrom.*, 2008, **277**, 291–295.
- 142 S. J. Kogikoski, A. Dutta and I. Bald, *ACS Nano*, 2021, **15**, 20562–20573.
- 143 R. Schürmann and I. Bald, *Nanoscale*, 2017, **9**, 1951–1955.
- 144 A. Dutta, R. Schürmann, S. J. Kogikoski, N. S. Mueller, S. Reich and I. Bald, *ACS Catal.*, 2021, **11**, 8370–8381.
- 145 N. L. Asfandiarov, S. A. Pshenichnyuk, R. G. Rakhmeyer, R. F. Tuktarov, N. L. Zaitsev, A. S. Vorobev, J. Kočíšek, J. Fedor and A. Modelli, *J. Chem. Phys.*, 2019, **150**, 114304.
- 146 N. Asfandiarov, M. Muftakhov, R. Rakhmiev, A. Safronov, A. Markova and S. Pshenichnyuk, *J. Electron Spectrosc. Related Phenomena*, 2022, **256**, 147178.
- 147 N. L. Asfandiarov, M. V. Muftakhov and S. A. Pshenichnyuk, *J. Chem. Phys.*, 2023, **158**, 194305.
- 148 N. L. Asfandiarov, M. V. Muftakhov, S. A. Pshenichnyuk, R. G. Rakhmiev, A. M. Safronov, A. V. Markova, A. S. Vorobev, T. F. M. Luxford, J. Kočíšek and J. Fedor, *J. Chem. Phys.*, 2021, **155**, 244302.
- 149 K. Falkiewicz, W. Kozak, M. Zdrowicz, P. Spisz, L. Chomicz-Mańka, M. Torchala and J. Rak, *J. Phys. Chem. B*, 2023, 2565–2574.
- 150 H. Abdoul-Carime, P. Limão-Vieira, S. Gohlke, I. Petrushko, N. J. Mason and E. Illenberger, *Chem. Phys. Lett.*, 2004, **393**, 442–447.
- 151 S. Denifl, P. Candori, S. Ptasinska, P. Limão-Vieira, V. Grill, T. D. Märk and P. Scheier, *Eur. Phys. J. D*, 2005, **35**, 391–398.
- 152 C.-R. Wang, A. Hu and Q.-B. Lu, *J. Chem. Phys.*, 2006, **124**, 241102.
- 153 J. Ma, T. Bahry, S. A. Denisov, A. Adhikary and M. Mostafavi, *J. Phys. Chem. A*, 2021, **125**, 7967–7975.
- 154 M. Saqib, E. Arthur-Baidoo, F. Izadi, A. Szczyrba, M. Datta, S. Demkowicz, J. Rak and S. Denifl, *J. Phys. Chem. Lett.*, 2023, **127**, 8948–8955.
- 155 M. Durante, R. Orecchia and J. S. Loeffler, *Nat. Rev. Clin. Oncol.*, 2017, **14**, 483–495.
- 156 J. Kopyra, A. Keller and I. Bald, *RSC Adv.*, 2014, **4**, 6825–6829.
- 157 C. Chatgililoglu, *Reactivity of Nucleic Acid Sugar Radicals*, John Wiley Sons, Ltd, 2009, ch. 4, pp. 99–133.
- 158 A. Kumar and M. D. Sevilla, *Chem. Rev.*, 2010, **110**, 7002–7023.
- 159 J. Gu, Y. Xie and H. F. Schaefer III, *ChemPhysChem*, 2006, **7**, 1885–1887.
- 160 K. Khistyayev, A. Golan, K. B. Bravaya, N. Orms, A. I. Krylov and M. Ahmed, *J. Phys. Chem. A*, 2013, **117**, 6789–6797.
- 161 B. Boudaïffa, *Science*, 2000, **287**, 1658–1660.
- 162 S. Ptasinska, S. Denifl, P. Scheier and T. D. Märk, *J. Chem. Phys.*, 2004, **120**, 8505–8511.
- 163 I. Bald, I. Dabkowska and E. Illenberger, *Angew. Chem., Int. Ed.*, 2008, **47**, 8518–8520.
- 164 H. Czapinska, M. Winiewska-Szajewska, A. Szymaniec-Rutkowska, A. Piasecka, M. Bochtler and J. Poznański, *J. Phys. Chem. B*, 2021, **125**, 2491–2503.
- 165 G. E. Adams, *Radiat. Res.*, 1992, **132**, 129–139.
- 166 P. Wardman, *Clin. Oncol.*, 2007, **19**, 397–417.
- 167 B. T. Oronsky, S. J. Knox and J. J. Scicinski, *Transl. Oncol.*, 2012, **5**, 66–71.
- 168 D. A. Wink, Y. Vodovotz, J. Laval, F. Laval, M. W. Dewhirst and J. B. Mitchell, *Carcinogenesis*, 1998, **19**, 711–721.
- 169 M. Lepoivre, F. Fieschi, J. Coves, L. Thelander and M. Fontecave, *Biochem. Biophys. Res. Commun.*, 1991, **179**, 442–448.
- 170 R. Willson, W. Cramp and R. Ings, *Int. J. Radiat. Biol. Relat. Stud. Phys., Chem. Med.*, 1974, **26**, 557–569.
- 171 M. R. Horsman, L. S. Mortensen, J. B. Petersen, M. Busk and J. Overgaard, *Nat. Rev. Clin. Oncol.*, 2012, **9**, 674–687.
- 172 K. Nepali, H.-Y. Lee and J.-P. Liou, *J. Med. Chem.*, 2019, **62**, 2851–2893.
- 173 N. Boechat, A. S. Carvalho, K. Salomão, S. L. D. Castro, C. F. Araujo-Lima, F. V. Mello, I. Felzenszwalb, C. A. Aiub, T. R. Conde and H. P. Zamith, *et al.*, *Mem. Inst. Oswaldo Cruz*, 2015, **110**, 492–499.
- 174 A. C. M. Von Trompowsky, T. R. Conde, R. C. Lemos, B. M. C. Quaresma, M. C. S. Pitombeira, A. S. de Carvalho, N. Boechat, K. Salomão, S. L. de Castro and H. P. D. S. Zamith, *Mem. Inst. Oswaldo Cruz*, 2019, **114**, e190017.
- 175 D. Christen, J. H. Griffiths and J. Sheridan, *Zeitschrift für Naturforschung A*, 1981, **36**, 1378–1385.
- 176 S. A. Pshenichnyuk, I. I. Fabrikant, A. Modelli, S. Ptasinska and A. S. Komolov, *J. Phys.: Conf. Ser.*, 2020, **1412**, 212003.
- 177 F. Kossoski and M. H. Bettega, *J. Chem. Phys.*, 2013, **138**, 234311.
- 178 A. Ribar, K. Fink, Z. Li, S. Ptasinska, I. Carmichael, L. Feketeová and S. Denifl, *Phys. Chem. Chem. Phys.*, 2017, **19**, 6406–6415.
- 179 T. Jani, P. C. Vinodkumar and M. Vinodkumar, *J. Phys. Chem. A*, 2023, **127**, 4996–5004.
- 180 A. Modelli and P. D. Burrow, *J. Phys. Chem. A*, 2004, **108**, 5721–5726.
- 181 Z. Li, I. Carmichael and S. Ptasinska, *Phys. Chem. Chem. Phys.*, 2018, **20**, 18271–18278.
- 182 A. A. Wallace, Y. Dauletyarov and A. Sanov, *J. Phys. Chem. A*, 2021, **125**, 317–326.
- 183 L. Feketeová, A. L. Albright, B. S. Sørensen, M. R. Horsman, J. White, R. A. OHair and N. Bassler, *Int. J. Mass Spectrom.*, 2014, **365–366**, 56–63.
- 184 V. S. Prabhudesai, A. H. Kelkar, D. Nandi and E. Krishnakumar, *Phys. Rev. Lett.*, 2005, **95**, 143202.
- 185 M. Zawadzki, T. F. M. Luxford and J. Kočíšek, *J. Phys. Chem. A*, 2020, **124**, 9427–9435.
- 186 A. Ribar, K. Fink, M. Probst, S. E. Huber, L. Feketeová and S. Denifl, *Chem. – Eur. J.*, 2017, **23**, 12892–12899.
- 187 K. Tanzer, L. Feketeová, B. Puschnigg, P. Scheier, E. Illenberger and S. Denifl, *Angew. Chem., Int. Ed.*, 2014, **53**, 12240–12243.
- 188 K. Tanzer, L. Feketeová, B. Puschnigg, P. Scheier, E. Illenberger and S. Denifl, *J. Phys. Chem. A*, 2015, **119**, 6668–6675.



- 189 J. Kopyra, K. K. Kopyra, H. Abdoul-Carime and D. Branowska, *J. Chem. Phys.*, 2018, **148**, 234301.
- 190 D. Barreiro-Lage, C. Nicolafrancesco, J. Kočišek, A. Luna, J. Kopyra, M. Alcamí, B. A. Huber, F. Martín, A. Domaracka, P. Rousseau and S. Díaz-Tendero, *Phys. Chem. Chem. Phys.*, 2022, **24**, 941–954.
- 191 Y. V. Vasil'ev, B. J. Figard, V. G. Voinov, D. F. Barofsky and M. L. Deinzer, *J. Am. Chem. Soc.*, 2006, **128**, 5506–5515.
- 192 F. Kossoski and M. T. D. N. Varella, *J. Chem. Phys.*, 2017, **147**, 164310.
- 193 C. Desfrancois, V. Périquet, S. Carles, J. P. Schermann, D. M. A. Smith and L. Adamowicz, *J. Chem. Phys.*, 1999, **110**, 4309–4314.
- 194 D. M. A. Smith, J. Smets, Y. Elkadi and L. Adamowicz, *J. Phys. Chem. A*, 1997, **101**, 8123–8127.
- 195 M. Zawadzki, M. Ranković, J. Kočišek and J. Fedor, *Phys. Chem. Chem. Phys.*, 2018, **20**, 6838–6844.
- 196 A. I. Lozano, L. Álvarez, A. García-Abenza, C. Guerra, F. Kossoski, J. Rosado, F. Blanco, J. C. Oller, M. Hasan, M. Centurion, T. Weber, D. S. Slaughter, D. M. Mootheril, A. Dorn, S. Kumar, P. Limão-Vieira, R. Colmenares and G. García, *Int. J. Mol. Sci.*, 2023, **24**, 12182.
- 197 R. Willson, B. Gilbert, P. Marshall and R. Norman, *Int. J. Radiat. Biol. Relat. Stud. Phys., Chem. Med.*, 1974, **26**, 427–434.
- 198 C. Lochmann, T. F. Luxford, S. Makurat, A. Pysanenko, J. Kočišek, J. Rak and S. Denifl, *Pharmaceuticals*, 2022, **15**, 1–12.
- 199 S. Kumar, I. Ben Chouikha, B. Kerkeni, G. García and P. Limão-Vieira, *Molecules*, 2022, **27**, 4134.
- 200 R. Meißner, L. Feketeová, A. Bayer, P. Limão-Vieira and S. Denifl, *J. Chem. Phys.*, 2021, **154**, 074306.
- 201 C. L. Brito, R. S. Lins, M. Bertotti, E. I. Ferreira and M. A. La-Scalea, *Electrochim. Acta*, 2022, **403**, 139709.
- 202 E. Gattavecchia, D. Tonelli and P. Fuochoi, *Int. J. Radiat. Biol. Relat. Stud. Phys., Chem. Med.*, 1984, **45**, 469–477.
- 203 R. Meißner, L. Feketeová, E. Illenberger and S. Denifl, *Int. J. Mol. Sci.*, 2019, **20**, 3496.
- 204 M. Ončák, R. Meißner, E. Arthur-Baidoo, S. Denifl, T. F. Luxford, A. Pysanenko, M. Fárnik, J. Pinkas and J. Kočišek, *Int. J. Mol. Sci.*, 2019, **20**, 1–12.
- 205 T. C. Johnstone, J. J. Wilson and S. J. Lippard, *Inorg. Chem.*, 2013, **52**, 12234–12249.
- 206 J. Reedijk, *Inorg. Chim. Acta*, 2016, **452**, 268–272.
- 207 K. Chválová, V. Brabec and J. Kašpárková, *Nucleic Acids Res.*, 2007, **35**, 1812–1821.
- 208 V. Brabec and M. Leng, *Proc. Natl. Acad. Sci. U. S. A.*, 1993, **90**, 5345–5349.
- 209 A. Eastman, *The Mechanism of Action of Cisplatin: From Adducts to Apoptosis*, John Wiley Sons, Ltd, 1999, ch. 4, pp. 111–134.
- 210 Q. B. Lu, *J. Med. Chem.*, 2007, **50**, 2601–2604.
- 211 Q. Zhang and Q. Lu, *Sci. Rep.*, 2021, **11**, 788.
- 212 T. Luo, J. Yu, J. Nguyen, C.-R. Wang, R. G. Bristow, D. A. Jaffray, X. Z. Zhou, K. P. Lu and Q.-B. Lu, *Proc. Natl. Acad. Sci. U. S. A.*, 2012, **109**, 10175–10180.
- 213 E. Alizadeh and L. Sanche, *Eur. Phys. J. D*, 2014, **68**, 97.
- 214 M. Rezaee, L. Sanche and D. J. Hunting, *Radiat. Res.*, 2013, **179**, 323–331.
- 215 S. Kouass Sahbani, M. Rezaee, P. Cloutier, L. Sanche and D. Hunting, *Chem.-Biol. Interact.*, 2014, **217**, 9–18.
- 216 J. Kopyra, C. Koenig-Lehmann, I. Bald and E. Illenberger, *Angew. Chem., Int. Ed.*, 2009, **48**, 7904–7907.
- 217 H. Y. Chen, H. F. Chen, C. L. Kao, P. Y. Yang and S. C. Hsu, *Phys. Chem. Chem. Phys.*, 2014, **16**, 19290–19297.
- 218 Q. Bao, Y. Chen, Y. Zheng and L. Sanche, *J. Phys. Chem. C*, 2014, **118**, 15516–15524.
- 219 M. Rezaee, E. Alizadeh, P. Cloutier, D. J. Hunting and L. Sanche, *ChemMedChem*, 2014, **9**, 1145–1149.
- 220 Y. Dong, L. Zhou, Q. Tian, Y. Zheng and L. Sanche, *J. Phys. Chem. C*, 2017, **121**, 17505–17513.
- 221 Y. Dong, Y. Wang, P. Zhuang, X. Fu, Y. Zheng and L. Sanche, *J. Phys. Chem. B*, 2020, **124**, 3315–3325.
- 222 B. Behmand, P. Cloutier, S. Girouard, J. R. Wagner, L. Sanche and D. J. Hunting, *J. Phys. Chem. B*, 2013, **117**, 15994–15999.
- 223 B. Behmand, J. R. Wagner, L. Sanche and D. J. Hunting, *J. Phys. Chem. B*, 2014, **118**, 4803–4808.
- 224 B. Behmand, J. L. Marignier, M. Mostafavi, J. R. Wagner, D. J. Hunting and L. Sanche, *J. Phys. Chem. B*, 2015, **119**, 9496–9500.
- 225 B. Behmand, A. M. Noronha, C. J. Wilds, J. L. Marignier, M. Mostafavi, J. R. Wagner, D. J. Hunting and L. Sanche, *J. Radiat. Res.*, 2020, **61**, 343–351.
- 226 M. A. Śmiałek, S. Ptasnińska, J. Gow, S. V. Hoffmann and N. J. Mason, *Eur. Phys. J. D*, 2015, **69**, 121.
- 227 K. Tanzer, A. Pelc, S. Huber, M. Śmiałek, P. Scheier, M. Probst and S. Denifl, *Int. J. Mass Spectrom.*, 2014, **365–366**, 152–156.
- 228 Š. Matejčík, V. Foltin, M. Stano and J. Skalný, *Int. J. Mass Spectrom.*, 2003, **223–224**, 9–19.
- 229 Y. V. Vasilev, V. G. Voinov, D. F. Barofsky and M. L. Deinzer, *Int. J. Mass Spectrom.*, 2008, **277**, 142–150.
- 230 M. Cipriani, S. Svavarsson, F. F. da Silva, H. Lu, L. McElwee-White and O. Ingólfsson, *Int. J. Mol. Sci.*, 2021, **22**, 8984.
- 231 F. Ferreira da Silva, R. M. Thorman, R. Bjornsson, H. Lu, L. McElwee-White and O. Ingólfsson, *Phys. Chem. Chem. Phys.*, 2020, **22**, 6100–6108.
- 232 J. Langer, M. Zawadzki, M. Fárnik, J. Pinkas, J. Fedor and J. Kočišek, *Eur. Phys. J. D*, 2018, **72**, 112.
- 233 E. Arthur-Baidoo, M. Ončák and S. Denifl, *J. Chem. Phys.*, 2022, **157**, 074301.
- 234 S. King, *Free Radical Biol. Med.*, 2004, **37**, 737–744.
- 235 J. Yarbro, *Semin. Oncol.*, 1992, **19**, 1–10.
- 236 K. Sakano, S. Oikawa, K. Hasegawa and S. Kawanishi, *Jpn. J. Cancer Res.*, 2001, **92**, 1166–1174.
- 237 S. E. Huber, M. A. Śmiałek, K. Tanzer and S. Denifl, *J. Chem. Phys.*, 2016, **144**, 224309.
- 238 J. Kočišek, P. Papp, P. Mach, Y. Vasil'ev, M. Deinzer and S. Matejčík, *J. Phys. Chem. A*, 2010, **114**, 1677–1683.
- 239 A. M. Weljie and F. R. Jirik, *Int. J. Biochem. Cell Biol.*, 2011, **43**, 981–989.



- 240 M. Bonora, S. Patergnani, A. Rimessi, E. De Marchi, J. M. Suski, A. Bononi, C. Giorgi, S. Marchi, S. Missiroli, F. Poletti, M. R. Wieckowski and P. Pinton, *Purinergic Signalling*, 2012, **8**, 343–357.
- 241 F. FerreiradaSilva, M. T. doN. Varella, N. C. Jones, S. VronningHoffmann, S. Denifl, I. Bald and J. Kopyra, *Chem. – Eur. J.*, 2019, **25**, 5498–5506.
- 242 T. J. Jorgensen, *Strange Glow: The Story of Radiation*, Princeton University Press, 2016.
- 243 K. Kobayashi, *Chem. Rev.*, 2019, **119**, 4413–4462.
- 244 M. Maestre-Reyna, P.-H. Wang, E. Nango, Y. Hosokawa, M. Saft, A. Furrer, C.-H. Yang, E. P. G. N. Putu, W.-J. Wu, H.-J. Emmerich, N. Caramello, S. Franz-Badur, C. Yang, S. Engilberge, M. Wranik, H. L. Glover, T. Weinert, H.-Y. Wu, C.-C. Lee, W.-C. Huang, K.-F. Huang, Y.-K. Chang, J.-H. Liao, J.-H. Weng, W. Gad, C.-W. Chang, A. H. Pang, K.-C. Yang, W.-T. Lin, Y.-C. Chang, D. Gashi, E. Beale, D. Ozerov, K. Nass, G. Knopp, P. J. M. Johnson, C. Cirelli, C. Milne, C. Bacellar, M. Sugahara, S. Owada, Y. Joti, A. Yamashita, R. Tanaka, T. Tanaka, F. Luo, K. Tono, W. Zarzycka, P. Müller, M. A. Alahmad, F. Bezold, V. Fuchs, P. Gnau, S. Kiontke, L. Korf, V. Reithofer, C. J. Rosner, E. M. Seiler, M. Watad, L. Werel, R. Spadaccini, J. Yamamoto, S. Iwata, D. Zhong, J. Standfuss, A. Royant, Y. Bessho, L.-O. Essen and M.-D. Tsai, *Science*, 2023, **382**, eadd7795.
- 245 N.-E. Christou, V. Apostolopoulou, D. V. M. Melo, M. Ruppert, A. Fadini, A. Henkel, J. Sprenger, D. Oberthuer, S. Günther, A. Pateras, A. R. Mashhour, O. M. Yefanov, M. Galchenkova, P. Y. A. Reinke, V. Kremling, T. E. S. Scheer, E. R. Lange, P. Middendorf, R. Schubert, E. D. Zitter, K. Lumbao-Conradson, J. Herrmann, S. Rahighi, A. Kunavar, E. V. Beale, J. H. Beale, C. Cirelli, P. J. M. Johnson, F. Dworkowski, D. Ozerov, Q. Bertrand, M. Wranik, C. Bacellar, S. Bajt, S. Wakatsuki, J. A. Sellberg, N. Huse, D. Turk, H. N. Chapman and T. J. Lane, *Science*, 2023, **382**, 1015–1020.
- 246 S. Kogikoski, J. Ameixa, A. Mostafa and I. Bald, *Chem. Commun.*, 2023, **59**, 4726–4741.
- 247 X. Xing, S. Sato, N.-K. Wong, K. Hidaka, H. Sugiyama and M. Endo, *Nucleic Acids Res.*, 2020, **48**, 4041–4051.
- 248 J. Reindl, A. M. Abrantes, V. Ahire, O. Azimzadeh, S. Baatout, A. Baeyens, B. Baselet, V. Chauhan, F. Da Pieve, W. Delbart, C. P. Dobney, N. F. J. Edin, M. Falk, N. Foray, A. François, S. Frelon, U. S. Gaipf, A. G. Georgakilas, O. Guipaud, M. Hausmann, A. J. Michaelidesova, M. Kadhim, I. A. Marques, M. Milic, D. Mistry, S. Moertl, A. Montoro, E. Obrador, A. S. Pires, R. Quintens, N. Rajan, F. Rödel, P. Rogan, D. Savu, G. Schettino, K. Tabury, G. I. Terzoudi, S. Triantopoulou, K. Viktorsson and A.-S. Wozny, *Molecular Radiation Biology*, ed. S. Baatout, Springer International Publishing, Cham, 2023, pp. 83–189.
- 249 J. Rackwitz and I. Bald, *Chem. – Eur. J.*, 2018, **24**, 4680–4688.
- 250 W. Li, E. Mjekiqi, W. Douma, X. Wang, O. Kavatsyuk, R. Hoekstra, J.-C. Pouilly and T. Schlathölder, *Chem. – Eur. J.*, 2019, **25**, 16114–16119.
- 251 M. K. Scheller, R. N. Compton and L. S. Cederbaum, *Science*, 1995, **270**, 1160–1166.
- 252 A. Dreuw and L. S. Cederbaum, *Chem. Rev.*, 2002, **102**, 181–200.
- 253 A. I. Boldyrev, M. Gutowski and J. Simons, *Acc. Chem. Res.*, 1996, **29**, 497–502.
- 254 X.-B. Wang and L.-S. Wang, *Ann. Rev. Phys. Chem.*, 2009, **60**, 105–126.
- 255 M. E. Castellani, D. Avagliano, L. González and J. R. R. Verlet, *J. Phys. Chem. Lett.*, 2020, **11**, 8195–8201.
- 256 M. E. Castellani, D. Avagliano and J. R. R. Verlet, *J. Phys. Chem. A*, 2021, **125**, 3646–3652.
- 257 J. A. Gibbard and J. R. R. Verlet, *J. Chem. Phys.*, 2023, **158**, 154306.
- 258 R. N. Compton, A. A. Tuinman, C. E. Klots, M. R. Pederson and D. C. Patton, *Phys. Rev. Lett.*, 1997, **78**, 4367–4370.
- 259 M. Rezaee, R. P. Hill and D. A. Jaffray, *Radiat. Res.*, 2017, **188**, 123–143.
- 260 L. Zhou, W. Liu, N. Brodeur, P. Cloutier, Y. Zheng and L. Sanche, *J. Chem. Phys.*, 2019, **150**, 195101.
- 261 R. Schürmann, T. Tsering, K. Tanzer, S. Denifl, S. V. K. Kumar and I. Bald, *Angew. Chem., Int. Ed.*, 2017, **56**, 10952–10955.
- 262 Y. Zheng and L. Sanche, *Appl. Phys. Rev.*, 2018, **5**, 021302.
- 263 D. Reimnitz, M. Davidková, O. Mestek, J. Pinkas and J. Kočíšek, *Radiat. Phys. Chem.*, 2017, **141**, 229–234.
- 264 M. Zdrowowicz, P. Spisz, A. Hać, A. Herman-Antosiewicz and J. Rak, *Int. J. Mol. Sci.*, 2022, **23**, 1429.
- 265 P. Nag, M. Ranković, H. C. Schewe, J. Rakovský, L. Sala, J. Kočíšek and J. Fedor, *J. Phys. B: At. Mol. Phys.*, 2023, **56**, 215201.
- 266 L. Sala, J. Rakovský, A. Zerolová and J. Kočíšek, *J. Phys. B: At. Mol. Phys.*, 2023, **56**, 185101.
- 267 J. Országh, A. Ribar, M. Danko, D. Bodewits, T. Matejčík and W. Barszczewska, *ChemPhysChem*, 2022, **23**, e202100705.
- 268 Z. Chen, Z. Li, J. Hu and S. X. Tian, *Acc. Chem. Res.*, 2022, **55**, 3071–3079.
- 269 T. E. Gartmann, S. Hartweg, L. Ban, E. Chasovskikh, B. L. Yoder and R. Signorell, *Phys. Chem. Chem. Phys.*, 2018, **20**, 16364–16371.
- 270 S. Amanatidis, B. L. Yoder and R. Signorell, *J. Chem. Phys.*, 2017, **146**, 224204.
- 271 H. Tsuchida, T. Kai, K. Kitajima, Y. Matsuya, T. Majima and M. Saito, *Eur. Phys. J. D*, 2020, **74**, 212.
- 272 K. Kitajima, H. Tsuchida, T. Majima and M. Saito, *J. Chem. Phys.*, 2019, **150**, 095102.
- 273 T. Majima, S. Mizutani, Y. Mizunami, K. Kitajima, H. Tsuchida and M. Saito, *J. Chem. Phys.*, 2020, **153**, 224201.
- 274 K. Kitajima, T. Majima, T. Nishio, Y. Oonishi, S. Mizutani, J. ya Kohnno, M. Saito and H. Tsuchida, *Nucl. Instrum. Methods Phys. Res., Sect. B*, 2018, **424**, 10–16.
- 275 Y. Gao, Y. Zheng and L. Sanche, *Int. J. Mol. Sci.*, 2021, **22**, 7879.
- 276 E. Alizadeh, D. Chakraborty and S. Ptasińska, *Biophys.*, 2022, **2**, 475–497.



- 277 A. Sieradzka and J. D. Gorfinkiel, *J. Chem. Phys.*, 2017, **147**, 034302.
- 278 L. M. Cornetta, K. Coutinho and M. T. D. N. Varella, *J. Chem. Phys.*, 2020, **152**, 084301.
- 279 J. D. Gorfinkiel, *J. Phys.: Conf. Ser.*, 2020, **1412**, 052003.
- 280 A. Lietard, G. Mensa-Bonsu and J. R. R. Verlet, *Nat. Chem.*, 2021, **13**, 737–742.
- 281 G. A. Cooper, C. J. Clarke and J. R. R. Verlet, *J. Am. Chem. Soc.*, 2023, **145**, 1319–1326.
- 282 M. Smyth, J. Kohanoff and I. I. Fabrikant, *J. Chem. Phys.*, 2014, **140**, 184313.
- 283 I. Anusiewicz, P. Skurski and J. Simons, *J. Phys. Chem. A*, 2020, **124**, 2064–2076.
- 284 M. Mukherjee, D. Tripathi and A. K. Dutta, *J. Chem. Phys.*, 2020, **153**, 044305.
- 285 S. Ptasińska, *Atoms*, 2021, **9**, 77.
- 286 J. McConkey, C. Malone, P. Johnson, C. Winstead, V. McKoy and I. Kanik, *Phys. Rep.*, 2008, **466**, 1–103.
- 287 A. Ribar, M. Danko, J. Országh, F. Ferreira da Silva, I. Utke and Š. Matejčík, *Eur. Phys. J. D*, 2015, **69**, 117.
- 288 J. Országh, A. Ribar, M. Danko, D. Bodewits, T. Matejčík and W. Barszczewska, *ChemPhysChem*, 2022, **23**, e202100705.
- 289 H. Abdoul-Carime, F. Mounier, F. Charlieux and H. André, *Rev. Sci. Instrum.*, 2023, **94**, 045104.
- 290 F. Charlieux and H. Abdoul-Carime, *ChemPhysChem*, 2023, **24**, e202200722.
- 291 Z. Li, A. R. Milosavljević, I. Carmichael and S. Ptasińska, *Phys. Rev. Lett.*, 2017, **119**, 053402.
- 292 C. D. Lane and T. M. Orlando, *J. Chem. Phys.*, 2006, **124**, 164702.
- 293 S. D. Brinkevich, A. Y. Maliborskii, I. A. Kapusto, R. L. Sverdlov, Y. V. Grigor'ev, O. A. Ivashkevich and O. I. Shadyro, *High Energy Chemistry*, 2019, **53**, 147–154.
- 294 H. C. Kolb, M. G. Finn and K. B. Sharpless, *Angew. Chem., Int. Ed.*, 2001, **40**, 2004–2021.
- 295 X. Jiang, X. Hao, L. Jing, G. Wu, D. Kang, X. Liu and P. Zhan, *Expert Opin. Drug Discovery*, 2019, **14**, 779–789.
- 296 M. Rezaee, D. J. Hunting and L. Sanche, *Int. J. Radiat. Oncol. Biol. Phys.*, 2013, **87**, 847–853.
- 297 M. R. Gill and K. A. Vallis, *Chem. Soc. Rev.*, 2019, **48**, 540–557.
- 298 R. Carter, A. Westhorpe, M. J. Romero, A. Habtemariam, C. R. Gallevo, Y. Bark, N. Menezes, P. J. Sadler and R. A. Sharma, *Sci. Rep.*, 2016, **6**, 20596.



2.

Electron attachment to isolated and
microhydrated favipiravir



Cite this: DOI: 10.1039/d1cp02686k

Electron attachment to isolated and microhydrated favipiravir†

 Barbora Sedmidubská,^{ib}ab Thomas F. M. Luxford^{ib}a and Jaroslav Kočíšek^{ib}*a

Electron attachment and its equivalent in complex environments, single-electron reduction, are important in many biological processes. Here, we experimentally study the electron attachment to favipiravir, a well-known antiviral agent. Electron attachment spectroscopy is used to explore the energetics of associative (AEA) and dissociative (DEA) electron attachment to isolated favipiravir. AEA dominates the interaction and the yields of the fragment anions after DEA are an order of magnitude lower than that of the parent anion. DEA primary proceeds *via* decomposition of the CONH₂ functional group, which is supported by reaction threshold calculations using *ab initio* methods. Mass spectrometry of small favipiravir–water clusters demonstrates that a lot of energy is transferred to the solvent upon electron attachment. The energy gained upon electron attachment, and the high stability of the parent anion were previously suggested as important properties for the action of several electron-affinic radiosensitizers. If any of these mechanisms cause synergism in chemo-radiation therapy, favipiravir could be repurposed as a radiosensitizer.

 Received 14th June 2021,
Accepted 6th August 2021

DOI: 10.1039/d1cp02686k

rsc.li/pccp

^a J. Heyrovský Institute of Physical Chemistry of the Czech Academy of Sciences, Dolejškova 3, 18223 Prague, Czech Republic.
E-mail: jaroslav.kocisek@jh-inst.cas.cz

^b Department of Nuclear Chemistry, Faculty of Nuclear Sciences and Physical Engineering, Břehová 7, 11519 Prague, Czech Republic

† Electronic supplementary information (ESI) available: Low *m/z* part of the spectra depicted in Fig. 6, panels (c) and (d). Comparison of the reaction energies calculated using B3LYP and M062x functionals, Cartesian coordinates of favipiravir conformers and its DEA anion and neutral fragments at B3LYP and M062x levels of theory. See DOI: 10.1039/d1cp02686k

1 Introduction

The present study is motivated by the fact that many biological processes based on reduction can be related to electron attachment (EA). This relation was explored by the Modelli and Pshenichnyuk groups for a wide range of biological processes, from metabolic pathways to the functionality of the olfactory system.^{1–7} The electron reduction properties can also influence the transport of drugs through biological membranes and influence their target binding properties.^{8,9} Recently, the RNA


Barbora Sedmidubská

Barbora Sedmidubská received her undergraduate and MSc (2020) degree in the field of nuclear chemistry and now she is continuing PhD studies at the Faculty of Nuclear Sciences and Physical Engineering, Czech Technical University in Prague. Her main research interest is in the molecular understanding of radiation chemistry in living tissues. Her PhD project is focused on noncovalent interactions of radiosensitizers and Fullerenes.


Thomas F. M. Luxford

Thomas F. M. Luxford received his undergraduate and MSc degrees from the University of York (UK), and his PhD from Herriot-Watt University in Edinburgh (UK, 2017). He is currently a research assistant at the J Heyrovský Institute of Physical Chemistry in Prague (Czech Republic), as part of the Department of Dynamics of Molecules and Clusters. His research is primarily focused on better understanding the fundamental interactions of species in the gas phase, and he is currently studying the electron-induced reactivity of molecules.

inhibitor efficiency of favipiravir tautomers was related to the energy difference between its highest occupied (HOMO) and lowest unoccupied (LUMO) molecular orbitals.¹⁰ Unoccupied orbitals can become singly occupied upon electron attachment and appear as so-called shape resonances in the electron scattering spectrum. A present study of the electron attachment to favipiravir may therefore provide an important key to better understand its activity.

Another important motivation is based on the relation of low-energy electrons to the synergism observed in the concomitant chemo-radiation therapy of cancer.^{11,12} Two facts motivated a range of studies on the relation of low-energy electrons to the synergistic action of radiation with a range of chemotherapeutic and radio-sensitizing drugs.^{13,14} The first fact is a large amount of available secondary low-energy electrons in the irradiated tissue.^{15,16} The second fact is that despite the different possible modes of action,¹⁷ most of the known small molecule radiosensitizers and their important functional groups have high electron affinities.¹⁸ Processes such as the formation of reactive anions and radical species *via* dissociative electron attachment,^{19–22} enhanced linear energy transfer,²³ transport properties⁸ due to associative electron attachment, or DNA sensitization^{24–30} have been proposed as possible sources of synergism observed in concomitant chemo-radiation therapy. Several of the processes were then used to suggest novel radiosensitizers.^{31–34} However, in many cases, the suggested molecules with “ideal” electron-attachment properties fail to exhibit the synergism³⁵ or are biologically incompatible.³⁶ Since drug repurposing³⁷ is becoming still more important and antiviral drugs are often chosen as cancer chemo or even chemo-radio therapeutics,^{38–43} we explore favipiravir as a promising candidate for an electron affinic radiosensitizer.

Favipiravir (Fig. 1) has already been established as a broad-range antiviral^{44–47} with good biocompatibility⁴⁸ and known pharmacokinetics.^{49,50} Here, we explore its behavior in the reactions with low-energy electrons using electron attachment

spectroscopy of the isolated and microhydrated molecule and perform basic computational modeling to support our experimental data.

2 Methods

2.1 Experimental

Favipiravir was purchased from Santiago Labs with stated purity of 99% and its electron-induced chemistry was explored on two experimental setups. The isolated molecule was studied using the TEM-QMS setup⁵¹ and hydration effects were studied using the CLUster Beam (CLUB) apparatus in the M. Fárník group.⁵²

The TEM-QMS apparatus is an electron attachment spectrometer combining a trochoidal electron monochromator (TEM) with a quadrupole mass spectrometer (QMS) analyser originally built in the M. Allan group.⁵³ With the TEM,⁵⁴ electrons thermo-emitted from an iridium-yttrium cathode, are selected according to their kinetic energy, narrowing the initial electron energy distribution function. In the present experiment, the electron-energy resolution was around 150 meV as estimated from the FWHM of the 0 eV peak in the anion yield for AEA to sulphur hexafluoride.⁵⁵ The electrons collide with sample molecules in the reaction chamber and the formed ions are extracted towards the QMS. Two modes of operation are possible, with ion yield measurement as a function of incident electron energy at a constant m/z of QMS or ion yield measurement as a function of m/z at constant incident electron energy. Favipiravir was introduced using the direct insertion probe.⁵⁶ Sample powder was loaded into a glass bulb and placed at the end of the probe, which was inserted into a resistively heated copper cylinder with the constant temperature kept at 340 K. The sublimed molecules effused into the reaction zone through a 1 cm long capillary. For calibration of the energy axis, we used SF₆ and CO₂ gases, which were introduced through the same inlet. The 4.3 eV resonance of O⁻ from CO₂⁵⁷ was used to calibrate the electron-energy axis and 0 eV resonance of SF₆⁻ from SF₆ to determine the energy threshold for electron transmission through the TEM. In the present case, the threshold is around 0.1 eV and constant electron current is reached around 0.25 eV as demonstrated on SF₆⁻ signal in Fig. 2. Anion yields lower than this value presented in this work, particularly the yield of parent anion, are therefore underestimated.

On the CLUB setup, we only used the neutral cluster source and reflectron time-of-flight mass spectrometer. Experimental details for the negative and positive mass spectra measurements can be found in ref. 58 and 59, respectively. The molecular target was prepared by co-expansion of He buffer gas and favipiravir vapors through a conical 90 μm nozzle into the vacuum. Clusters of microhydrated molecules were prepared by an approach developed in our laboratory based on the addition of a small amount of water into the buffer gas through the Nafion membrane.⁶⁰ During all experiments, the sample was sublimed at a temperature of approximately 85 °C. To test



Jaroslav Kočíšek

Jaroslav Kočíšek received PhDs in plasma physics from Comenius University in Bratislava (2010) and in photo-dissociation dynamics from Charles University in Prague (2013). After postdocs studying electron scattering at the University of Fribourg and collisions of multiply charged ions at GANIL, he started a junior research group at J. Heyrovský Institute of Physical Chemistry in 2016. Since 2019, he is holding a recognized J. Heyrovský Young Scientist position. His

research is focused on environmental effects on reaction dynamics and elementary processes in radiation interaction with living tissue, studied experimentally on model systems ranging from isolated molecules and clusters to self-assembled nanostructures.

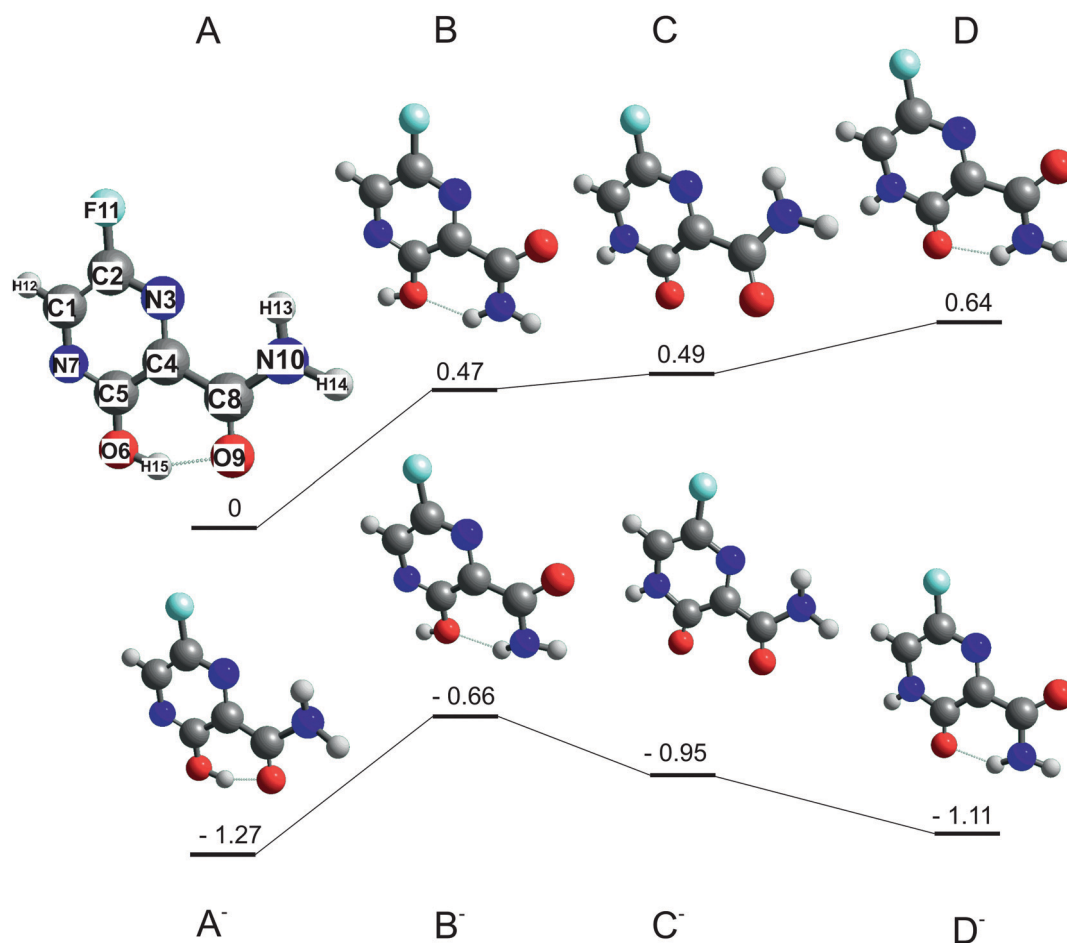


Fig. 1 Optimized structures of stable conformers A, B and keto tautomers B, C of favipiravir and their respective anions. Energies in eV relative to the most stable neutral conformer A calculated at the B3LYP/aug-cc-pVTZ level of theory.

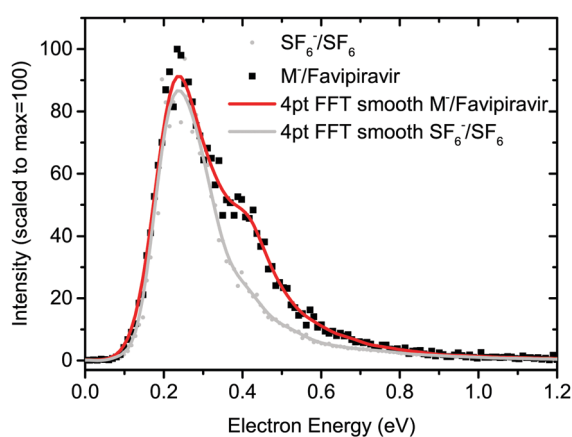


Fig. 2 Electron energy-dependent ion yields for AEA to favipiravir and sulfur hexafluoride. The drop of the anion yield below ~ 0.25 eV is caused by decrease of the incident electron current below this value. Anion yields at energies lower than ~ 0.25 eV presented in this work are, therefore, underestimated.

the thermal stability of the molecule, we heated the sample up to 118 °C. Even at this elevated temperature, we did not observe any new product ions due to thermal decomposition in the ionization MS (see ESI[†]).

2.2 *Ab initio* calculations

Two favipiravir conformers, differing in the orientation of the CONH₂ functional group, its keto form, and their respective anions, were pre-optimized at the B3LYP/6-31(d) level of theory and then optimized at the B3LYP/aug-cc-pVTZ level of theory. The structures of neutrals and respective energies of neutrals and anions optimized at the B3LYP/aug-cc-pVTZ level of theory are in Fig. 1. The order of the conformers was checked by energy calculation using G3MP2⁶¹ method and method error by re-optimizing the B3LYP⁶² structures using M062x⁶³ functional and the same aug-cc-pVTZ basis set. Adiabatic electron affinities were calculated as a difference of the neutral and anion energies in their optimized geometry and they are listed together with other parameters in Table 1.

Then, energetic thresholds for individual reaction channels of DEA to favipiravir were calculated at the B3LYP/aug-cc-pVTZ theory to support the experimental results. Threshold energies were obtained using the formula:

$$E_{\text{th}} = E_{\text{M}_a^-} + E_{\text{M}_b} - E_{\text{M}} \quad (1)$$

where $E_{\text{M}_a^-}$ and E_{M_b} are the energies of the anion and neutral fragments respectively (if there are multiple neutral fragments,

Table 1 Relative energies and dipole moments of optimized ground state neutral and anion conformers of favipiravir computed at the B3LYP/aug-cc-pVTZ, G3MP2 and M062x/aug-cc-pVTZ level of theory. All energies are in eV relative to the conformer A, which is the lowest energy neutral conformer at all levels of theory. All dipole moments are in D

Conformer	Energy B3LYP	Energy G3MP2	Energy M062x	Dipole moment B3LYP
A	0	0	0	3.2
B	0.47	0.44	0.79	5.7
C	0.49	0.57	0.34	6
D	0.64	0.72	1.09	5.3
A ⁻	-1.27	-1.14	-0.68	4.8
B ⁻	-0.66	-0.54	-0.3	7.8
C ⁻	-0.95	-0.91	-0.9	9.2
D ⁻	-1.11	-0.73	-0.5	9.1

then E_{M_b} is the sum of all neutral fragment energies), and E_M is the energy of the neutral parent molecule. These energies correspond to the sum of electronic and zero-point correction energies in the Gaussian output file. Again the method error was checked by recalculating the values at M062x/aug-cc-pVTZ level (see ESI[†]).

Finally, virtual orbital energies of favipiravir were calculated at the HF/6-31G* level of theory, using the structures optimised at the B3LYP/aug-cc-pVTZ level of theory. These energies were then scaled to obtain vertical attachment energies according to the empirical formula of Aflatooni *et al.*⁶⁴:

$$\text{VAE} = [\epsilon_{\text{VO}} - 2.5553]/1.3749 \quad (2)$$

where VAE is the vertical attachment energy and ϵ_{VO} is the virtual orbital energy.

All calculations were performed in Gaussian 16⁶⁵ and the results were analyzed and visualized using Chemcraft.⁶⁶

3 Results and discussion

3.1 Isolated molecule

Structures of the most stable isomers and keto tautomers of favipiravir are shown in Fig. 1. Conformer A is the most stable conformer of neutral favipiravir, independent of the computational method (Table 1), due to the aromatic nature of the ring and being stabilized by O(9)–H(15) hydrogen bond (atom numbers are shown on the structure of conformer A of Fig. 1). The energy of the conformer is (depending on the method) ~ 0.5 eV below the other studied structures and therefore will dominate the gas phase distribution of the sublimed favipiravir. The recent work of Antonov⁶⁷ also demonstrated the stability of this conformer in various solvents. We will therefore relate all energies in the following discussion to this most stable conformer A. The energy difference due to different conformers of the neutral precursor molecule may be easily estimated from Table 1.

The calculated adiabatic electron affinity of the molecule is 1.3 eV (Fig. 1 and Table 1). Therefore, favipiravir can form a stable valence-bound anion, which is also close in geometry to the neutral molecule. However, in its anionic state, the energy gap between the enol A conformer and keto D conformer is

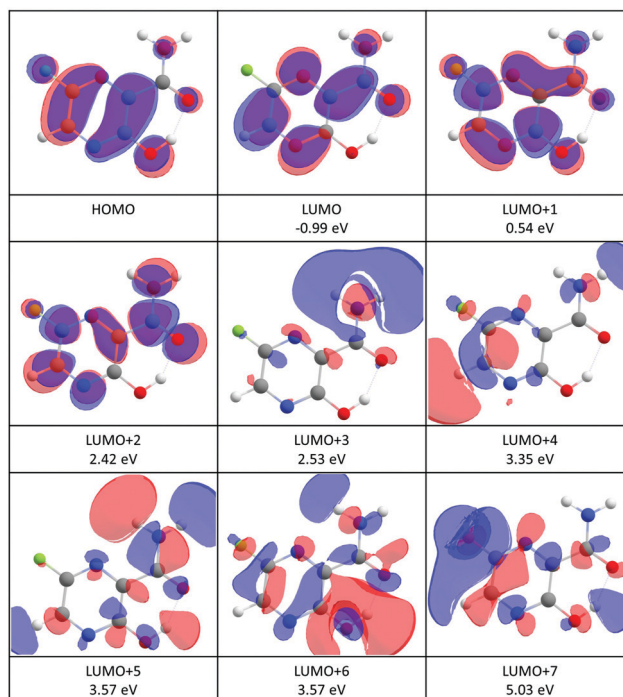


Fig. 3 Contour plots of the highest occupied (HOMO) and low-lying virtual orbitals of favipiravir. The orbitals were calculated at the HF/6-31G(d) level of theory. The numbers in eV are vertical attachment energies according to the formula (2).

much lower than in the case of the neutral molecule and therefore both forms may be present. This may influence the dissociation dynamics, as will be discussed later.

An estimated value of the vertical electron affinity at the B3LYP/aug-cc-pVTZ level of theory is 0.3 eV. The value may vary due to the limitations of the DFT approach,⁶⁸ however, its positive character is clear also from our estimation of the negative value of the LUMO vertical attachment energy (Fig. 3).

Favipiravir has a large dipole moment. The most stable conformer A has the lowest dipole moment (3.3 D) of all explored conformers, above the commonly set limits for the formation of dipole supported states of the anion (ref. 69 and references cited therein).

The incident electron energy dependent ion yields for the most stable anionic products of electron attachment to isolated favipiravir are shown in Fig. 4 and relative intensities of the bands, obtained as the area of Gaussian peaks fitted to the data, are listed in Table 2. The yields peak at energies of around 0, 1, 2, 3, 4, 5, 7, and 9 eV. The 0 eV peak is observed only for the parent anion. The 2, 3, and 5 eV peaks can be assigned to shape resonances according to estimated vertical attachment energies of LUMO+2, 4, and 7 (see Fig. 3). The yields peaking at 1 or 4 eV can also be due to the attachment to virtual orbitals, however, their low energy onset may be shifted due to the reaction endothermicity, which will be discussed later. The high energy peaks in the spectrum can be formed by core excited Feshbach resonances or core excited shape resonances. Unfortunately, the photo-electron spectrum of favipiravir, which would allow

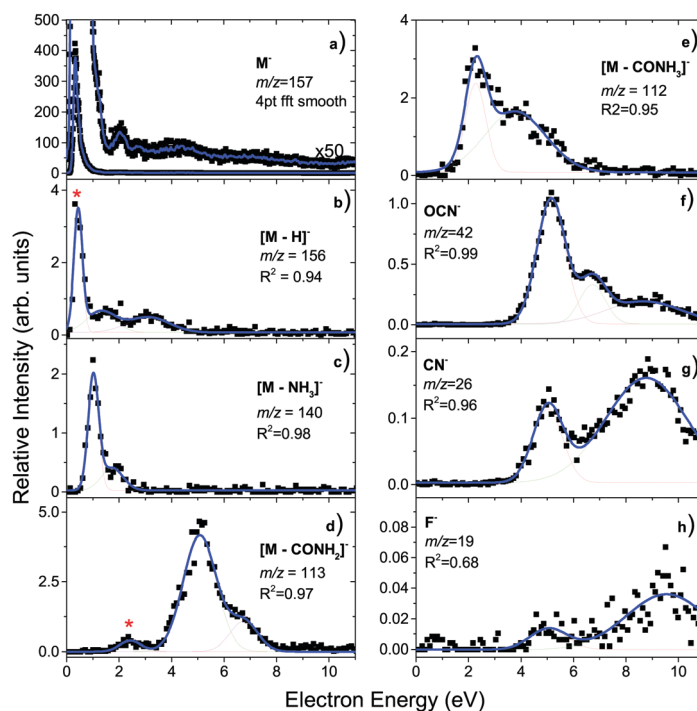


Fig. 4 Electron-energy dependent ion yields for the main products of EA to favipiravir. The contributions of ion signal from neighboring m/z due to low selectivity of QMS are marked by *.

us to better identify the Feshbach resonances^{70–72} has not yet been measured.

Positions of the Feshbach resonances can be, however, estimated on the basis of known resonances for components of the molecule,^{56,73} such as pyrazine or small amides. From the known electron energy loss spectrum of pyrazine,⁷⁴ which matches the central favipiravir ring structure, we expect that Feshbach resonances in favipiravir can occur as low as at 4 eV. Further excited states of pyrazine are available at 5 eV, 6.5 eV, and 7.5 eV. For the amide functional group, excited states may be expected at higher energies of 7 eV and 9 eV, based on electron energy loss and DEA data of small amides.^{75,76} However, for amides also an alternative process of core excited shape resonances was suggested,⁷⁷ but has yet to be confirmed.⁷⁸

The product anion yield is dominated by the parent favipiravir anion M^- . Several mechanisms for the formation of the anion at low energies are possible. As we discussed in the previous paragraphs, the attachment is exothermic and therefore attachment at 0 eV can be expected. The high dipole moment and similar geometries of the neutral and anion allow for dipole-supported vibrational Feshbach resonances, which are known DEA to various molecules.^{79–81} The electron-energy dependent ion yield curve of the M^- anion is shown in detail in Fig. 2. First, we can not see the onset at expected 0 eV but at ~ 0.1 eV due to the electron transmission function of the monochromator, which can be well demonstrated on the comparison with SF_6^- ion yield with the known 0 eV resonance and similar onset. Second, there is a small bump at energies ~ 0.4 eV, which may be an indication of vibrational structure. However, the vibrational mode can not be unambiguously

assigned because the spectrum is shifted by the electron transmission function of the monochromator. In bare pyrazine (the central cyclic structure of favipiravir), the structures in electron scattering were assigned to breathing modes of the ring.⁸² In the present case, the energy is high, if we exclude a possibility that more structures occur in the part of the ion yield to which we are blind, the modes involved will be rather O–H or C–H stretches. However, the bump in the spectrum may also be simply an experimental artefact or indication of attachment *via* the low-lying π shape resonance. Vertical attachment to LUMO+1 may occur for electrons with energies ~ 0.5 eV (Fig. 3) according to the scaling of Aflatooni *et al.*⁶⁴

A clear structure around 2 eV in the spectrum of M^- , in the panel a) of Fig. 4 can be also assigned to a shape resonance of LUMO+2.

We can see that for several bands in the spectrum of favipiravir, there are multiple possible explanations of the undergoing attachment mechanism. Their unambiguous identification requires further experiments. We will not speculate here and will instead focus on the exit channel of the DEA, which was directly studied in the present experiment.

The main DEA channels of favipiravir are listed in Table 2, together with their calculated threshold energies and information about the relative intensities of the main peaks in the experimentally measured ion yields (Fig. 4). As already mentioned, AEA dominates the interaction. In Table 2, where the intensity of the near 0 eV peak of M^- is set to 100, the intensity of the second most intense peak in the yield of EA products to favipiravir corresponds to the loss of the $CONH_2$ functional group at energies of incident electrons ~ 5 eV, which has a

Table 2 Main EA channels. Reaction thresholds obtained from calculations using B3LYP functional with the aug-cc-pVTZ basis set. Peak positions and relative intensities of anions from electron-energy dependent ion yields. All energies are presented in units of eV. Relative intensities in arbitrary units with maximum set to 100. The error of the relative intensity is influenced by the settings of the ion optics of the mass spectrometer and may reach 20%. The error of the peak position is on the level of the current TEM resolution ~ 150 meV. Structures of fragment conformers labelled A, B, C... are available in the ESI

m/z	Anion	Neutral	$M + e^- \rightarrow$ products calculated threshold	Experimental peak energy (relative intensity)		
157	$C_5H_4FN_3O_2^-$			$\sim 0(100)$;	2.2(0.06)	
156	$C_5H_3FN_3O_2^-$			1.8(0.2);	3.2(0.12)	
	[M-H] ⁻ A	H(15)	0.64			
	[M-H] ⁻ B	H(13)	1.03			
	[M-H] ⁻ C	H(15)	1.03			
	[M-H] ⁻ D	H(12)	2.05			
	[M-H] ⁻ E	H(13)	2.22			
	[M-H] ⁻ F	H(12)	2.50			
140	$C_5HFN_2O_2^-$			1.1(1.4);	1.9(0.26)	
	[M-NH ₃] ⁻	NH ₃	0.17			
	[M-OH] ⁻ A	OH	2.96			
	[M-OH] ⁻ B	OH	3.17			
	[M-OH] ⁻ C	OH	4.92			
	[M-OH] ⁻ D	OH	5.03			
113	$C_4H_2FN_2O^-$			5.0(6.0);	6.8(1.1)	8.5(0.67)
	[M-CONH ₂] ⁻ A	CO + NH ₂	3.24			
	[M-CONH ₂] ⁻ B	CO + NH ₂	3.46			
	[M-CONH ₂] ⁻ C	CO + NH ₂	3.62			
	[M-CONH ₂] ⁻ A	CONH ₂	4.39			
	[M-CONH ₂] ⁻ B	CONH ₂	4.61			
	[M-CONH ₂] ⁻ C	CONH ₂	4.77			
112	$C_4HFN_2O^-$			2.3(1.8);	4.3(3.3)	
	[M-CONH ₃] ⁻ A	CONH ₃	0.86			
	[M-CONH ₃] ⁻ A	CO + NH ₃	1.31			
	[M-CONH ₃] ⁻ B	CONH ₃	1.96			
	[M-CONH ₃] ⁻ B	CO + NH ₃	2.41			
	[M-CONH ₃] ⁻ C	CONH ₃	2.35			
	[M-CONH ₃] ⁻ C	CO + NH ₃	2.8			
	[M-CONH ₃] ⁻ D	CONH ₃	2.4			
	[M-CONH ₃] ⁻ D	CO + NH ₃	2.85			
42	OCN ⁻	—	—	5.0(1.4);	6.6(0.4);	
	OCN ⁻	$C_4H_4FN_2O$	1.93			
	OCN ⁻	$H_2 + C_4H_2FN_2O$ A	4.1			
	OCN ⁻	$H_2 + C_4H_2FN_2O$ B	4.87			
	OCN ⁻	$H_2 + C_4H_2FN_2O$ C	4.95			
26	CN ⁻	—	—	5.0(0.17);	8.7(0.55)	
	CN ⁻	$H_2O + C_4H_2FN_2O$ A	1.85			
	CN ⁻	$C_4H_4FN_2O_2$	1.97			
	CN ⁻	$HF + C_4H_3N_2O_2$	2.61			
	CN ⁻	$H_2O + C_4H_2FN_2O$ B	2.62			
	CN ⁻	$H_2O + C_4H_2FN_2O$ C	2.7			
19	F ⁻	—	—	5.0(0.02);	9.4(0.1)	
	F ⁻	(M-F) A	1.72			
	F ⁻	(M-F) B	2.15			
	F ⁻	(M-F) C	2.15			
	F ⁻	(M-F) D	2.34			

relative intensity of 6. It is important to mention that the relative intensity ratios in the present experiment may be influenced by the ion optics and quadrupole mass filter transmission settings, which are mass-dependent. To minimize these effects we tuned the ion optics for maximum transmission at $m/z = 79$, Br⁻ anion, which is present as a background in the TEM-QMS setup and is approximately in the center of the m/z fragment distribution. However, the relative intensities may still vary by up to $\sim 20\%$.

[M-CONH₂]⁻ can be formed by the simple breaking of the C(4)–C(8) bond. The electron energy-dependent spectrum for its formation is shown on panel d) of Fig. 4. The calculated threshold energy for this process is 4 eV (Table 2). This means that there is sufficient energy in the system for this process to occur at incident electron energies above 4 eV, while it is energetically inaccessible at incident electron energies below 4 eV. The onset of the most intense peak in the spectrum is around 3.5 eV, below the calculated reaction threshold for

simple C(4)–C(8) bond cleavage, and is therefore energetically inaccessible. Only when we consider further dissociation of the CONH₂ fragment into more stable CO and NH₂ molecules, the calculated threshold energy shifts below the experimentally observed threshold. Additionally, there is a peak with a maximum at around 2 eV, which is an experimental artefact, caused by the low selectivity of the QMS. The low energy peak is a contribution from neighboring intense fragment ion, [M–CONH₃][–], as can be read from its spectra discussed in the next paragraph.

The second most intense fragment ion is [M–CONH₃][–], whose spectrum is shown in Fig. 4, panel e). In certain configurations of the anion, the H(15) hydrogen of the OH group can be easily transferred to the amino group. Then, the formation of CO and NH₃ neutral fragments together with the C₄HFNO[–] anion is possible at energies as low as 0.86 eV, explaining the first peak in the ion yield. The second peak in the spectrum can be due to anions formed after H(12) removal, which requires more than 2 eV.

The spectrum of the third most intense fragment, OCN[–] is shown in panel f) of Fig. 4. Due to its high electron affinity (EA), OCN[–] is a common ion formed by DEA to many biologically relevant molecules in the gas phase,^{83–90} as well as clusters⁵⁸ and molecules deposited on surfaces.^{91,92} The high electron affinity of OCN[–] (~3.6 eV)⁹³ allows for very complex rearrangement and fragmentation reactions to be induced by the attachment of low-energy electrons.^{83,86} In the present case, the most straightforward pathway for OCN[–] extraction is the cleavage of C(4)–C(8) bond followed by the elimination of H₂ from the resulting CONH₂[–] anion. As we have seen already for the [M–CONH₂][–] channel the C(4)–C(8) bond is strong and therefore the reaction energies for such mechanism are above 4 eV. Within experimental and computational errors, the mechanisms can still explain all the peaks observed in the OCN[–] spectrum. However, we also found a more energetically favorable channel, which can be opened by hydrogen transfer to C(4) carbon allowing for N(7)C(5)O(6) anion extraction at energies below 2 eV together with a C₄H₄FN₂O neutral co-fragment.

Another intense fragmentation channel results in an ion corresponding to the neutral loss of 17 Da from the parent ion (Fig. 4, panel c)), which could correspond to either OH or NH₃ loss. The calculated reaction thresholds allow us to exclude the OH loss channel, as it occurs only at energies above 2.9 eV, higher than both observed peaks in the spectrum of this anion. On the other hand, the elimination of NH₃ has a threshold of only 0.17 eV, which is well below the onset of the observed signal, meaning that it is accessible.

The [M–H][–] ion yield is dominated by a near 0 eV peak, which is due to the low selectivity of QMS and overlap with the neighboring signal of the M[–] anion, which can not be fully separated in the present experiment. Energetically, this channel is only accessible above 0.64 eV. H(15) or H(13) hydrogen loss may occur at energies of the first real peak in the spectrum with a maximum at ~1.8 eV and cleavage of H(12) is possible at the higher energies of the second peak with a maximum at ~3.2 eV.

Another common biomolecular fragment ion with high electron affinity, CN[–] can be formed from the decomposition of the CONH₂ functional group or the ring of favipiravir. The energetic thresholds for both mechanisms are similar, at 1.85 eV and 1.97 eV respectively. In the first mechanism, a stable water molecule is formed as a neutral co-product. In the second mechanism, the C(1)–N(7) atoms are easiest to extract after hydrogen migration from C(1) to C(2). We also found several other possible reaction pathways that are possible for the observed CN[–] formation, with an onset around 4 eV (Fig. 4, panel g). In some cases, the reaction energy is lowered by closing the ring after the extraction of CN[–] anion forming the C₃N ring. Such rearrangement, however, may proceed over a reaction barrier, which can not be identified using the simple calculations present here.

Finally, with a relative intensity of only ~0.1% that of the parent ion signal, we observe F[–] (Fig. 4, panel h)). The signal levels for this ion are near the detection limits of the setup, there appear to be three peaks in the spectrum, at ~1 eV, ~5 eV, and ~9.5 eV. The calculated threshold energy for simple cleavage of the C(2)–F(11) bond is 2.15 eV, which explains the two higher energy resonances, but not the low energy resonance. This unassigned low-energy signal is possibly an experimental artefact, and is most likely caused by background ions in the experiment.

3.2 Hydration

To explore environmental effects, we measured EA to favipiravir in clusters with attached water molecules, prepared in a molecular beam using the CLUB experimental setup. Negative ion spectra of the molecule under dry and hydrated conditions taken in the energy range 0.6 to 8.6 eV is shown in Fig. 5. We can see that for the dry conditions, the intensity of the DEA channels is already reduced with respect to parent anion intensity. Using the CLUB apparatus, we measured reasonable signal only for the *m/z* = 112, 113 fragment anions. Let's compare the relative intensities of these anions to the parent anion in the two experiments. Dividing the integral intensity of the fragment *m/z* = 112 + *m/z* = 113 ion signal by that of *m/z* = 157 parent ion signal from the energy dependent ion yields in Fig. 4, we obtain the ratio of fragment to parent ion signal in the QMS-TEM setup of ~1/10. Dividing the integral intensity of the the fragment *m/z* = 112 + *m/z* = 113 peak to that of *m/z* = 157 parent peak in the cumulative MS in Fig. 5, we obtain the ratio of fragment to parent ion signal in CLUB experiment at dry conditions to be 1/33, which is much lower. Additionally, the ratio 1/33 is only the highest estimate, since the electron current in CLUB experiment significantly drops in the near 0 eV region of the parent ion resonance, resulting in an apparent reduction of the parent ion signal.

The main reasons for suppression of fragmentation in the CLUB experiment under dry conditions is the detection time of only tens of microseconds, in comparison to the TEM-QMS experiment, where it is hundreds of microseconds. The much shorter detection timescale of the CLUB setup means that there is less time for fragmentation or autodetachment to occur.

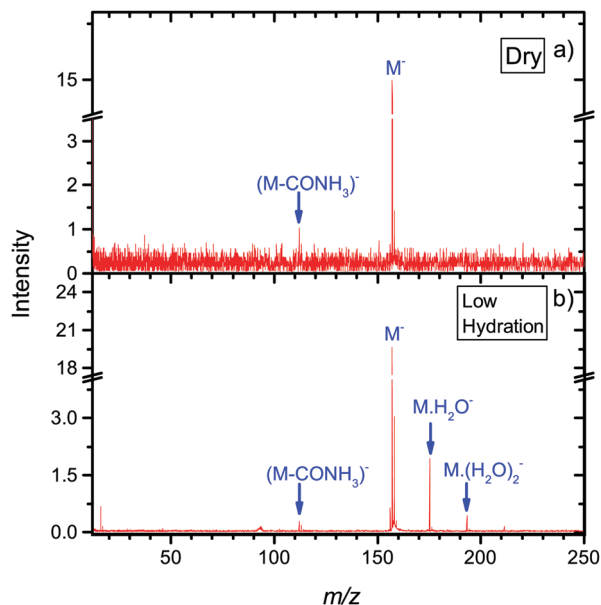


Fig. 5 Mass spectra from the CLUB experiment of anions formed after electron attachment to isolated or microhydrated neutral favipiravir in molecular beams. Negative ion MS are prepared by summing spectra taken with 0.2 eV step in the 0.6 eV to 8.6 eV range.

These effects of the detection time scale were studied in detail by Asfandiarov and co-workers.^{94,95} Another parameter influencing the fragmentation is the temperature of the precursor molecules, which is lower in the molecular beam of the CLUB than in the effusive beam of the TEM-QMS.⁹⁶

Further stabilization of parent anion with respect to both DEA and autodetachment can be induced by hydration. Under hydrated conditions the ratio of $m/z = 112, 113$ to parent anion signal further decreases to $\sim 1/90$.

Under hydrated conditions, anions are stabilized by energy transfer to the solvent. The total energy available for transfer to surrounding water molecules and their subsequent evaporation (TET) can be written as a sum of adiabatic electron affinity (AEA) and energy of the incoming electron (E_e):

$$\text{TET} = E_e + \text{AEA} \quad (3)$$

For halouracils, energy of several eV was estimated to be transferred to the solvent after electron attachment.²³ We also postulated that such energy transfer to the solvent can increase linear energy transfer (LET) value after interaction of the ionizing radiation with an environment containing electron affinic molecules and can explain their radiosensitizing action. The largest effect was previously observed for bromouracil, for which the number of evaporated water molecules after electron attachment was similar to that after electron ionization. In Fig. 6 we can see that the situation is also very similar for favipiravir. The figure shows a comparison of electron impact ionization MS of favipiravir at 70 eV and negative ion MS after electron attachment at 1.4 eV for two different hydration conditions. We can see that the observed numbers of water molecules, n , m , and p , attached to anions $M(\text{H}_2\text{O})_n^-$ and cations $M(\text{H}_2\text{O})_m^+$ and $M(\text{H}_2\text{O})_p^+$ are similar. Despite the well-known fragmentation efficiency of electron impact ionization,⁹⁷ the “soft” EA leads to a

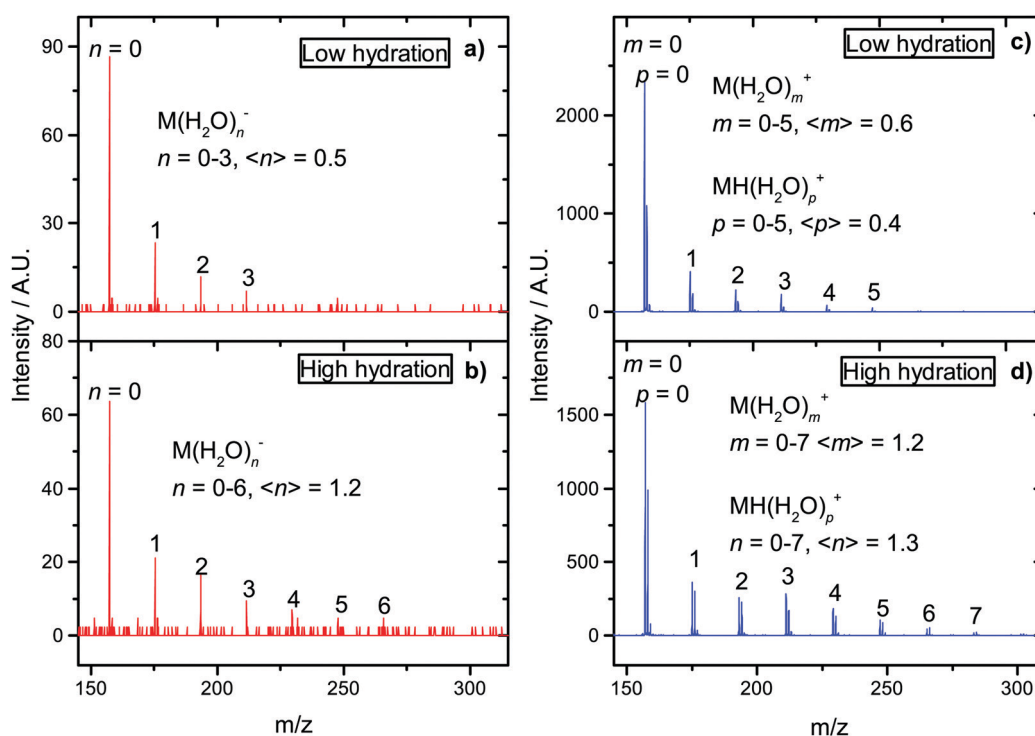


Fig. 6 Mass spectra from the CLUB experiment for hydrated favipiravir in molecular beams. Negative ion MS (a) and (b) at the electron-energy 1.4 eV and positive ion MS (c) and (d) at the electron-energy 70 eV. The values in brackets represents peak intensity weighted average.

similar fragmentation, in the form of loss of neutral water molecules from the clusters. This is caused by the high electron affinity of favipiravir, which results in water evaporation from cluster after electron attachment. Therefore, if our hypothesis that energy transfer to the solvent after EA enhances LET and causes radiosensitization is correct, favipiravir should demonstrate radiosensitizing effects comparable to halogenated uracils.

4 Conclusions

We present an experimental study of electron attachment to favipiravir as an interesting hetero-aromatic, important biochemical, and promising radiosensitizing molecule. Electron attachment to favipiravir leads primarily to the formation of the parent anion with a long lifetime. Such stability may be important for the transport and radiosensitizing properties of the molecule⁸ but may also allow for multiple electron reduction.^{9,8} The threshold DFT calculations helped us to interpret the fragmentation pattern of the molecule with main fragmentation reactions occurring on the CONH₂ group. The estimation of vertical attachment energies demonstrates several possible virtual states available for attachment *via* shape resonances that may be related to favipiravir's antiviral action.¹⁰ The mass spectrometry of small clusters of the form Fav(H₂O)_n, reveals that a large amount of energy is transferred to the solvent after electron attachment. This energy may contribute to favipiravir's reactivity in its reduced form but also support our hypothesis that favipiravir may be repurposed as a radiosensitizer.

Conflicts of interest

There are no conflicts to declare.

Acknowledgements

The authors appreciate the support of the Czech Science Foundation, grant number 19-01159S. We would like to thank R. Čurík and M. Tarana for providing us with computational equipment and software available at the Department of Theoretical Chemistry of J. Heyrovský Institute of Physical Chemistry.

Notes and references

- S. A. Pshenichnyuk and A. Modelli, *J. Chem. Phys.*, 2014, **140**, 034313.
- S. A. Pshenichnyuk and A. Modelli, in *ETS and DEAS Studies of the Reduction of Xenobiotics in Mitochondrial Intermembrane Space*, ed. V. Weissig and M. Edeas, Springer New York, New York, NY, 2015, pp. 285–305.
- S. A. Pshenichnyuk and A. S. Komolov, *J. Phys. Chem. Lett.*, 2015, **6**, 1104–1110.
- S. A. Pshenichnyuk, A. Modelli, E. F. Lazneva and A. S. Komolov, *J. Phys. Chem. A*, 2016, **120**, 2667–2676.
- S. A. Pshenichnyuk, R. G. Rakhmeyer, N. L. Asfandiarov, A. S. Komolov, A. Modelli and D. Jones, *J. Phys. Chem. Lett.*, 2018, **9**, 2320–2325.
- S. A. Pshenichnyuk, A. Modelli and A. S. Komolov, *Int. Rev. Phys. Chem.*, 2018, **37**, 125–170.
- S. A. Pshenichnyuk and A. Modelli, in *Electron Attachment to Isolated Molecules as a Probe to Understand Mitochondrial Reductive Processes*, ed. V. Weissig and M. Edeas, Springer US, New York, NY, 2021, pp. 101–124.
- R. Meißner, J. Kočíšek, L. Feketeová, J. Fedor, M. Fárník, P. Limão-Vieira, E. Illenberger and S. Denifl, *Nat. Commun.*, 2019, **10**, 2388.
- C. W. Fong, Toxicology of platinum anticancer drugs: oxidative stress and antioxidant effect of stable free radical Pt-nitroxides, Eigenenergy, Adelaide, Australia research report, 2019.
- H. M. Yasir and F. H. Hanoon, IOP Conference Series: Materials Science and Engineering, 2020, vol. 928, p. 072066.
- R. Schürmann, S. Vogel, K. Ebel and I. Bald, *Chem. – Eur. J.*, 2018, **24**, 10271–10279.
- Y. Dong, Y. Wang, P. Zhuang, X. Fu, Y. Zheng and L. Sanche, *J. Phys. Chem. B*, 2020, **124**, 3315–3325.
- Advances In Atomic, Molecular, and Optical Physics*, ed. E. Arimondo, C. C. Lin and S. F. Yelin, Academic Press, 2017, vol. 66, pp. 545–657.
- J. D. Gorfinkiel and S. Ptasinska, *J. Phys. B: At., Mol. Opt. Phys.*, 2017, **50**, 182001.
- S. M. Pimblott and J. A. LaVerne, *Radiat. Phys. Chem.*, 2007, **76**, 1244–1247.
- E. Alizadeh and L. Sanche, *Chem. Rev.*, 2012, **112**, 5578–5602.
- C. D. Willey, E. S.-H. Yang and J. A. Bonner, in *Clinical Radiation Oncology*, ed. L. L. Gunderson and J. E. Tepper, Elsevier, Philadelphia, 4th edn, 2016, pp. 63–79.e4.
- P. Wardman, *Clin. Oncol.*, 2007, **19**, 397–417.
- L. Chomicz, M. Zdrowowicz, F. Kasprzykowski, J. Rak, A. Buonaugurio, Y. Wang and K. H. Bowen, *J. Phys. Chem. Lett.*, 2013, **4**, 2853–2857.
- J. Kopyra, C. Koenig-Lehmann, I. Bald and E. Illenberger, *Angew. Chem., Int. Ed.*, 2009, **48**, 7904–7907.
- J. Rak, L. Chomicz, J. Wiczak, K. Westphal, M. Zdrowowicz, P. Wityk, M. Żyndul, S. Makurat and Ł. Golon, *J. Phys. Chem. B*, 2015, **119**, 8227–8238.
- C. R. Wang, J. Nguyen and Q. B. Lu, *J. Am. Chem. Soc.*, 2009, **131**, 11320–11322.
- J. Poštulka, P. Slaviček, J. Fedor, M. Fárník and J. Kočíšek, *J. Phys. Chem. B*, 2017, **121**, 8965–8974.
- M. Rezaee, D. J. Hunting and L. Sanche, *Int. J. Radiat. Oncol., Biol., Phys.*, 2013, **87**, 847–853.
- D. Reimnitz, M. Davidková, O. Mestek, J. Pinkas and J. Kočíšek, *Radiat. Phys. Chem.*, 2017, **141**, 229–234.
- Y. Dong, L. Zhou, Q. Tian, Y. Zheng and L. Sanche, *J. Phys. Chem. C*, 2017, **121**, 17505–17513.
- C. Wagner and H.-A. Wagenknecht, *Chem. – Eur. J.*, 2005, **11**, 1871–1876.
- F. Xiao, X. Luo, X. Fu and Y. Zheng, *J. Phys. Chem. B*, 2013, **117**, 4893–4900.

- 29 J. Rackwitz, M. L. Ranković, A. R. Milosavljević and I. Bald, *Eur. Phys. J. D*, 2017, **71**, 32.
- 30 J. Rackwitz, J. Kopyra, I. Dabkowska, K. Ebel, M. L. Ranković, A. R. Milosavljević and I. Bald, *Angew. Chem., Int. Ed.*, 2016, **55**, 10248–10252.
- 31 L. Chomicz, M. Zdrowowicz, F. Kasprzykowski, J. Rak, A. Buonaugurio, Y. Wang and K. H. Bowen, *J. Phys. Chem. Lett.*, 2013, **4**, 2853–2857.
- 32 M. Zdrowowicz, L. Chomicz, M. Żyndul, P. Wityk, J. Rak, T. J. Wiegand, C. G. Hanson, A. Adhikary and M. D. Sevilla, *Phys. Chem. Chem. Phys.*, 2015, **17**, 16907–16916.
- 33 J. Ameixa, E. Arthur-Baidoo, R. MeiÅŸner, S. Makurat, W. Kozak, K. Butowska, F. Ferreira da Silva, J. Rak and S. Denifl, *J. Chem. Phys.*, 2018, **149**, 164307.
- 34 R. MeiÅŸner, S. Makurat, W. Kozak, P. Limão-Vieira, J. Rak and S. Denifl, *J. Phys. Chem. B*, 2019, **123**, 1274–1282.
- 35 P. Spisz, M. Zdrowowicz, W. Kozak, L. Chomicz-Mańka, K. Falkiewicz, S. Makurat, A. Sikorski, D. Wyrzykowski, J. Rak, E. Arthur-Baidoo, P. Ziegler, M. S. Rodrigues Costa and S. Denifl, *J. Phys. Chem. B*, 2020, **124**, 5600–5613.
- 36 T. F. M. Luxford, S. A. Pshenichnyuk, N. L. Asfandiarov, T. Perečko, M. Falk and J. Kočišek, *Int. J. Mol. Sci.*, 2020, **21**, 8173.
- 37 S. Pushpakom, F. Iorio, P. A. Evers, K. J. Escott, S. Hopper, A. Wells, A. Doig, T. Williams, J. Latimer, C. McNamee, A. Norris, P. Sanseau, D. Cavalla and M. Pirmohamed, *Nat. Rev. Drug Discovery*, 2019, **18**, 41–58.
- 38 S. H. Kim, J. H. Kim, A. Kolozsvary, S. L. Brown and S. O. Freytag, *J. Neuro-Oncol.*, 1997, **33**, 189–194.
- 39 L. Sleire, H. E. Førde, I. A. Netland, L. Leiss, B. S. Skeie and P. Øyvind Enger, *Pharmacol. Res.*, 2017, **124**, 74–91.
- 40 X. Zhang, F. Wang, C. Zhang, S. Wu, X. Zheng, T. Gong, R. Ding, K. Chen and D. Bai, *Inorg. Chem. Commun.*, 2018, **94**, 92–97.
- 41 Z. Zhang, L. Zhou, N. Xie, E. C. Nice, T. Zhang, Y. Cui and C. Huang, *Signal Transduction Targeted Ther.*, 2020, **5**, 113.
- 42 D. Bai, Y. Tian, K. Chen, X. Zhang, F. Wang, Y. Cheng, X. Zheng, K. Xiao and X. Dong, *Dyes Pigm.*, 2020, **182**, 108635.
- 43 S. Huq, J. Kedda, T. Zhao, R. Serra, A. Ding, M. Morales, J. Ehresman, H. Brem, G. L. Gallia, D. M. Sciubba and B. Tyler, *Neurosurgery*, 2020, **67**, 309.
- 44 M. Van Herp, H. Declerck and T. Decroo, *Lancet*, 2015, **385**, 2350.
- 45 K. Rosenke, H. Feldmann, J. Westover, P. W. Hanley, C. Martellaro, F. Feldmann, G. Saturday, J. Lovaglio, D. Scott, Y. Furuta, T. Komeno, B. Gowen and D. Safronetz, *Emerging Infectious Disease J.*, 2018, **24**, 1696.
- 46 Z. F. Udawadia, P. Singh, H. Barkate, S. Patil, S. Rangwala, A. Pendse, J. Kadam, W. Wu, C. F. Caracta and M. Tandon, *Int. J. Infect. Dis.*, 2021, **103**, 62–71.
- 47 K. Shiraki and T. Daikoku, *Pharmacol. Ther.*, 2020, **209**, 107512.
- 48 Y. Furuta, K. Takahashi, Y. Fukuda, M. Kuno, T. Kamiyama, K. Kozaki, N. Nomura, H. Egawa, S. Minami, Y. Watanabe, H. Narita and K. Shiraki, *Antimicrob. Agents Chemother.*, 2002, **46**, 977–981.
- 49 Y.-X. Du and X.-P. Chen, *Clin. Pharm. Ther.*, 2020, **108**, 242–247.
- 50 M. G. Ison and M. H. Scheetz, *EBioMedicine*, 2021, **63**, 103204.
- 51 J. Langer, M. Zawadzki, M. Fárník, J. Pinkas, J. Fedor and J. Kočišek, *Eur. Phys. J. D*, 2018, **72**, 112.
- 52 M. Fárník and J. Lengyel, *Mass Spectrom. Rev.*, 2018, **37**, 630–651.
- 53 M. Stepanović, Y. Pariat and M. Allan, *J. Chem. Phys.*, 1999, **110**, 11376–11382.
- 54 A. Stamatovic and G. J. Schulz, *Rev. Sci. Instrum.*, 1970, **41**, 423–427.
- 55 L. G. Christophorou and J. K. Olthoff, *J. Phys. Chem. Ref. Data*, 2000, **29**, 267–330.
- 56 M. Zawadzki, T. F. M. Luxford and J. Kočišek, *J. Phys. Chem. A*, 2020, **124**, 9427–9435.
- 57 R. Dressler and M. Allan, *Chem. Phys.*, 1985, **92**, 449–455.
- 58 J. Kočišek, K. Grygoryeva, J. Lengyel, M. Fárník and J. Fedor, *Eur. Phys. J. D*, 2016, **70**, 98.
- 59 J. Kočišek, J. Lengyel and M. Fárník, *J. Chem. Phys.*, 2013, **138**, 124306.
- 60 J. Kočišek, A. Pysanenko, M. Fárník and J. Fedor, *J. Phys. Chem. Lett.*, 2016, **7**, 3401–3405.
- 61 L. A. Curtiss, K. Raghavachari and J. A. Pople, *J. Chem. Phys.*, 1993, **98**, 1293–1298.
- 62 A. D. Becke, *J. Chem. Phys.*, 1993, **98**, 5648–5652.
- 63 Y. Zhao and D. G. Truhlar, *Theor. Chem. Acc.*, 2008, **120**, 215–241.
- 64 K. Aflatooni, G. A. Gallup and P. D. Burrow, *J. Phys. Chem. A*, 1998, **102**, 6205–6207.
- 65 M. J. Frisch, G. W. Trucks, H. B. Schlegel, G. E. Scuseria, M. A. Robb, J. R. Cheeseman, G. Scalmani, V. Barone, G. A. Petersson, H. Nakatsuji, X. Li, M. Caricato, A. V. Marenich, J. Bloino, B. G. Janesko, R. Gomperts, B. Mennucci, H. P. Hratchian, J. V. Ortiz, A. F. Izmaylov, J. L. Sonnenberg, D. Williams-Young, F. Ding, F. Lipparini, F. Egidi, J. Goings, B. Peng, A. Petrone, T. Henderson, D. Ranasinghe, V. G. Zakrzewski, J. Gao, N. Rega, G. Zheng, W. Liang, M. Hada, M. Ehara, K. Toyota, R. Fukuda, J. Hasegawa, M. Ishida, T. Nakajima, Y. Honda, O. Kitao, H. Nakai, T. Vreven, K. Throssell, J. A. Montgomery, Jr., J. E. Peralta, F. Ogliaro, M. J. Bearpark, J. J. Heyd, E. N. Brothers, K. N. Kudin, V. N. Staroverov, T. A. Keith, R. Kobayashi, J. Normand, K. Raghavachari, A. P. Rendell, J. C. Burant, S. S. Iyengar, J. Tomasi, M. Cossi, J. M. Millam, M. Klene, C. Adamo, R. Cammi, J. W. Ochterski, R. L. Martin, K. Morokuma, O. Farkas, J. B. Foresman and D. J. Fox, *Gaussian ~ 16 Revision C.01*, Gaussian Inc., Wallingford CT, 2016.
- 66 G. Zhurko, *Chemcraft – Graphical Program for Visualization of Quantum Chemistry Computations*, available online: <https://chemcraftprog.com>.
- 67 L. Antonov, *Theor. Chem. Acc.*, 2020, **139**, 145.
- 68 J. Simons, *Annu. Rev. Phys. Chem.*, 2011, **62**, 107–128.
- 69 H. Hao, J. Shee, S. Upadhyay, C. Ataca, K. D. Jordan and B. M. Rubenstein, *J. Phys. Chem. Lett.*, 2018, **9**, 6185–6190.

- 70 L. Sanche and G. J. Schulz, *Phys. Rev. A*, 1972, **5**, 1672–1683.
- 71 D. Spence, *J. Chem. Phys.*, 1977, **66**, 669–674.
- 72 M. Zawadzki, M. Ranković, J. Kočišek and J. Fedor, *Phys. Chem. Chem. Phys.*, 2018, **20**, 6838–6844.
- 73 V. S. Prabhudesai, A. H. Kelkar, D. Nandi and E. Krishnakumar, *Phys. Rev. Lett.*, 2005, **95**, 143202.
- 74 C. Fridh, L. Åsbrink, B. Jonsson and E. Lindholm, *Int. J. Mass Spectrom. Ion Phys.*, 1972, **8**, 101–118.
- 75 M. V. Muftakhov and A. I. Fokin, *Rapid Commun. Mass Spectrom.*, 1997, **11**, 1923–1925.
- 76 J. Gingell, N. Mason, H. Zhao, I. Walker and M. Siggel, *Chem. Phys.*, 1997, **220**, 191–205.
- 77 Z. Li, M. Ryszka, M. M. Dawley, I. Carmichael, K. B. Bravaya and S. Ptasińska, *Phys. Rev. Lett.*, 2019, **122**, 073002.
- 78 J. Fedor, *Phys. Rev. Lett.*, 2020, **124**, 199301.
- 79 R. Abouaf and H. Dunet, *Eur. Phys. J. D*, 2005, **35**, 405–410.
- 80 P. D. Burrow, G. A. Gallup, A. M. Scheer, S. Denifl, S. Ptasińska, T. Märk and P. Scheier, *J. Chem. Phys.*, 2006, **124**, 124310.
- 81 M. Allan, M. Lacko, P. Papp, Š. Matejčík, M. Zlatar, I. I. Fabrikant, J. Kočišek and J. Fedor, *Phys. Chem. Chem. Phys.*, 2018, **20**, 11692–11701.
- 82 I. Nenner and G. J. Schulz, *J. Chem. Phys.*, 1975, **62**, 1747–1758.
- 83 C. Koenig-Lehmann, J. Kopyra, I. Dabkowska, J. Kočišek and E. Illenberger, *Phys. Chem. Chem. Phys.*, 2008, **10**, 6954–6961.
- 84 T. Hamann, A. Edtbauer, F. Ferreira da Silva, S. Denifl, P. Scheier and P. Swiderek, *Phys. Chem. Chem. Phys.*, 2011, **13**, 12305–12313.
- 85 A. Keller, J. Kopyra, K. V. Gothelf and I. Bald, *New J. Phys.*, 2013, **15**, 083045.
- 86 F. Ferreira da Silva, C. Matias, D. Almeida, G. García, O. Ingólfsson, H. D. Flosadóttir, B. Ómarsson, S. Ptasińska, B. Puschnigg, P. Scheier, P. Limão-Vieira and S. Denifl, *J. Am. Soc. Mass Spectrom.*, 2013, **24**, 1787–1797.
- 87 M. M. Dawley and S. Ptasińska, *Int. J. Mass Spectrom.*, 2014, **365–366**, 143–151.
- 88 M. M. Dawley, K. Tanzer, I. Carmichael, S. Denifl and S. Ptasińska, *J. Chem. Phys.*, 2015, **142**, 215101.
- 89 M. Muftakhov, P. Shchukin and R. Khatymov, *Radiat. Phys. Chem.*, 2021, **184**, 109464.
- 90 M. V. Muftakhov and P. V. Shchukin, *Rapid Commun. Mass Spectrom.*, 2019, **33**, 482–490.
- 91 M. M. Dawley, C. Pirim and T. M. Orlando, *J. Phys. Chem. A*, 2014, **118**, 1228–1236.
- 92 H. Abdoul-Carime, P. Cloutier and L. Sanche, *Radiat. Res.*, 2001, **155**, 625–633.
- 93 S. E. Bradforth, E. H. Kim, D. W. Arnold and D. M. Neumark, *J. Chem. Phys.*, 1993, **98**, 800–810.
- 94 N. L. Asfandiarov, S. A. Pshenichnyuk, R. G. Rakhmeyer, R. F. Tuktarov, N. L. Zaitsev, A. S. Vorobev, J. Kočišek, J. Fedor and A. Modelli, *J. Chem. Phys.*, 2019, **150**, 114304.
- 95 N. L. Asfandiarov, M. V. Muftakhov, S. A. Pshenichnyuk, P. Papp, M. Danko, M. Lacko, J. Blaško, Š. Matejčík and A. Modelli, *J. Chem. Phys.*, 2017, **147**, 234302.
- 96 H. Pauly, *Atomic and Molecular Beam Methods*, vol. 1, 1998.
- 97 J. Lengyel, A. Pysanenko, V. Poterya, J. Kočišek and M. Fárník, *Chem. Phys. Lett.*, 2014, **612**, 256–261.
- 98 R. Schürmann, T. F. M. Luxford, I. S. Vinklárek, J. Kočišek, M. Zawadzki and I. Bald, *J. Chem. Phys.*, 2020, **153**, 104303.

3.

Dissociative Electron Attachment Dynamics
of a Promising Cancer Drug Indicates Its
Radiosensitizing Potential

Dissociative Electron Attachment Dynamics of a Promising Cancer Drug Indicates Its Radiosensitizing Potential

Farhad Izadi,^[a,b] Thomas F.M. Luxford,^[c] Barbora Sedmidubská,^[c,d] Eugene Arthur-Baidoo,^[a,b] Jaroslav Kočíšek^[c], Milan Ončák^{*[a]}, Stephan Denifl^{*[a,b]}

[a] Farhad Izadi, Eugene Arthur-Baidoo, Prof. Dr. Milan Ončák *, Prof. Dr. Stephan Denifl *
Institut für Ionenphysik und Angewandte Physik, Universität Innsbruck, Technikerstrasse 25, A-6020 Innsbruck, Austria
farhad.izadi@gmail.com; eugene.arthurbaidoo@gmail.com; Milan.Oncak@uibk.ac.at; Stephan.Denifl@uibk.ac.at

[b] Farhad Izadi, Eugene Arthur-Baidoo, Prof. Dr. Stephan Denifl
Center for Biomolecular Sciences Innsbruck, Universität Innsbruck, Technikerstrasse 25, A-6020 Innsbruck, Austria

[c] Dr. Thomas F.M. Luxford, Barbora Sedmidubská, Dr. Jaroslav Kočíšek
J. Heyrovský Institute of Physical Chemistry of the Czech Academy of Sciences, v.v.i., Dolejškova 3, 18223 Prague, Czech Republic
thomas.luxford@gmail.com; barbora.sedmidubska@jh-inst.cas.cz; jaroslav.kocisek@jh-inst.cas.cz

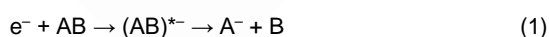
[d] Barbora Sedmidubská
Department of Nuclear Chemistry, Faculty of Nuclear Sciences and Physical Engineering, Czech Technical University in Prague, Břehová 78/7, 115 19 Prague, Czech Republic

Supporting information for this article is given via a link at the end of the document.

Abstract: 2-Bromo-1-(3,3-dinitroazetidin-1-yl)ethan-1-one (RRx-001) is a hypoxic cell chemotherapeutics with already demonstrated synergism in combined chemo-radiation therapy. The interaction of the compound with secondary low-energy electrons formed in large amounts during the physico-chemical phase of the irradiation may lead to these synergistic effects. The present study focuses on the first step of RRx-001 interaction with low-energy electrons in which a transient anion is formed and fragmented. Combination of two experiments allows us to disentangle the decay of the RRx-001 anion on different timescales. Sole presence of the electron initiates rapid dissociation of NO₂ and HNO₂ neutrals while NO₂⁻ and Br⁻ anions are produced both directly and via intermediate complexes. Based on our quantum chemical calculations, we propose that bidirectional state switching between π*(NO₂) and σ*(C–Br) states explains the experimental spectra. The fast dynamics monitored will impact the condensed phase chemistry of the anion as well.

Introduction

Collisions of free low-energy electrons with molecules are of fundamental importance for many processes in nature^[1] as well as in technical applications.^[2] Below typical electron kinetic energies of about 15 eV, dissociative electron attachment (DEA) is a significant process,^[3] which can be written in the simplest scheme for a molecule AB,



Here (AB)^{*-} represents the temporary negative ion (TNI), also called resonance, which is initially formed by the attachment of an electron matching the energy of the TNI state.^[4] This initial transition occurs on femtosecond timescales. The TNI may decay in A⁻ and B which stand for the formed fragment anion and the corresponding neutral species, respectively. This dissociation process competes with spontaneous emission of the excess

electron (autodetachment) as well as intra-molecular vibrational redistribution (IVR) of the energy deposited by excess electron.^[5] IVR, if available, may lead to stabilization of the TNI towards longer timescales.

Anions decaying on this timescale (metastable anions) are particularly interesting for mass spectrometry since the detection window of anions opens here.^{[6][7]} On the other hand, this fact means that it is very challenging to study the dynamics of TNI formation and DEA on earlier timescales. Pulsed radiolysis coupled with transient absorption spectroscopy has been a successfully applied experimental technique to probe the formation of anions and their decay in bulk solution on fast time scales.^[8,9] In terms of experiments in the gas phase, pump-probe photoelectron spectroscopy of anions was used to gain insight into the formation and decay of TNIs.^[10] To mimic the initial electron attachment in such studies, electron transfer by photoexcitation of anionic iodide in a cluster was exploited.^[11] From a theoretical point of view, the coupling of resonant states in anionic molecular systems in the gas phase raised strong interest.^[12] Such coupling schemes may also enable efficient dissociation of the formed TNI.^[13,14]

A potential candidate for efficient DEA is 2-bromo-1-(3,3-dinitroazetidin-1-yl)ethan-1-one (C₅H₆BrN₃O₅, RRx-001, here further denoted as RRx). The molecular structure of the compound, which includes an acyl-bromide and a geminal dinitroazetidine group, is shown in Figure 1. Previous radiobiological studies suggested that RRx could be a promising cancer therapeutic as a stand-alone drug as well as hypoxic tumor cell radiosensitizer.^[15,16] This energetic heterocyclic dinitroazetidine compound was derived from 1,3,3-trinitroazetidine, which found initial application as a fuel in aerospace.^[16] So far, this compound has been studied up to phase III clinical trials for the treatment of multiple solid tumors as well as a supportive care drug.^[17] Besides its potential for radiotheranostics, where it is exposed also to low-energy secondary electrons formed during irradiation of biological matter,^[18] RRx is a highly interesting compound from the chemical

perspective. The two NO_2 groups and a bromine atom (Figure 1) can compete for the incoming electron by their high electron affinities of 2.27 eV^[19] and 3.36 eV^[20], respectively (experimentally determined values).

In this study, we investigated the attachment of a free electron to RRx in the gas phase. Using experimental electron attachment spectroscopy combined with mass spectrometry and computational modeling employing Gaussian^[21] and Molpro^[22] software packages for single and multi-reference calculations, respectively, we follow here this competition on the fast timescale. In addition, we also explore the dissociation dynamics of RRx on longer timescales up to a few hundred microseconds and demonstrate that the molecule effectively decomposes into reactive anionic and neutral species.

Results and Discussion

The negative ion mass spectra of RRx measured with two different experimental setups having different detection times are shown in Figure 1. The spectra show the resulting intensities of the different anions formed as a function of the m/z . The spectrum shown in Figure 1a was measured with the Wippi apparatus (quadrupole mass spectrometer) having a considerably longer detection time of $t_{\text{det}} \sim 300 \mu\text{s}$ compared to the CLUB apparatus employing a time-of-flight (TOF) mass spectrometer. For the latter setup, the detection time is $\sim 10 \mu\text{s}$. The corresponding TOF spectrum is shown in Figure 1b. Since electron attachment is a resonance process, the intensities in the plots were obtained by integrating raw spectra at different electron energies. Also at a few microsecond detection times, no molecular anion with the expected main isotope peaks at m/z 267 and 269 is observed. However, comparing with the spectrum at longer timescales in Figure 1a, the ratio between lower- and higher-mass fragment anions is substantially changed here: $(\text{RRx}-\text{NO}_2)^-$ and $(\text{RRx}-\text{HNO}_2)^-$ dominate in the spectrum, while Br^- and NO_2^- are less intense. The combined view of the Wippi and CLUB data indicates that the dissociation dynamics is not yet completed on the early microsecond time scale. In detail, the heavier anions $(\text{RRx}-\text{NO}_2)^-$ and $(\text{RRx}-\text{HNO}_2)^-$ may be metastable and decay into Br^- and NO_2^- fragments. We can also observe within these two-step dissociation processes that $(\text{RRx}-\text{HNO}_2)^-$ decays faster than $(\text{RRx}-\text{NO}_2)^-$ since the abundance at m/z 220 and 222 is reduced more in comparison to m/z 221 and 223 at longer times (see inset in Figure 1b). We also note that Br^- is produced in much higher amounts than NO_2^- .

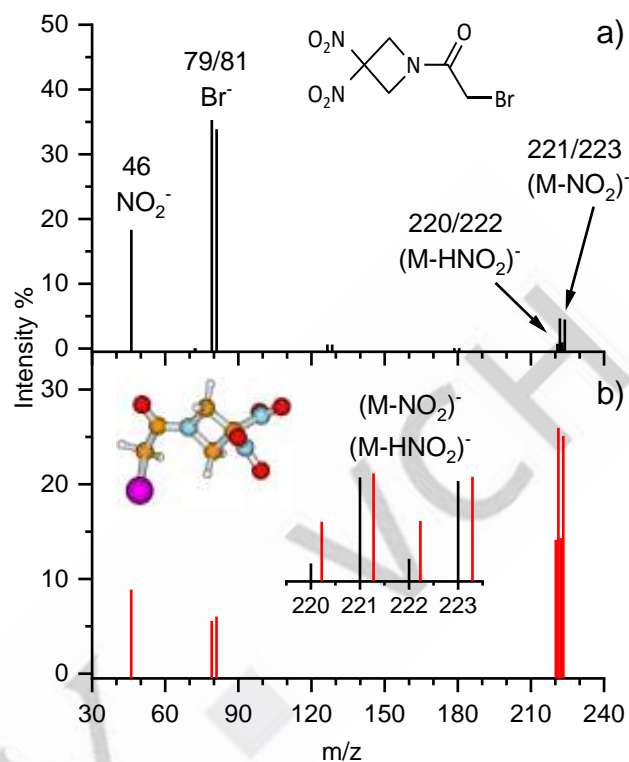


Figure 1. DEA mass spectra of isolated RRx (denoted as M in the two panels) after electron attachment from a) Wippi experiment, $t_{\text{det}} \sim 300 \mu\text{s}$ and b) CLUB experiment, $t_{\text{det}} \sim 10 \mu\text{s}$. Relative intensities were obtained by integrating raw mass spectra for different electron energies from -0.9 eV . The inset shows relative change of intensities for $(\text{RRx}-\text{NO}_2)^-$ and $(\text{RRx}-\text{HNO}_2)^-$ fragment anions by comparing them scaled to the same maximum in the zoomed region. Panel a) shows the skeletal formula of the RRx molecule and in panel b) the structure obtained at the B3LYP/aug-cc-pVTZ level is included. Color code: hydrogen – grey, carbon – brown, nitrogen – blue, oxygen – red, bromine – violet.

The dissociation products observed in the mass spectra can be interpreted based on the calculated energetics shown in the reaction scheme in Figure 2. If the anion follows the $\sigma^*(\text{C}-\text{Br})$ pathway, Br^- most probably leaves the molecule upon pre-dissociation. Within the $\pi^*(\text{NO}_2)$ pathway, there are several reaction channels possible. The NO_2 moiety might leave the ion directly with the reaction energy of -0.66 eV , forming an ion at m/z 221 that might further dissociate to produce NO_2^- in an almost

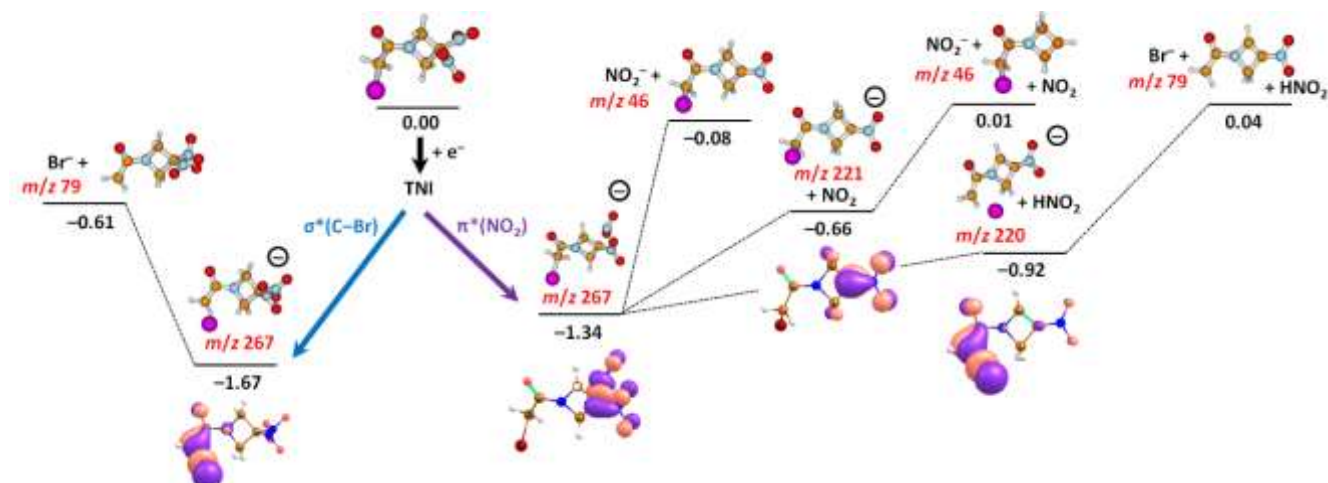


Figure 2. Suggested main reaction pathways upon electron attachment to RRx-001 calculated at the CCSD/aug-cc-pVDZ//B3LYP/aug-cc-pVDZ level, energies are given in eV with respect to the minimum of the neutral molecule. Singly occupied orbitals and the highest-occupied orbital of $(\text{RRx-NO}_2)^-$ are shown as calculated at the B3LYP level. See the SI (Figure S1) for higher-lying dissociation channels and the $(\text{RRx})^-$ structure formed upon electron attachment without pre-dissociation.

thermoneutral reaction (0.01 eV). Alternatively, the NO_2 moiety might roam in the vicinity of the $(\text{RRx-NO}_2)^-$ fragment, accepting a hydrogen atom from a CH_2 group to form a neutral HNO_2 molecule that leaves the ion in an exothermic reaction (-0.92 eV). The resulting ion at m/z 220 might dissociate further to form Br^- , again in an almost thermoneutral reaction (0.04 eV). The singly occupied molecular orbital (SOMO) in the $(\text{RRx-HNO}_2)^-$ anion at m/z 220 indicates that a non-covalent type of anionic complex is formed, with a C-Br distance of 2.80 Å and charge mainly localized on Br (-0.59 e). Such an exotic complex was computationally predicted first time for intact bromo-substituted nucleobase anions in the gas phase and the solution.^[23] While for these compounds the DEA reaction leading to Br^- release was predicted to be substantially exothermic (> 2 eV) in solution, the overall reaction energy for the isolated molecule in the gas phase was about +0.4 eV. Later mass spectrometric studies with 8-bromoadenine confirmed the existence of such molecular anion complex.^[24] In the present study, non-covalent type of anionic complex can be detected on mass spectrometric timescales, but it can dissociate via Br^- release with the reaction energy close to 0 eV (see Figure 2). A similar complex is also formed in the case of for C-Br pre-dissociation at -1.67 eV. There, the C-Br bond is 3.02 Å long. It is worth noting that recent studies demonstrate that these non-covalent anions, if present, determine the TNI dissociation dynamics in solution.^[25] The $(\text{RRx-NO}_2)^-$ complex has a more compact structure with covalent bonds to both NO_2 and Br. For this intermediate, the energetics and charge localization on NO_2 (-0.48 eV) set NO_2^- release as the primary dissociation channel.

Figure 2 indicates that the lowest-lying DEA pathways considered in the calculations would be exothermic or nearly exothermic for all four abundant fragment anions found in the experimental spectra. Along the pathways, no significant barriers are present, which would hinder the dissociation by electrons having an initial kinetic energy of nearly zero eV. This computational prediction is supported by the single negative ion mass spectra at various electron energies which is shown in the Supporting Information

(Figure S2). The ion intensities found in the negative ion mass spectrum at zero eV clearly point out that all discussed fragments are formed at this electron energy at their utmost intensity. At the incident electron energy of zero eV, the excess energy of TNI is sufficient to induce the dissociation. For some pathways, also molecular rearrangement delivers additional energy for decisive bond cleavage. In this context, it should be also mentioned that in the Wippi experiment, the molecules sublimed in the oven are directly transferred to the interaction region with the electron beam, while in the CLUB experiment, the molecules are sublimed and co-expanded with He gas into the vacuum. In the latter case, they can undergo cooling of translational but also vibrational degrees of freedom which may extend the lifetime of the anion or leads to closing of the endothermic dissociation channels. These effects will influence the relative abundance of the product anions in the mass spectra.

The experimental and theoretical observations presented so far point out the strong competition of the electron affine NO_2 group and the bromine atom, competing for the negative excess charge. We also looked at this competition during the formation of the TNI and its early decay on fast timescales of femto- to picoseconds. Computational insight can be obtained from the semi-quantitative potential energy surface (PES) analysis shown in Figure 3b. RRx has high vertical and adiabatic electron affinities of 0.85 eV and 1.67 eV, respectively (at the CCSD/aug-cc-pVDZ//B3LYP/aug-cc-pVDZ level). Two lowest electronic states, allowing for electron attachment, correspond to an electron positioned in $\pi^*(\text{NO}_2)$ orbitals of both NO_2 groups, either in symmetric or antisymmetric combination as shown in Figure 3a. In the Franck-Condon (FC) region, they are almost degenerate at TD-CAM-B3LYP/aug-cc-pVTZ and MRCI(3,5)/6-31g* levels (difference of 0.14 and 0.04 eV, respectively), the EOM-CCSD/6-31g* predicts a larger gap of 0.51 eV, probably due to the single-reference treatment. At the MRCI level, the third valence electronic state lies about 1.4 eV above the $\pi^*(\text{NO}_2)$ states, with the odd electron occupying the

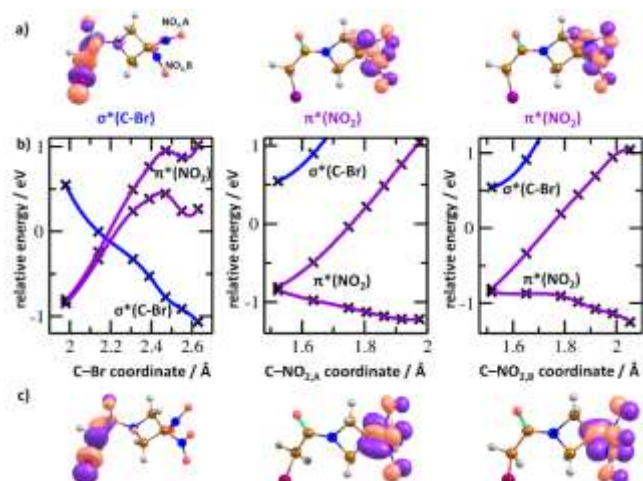


Figure 3. a) Orbitals occupied by the odd electron for three lowest-lying valence electronic states of the RRx anion as obtained at the TD-CAM-B3LYP/aug-cc-pVTZ level. Color code: hydrogen – grey, carbon – brown, nitrogen – blue, oxygen – red, bromine – violet. b) Interpolation curves in the RRx anion along C–Br and C–NO₂ coordinates for the lowest three electronic states of valence character between the structure of the neutral RRx-001 molecule and pre-dissociation transition states (as optimized at the B3LYP/aug-cc-pVDZ level). Crosses show points calculated at the MRCI(3,5)/6-31g* level, splines are added to guide the eye. The energy is given with respect to the ground state of the neutral molecule as obtained by setting the energy of the anion in the minimum of the neutral molecule to negative of the vertical electron affinity calculated at the CCSD/aug-cc-pVDZ level (0.85 eV). c) Orbitals occupied by the odd electron for the last points of the respective interpolations in b) at the CAM-B3LYP/aug-cc-pVTZ level.

$\sigma^*(\text{C-Br})$ orbital. Depending on the electronic state that is reached after the initial electron attachment step, pre-dissociation of either NO₂ or Br moieties takes place. For prolongation of the C–Br distance, the $\sigma^*(\text{C-Br})$ state is moving down in energy without any barrier, becoming the ground electronic state at the C–Br distance of about 2.2 Å; eventually, the charge of Br reaches –0.66 e. For dissociation along the C–NO₂ coordinate, we also obtained a barrierless pathway from the structure of the neutral molecule, keeping the $\pi^*(\text{NO}_2)$ character of the electronic ground state. When reaching a minimum of the pre-dissociated state, the charge on the loosely bound NO₂ moiety is –0.38 e. Both pathways can result in transient parent anion structures with NO₂ or Br moieties loosely bound to a polarized co-fragment, which further decay as shown in Figure 2.

The interpolation curves of PES present in Figure 3b also show conical intersections between π^* and σ^* states, which would allow for state switching during the fast dissociation. As shown for less complex systems without pronounced local minima on the PES surface, a coupling of π^* and σ^* states can result in complex transient anion dynamics.^[14] Using the Wippi apparatus, we measured the anion efficiency curves of the four major anions formed upon DEA to RRx, NO₂[–], Br[–], (RRx–HNO₂)[–] and (RRx–NO₂)[–]. The corresponding anion yields for the different fragments are presented in Figure 4. All fragment anions exhibit a peak near zero eV, as expected by the energetics of the dissociation

pathways shown in Figure 2. Scaling all four anion efficiency curves to the zero eV feature reveals a striking difference of the ion yields: The NO₂[–] and Br[–] ion yields show a pronounced tail of the first peak which is missing for (RRx–HNO₂)[–] and (RRx–NO₂)[–]. The anion efficiency curves of the latter two anions can be fitted by an (asymmetric) single peak, while the fits of the experimental NO₂[–] and Br[–] data identify a second resonance in the broad tail of the zero eV peak (all fits are shown in the SI, Figure S4). The second resonance leading to NO₂[–] and Br[–] is found at 0.52 and 0.56 eV, respectively. Since the corresponding thresholds of these resonance features are below the threshold of higher-lying dissociation channels (≥ 0.47 eV, see Figure S1), the reaction scheme shown in Figure 2 still applies. However, the difference to the zero eV peak is found in the fast TNI dynamics since we assign this yield to the initial electron attachment into the $\sigma^*(\text{C-Br})$ orbital (based on the interpolation curves shown in Figures 3b). While for predissociation of Br[–] the excess electron just needs to remain in this orbital, NO₂[–] formation requires state switching at the conical intersection. Regarding (RRx–HNO₂)[–] and (RRx–NO₂)[–], their anion efficiency curves suggest therefore that both anions just form by the initial occupation of the $\pi^*(\text{NO}_2)$ orbital without involvement of the $\sigma^*(\text{C-Br})$ orbital on the fast timescale. We also note that the resonance near 0.5 eV is about a factor 3 broader compared to the narrow contribution near zero eV. The width of the resonance may provide basic information about the temporary negative ion state involved. The longer life-time of π^* resonances compared to σ^* resonances is associated to a small width of the former.^[26] Thus, the contribution at about zero eV indicates involvement of a π^* state since it nearly reflects the energy distribution function of the electron beam. The narrow width and the high intensity of the zero eV contribution indicate an s-wave electron attachment process in which the incoming electron is captured with a cross-section within the $E^{-0.5}$ limit with E as the initial kinetic energy of the electron. The yield of the TNI formed near 0.5 eV is further reduced due to the possibility of autodetachment nearly till the conical intersection at the C–Br distance of about 2.2 Å. This explains the significant intensity difference for the two resonances observed in the anion efficiency curves.

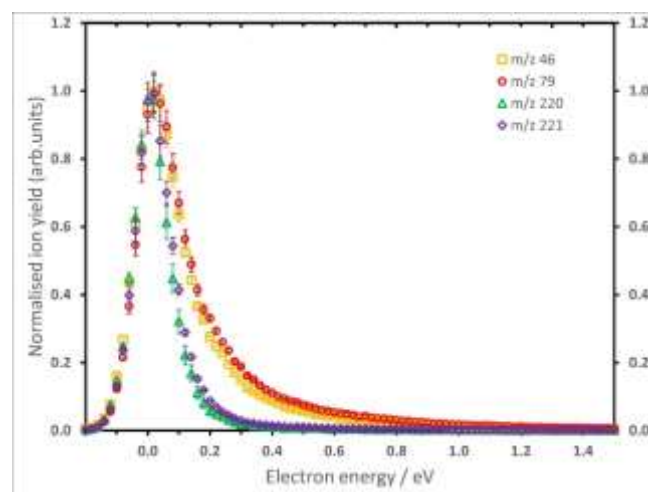


Figure 4. Anion efficiency curves of the fragment anions NO_2^- (m/z 46), Br^- (m/z 79), $(\text{RRx-HNO}_2)^-$ (m/z 220) and $(\text{RRx-NO}_2)^-$ (m/z 221) formed upon electron attachment to RRx. The respective ion yields were scaled at the zero eV resonance. The statistical error margins shown for each data point refer to the standard error of the mean from individual measurements.

Conclusion

The present electron attachment results for RRx indicate that the compound is highly susceptible to low-energy electrons. The Br^- represents the most abundant fragment anion just a few hundred microseconds after TNI formation. This observation disproves the hypothesis of a fast, simple dissociation process upon formation of the repulsive $\sigma^*(\text{C-Br})$ state since the dissociation takes unexpectedly long for an exothermic dissociation process. Instead, the present calculations point out the formation of a non-covalent type of anionic complex $\text{Br}^--(\text{RRx-HNO}_2)^-$, which is found in the mass spectrum with high abundance at earlier times. The analogous mechanism applies to the reaction channel leading to the formation of NO_2^- which represents, on late timescales, an independent competitive pathway to the release of Br^- . However, the feeding of the pathways on fast timescales occurs also upon a conical intersection of $\pi^*(\text{NO}_2)$ and $\sigma^*(\text{C-Br})$ states. Previously the σ^* predissociation of π^* resonance states was theoretically proposed to be an efficient DEA mechanism for various molecules.^[26–28] To mention a system of biological relevance, the formation of a single-strand break in (dry) DNA was proposed to be formed by the initial formation of a π^* resonance of the nucleobase with subsequent electron transfer into a C-O σ^* orbital of the phosphate group.^[29,30] Experimental data also suggested the general preference of the $\pi^* \rightarrow \sigma^*$ coupling scheme since the non-dissociative π^* resonances are characterized by longer lifetimes than σ^* resonances with respect to spontaneous electron emission.^[26] For anionic RRx, the conical intersection, which is energetically found below the autodetachment continuum, allows to experimentally observe the reversed $\sigma^* \rightarrow \pi^*$ coupling scheme as well. Its appearance is indicated in the form of the resonance at ~ 0.5 eV in the NO_2^- ion yield. We also note that the involved π^* state is of dissociative character here, unlike the molecular-non-dissociative π^* resonances reported for other anionic systems.^[26–28]

Radiobiological experiments indicated that RRx develops a high biological activity in cells. Experiments in the gas phase like the present one enable exploration of intermediate processes of radiation damage and to distinguish direct from indirect effects.^[31] A possible hypothesis may be that RRx may also become activated as a potential radiosensitizer by low-energy secondary electrons formed in irradiated cells. A previous electron attachment study with the radiosensitizer nimorazole demonstrated indeed such a possibility of activation mechanism.^[32] The present results for RRx indicate efficient release of nitrite, nitrogen dioxide, and nitrous acid, which can undergo a range of electron transfer, addition, and abstraction reactions,^[33] mainly resulting in a vasodilator effect^[34] or an increase of oxidative stress via enhanced OH formation.^[35] This would represent a novel mechanism for the oxygenation of hypoxic tumor cells in addition to the previously suggested

reduction of serum nitrite to nitric oxide by RRx-bound hemoglobin.^[36] Reoxygenation of hypoxic tumor cells would lead to a lowered resistance of these cells towards ionizing radiation.^[37] However, it should be noted that the dissociation processes monitored presently on the microsecond timescale may be quenched in a molecular environment by, e.g., fast intermolecular energy dissipation^[38] or stabilizing proton transfer.^[30] In such a case, the anionic system relaxes before dissociation occurs. On the other hand, this may not apply to fast processes like shown by previous solution phase studies of an excited nucleoside anion.^[9] Thus the initially populated states of the TNI studied here will be the same in solution and therefore the present results provide deeper fundamental insight into the initial steps in the radiation chemistry of this potential radiosensitizer, irrespective of the environment. We also point out the importance of studying the dynamics of formation and degradation of negative ions for other classes of molecules, like for example photocatalysts used for photoredox-mediated organic reactions and polymerizations.^[39]

Supporting Information

The supporting information presents the Experimental and Computational Methods, Supplementary Figures S1-S4, Supplementary Table S1, Cartesian coordinates of structures, and raw data. Authors have cited additional references within the Supporting Information.^[40]

Acknowledgements

This research was funded in part by the Austrian Science Fund (FWF) [Grant-DOIs 10.55776/P30332 and 10.55776/I5390]. For open access purposes, the author has applied a CC BY public copyright license to any author accepted manuscript version arising from this submission. The computational results presented have been achieved using the HPC infrastructure LEO of the University of Innsbruck. The authors acknowledge the support of the Ministry of Education, Youth, and Sports of the Czech Republic via project CZ.02.01.01/00/22_008/0004649 QUEENTECH co-funded by the European Union. J.K. acknowledges the support by the Czech Science Foundation, Project No. 21-26601X. F.I. was supported by COST Action CA20129 - Multiscale Irradiation and Chemistry Driven Processes and Related Technologies (MultiChem), supported by COST (European Cooperation in Science and Technology).

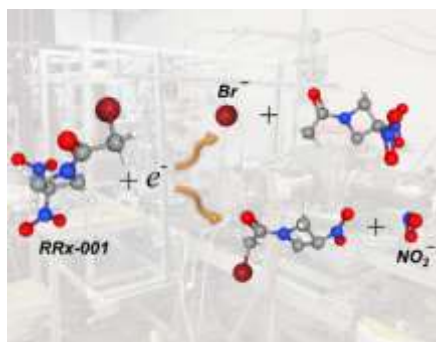
Keywords: radiosensitizers • gas phase reactions • low-energy electron • dissociative electron attachment • reaction mechanisms

- [1] a) E. Alizadeh, T. M. Orlando, L. Sanche, *Annual review of physical chemistry* **2015**, *66*, 379; b) C. R. Arumainayagam, R. T. Garrod, M. C. Boyer, A. K. Hay, S. T. Bao, J. S. Campbell, J. Wang, C. M. Nowak, M. R. Arumainayagam, P. J. Hodge, *Chemical Society reviews* **2019**, *48*, 2293.

- [2] M. Huth, F. Porrati, C. Schwalb, M. Winhold, R. Sachser, M. Dukic, J. Adams, G. Fantner, *Beilstein journal of nanotechnology* **2012**, *3*, 597.
- [3] a) F. Izadi, E. Arthur-Baidoo, L. T. Strover, L.-J. Yu, M. L. Coote, G. Moad, S. Denifl, *Angewandte Chemie (International ed. in English)* **2021**, *60*, 19128; b) I. I. Fabrikant, H. Hotop, *Phys. Rev. A* **2001**, *63*.
- [4] a) I. Baccarelli, I. Bald, F. A. Gianturco, E. Illenberger, J. Kopyra, *Physics Reports* **2011**, *508*, 1; b) S. Ptasinska, S. Denifl, P. Scheier, E. Illenberger, T. D. Märk, *Angewandte Chemie (International ed. in English)* **2005**, *44*, 6941.
- [5] J. Troe, T. M. Miller, A. A. Viggiano, *The Journal of chemical physics* **2007**, *127*, 244303.
- [6] a) F. F. Da Silva, C. Matias, D. Almeida, G. García, O. Ingólfsson, H. D. Flosadóttir, B. Ómarsson, S. Ptasinska, B. Puschnigg, P. Scheier et al., *Journal of the American Society for Mass Spectrometry* **2013**, *24*, 1787; b) H. D. Flosadóttir, S. Denifl, F. Zappa, N. Wendt, A. Mauracher, A. Bacher, H. Jónsson, T. D. Märk, P. Scheier, O. Ingólfsson, *Angewandte Chemie (International ed. in English)* **2007**, *46*, 8057.
- [7] N. L. Asfandiarov, R. V. Galeev, S. A. Pshenichnyuk, *The Journal of chemical physics* **2022**, *157*, 84304.
- [8] J. Ma, F. Wang, S. A. Denisov, A. Adhikary, M. Mostafavi, *Science advances* **2017**, *3*, e1701669.
- [9] J. Ma, A. Kumar, Y. Muroya, S. Yamashita, T. Sakurai, S. A. Denisov, M. D. Sevilla, A. Adhikary, S. Seki, M. Mostafavi, *Nature communications* **2019**, *10*, 102.
- [10] a) J. P. Rogers, C. S. Anstöter, J. R. R. Verlet, *Nature chemistry* **2018**, *10*, 341; b) M. A. Yandell, S. B. King, D. M. Neumark, *Journal of the American Chemical Society* **2013**, *135*, 2128.
- [11] L. Lehr, M. T. Zanni, C. Frischkorn, R. Weinkauff, D. M. Neumark, *Science (New York, N.Y.)* **1999**, *284*, 635.
- [12] a) S. Feuerbacher, T. Sommerfeld, L. S. Cederbaum, *The Journal of chemical physics* **2004**, *120*, 3201; b) K. Chatterjee, Z. Koczor-Benda, X. Feng, A. I. Krylov, T.-C. Jagau, *Journal of chemical theory and computation* **2023**, *19*, 5821.
- [13] J. A. Gyamfi, T.-C. Jagau, *The journal of physical chemistry letters* **2022**, *13*, 8477.
- [14] M. Zawadzki, M. Čížek, K. Houfek, R. Čurík, M. Ferus, S. Civiš, J. Kočišek, J. Fedor, *Physical review letters* **2018**, *121*, 143402.
- [15] a) S. Ning, M. Bednarski, B. Oronsky, J. Scicinski, G. Saul, S. J. Knox, *Cancer research* **2012**, *72*, 2600; b) B. Oronsky, J. Scicinski, S. Ning, D. Peehl, A. Oronsky, P. Cabrales, M. Bednarski, S. Knox, *Investigational new drugs* **2016**, *34*, 371.
- [16] B. Oronsky, X. Guo, X. Wang, P. Cabrales, D. Sher, L. Cannizzo, B. Wardle, N. Abrouk, M. Lybeck, S. Caroen et al., *Journal of medicinal chemistry* **2021**, *64*, 7261.
- [17] N. Jayabalan, B. Oronsky, P. Cabrales, T. Reid, S. Caroen, A. M. Johnson, N. A. Birch, J. D. O'Sullivan, R. Gordon, *Drugs* **2023**, *83*, 389.
- [18] a) L. Sanche, *Nature* **2009**, *461*, 358; b) S. M. Pimblott, J. A. LaVerne, *Radiation Physics and Chemistry* **2007**, *76*, 1244; c) R. Schürmann, S. Vogel, K. Ebel, I. Bald, *Chemistry (Weinheim an der Bergstrasse, Germany)* **2018**, *24*, 10271.
- [19] K. M. Ervin, J. Ho, W. C. Lineberger, *J. Phys. Chem.* **1988**, *92*, 5405.
- [20] C. Blondel, P. Cacciani, C. Delsart, R. Trainham, *Physical review. A, General physics* **1989**, *40*, 3698.
- [21] M. J. Frisch, G. W. Trucks, H. B. Schlegel, G. E. Scuseria, M. A. Robb, J. R. Cheeseman, G. Scalmani, V. Barone, G. A. Petersson, H. Nakatsuji, X. Li, M. Caricato, A. V. Marenich, J. Bloino, B. G. Janesko, R. Gomperts, B. Mennucci, H. P. Hratchian, J. V. Ortiz, A. F. Izmaylov, J. L. Sonnenberg, D. Williams-Young, F. Ding, F. Lipparini, F. Egidi, J. Goings, B. Peng, A. Petrone, T. Henderson, D. Ranasinghe, V. G. Zakrzewski, J. Gao, N. Rega, G. Zheng, W. Liang, M. Hada, M. Ehara, K. Toyota, R. Fukuda, J. Hasegawa, M. Ishida, T. Nakajima, Y. Honda, O. Kitao, H. Nakai, T. Vreven, K. Throssell, J. A. Montgomery, Jr., J. E. Peralta, F. Ogliaro, M. J. Bearpark, J. J. Heyd, E. N. Brothers, K. N. Kudin, V. N. Staroverov, T. A. Keith, R. Kobayashi, J. Normand, K. Raghavachari, A. P. Rendell, J. C. Burant, S. S. Iyengar, J. Tomasi, M. Cossi, J. M. Millam, M. Klene, C. Adamo, R. Cammi, J. W. Ochterski, R. L. Martin, K. Morokuma, O. Farkas, J. B. Foresman, and D. J. Fox, *Gaussian 16, Revision A.03*, Gaussian, Inc., Wallingford CT.

- [22] a) H.-J. Werner, P. J. Knowles, G. Knizia, F. R. Manby, M. Schütz, *WIREs Comput Mol Sci* **2012**, *2*, 242; b) H.-J. Werner, P. J. Knowles, G. Knizia, F. R. Manby, M. Schütz, P. Celani, W. Györffy, D. Kats, T. Korona, R. Lindh, A. Mitrushenkov, G. Rauhut, K. R. Shamasundar, T. B. Adler, R. D. Amos, A. Bernhardsson, A. Berning, D. L. Cooper, M. J. O. Deegan, A. J. Dobbyn, F. Eckert, E. Goll, C. Hampel, A. Hesselmann, G. Hetzer, T. Hrenar, G. Jansen, C. Köppl, Y. Liu, A. W. Lloyd, R. A. Mata, A. J. May, S. J. McNicholas, W. Meyer, M. E. Mura, A. Nicklass, D. P. O'Neill, P. Palmieri, D. Peng, K. Pflüger, R. Pitzer, M. Reiher, T. Shiozaki, H. Stoll, A. J. Stone, R. Tarroni, T. Thorsteinsson, M. Wang, *MOLPRO, version 2012.1, a package of ab initio programs. see <http://www.molpro.net>*.
- [23] L. Chomicz, J. Rak, P. Storoniak, *The journal of physical chemistry. B* **2012**, *116*, 5612.
- [24] R. Schürmann, K. Tanzer, I. Dąbkowska, S. Denifl, I. Bald, *The journal of physical chemistry. B* **2017**, *121*, 5730.
- [25] a) N. L. Asfandiarov, S. A. Pshenichnyuk, R. G. Rakhmeyer, R. F. Tuktarov, N. L. Zaitsev, A. S. Vorob'ev, J. Kočíšek, J. Fedor, A. Modelli, *The Journal of chemical physics* **2019**, *150*, 114304; b) L. Sala, B. Sedmidubská, I. Vinklár, M. Fárník, R. Schürmann, I. Bald, J. Med, P. Slavíček, J. Kočíšek, *Physical chemistry chemical physics : PCCP* **2021**, *23*, 18173.
- [26] A. M. Scheer, K. Aflatoon, G. A. Gallup, P. D. Burrow, *Physical review letters* **2004**, *92*, 68102.
- [27] F. Kossoski, M. Barbatti, *Chemical science* **2020**, *11*, 9827.
- [28] L. M. Cornetta, T. J. Martinez, M. T. d. N. Varela, *Physical chemistry chemical physics : PCCP* **2022**, *24*, 6845.
- [29] J. Simons, *Accounts of chemical research* **2006**, *39*, 772.
- [30] L. Chomicz-Mańka, A. Czaja, K. Falkiewicz, M. Zdrowowicz, K. Biernacki, S. Demkowicz, F. Izadi, E. Arthur-Baidoo, S. Denifl, Z. Zhu et al., *Journal of the American Chemical Society* **2023**, *145*, 9059.
- [31] F. Chevalier, T. Schlathöller, J.-C. Pouilly, *Chembiochem : a European journal of chemical biology* **2023**, *24*, e202300543.
- [32] R. Meißner, J. Kočíšek, L. Feketeová, J. Fedor, M. Fárník, P. Limão-Vieira, E. Illenberger, S. Denifl, *Nature communications* **2019**, *10*, 2388.
- [33] O. Augusto, M. G. Bonini, A. M. Amanso, E. Linares, C. C. X. Santos, S. L. de Menezes, *Free radical biology & medicine* **2002**, *32*, 841.
- [34] K. Cosby, K. S. Partovi, J. H. Crawford, R. P. Patel, C. D. Reiter, S. Martyr, B. K. Yang, M. A. Waclawiw, G. Zalos, X. Xu et al., *Nature medicine* **2003**, *9*, 1498.
- [35] J. Mack, J. R. Bolton, *Journal of Photochemistry and Photobiology A: Chemistry* **1999**, *128*, 1.
- [36] J. Sciacinski, B. Oronsky, S. Ning, S. Knox, D. Peehl, M. M. Kim, P. Langecker, G. Fanger, *Redox biology* **2015**, *6*, 1.
- [37] a) J. M. Brown, W. R. Wilson, *Nature reviews. Cancer* **2004**, *4*, 437; b) M. Zdrowowicz, L. Chomicz-Mańka, K. Butowska, P. Spisz, K. Falkiewicz, A. Czaja, J. Rak in *Practical Aspects of Computational Chemistry V* (Eds.: J. Leszczynski, M. K. Shukla), Springer International Publishing, Cham, **2022**, pp. 125–169.
- [38] C. G. Elles, F. F. Crim, *Annual review of physical chemistry* **2006**, *57*, 273.
- [39] Y. Kwon, J. Lee, Y. Noh, D. Kim, Y. Lee, C. Yu, J. C. Roldao, S. Feng, J. Gierschner, R. Wannemacher et al., *Nature communications* **2023**, *14*, 92.
- [40] a) M. Saqib, F. Izadi, L. U. Isierhienrhien, M. Ončák, S. Denifl, *Physical chemistry chemical physics : PCCP* **2023**, *25*, 13892; b) G. A. Gallup, K. Aflatoon, P. D. Burrow, *The Journal of chemical physics* **2003**, *118*, 2562; c) M. Fárník, J. Fedor, J. Kočíšek, J. Lengyel, E. Pluhařová, V. Poterya, A. Pysanenko, *Physical chemistry chemical physics : PCCP* **2021**, *23*, 3195; d) J. Kočíšek, K. Grygoryeva, J. Lengyel, M. Fárník, J. Fedor, *Eur. Phys. J. D* **2016**, *70*; e) R. L. Martin, *The Journal of chemical physics* **2003**, *118*, 4775; f) C. M. Breneman, K. B. Wiberg, *J Comput Chem* **1990**, *11*, 361.

Entry for the Table of Contents



Text for Table of Contents: 2-Bromo-1-(3,3-dinitroazetidin-1-yl)ethan-1-one (RRx-001) has been suggested as a potential radiosensitizer. Here we explored the decay of the molecule upon electron attachment. The main dissociation processes of the formed anion are characterized by loss of either a bromine atom or a NO_2 group, both competing for the excess electron. The fast chemistry observed may also indicate an alternative avenue for oxygenation of hypoxic tumor cells.

Abstract

In concomitant chemoradiotherapy (CCRT), there is an effort to increase its effectiveness and alleviate toxicity for healthy cells. It may be achieved via synergism and targeted drug delivery (TGD). TGD is the selective drug transport to sites of interest, protecting healthy tissue from chemotherapeutic toxicity. The synergism, the highest chemoradioterapeutic effect, results from complex interactions between both treatment modalities, as the interaction of the radiosensitizing chemo-drug with secondary low-energy electrons (LEEs) arising in irradiated tissue. In light of that, work focuses on the radiosensitization process to investigate the radiosensitizing potential and mechanisms of selected molecules based on interaction with LEE; there is an aim to obtain new information to design more effective radiosensitizers with lower toxicity. The theoretical part deals with existing radiosensitizers and their model compounds from the point of view of interaction with LEEs. The experimental part combines electron attachment experiments in the gas phase and *ab initio* calculations of electron affinities of studied molecules, pulse radiolysis experiments in solution, and microtron irradiation with NMR spectroscopic evaluation. Based on the study of interaction with (secondary) LEEs, the radiosensitizing potential was confirmed for the antiviral agent favipiravir; significant interaction was proven for radiosensitizing chemotherapeutic RRx-001 as well, so as a strong interaction of solvated electrons with fullerenols as a radiosensitizing carrier drug for TGM in CCRT.

Résumé

Dans la chimioradiothérapie concomitante utilisée pour le traitement du cancer, il y a des efforts pour augmenter son efficacité tout en atténuant les effets secondaires. Une augmentation des effets de la chimioradiothérapie est possible grâce au synergisme, l'effet maximal potentiel de la chimioradiothérapie, résultant de la somme des effets des deux traitements et de leurs interactions complexes. Dans ces interactions complexes, c'est l'interaction d'un agent radiosensibilisant avec des électrons de basse énergie (EBE) générés dans les tissus irradiés. Dans ce contexte, on parle de la radiosensibilisation des tissus vivants après irradiation par des rayonnements ionisants, en présence simultanée d'un radiosensibilisant au moment de l'irradiation. En revanche, les effets secondaires proviennent, entre autres, principalement de la toxicité pour les cellules saines. Une toxicité réduite pour les cellules saines peut être obtenue par l'utilisation de la délivrance ciblée de médicaments (DCM). La DCM permet un transport sélectif des médicaments vers des sites d'intérêt, protégeant ainsi les tissus sains des effets toxiques des agents chimiothérapeutiques. Dans ce contexte, cette thèse se concentre sur le processus de radiosensibilisation afin d'étudier le potentiel et les mécanismes radiosensibilisants des molécules sélectionnées, basés sur leur interaction avec les EBE. Nous examinons le potentiel de radiosensibilisation également en cas de molécules choisies pour la DCM. L'objectif de cette thèse est d'obtenir de nouvelles informations permettant de concevoir des radiosensibilisateurs plus efficaces et moins toxiques, pour la chimioradiothérapie plus efficace tout en réduisant ses effets secondaires.

La partie théorique de la thèse aborde la chimioradiothérapie, les cytostatiques présentant des propriétés radiosensibilisantes, ainsi que leurs composés modèles, du point de vue de l'interaction avec les EBE. La thèse examine les électrons de basse énergie, leur origine, leurs propriétés et leurs interactions avec la matière. La partie expérimentale combine des expériences d'attachement électronique en phase gazeuse et des calculs *ab initio* des affinités électroniques des molécules étudiées et de leurs fragments, ainsi que des expériences de radiolyse pulsée en solution et des irradiations de solutions par microtron, suivies d'évaluations par spectroscopie de résonance magnétique nucléaire.

Les études portaient principalement sur trois molécules, et les deux des eux ont été sélectionnées en raison de leur utilisations à médecine, leur biocompatibilité et des cinétiques déjà décrites. La molécule favipiravir est un antiviral utilisé, par exemple, pour le traitement de l'Ebola ou du COVID-19. Cette molécule est intéressante pour le potentiel radiosensibilisant en raison de ses groupes fonctionnels très réactifs avec les EBE. Pour favipiravir, cette interaction a été étudiée en phase gazeuse afin d'évaluer son potentiel radiosensibilisant. Le choix d'un antiviral revêt également un intérêt particulier en raison de son activité antivirale, étant donné que certains types de cancers ont une origine virale. La molécule RRx-001 agit à la fois comme radiosensibilisant et comme agent chimiothérapeutique, comme le confirment les essais cliniques. Par ailleurs, elle présente une toxicité bien inférieure à celle du cisplatine, un agent radiosensibilisant et chimiothérapeutique couramment utilisé. Dans ce cas, nous avons cherché à déterminer si la radiosensibilisation était due à l'interaction avec des EBE et à décrire cette interaction jusqu'aux produits finaux. La troisième molécule étudiée était le fullerénol, étudié pour son potentiel de radiosensibilisation et son effet possible DCM.

Sur la base de l'étude des interactions avec les EBE secondaires, le potentiel radiosensibilisant a été confirmé pour l'agent antiviral favipiravir. Une interaction significative a été démontrée pour le radiosensibilisant chimiothérapeutique RRx-001, ainsi qu'une forte interaction des électrons solvatés avec les fullerénols, qui agissent comme une plateforme radiosensibilisante pour la DCM.